UNIVERSITY
OF WARSAW

FACULTY OF
PHYSICS

Multiloop Corrections to Semileptonic Decays of the B Meson

Mateusz Czaja

**A thesis presented in partial fulfilment of the requirements
for the degree of Doctor of Philosophy,
prepared under the supervision of Prof. Dr hab. Mikołaj Misiak.**

Doctoral School of Exact and Natural Sciences
University of Warsaw

Warsaw, Poland
April 2025

Table of Contents

Acknowledgments

I would like to give my most sincere thanks to everyone who supported me throughout my decade-long studies. First of all, I express my deepest gratitude to my supervisor, prof. Mikołaj Misiak, for his scientific guidance over the last six years, endless hours of thorough discussions, patience, and help in navigating the academic world. I thank dr. Abdur Rehman for our fruitful cooperation during the work on our common articles [1, 2]. I am also grateful to all the professors and staff of our faculty for their commitment to the highest standard of education. My heartfelt gratitude goes to my parents, Marta and Krzysztof, for their love, kindness, and care. I also thank my father for helping me with technical aspects of large document preparation. Last but not least, I appreciate the useful discussions I have had with dr Matteo Fael, prof. Matthias Steinhauser, prof. Paolo Gambino, and dr Florian Herren.

Thank you!

The work on this thesis was supported in part by the National Science Center, Poland, under the research project 2020/37/B/ST2/02746.

Abstract

The inclusive semileptonic decay of the B meson serves as the "standard candle" process for the determination of the Cabibbo–Kobayashi–Maskawa matrix element V_{cb} in the Standard Model. It can also be used to fix values of the masses of the bottom and charm quarks and non-perturbative parameters used in the theory of all inclusive decays of the B meson. The recently developed techniques of reparametrization-invariance-improved Heavy Quark Expansion motivate the investigation of the leptonic invariant mass spectrum of this decay. In the present thesis, I describe the calculation of this spectrum in the leading order in the Heavy Quark Expansion and up to the next-to-next-to-leading order in Quantum Chromodynamics. The results contain the contribution from the $b \to cc\bar{c}l\bar{\nu}_l$ channel omitted in previous determinations, making the analysis fully inclusive. The spectrum is presented as a fit to precise numerical values obtained with the Auxiliary Mass Flow algorithm, and are followed by an examination of the impact of the Next-to-Next-to-Leading correction on its moments.

In the preparation of this dissertation, I placed an emphasis on the description of the field-theoretic framework used to obtain perturbative corrections in particle physics and of the contemporary methods of computing multi-loop, multi-scale Feynman diagrams. To this end, the calculation of a two loop diagram contributing to the considered process is presented in detail. The practical aspects of dimensional regularization, Clifford and $\mathfrak{su}(N)$ algebras are summarized with a subsequent overview of the techniques of Integration By Parts reduction, differential equations, ϵ-form, and Auxiliary Mass Flow.

The technical chapters of the thesis are followed by an outline of the modern theory of inclusive decays of hadrons containing a heavy quark. The leading order approximation of the semileptonic transition in the Standard Model is derived within the framework of an Effective Field Theory. The Heavy Quark Effective Theory and the resulting Heavy Quark Expansion are presented in the context of the semileptonic decay. The reparametrization invariance and its consequences are then reviewed. Finally, I construct the effective width technique for the leptonic invariant mass spectrum that greatly facilitates the computation of higher-order perturbative corrections.

The presented results can serve to improve the future extractions of phenomenologically significant quantities from the data provided by the Belle, Belle II, and LHCb experiments. The precision of these extractions is an important limiting factor of the predictions of rare processes that can guide the search for physics beyond the Standard Model.

Streszczenie

Proces inkluzywnego, semileptonowego rozpadu mezonu B jest wykorzystywany jako „świeca standardowa" przy wyznaczaniu elementu macierzy Cabibbo–Kobayashiego–Maskawy $|V_{cb}|$ w Modelu Standardowym. Może również być użyty do uzyskania wartości masy kwarków pięknego i powabnego oraz nieperturbacyjnych parametrów używanych w teorii wszystkich inkluzywnych rozpadów mezonu B. Niedawno opublikowana metoda, polegająca na ulepszeniu Rozwinięcia Ciężkich Kwarków dzięki niezmienniczości reparametryzacyjnej, motywuje badanie spektrum w masie inwariantnej pary leptonów tego rozpadu. W poniższej rozprawie opisuję obliczenie tego spektrum w wiodącym rzędzie Rozwinięcia Ciężkich Kwarków i w drugim niewiodącym rzędzie Chromodynamiki Kwantowej. Uzyskane wyniki obejmują wkład kanału $b \to cc\bar{c}l\bar{\nu}_l$ pominiętego w poprzednich ewaluacjach dzięki czemu analiza stała się w pełni inkluzywna. Spektrum prezentuję w postaci dopasowania do precyzyjnych numerycznych wartości wyznaczonych za pomocą algorytmu Pływu Masy Pomocniczej. Następnie analizuję wpływ drugiej niewiodącej poprawki na momenty spektrum.

Podczas przygotowywania tej rozprawy, położyłem nacisk na opis teoriopolowego podejścia do obliczeń poprawek perturbacyjnych w fizyce cząstek elementarnych, a także współczesnych metod analizy wielopętlowych, wieloskalowych diagramów Feynmana. W tym celu przedstawiłem ze szczegółami obliczenie jednego z dwupętlowych diagramów, dających wkład do rozważanego procesu. Zaprezentowałem również praktyczne aspekty regularyzacji wymiarowej oraz algebr Clifforda i $\mathfrak{su}(N)$ wraz z przeglądem technik: redukcji poprzez tożsamości całkowania przez części, równań różniczkowych, formy ϵ-owej i Pływu Masy Inwariantnej.

Trzeci rozdział rozprawy otwiera zarys współczesnej teorii inkluzywnych rozpadów hadronów zawierających ciężki kwark. Wiodące przybliżenie semileptonowej przemiany w Modelu Standardowym jest wyprowadzone w ramach formalizmu Efektywnych Teorii Pola. Efektywna Teoria Ciężkich kwarków i wynikające z niej Rozwinięcie Ciężkich Kwarków są zaprezentowane w kontekście rozpadu semileptonowego. Opisana została również niezmienniczość reparametryzacyjna i jej konsekwencje. Przedstawiłem także wyprowadzenie techniki szerokości efektywnej dla spektrum w masie inwariantnej leptonów, która znacznie ułatwia obliczenia wyższych poprawek perturbacyjnych.

Zaprezentowane wyniki mogą pomóc w ulepszeniu przyszłego wyznaczania fenomenologicznie istotnych wielkości z danych zebranych przez eksperymenty Belle, Belle II i LHCb. Precyzja tego wyznaczania jest ważnym czynnikiem warunkującym dokładność przewidywań rzadkich procesów mogących pokierować poszukiwaniami teorii fizycznej wychodzącej poza Model Standardowy.

List of Publications

This thesis is primarily based on the article [1]:

M. Czaja, M. Misiak, and A. Rehman, "Complete $\mathcal{O}\left(\alpha_s^2\right)$ corrections to the leptonic invariant mass spectrum in $b \to X_c l \overline{\nu}_l$ decay", JHEP **02** (2025), 021 doi:10.1007/JHEP02(2025)021 [arXiv:2411.12866 [hep-ph]].

The other articles published during my doctoral studies are:

M. Czaja, M. Czakon, T. Huber, M. Misiak, M.Niggetiedt, at al., "The $Q_{1,2}$–Q_7 interference contributions to $b \to s\gamma$ at $\mathcal{O}(\alpha_{\rm s}^2)$ for the physical value of m_c", Eur. Phys. J. C **12** (2023), 1108 doi:10.1140/epjc/s10052-023-12270-8 [arXiv:2309.14707 [hep-ph]].

M. Czaja, M. Misiak, "Current Status of the Standard Model Prediction for the $B_s \to \mu^+\mu^-$ Branching Ratio", Symmetry **16** (2024) no.7, 917 doi:10.3390/sym16070917 [arXiv:2407.03810 [hep-ph]].

Introduction

In the process of developing a physical description of nature, one is bound to encounter quantities with values that cannot be reasoned from this description alone but rather have to be tailored *a posteriori* such that a certain chosen subset of predictions fits the observed behavior. The predictive value of a theory should be judged by the comparison of the smallest possible size of this set needed to fix all parameters to the amount of all quantitative predictions given by the theory. Demanding that the theory respects certain symmetries can reduce the number of free constants. The parameter spaces of various physical models developed over the last century vary greatly in size and substance. The hypothesized M theory is specified by a single dimensionful scale and a single dimensionless ratio. On the other hand, "bottom up" effective field theories such as the Standard Model Effective Field Theory (SMEFT) or the Higgs Effective Field Theory depend in principle on an infinite tower of Wilson coefficients but of diminishing phenomenological importance.

Both extremes have their virtues. Models with a small number of free parameters possess an indisputable aesthetic quality and one is naturally inclined to believe that the final, noumenal or in any way "true" description will be free of any ambiguity. The discussion of the existence, or even approachability of such a theory lies in the domain of philosophy. It is this author's conviction, that the criteria used in physical modeling should instead be first of all pragmatic, and the theory itself adjusted to the contemporary measurement technology and aimed at guiding the development of future generations of experiments. To this end, models in the second extreme can serve an important purpose. Such formulations obviously cannot be expected to be predictive by themselves, but rather should be treated as universal parametrizations of theories respecting certain assumptions. The applicability of a predictive high energy theory T_{H+L} with parameters C_{H+L} describing known particles L along with some yet unobserved, heavy degrees of freedom H can be assessed by studying the effects of H on the dynamics of L with the latter fixed by experiment. To do so systematically, one can treat the most generic model T_L matching the particle content and the dynamics of L as the low energy effective theory of T_{H+L} which uniquely fixes all parameters C_L of T_L in terms of C_{H+L}. In this sense, the space of C_L parametrizes all possible T_{H+L} that can predict the already known behavior of L. On the other hand, C_L are experimentally known up to some finite precision, which puts bounds on C_{H+L} or even excludes T_{H+L} entirely without any direct search for H. The findings of such analyses have been guiding the general strategy of experimental particle physics for decades.

The Standard Model (SM) of particle physics lies between the above two opposites. It is based on two primary principles: gauge invariance and renormalizability. The first is formalized by introducing a gauge symmetry group $G_{SM} = SU(3) \otimes SU(2) \otimes U(1)$, and specifying that the dynamical fields transform in certain representations of this group. The fermionic matter content of the SM is as follows:

- left-handed fields ψ_{Qj}, $j \in \{1, 2, 3\}$ transforming in the fundamental representations of $SU(3)$ and $SU(2)$, with $U(1)$ hypercharge $Y_Q = 1/6$ (quark doublets),
- left-handed fields ψ_{Lj} in the fundamental representation of $SU(2)$, uncharged under $SU(3)$, and with hypercharge $Y_L = -1/2$ (lepton doublets),

- right-handed fields ψ_{Uj} and ψ_{Dj}, in the fundamental representation of $SU(3)$, uncharged under $SU(2)$, with hypercharges $Y_U = 2/3$ and $Y_D = -1/3$, respectively (up- and down-type quark singlets),

- right-handed fields ψ_{Ej}, uncharged under $SU(3)$ and $SU(2)$, with hypercharge $Y_E = -1$ (lepton singlets).

Some additional structure is needed to describe the neutrino masses required by the observed neutrino flavor oscillations. The nature of these masses will play no role in the present thesis, but for definiteness, in the counting of SM parameters, I assume a model with no Majorana mass terms and with right-handed Dirac neutrino gauge singlets. This introduces the final three right handed fermion fields $\psi_{\nu j}$ that are uncharged under $SU(3)$ and $SU(2)$ and with hypercharge $Y_\nu = 0$. To preserve the local symmetry, for each gauge group generator one introduces a vector boson that couples to the fermions through the corresponding covariant derivative. There is a single fermion-gauge boson coupling constant for each of the three simple components of G_{SM}. The electroweak part of the gauge symmetry is spontaneously broken by the introduction of a Lorentz scalar Higgs $SU(2)$ doublet with a "Mexican hat" shaped classical potential that can be parameterized by the Higgs mass and the vacuum expectation value v. The *a priori* massless fermionic fields are coupled to the Higgs doublet via Yukawa interactions. The most general parametrization allows for 36 complex Yukawa couplings that can be collected in four 3×3 matrices $\Gamma^{(x)}_{ij}$ with $x \in \{u, d, l, \nu\}$. The actual number of free parameters is much smaller, as the majority of the Yukawa matrix element parameters can be absorbed into the fields via unitary field redefinitions in the generation space. After the spontaneous symmetry breaking, one can express the remaining Yukawa coupling parameters in terms of 12 real fermion masses and 8 real generation-mixing angles. The criterion of renormalizability excludes from the SM Lagrangian terms with couplings of negative mass-dimension. This, in turn, limits the allowed interaction terms to the ones described above. Overall, such a formulation of the SM depends on 25 real parameters that have to be fixed by experiment: the three gauge couplings, the 20 irreducible Yukawa parameters, and the two Higgs-doublet potential parameters[†].

The continuing effort to improve the extraction of SM parameters is motivated by the growing emphasis on the high precision searches for physics beyond the SM. Despite the great success of the SM as a theory in collider experiments up to collision energies $\mathcal{O}(10)$TeV, a number of fundamental questions remain unanswered. The SM does not explain, in particular, the observed matter-antimatter asymmetry, the tiny enough neutron electric dipole moment [14], or the nature of Dark Matter. Moreover, it does not contain any description of gravity. While the LHC still has several decades of data gathering ahead and substantial upgrades to come, the lack of direct detection of any of the multitude degrees of freedom proposed by theorists up to 14TeV motivates a growing emphasis on the high precision searches for physics beyond the SM. This strategy in essence follows the one outlined above, with the SM treated as the leading approximation of the non-renormalizable SMEFT limited only by the particle content and symmetries of the SM. A scenario in which the SMEFT with some non-vanishing Wilson coefficients gives a significantly better prediction than the SM will constitute a clear signal of New Physics. Within this approach, the space of possible beyond SM theories narrows with the increasing precision of SM predictions but the experimental

[†]The SM parameter counting here does not include $\theta_{\rm QCD}$ and $\theta_{\rm weak}$ that correspond to certain total derivatives in the Lagrangian density, and may manifest themselves via topological quantum effects only [3–9].

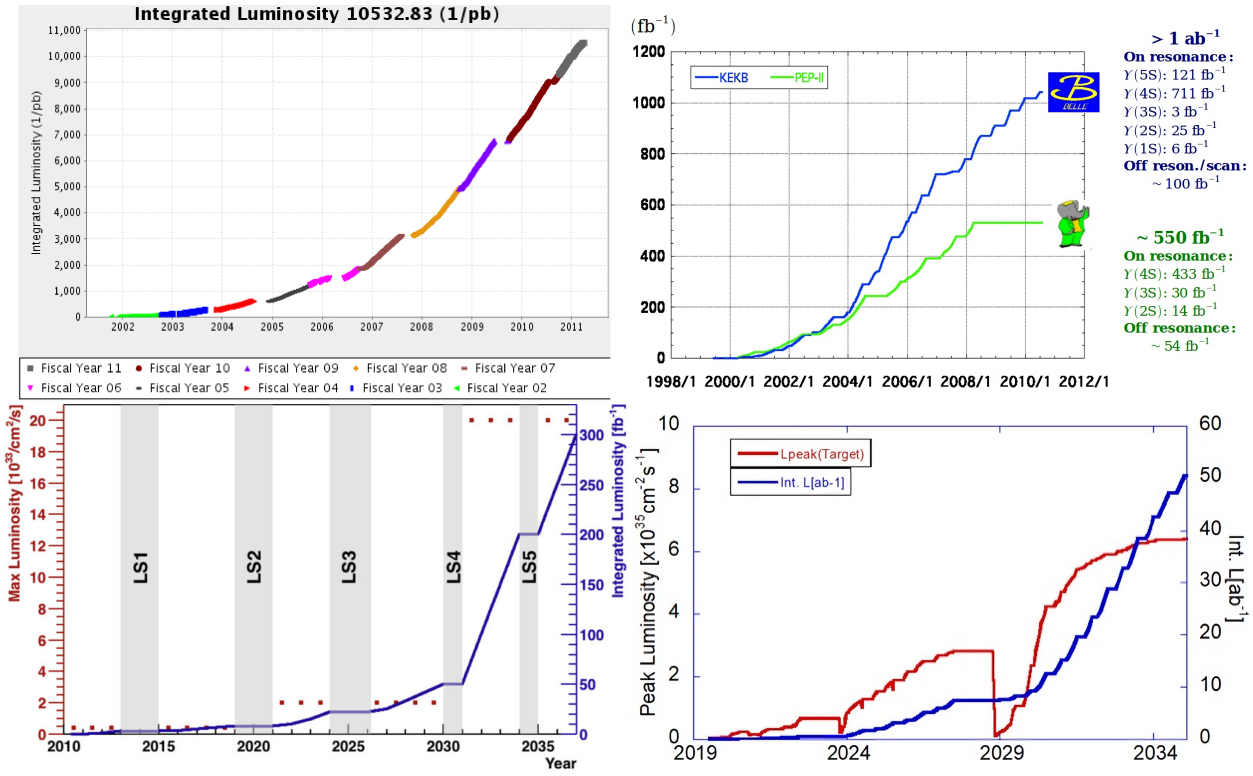

Figure 2: The integrated luminosity plots of several past, present, and future collider experiments: Tevatron (top left), Belle I and BaBar (top right), LHCb (bottom left), and Belle II (bottom right). Figures taken from refs. [10–13].

constraints on the SMEFT Wilson coefficients can shed light on physics beyond SM only if the values of the SM free parameters are well under control.

The precision studies of the SM became feasible due to the continuous increase in luminosity of accelerators and the resulting rise in the number of detected events. Maximizing the amount of data gathered in collider experiments is the principal aim of all detector designs and their subsequent upgrades. In the case of experiments covering b hadron physics, the statistics collected in the previous generation of B factories is already significant, and is expected to increase more than tenfold (see figure 2). The Belle II collaboration continues to establish new instantaneous luminosity records and, by the time of publication of this thesis, accumulated around half of the integrated luminosity of Belle I and BaBar combined. The efficiency of hadron colliders is also steadily improving. For example, in 2024 alone, the LHCb experiment almost matched the entire integrated luminosity of Tevatron. Such a wealth of results will allow the experimental community to reduce statistical errors in many crucial observables. With a data set increased n times, one can roughly project this reduction to be by a factor $\mathcal{O}(\sqrt{n})$; an estimate confirmed for some sample observables in table 1 [15]. It is thus reasonable to anticipate that the upcoming two decades could bring improvements in experimental accuracy of flavor physics observables by a factor of 3 or even higher, provided that systematic uncertainties can be reduced as well. This in turn motivates greatest possible efforts to bring the uncertainties down also on the theory side.

While many properties of hadrons and leptons, can be extracted directly from the differential cross sections and decay widths, quantities describing the constituent particles are more elusive. Due to the strong confinement, quarks cannot be produced by themselves but only bound into hadrons of various kinds. This introduces much difficulty already in prop-

Observable	5 ab^{-1}	50 ab^{-1}	Observable	5 ab^{-1}	50 ab^{-1}
$\mathcal{B}(B^+ \to \bar{D}^0\tau^+\nu_\tau)$	7.9%	2.5%	$\mathcal{B}(B^0 \to D^-\tau^+\nu_\tau)$	28.5%	9.0%
$\mathcal{A}_{\rm CP}(B \to X_s\gamma)$	0.009	0.003	$\lvert V_{ub}\rvert$	1.0%	0.3%
R_K	7%	2%	R_{K^*}	9%	3%

Table 1: Expected uncertainties of some quantities with Belle II data at two sample values of integrated luminosity. Values given in percentages are relative to the mean value of the currently best known extractions while the ones given as numbers denote absolute errors. Percentages for the branching ratios in the first row denote total errors while all others values contain only the statistical contributions to the relevant measurement errors. The CP asymmetry of a process $\mathcal{A}_{\rm CP}(\text{process})$ is defined as $[\Gamma(\text{process}) - \Gamma(\overline{\text{process}})]/[\Gamma(\text{process}) + \Gamma(\overline{\text{process}})]$, where the overline denotes the CP-conjugation of the initial and final states. The symbol $\mathcal{B}(\text{process})$ denotes the branching ratio of a process while $R_{K^{(*)}}$ is the ratio $\mathcal{B}(B \to K^{(*)}\mu^+\mu^-)/\mathcal{B}(B \to K^{(*)}e^+e^-)$. Finally, $|V_{ub}|$ is the Cabibbo–Kobayashi–Maskawa (CKM) matrix parameter described below.

erly defining the quark masses which must be treated as renormalization-scheme-dependent quantities. In the perturbative regime of QCD, the standard definition of the on-shell mass as the location of the lowest energy pole of the two-point Green's function gives a poorly behaved series. This behavior can be improved in a carefully constructed renormalization scheme [16–26]. Whatever the details of the particular definition one chooses, the observed quark masses follow a very peculiar hierarchy. The ubiquitous up and down quarks have masses $\mathcal{O}(1\text{MeV})$ with most of the nucleon mass coming from the energy of the relativistic strongly interacting partons. The strange quark's mass is $\mathcal{O}(100\text{MeV})$, followed by the charm quark mass $\mathcal{O}(1\text{GeV})$. The third generation quarks b and t appear to have masses $\mathcal{O}(4\text{GeV})$ and $\mathcal{O}(170\text{GeV})$ respectively. The observed quark masses cover five orders of magnitude, implying a similar hierarchy among the fundamental Yukawa couplings to the Higgs doublet. Understanding such a hierarchy is one of the motivations for the precise study of the Yukawa sector of the SM, and is required to shed more light on the apparent quark mass hierarchy.

The development of the SM was in large part motivated by the need to explain the CP symmetry violation observed first in the decays of neutral Kaons. The wider subject of CP violation is directly connected to the puzzle of baryogenesis and the observed asymmetry between matter and antimatter, which remain as one of the most mysterious problems of modern particle physics and cosmology. With the apparent lack of strong CP violation, the only source of CP symmetry breaking in the renormalizable interactions of known particles comes from the non-vanishing imaginary parts of Yukawa couplings. In the quark sector with only two generations, these can be made zero with unitary field redefinitions. This led Kobayashi and Maskawa to postulate [27] the existence of the third generation of quarks 4 years before the discovery of mesons containing b quarks [28] and two decades before the experimental confirmation of the top at the Tevatron [29, 30]. The introduction of the third $SU(2) \otimes U(1)$ quark doublet increases the amount of independent, irreducible parameters describing the Yukawa couplings by three with one of them being the CP violating complex phase factor.

At the partonic level, CP violating processes in hadrons arise as a result of transitions between different quark flavors. In the SM, the latter are parameterized by the unitary CKM matrix V_{jk} which encapsulates the four mixing parameters left after quark field redefinitions, and describes the relation between quark weak interaction and mass eigenstates. The prob-

ability amplitude of a flavor transition is governed by the relevant CKM matrix element, as described by the following Feynman rules:

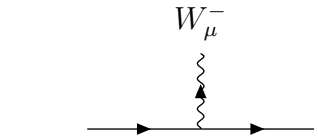

$$= \mathcal{A}^\mu V_{jk},$$

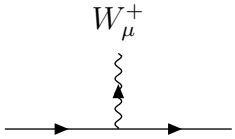

$$= \mathcal{A}^\mu V^*_{jk}, \quad \text{(I.1)}$$

where $\mathcal{A}^\mu \equiv -ig\gamma^\mu P_L/\sqrt{2}$, g is the $SU(2)$ coupling, γ^μ is one of the four Dirac matrices, and P_L is the projector onto left spinor components. It is important to stress that each element of the CKM matrix can be independently measured[†] without any ansatz on the structure of the CKM matrix. The unitarity of the obtained matrix is a strong test of the Kobayashi–Maskawa description of CP violation and of the SM as a whole. The recent progress on the determination of V_{ud} [32] has led to a 3σ deviation from the unitarity condition [31]

$$|V_{ud}|^2 + |V_{us}|^2 + |V_{ub}|^2 = 0.9985(5), \quad \text{(I.2)}$$

possibly hinting at a new "anomaly" of the SM.

In the SM, the CKM matrix can be parameterized in many different ways but in the context of b physics, it is done most conveniently using four real numbers: λ, γ, $|V_{ub}|$, and $|V_{cb}|$. With these, the CKM matrix takes the form

$$\begin{aligned} V &= \begin{pmatrix} V_{ud} & V_{us} & V_{ub} \\ V_{cd} & V_{cs} & V_{cb} \\ V_{td} & V_{ts} & V_{tb} \end{pmatrix} \\ &= \left(1 + \mathcal{O}(\lambda^3)\right) \begin{pmatrix} 1 - \frac{\lambda^2}{2} & \lambda & |V_{ub}|e^{-i\gamma} \\ -\lambda & 1 - \frac{\lambda^2}{2} & |V_{cb}| \\ |V_{cb}|\lambda - |V_{ub}|e^{i\gamma}\left(1 - \frac{\lambda^2}{2}\right) & -|V_{cb}|\left(1 - \frac{\lambda^2}{2}\right) - |V_{ub}|\lambda e^{i\gamma} & 1 \end{pmatrix}. \end{aligned} \quad \text{(I.3)}$$

The precise values and uncertainties of the free parameters vary with the particular extraction procedure, but the magnitudes of CKM matrix elements turn out to respect the following hierarchy:

$$\begin{pmatrix} |V_{ud}| & |V_{us}| & |V_{ub}| \\ |V_{cd}| & |V_{cs}| & |V_{cb}| \\ |V_{td}| & |V_{ts}| & |V_{tb}| \end{pmatrix} = \begin{pmatrix} \mathcal{O}(1) & \mathcal{O}(10^{-1}) & \mathcal{O}(10^{-3}) \\ \mathcal{O}(10^{-1}) & \mathcal{O}(1) & \mathcal{O}(10^{-2}) \\ \mathcal{O}(10^{-3}) & \mathcal{O}(10^{-2}) & \mathcal{O}(1) \end{pmatrix}. \quad \text{(I.4)}$$

The parameter $\lambda = 0.22650(48)$ is determined in measurements of semileptonic decays of charged Kaons and from β decay. Resolving the other three parameters relies on the study of B meson physics. The CKM phase $\gamma = 1.196^{+0.045}_{-0.043}$ is measured from a wide range of CP violating B decays[‡]. Both of these values were taken from the global analysis of ref. [31].

The values of $|V_{cb}|$ and $|V_{ub}|$ are obtained from semileptonic decays of the B mesons. Currently, the most precise determination of $|V_{cb}|$ comes from a fit of kinematic moments of the inclusive $B \to X_c l \bar{\nu}_l$ channel[††] shown in figure 3, summed over all possible hadronic states

[†] A review of different extraction strategies of each element is provided in section 12 of ref. [31]

[‡] A direct measurement from neutral Kaon mixing is less competitive due to larger hadronic uncertainties on the theory side of the analysis.

[††] The experimental and theoretical analysis is performed for the isospin- and CP-averaged quantities.

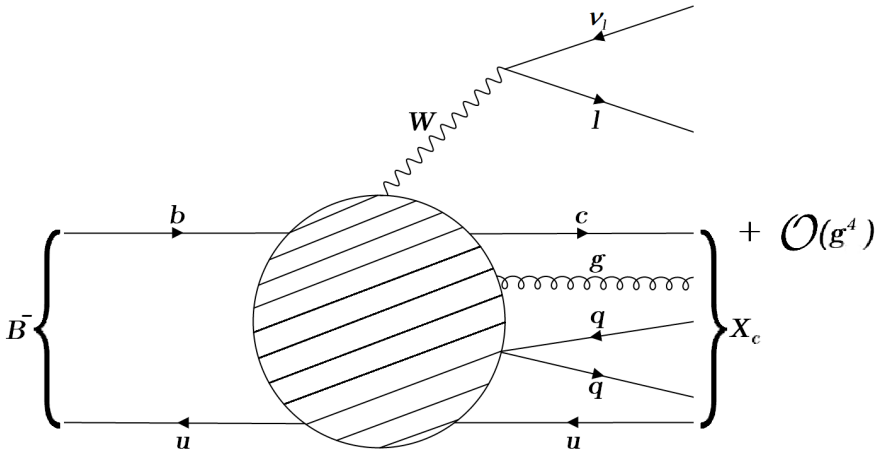

Figure 3: The inclusive semileptonic decay of the B^- meson: $B \to X_c l \bar{\nu}_l$

.

X_c that contain one unbalanced charm quark. The theory prediction of this decay, as well as of the B meson lifetimes and mixing has a fairly simple structure: sufficiently inclusive observables can be expanded into a series of terms suppressed by powers of $\overline{\Lambda}/m_b$, where $\overline{\Lambda} \simeq M_B - m_b \approx 0.15 m_b$, and M_B is the mass of the B meson. In each term of this, so called, Heavy Quark Expansion (HQE), the contributions from the perturbative and non-perturbative regimes of QCD factorize. The former can be calculated using Feynman diagrams and other techniques of perturbative Quantum Field Theory (QFT). Once a truncation order of the HQE is chosen, the latter are treated as parameters in a fit to experimental data of the moments of spectra of the $B \to X_c l \bar{\nu}_l$ decay. For example, the inclusive semileptonic decay width $\Gamma_{sl} \equiv \Gamma(B \to X_c l \bar{\nu}_l)$ in the HQE reads

$$\Gamma_{sl} = G_F^2 |V_{cb}|^2 m_b^5 \sum_k \frac{C_k^\Gamma \langle O_k^{(n_k)} \rangle}{m_b^{n_k - 3}} + \mathcal{O}\left(\alpha_{em}, \frac{m_b}{\text{electroweak scale}}\right), \tag{I.5}$$

where G_F is the Fermi constant measured in the muon decay and $\alpha_{em} \equiv e^2/(4\pi)$ is the fine structure constant of Quantum Electrodynamics (QED). The subleading electroweak corrections will be suppressed below.

The non-perturbative effects of the hadronic structure of the B meson are parameterized by the matrix elements $\langle O_k^{(n_k)} \rangle$ defined as:

$$\langle O_k^{(n_k)} \rangle \equiv \frac{\langle B(p_B) | O_k^{(n_k)}(x=0) | B(p_B) \rangle}{2M_B}. \tag{I.6}$$

The leading matrix element arises at $n_k = 3$ and reads (cf. section 3.3):

$$\langle O_\mu^{(3)} \rangle = \frac{\langle B | \bar{b} \gamma_\mu b | B \rangle}{2M_B} = v_\mu, \tag{I.7}$$

where $\bar{\psi} \equiv \psi^\dagger \gamma_0$. The higher dimension local operators $O_k^{(n_k)}$ are built from the fields b_v, gluon fields and the fields of lighter quarks. Here, b_v, given by

$$b_v(x) \equiv e^{i m_b v x} \frac{1 + \not{v}}{2} b(x), \tag{I.8}$$

is the Heavy Quark Effective Theory (HQET) rescaled field, v is the four-velocity of the B meson: $v \equiv p_B/M_B$, p_X the momentum of the particle X, and $\not{a} \equiv \gamma^\mu a_\mu$. The form

of the operators $O_k^{(n_k)}$ will be discussed in section 3.3 of this thesis. Here, it is sufficient to state that they scale as $\overline{\Lambda}^{n_k-3}$, providing the suppression factor $(\overline{\Lambda}/m_b)^{n_k-3} \equiv \hat{\Lambda}^{n_k-3}$ for each term of the HQE (I.5). The matrix elements of possible operators with $n_k = 4$ vanish by equations of motion of HQET, meaning that the first non-perturbative correction is suppressed by a factor of $\hat{\Lambda}^2 \approx 0.02$. An important observation is that the HQE matrix elements are universal for all observables in which one can establish an expansion analogous to eq. (I.5), in particular for the semileptonic decay moments.

The Wilson coefficients C_k^Γ in eq. (I.5) depend on the considered observable. They are computed in perturbative QCD in powers of $\alpha_s \equiv g_s^2/(4\pi)$ by matching the partonic matrix elements of the HQE operators $O_k^{(n_k)}$ to the corresponding correlators in full QCD (cf. section 3.3). In particular, eq. (I.7) leads to the following result for the semileptonic width in the leading order in the HQE:

$$\begin{aligned}\Gamma_{sl} =& |G_F|^2 |V_{cb}|^2 m_b^5 C_{part}^{\Gamma,\mu} \langle O_\mu^{(3)} \rangle + \mathcal{O}\left(\hat{\Lambda}^2\right) = \Gamma(b \to X_c l \bar{\nu}_l) + \mathcal{O}\left(\hat{\Lambda}^2\right) \\ =& \Gamma^{(0)} + \alpha_s \Gamma^{(1)} + \alpha_s^2 \Gamma^{(2)} + \mathcal{O}(\alpha_s^3) + \mathcal{O}\left(\hat{\Lambda}^2\right).\end{aligned} \tag{I.9}$$

The strategy of extracting the value of $|V_{cb}|$ is as follows. One considers a set of kinematic moments of the semileptonic decay that can be defined as

$$\langle M[w] \rangle \equiv \int dPS_{sl} w(v, p_l, p_{\bar{\nu}_l}) \frac{d\Gamma_{sl}}{dE_l dq^2 dr^2}, \tag{I.10}$$

where dPS_{sl} is the differential element of the allowed phase space of the outgoing particles and $w(v, p_l, p_{\bar{\nu}_l})$ is a certain weight function. In the above definition, E_l is the energy of the outgoing charged lepton in the rest frame of the B meson, $E_l \equiv v p_l$, $q \equiv p_l + p_{\bar{\nu}_l}$ is the four-momentum of the virtual W boson mediating the semileptonic transition, and $r \equiv p_B - q = m_b v - q$ is the total four-momentum of the produced hadronic system X_c. Sample kinematic moments include:

$$\begin{aligned}&\langle M[(m_b v - p_l - p_{\bar{\nu}_l})^{2k}] \rangle = \langle r^{2k} \rangle, \\ &\langle M[(v p_l)^k] \rangle = \langle E_l^k \rangle, \\ &\langle M[(p_l + p_{\bar{\nu}_l})^{2k}] \rangle = \langle q^{2k} \rangle,\end{aligned} \tag{I.11}$$

for $k \in \mathbb{N} \cup \{0\}$, which are the successive moments of spectra in r^2, E_l, and q^2 respectively. The HQE analogous to eq. (I.5) for each of such quantities can be established, and the Wilson coefficients computed up to a desired order in $\hat{\Lambda}$. Throughout this thesis, the charged leptons and quarks lighter than c will be treated as massless. Then, the results for the kinematic moments will depend on the masses m_b, m_c, $|V_{cb}|$, and a number of non-perturbative matrix elements $\langle O_k^{(n_k)} \rangle$. On the other hand, kinematic moments of the semileptonic decay can be obtained from the measurements of the spectra of the decay. Apart from the semileptonic data, extra information on the quark masses from $e^+e^- \to$hadrons is often included. If one obtains the theory-side expressions for more moments than the number of unknown parameters, the values of the quark masses, $|V_{cb}|$ and $\langle O_k^{(n_k)} \rangle$ can be resolved in a global fit to their measured values.

In practice, the semileptonic decay is measured only above a certain threshold $E_{l,0}$ on low E_l needed to suppress large backgrounds. This complication can be taken into account on the theory side by modifying the weight functions as $w \to w\Theta(v p_l - E_{l,0})$, where $\Theta(x)$ is the Heaviside step function. The directly measured quantities at particle colliders are numbers

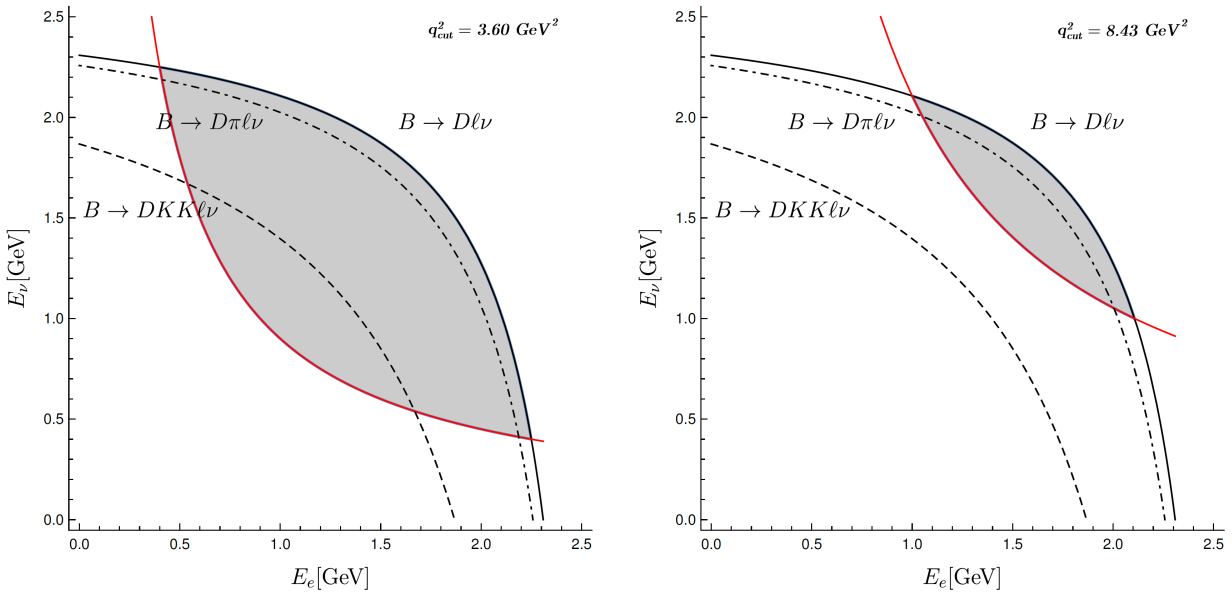

Figure 4: The region of phase space allowed after enforcing a cut on low q^2 for two values of q^2_{cut}. Figure taken from ref. [33].

of events in particular bins of the kinematic variables E_l, q^2, or r^2, which correspond to spectrum integrals over small intervals. A natural but naive idea would be to use such integrals of spectra on the theory side of the fit, using for example

$$\frac{d\Gamma_{sl}}{dq^2} = \langle M[\delta((p_l + p_{\bar{\nu}_l})^2 - q^2)]\rangle \,. \tag{I.12}$$

Unfortunately, the HQE for the spectra is poorly convergent, especially close to the endpoint of the phase space. Its integrals over bins are especially sensitive to the precise location of the interval, necessitating the use of moments with weight functions w analytical above the threshold $E_{l,0}$.

As observed in ref. [34], the Wilson coefficients of observables that do not depend on the velocity v satisfy a system of linear relations, which can be solved to reduce the number of terms of the HQE (I.5). Such observables are referred to as Reparametrization Invariant (RPI) ones. They became of particular interest in recent years. The benefit of using RPI becomes apparent already when one considers the HQE up to the $\hat{\Lambda}^3$ order, where there are 4 HQE operators for a generic observable and 3 for an RPI one. These numbers read 13 and 8 respectively at $\mathcal{O}(\hat{\Lambda}^4)$. This can be used either to improve the precision of the fit to experimental data at a fixed truncation order of the HQE, or to try to include more orders in $\hat{\Lambda}$. The total width Γ_{sl} is an obvious example of an RPI quantity. It also follows immediately from the corresponding weight function w in eq. (I.11) that the moments of the q^2 spectrum are RPI. The inclusion of the cut on low charged lepton energy in these moments would spoil this invariance, as the required theta function depends on v. This issue can be circumvented by demanding a cut on low q^2, i.e.

$$w = (p_l + p_{\bar{\nu}_l})^{2k} \Theta\left((p_l + p_{\bar{\nu}_l})^2 - q^2_{cut}\right) . \tag{I.13}$$

From purely kinematical considerations it follows that a cut

$$q^2 \geq q^2_{cut} = 2E_{l,0}\left(M_B - \frac{M_D^2}{M_B - 2E_{l,0}}\right) \tag{I.14}$$

eliminates the region of the phase space with $E_l < E_{l,0}$. This is illustrated in figure 4. The lower, red curve shows the lower bound of the inequality

$$q^2_{cut} \leq q^2 = 2E_l E_{\bar{\nu}_l}(1 - \cos\theta_{l\bar{\nu}_l}) \leq 4E_l E_{\bar{\nu}_l} \tag{I.15}$$

where $\theta_{l\bar{\nu}_l}$ is the angle formed by the outgoing leptons. The concave curves give upper limits on the allowed regions for production of different hadronic final states. The uppermost bound, shown with the solid black line, comes from the $B \to Dl\bar{\nu}_l$ channel and can be obtained as

$$\begin{aligned} M_D^2 \leq r^2 = (p_B - q)^2 &= M_B^2 - 2M_B(E_l + E_{\bar{\nu}_l}) + 2E_l E_{\bar{\nu}_l}(1 - \cos(\theta_{l\bar{\nu}_l})) \\ &\leq M_B^2 - 2M_B(E_l + E_{\bar{\nu}_l}) + 4E_l E_{\bar{\nu}_l}. \end{aligned} \tag{I.16}$$

The red and solid black lines cross at the two points satisfying

$$q^2_{cut} = 4E_l E_{\bar{\nu}_l} \qquad \wedge \qquad M_B^2 - M_D^2 - 2M_B(E_l + E_{\bar{\nu}_l}) + 4E_l E_{\bar{\nu}_l} = 0. \tag{I.17}$$

Solving these equations leads to the condition $E_l \geq E_{l,0}$, with $E_{l,0}$ satisfying eq. (I.14). This gives a prescription for choosing q^2_{cut} that gives the experimentally required lower bound on E_l. As the weight function (I.13) does not depend on v, the q^2 moments with a cut are still RPI, and depend on a reduced set of HQE matrix elements. Obtaining the q^2 moments with a cut on small values of q^2 is straightforward. One calculates the q^2 spectrum $d\Gamma_{sl}/dq^2$ and integrates it from q^2_{cut} to the largest kinematically allowed value $q^2_{max} = (M_B - M_D)^2$ with weight functions q^{2k}:

$$\langle q^{2k} \rangle_{q^2 \geq q^2_{cut}} = \int\limits_{q^2_{cut}}^{q^2_{max}} dq^2 \frac{d\Gamma_{sl}}{dq^2} q^{2k}. \tag{I.18}$$

The RPI improvement of the HQE and the need for an RP invariant cut on low E_l thus reestablishes the q^2 spectrum as the quantity of interest in the extraction of $|V_{cb}|$ and quark masses. The values obtained in a recent fit utilizing the moments of spectra in q^2, r^2, and E_l read [35]:

$$|V_{cb}| = 0.004197(48), \qquad m_b^{kin} = 4.573(12)\text{GeV}, \qquad \overline{m}_c(2\text{GeV}) = 1.090(10)\text{GeV}, \tag{I.19}$$

where the b-quark mass was determined in the kinetic scheme with the cutoff separating the perturbative and non-perturbative regimes set at 1GeV, and the $\overline{\text{MS}}$ renormalized c-quark mass at 2GeV. The Belle II results for the q^2 spectrum are shown in figure 5.

Using the strategy outlined above, the values of three free parameters of the SM can be extracted. The HQE makes the treatment of non-perturbative effects in inclusive processes of the B meson quite unique within hadron physics. The equivalent expansion for D decays has a suppression factor of $\bar{\Lambda}_D/m_c \approx 0.72$, making its behavior much poorer. The simple factorization of perturbative and non-perturbative effects for D mesons becomes dubious, due to larger theoretical uncertainties. As long as one considers the regions of phase space, where HQE can be successfully established, the hadronic structure effects in inclusive decays of the B meson are well under control. This establishes the study of the B meson as one of the primary areas of interest at the precision frontier of particle physics.

The determination of $|V_{ub}|$ from the analogous $B \to X_u l\bar{\nu}_l$ decay proves difficult due to the poor behavior of the HQE in the region of $(m_b - m_c)^2 < q^2 < m_b^2$ where this channel is not contaminated by the dominant $B \to X_c l\bar{\nu}_l$ background. The description of non-perturbative

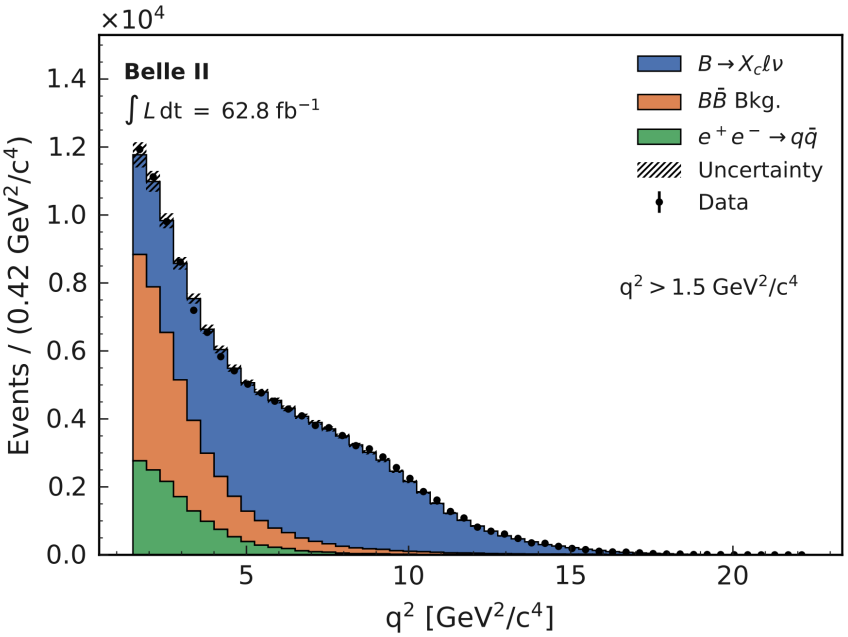

Figure 5: The q^2 spectrum obtained by Belle II. Figure taken from ref. [36].

effects in this region relies on unknown shape functions. The leading non-perturbative term is governed by a single such function, which receives important constraints from the photon energy spectrum of the $B \to X_s\gamma$ decay [37]. However, the most precise extraction of $|V_{ub}|$ comes from exclusive processes studied in lattice QCD, such as the $B \to \pi l\bar{\nu}_l$ or the purely leptonic $B \to l\bar{\nu}_l$ decays.

The study of b-quark physics has a rich history originating with the seminal work of Kobayashi and Maskawa [27]. The leading approximations for many observables in flavor physics have now been known for several decades. The semileptonic decay width of the B meson in the limit of heavy b quark and neglecting QCD corrections was computed (first as the equivalent $D \to Kl\bar{\nu}_l$ decay) 50 years ago [38] while the $\mathcal{O}(\alpha_s^1)$ effects and the lepton energy spectrum at this level were obtained in the late 1970s [39–42]. The fully differential decay rate, including the $\mathcal{O}(\alpha_s^1)$, together with the analysis of kinematic moments in the lepton energy and hadronic invariant mass were presented in 2004 and 2005 in refs. [43, 44]. The analysis of power corrections began in the early 1990s. The contribution suppressed by $\hat{\Lambda}^2$ neglecting QCD effects was published in refs. [45, 46] and the one suppressed by $\hat{\Lambda}^3$ in ref. [47]. The first results for the $\mathcal{O}(\alpha_s\hat{\Lambda}^2)$ correction were published a decade later in ref. [48], and completed in 2015 [49, 50]. The $\mathcal{O}(\alpha_s\hat{\Lambda}^3)$ correction was computed four years later in ref. [51]. Currently, the $\mathcal{O}(\hat{\Lambda}^4)$ and $\mathcal{O}(\hat{\Lambda}^5)$ corrections are only known without perturbative QCD effects. They are available in refs. [52] and [53] respectively. The results for the width at $\mathcal{O}(\alpha_s^2)$ were obtained first in the Brodsky-Lepage-Mackenzie approximation [54] in ref. [55]. The full correction was then published as an expansion in m_c/m_b in a series of articles [56–59], the last of which was published in 2008. Soon after, the fully differential analysis was published, first for the massless leptons in refs. [60, 61] and then extended to tauons in ref. [62]. The $\mathcal{O}(\alpha_s^3)$ correction to the full width was published in 2020 in ref. [63]. Following the discovery of the RPI-improved HQE in refs. [34, 64, 65] and the proposal of the above described method of extraction of $|V_{cb}|$ in ref. [33], the q^2 spectrum became the main focus of investigation of the inclusive semileptonic decay. The first results for q^2 moments at $\mathcal{O}(\alpha_s^3)$ without a cut on low values of q^2 were presented in 2022 in ref. [66].

This thesis describes the calculation of the q^2 spectrum in the leading order of the HQE and up to the $\mathcal{O}(\alpha_s^2)$ term. The result is obtained in powers of α_s:

$$\frac{d\Gamma(b \to X_c l \bar{\nu}_l)}{dq^2} = \frac{d\Gamma^{(0)}}{dq^2} + \alpha_s \frac{d\Gamma^{(1)}}{dq^2} + \alpha_s^2 \left(\frac{d\Gamma^{(2)}_{1c}}{dq^2} + \frac{d\Gamma^{(2)}_{3c}}{dq^2} \right) + \mathcal{O}(\alpha_s^3). \tag{I.20}$$

Determination of the Leading Order (LO) term $d\Gamma^{(0)}/dq^2$ requires evaluation of the imaginary part of a single 1-loop propagator diagram, the Next-to-LO (NLO) −of four 2-loop diagrams, and Next-to-NLO (NNLO) −of 39 distinct 3-loop diagrams. The LO and NLO diagrams are shown on the right panel of figure 6 in section 1.3 (page 41), while the NNLO diagrams are depicted in figure 16 in section 3.5 (page 132). The NNLO term in the above equation was split into the contribution coming from the $b \to X_{1c} l \bar{\nu}_l$ and the $b \to c c \bar{c} l \bar{\nu}_l$ channels, where X_{1c} contains exactly one charm quark and possibly some massless partons. The origin of this splitting is twofold. First, the single-charm contribution was obtained in parallel and independently by a competitive group and published in ref. [67]. In our calculation [1] we confirmed their findings using an alternative method described in chapters 2 and 3 of this thesis but also supplemented it with the triple-charm correction, making the $\mathcal{O}(\alpha_s^2)$ result fully inclusive. The $d\Gamma^{(2)}_{3c}/dq^2$ term is tiny when compared with the single-charm part and is constrained to a region of phase space where the HQE for the q^2 moments is poorly behaved. The result serves thus mainly as a confirmation that the effects of this channel do not spoil the well-behaved single-charm part. Nonetheless, the analysis presented in ref. [1] and in section 3.6 of this thesis constitute the first quantitative prediction for this channel, which hitherto was only roughly estimated by the size of its phase space.

The results presented and discussed in further chapters are only a single contribution to the general program of theoretical flavor physics and are limited to the calculation of perturbative effects. Nevertheless, they provide a great example of the progress made in recent years in the field of computing Feynman diagrams. This rich area of research benefits immensely from the efforts of great specialists from the frontier of computer science, mathematics, and physics. A significant part of this thesis is dedicated to the discussion of some of their findings. Even though many of these discoveries were made years ago, utilizing them to their full capabilities had to wait for the appropriate hardware to become readily available. Including each additional loop dramatically increases the number of diagrams and their complexity. The progress of perturbative calculations is thus often limited by the amount of memory available or the efficiency and number of CPUs employed at various stages of the computation. As these resources are now ubiquitous when compared to the technology accessible even a decade ago, tackling previously unattainable perturbative corrections becomes gradually more feasible.

The considered techniques have been developed in a way that facilitates their automation and scaling necessary for the cutting-edge problems. The general framework discussed below has been used not only in the preparation of this thesis, but also, fully or partially, in the computation of corrections to several other processes by different researches in the multi-loop community. These projects include results published for instance in refs. [68–77]. In this approach, the calculation is divided into the following steps:

1. Generation of the necessary Feynman diagrams and the corresponding expression for the amplitude.

2. Dividing the amplitude into a sum over all possible Dirac structures and extracting the coefficients of this sum using a set of projections.

3. Contracting the Dirac, Lorentz, and Color indices to obtain a manifestly scalar quantity.

4. Expressing the amplitude as a linear combination of Scalar Integrals (SIs).

5. Treating the SIs as seeds for the Integration-By-Parts (IBP) reduction.

6. Differentiating the leftover Master Integrals (MIs) with respect to all masses and kinematical invariants and treating the resulting SIs as seeds for a new IBP reduction.

7. Repeating the previous step and extending the set of MIs until it closes under differentiation.

8. Writing a system of first-order, linear Differential Equations (DEs) for MIs with coefficients dependent on masses, kinematical invariants and the space-time dimension.

9. Choosing a set of free variables best suited for the subsequent simplification of the DEs.

10. Rotating, if possible, the vector of MIs in such a way that the DE matrix has at most simple poles in the new set of free variables.

11. Finding, if possible, a rotation of the vector of MIs that brings the DEs to the so called ϵ-form (cf. section 2.3).

12. Writing, if possible, the general solution for the system of DEs order by order in the number of space-time dimensions in terms of Goncharov Polylogarithms.

13. Constructing the boundary conditions by solving DEs for MIs with the Feynman regulator as the free variable.

14. Reconstructing, if possible, the transcendental constants appearing in the boundary conditions.

In the above prescription, steps 5 and 13 are usually the most time and resource consuming, while step 9 requires some intuition and insight into the theory of DEs and cannot be simply automated. Step 10 is not possible for a class of integrals. An extension of this method to this class is possible, resulting in a more general iterated integrals in the solution to the DEs. The remaining steps are conceptually simpler, and can usually be performed with publicly available algorithms without any complicated optimization. If one does not require an analytic dependence of the amplitude on the masses and kinematic invariants, the Auxiliary Mass Flow (AMF) method applied at step 13 can instead be utilized immediately after step 5, to perform a scan of MIs over the space of values of masses and kinematical invariants. This is the approach we adopted in the calculation of the $\mathcal{O}(\alpha_s^2)$ corrections to the q^2 spectrum. Nevertheless, the full procedure was successfully applied to rederive the $\mathcal{O}(\alpha_s^0)$ and $\mathcal{O}(\alpha_s^1)$ results, and to obtain the contributions from diagrams with counterterms at the $\mathcal{O}(\alpha_s^2)$ level.

This thesis is organized as follows. Chapter 1 is dedicated to the general perturbative description of scattering and decays in QFT with the aim of relating observable quantities to scalar Feynman integrals. The subjects of Green's functions, LSZ formula, optical theorem, renormalization, dimensional regularization, Dirac algebra, and $\mathfrak{su}(N)$ algebra are discussed in subsequent sections. The general findings are implemented in an sample calculation

of one of the NLO diagrams contributing to the q^2 spectrum with the steps 1, 3, and 4 of the above algorithm outlined in sections 1.3 and 1.7. Chapter 2 follows the steps 5–14 with dedicated sections on the IBP reduction, DEs and the ϵ-form, and the Auxiliary Mass Flow method. The sample calculation is continued until the final result in sections 2.2, 2.4, and 2.6. Chapter 3 begins with the discussion of the theory of semileptonic transitions in the SM in section 3.1, and the HQE for inclusive decays of the B meson in sections 3.2 and 3.3. Sections 3.4 and 3.5 follow the steps taken in the computation of the corrections $d\Gamma_{1c}/dq^2$ and $d\Gamma_{3c}/dq^2$ introduced in eq. (I.20). Section 3.6 contains the analysis of the single- and triple-charm contributions to the NNLO QCD correction to the q^2 spectrum, and the final results for and the q^2 moments. The main results are summarized in the Conclusions.

Chapter 1:

Feynman Integrals

The purpose of this chapter is to describe the relation of physical quantities typical to collider experiments (e.g., cross sections, decay rates, branching ratios, various decay asymmetries) to scalar Feynman integrals, the evaluation of which often constitutes the most challenging part of a perturbative QFT calculation. Feynman integrals are terms in analytic expressions that are systematically associated to Feynman diagrams with the use of Feynman rules. These rules are mnemonic prescriptions relating elements of graphs: vertices, external and internal lines, to factors contributing to the probability amplitude. The relation between graphs and observables, although intuitive, can be laborious to establish on mathematical grounds. Even a sketch of this construction must be quite lengthy, and an exhaustive derivation would have to constitute a thesis on its own. Nevertheless, for the reader to have a comprehensive picture of the modern perturbative QFT framework, a discussion of this relation is required.

Most of the material presented in sections 1.1, 1.2, and 1.4 is covered more thoroughly by many standard QFT textbooks, such as refs [78–85]. Nevertheless, it is being included in this thesis to serve as a reminder and fix the notation, but also to relate the technical aspects of the computation of Feynman diagrams to the underlying physics and phenomenology. Section 1.5 discusses the generalization of the well-known Clifford algebra of γ-matrices to computations in D space-time dimensions. It covers the definition and analytic properties of chiral projectors in D dimensions in the so-called Naive Dimensional Regularization scheme, as well as a practical prescription for using these operators, which is applicable to computations of many decay observables. Section 1.6 describes properties of the $\mathfrak{su}(N)$ Lie algebras, with particular attention given to identities that play a role in the computation of the q^2 spectrum of the inclusive semileptonic decay of the b quark up to NNLO in QCD. A much more detailed discussion of the Lie algebra theory can be found in various pedagogical works, e.g, in refs [86–88]. Sections 1.3 and 1.7 aim to relate the theoretical conclusions of the preceding sections to the calculation of the q^2 spectrum by presenting in detail the computation of a sample two-loop diagram that contributes to this observable. This computation will be continued and concluded in Chapter 2.

1.1 Path Integral Formulation of Green's Functions

The starting point of this analysis is a definition of a fundamental quantity in QFT calculations: the n-point Green's function. This section will focus exclusively on the computation of such functions, while their relation to physical quantities is going to be described further on. Green's functions are vacuum expectation values of time-ordered products of n quantum fields evaluated at n different space-time points x_k:

$$\langle\Omega|T\hat{\phi}_{j_1}(x_1)\hat{\phi}_{j_2}(x_2)\dots\hat{\phi}_{j_n}(x_n)|\Omega\rangle\,. \tag{1.1}$$

In this definition, the state $|\Omega\rangle$ is the lowest-eigenvalue normalized eigenvector of the Hamiltonian of the considered theory: $\hat{H}\,|\Omega\rangle = E_0\,|\Omega\rangle$, commonly referred to as the ground state or the vacuum. For simplicity, the Hamiltonian is assumed to not be degenerate at this eigenvalue. Any possible spinor and Lorentz indices will be suppressed until the next section. The Heisenberg picture field operators $\hat{\phi}_{j_k}(x_k)$ belong to the set of degrees of freedom described by the theory. The time-ordering symbol T arranges the fields from the latest to the earliest in time:

$$\begin{aligned} &T\hat{\phi}_{j_1}(x_1)\hat{\phi}_{j_2}(x_2)\dots\hat{\phi}_{j_n}(x_n) \equiv \\ &\equiv \sum_{\sigma\in\mathfrak{S}_n}\left(\prod_{k=1}^{n-1}\Theta\left(x^0_{\sigma_k}-x^0_{\sigma_{k+1}}\right)\right) s(\sigma)\hat{\phi}_{j_{\sigma_1}}(x_{\sigma_1})\hat{\phi}_{j_{\sigma_2}}(x_{\sigma_2})\dots\hat{\phi}_{j_{\sigma_n}}(x_{\sigma_n}), \end{aligned} \tag{1.2}$$

where $\mathfrak{S}_n$ is the group of permutations of n elements, $\sigma_k \equiv \sigma(k)$. The symbol $s(\sigma)$ accounts for the anticommutation relations of fermionic operators:

$$s(\sigma) \equiv \begin{cases} 1 & \text{bosonic operators,} \\ sign(\sigma) & \text{fermionic operators.} \end{cases} \tag{1.3}$$

As bosonic and fermionic fields commute with each other, one can always split a mixed time-ordered product into separate parts for each spin. In each of the parts, $s(\sigma)$ is then well defined.

The 2-point free Green's function:

$$\langle 0|T\hat{\phi}_{j_1}(x_1)\hat{\phi}_{j_2}(x_2)|0\rangle \equiv \delta_{j_1,j_2}\tilde{\mathcal{P}}_{j_1}(x_1-x_2) \tag{1.4}$$

is of particular importance. The vector $|0\rangle$ denotes the lowest energy eigenstate in the theory without interactions. The quantity $\tilde{\mathcal{P}}_j(x_1-x_2)$ is referred to as the propagator of the free field $\hat{\phi}_j$. Its Fourier transform, $\mathcal{P}_j(p_1-p_2)$, together with vertex factors described below, constitute the building blocks of Feynman diagrams.

In eq. (1.1), the Green's functions were introduced in the formalism of Heisenberg operators $\hat{\phi}_j$ and the Fock space of state vectors. Practical calculations in this picture rely heavily on the algebra of canonical (anti)commutation relations and the Wick theorem [89]. These manipulations are often cumbersome and can obfuscate the physical meaning behind the considered objects. Green's functions can be instead elegantly described in the language of functional analysis. This description is primarily based on the path integral, i.e. the formal generalization of definite integration over sets of c-numbers to the space of complex-valued functions of space-time coordinates.

A generic path integral is of the form:

$$\int\limits_{\{t_1,\phi_1(\mathbf{x})\}}^{\{t_2,\phi_2(\mathbf{x})\}} \mathcal{D}\phi\mathcal{J}[\phi]. \tag{1.5}$$

The integration measure $\mathcal{D}\phi$ can be understood as the limit of a product of measures on an infinitely dense square lattice:

$$\frac{1}{C(s)}\prod_j \frac{d\phi(x_j)}{C(s)} \xrightarrow{s\to 0} \mathcal{D}\phi, \tag{1.6}$$

where x_j are lattice points separated by lattice spacing s. Whenever a functional object is defined through a discretization, such as in the limit (1.6), the appearance of factors $C(s)$ dependent on the spacing can be expected. Such quantities tend to vanish or be divergent in the limit of continuous space-time, but cancel out in the computation of physical observables. The form of the constant $C(s)$ depends on the considered field but will play no role in the discussion below. Note that $\phi(x)$ and $\phi(x_j)$ are now real- or complex-valued functions or *paths*, as opposed to $\hat{\phi}(x)$ which was a linear operator acting on a vector space. Path integration in this picture is an infinite-dimensional integration over all possible values of a path independently at each point of space-time. A path integral parameterized in this way can thus formally cover the space of functions satisfying the boundary conditions of the path integral in eq. (1.5). The integration boundaries $\{t_1, \phi_1(\mathbf{x})\}$ and $\{t_2, \phi_2(\mathbf{x})\}$ constrain the space of paths in such a way that $\phi(t_{1(2)}, \mathbf{x}) = \phi_{1(2)}(\mathbf{x})$ for some set functions $\phi_{1(2)}(\mathbf{x})$[†]. Finally, the integrand $\mathcal{J}[\phi]$ is a functional that assigns c-numbers to paths $\phi(x)$.

By linearity of time evolution of quantum systems, one should expect that the probability amplitude of an initial state $|\phi_i\rangle$ prepared at time t_i to be observed at a later time t_f as a final state $|\phi_f\rangle$:

$$K(\phi_f, t_f, \phi_i, t_i) \equiv \langle \phi_f | e^{-i(t_f - t_i)\hat{H}} | \phi_i \rangle \,, \tag{1.7}$$

should display an interference structure known from the theory of wave propagation, i.e. superposition. The states $|\phi_{i/f}\rangle$ are chosen to be formal eigenstates of the dynamical quantum fields of the QFT (c.f. eqs (1.18) and (1.19)). The path integral of eq. (1.5) innately reflects this fundamental aspect of quantum theories: it is a sum of contributions from every way a physical system can evolve, just as the probability amplitude can be written as a sum of contributions from separate evolutions of vectors from some chosen basis. The functional analysis formalism provides therefore a very natural prescription for a general transition amplitude:

$$K(\phi_f, t_f, \phi_i, t_i) = \int\limits_{\{t_i, \phi_i(\mathbf{x})\}}^{\{t_f, \phi_f(\mathbf{x})\}} \mathcal{D}\phi \mathcal{J}[\phi]. \tag{1.8}$$

The form of the proper functional $\mathcal{J}$ can be derived as follows.

In analogy to the Huygens–Fresnel principle, the amplitude must obey the composition law:

$$K(\phi_f, t_f, \phi_i, t_i) = \int \mathcal{D}\phi_m K(\phi_f, t_f, \phi_m, t_m) K(\phi_m, t_m, \phi_i, t_i), \tag{1.9}$$

for any t_m. Note that the function $\phi_m = \phi_m(\mathbf{x})$ is only a function of space with time fixed to t_m. The transition amplitude can therefore be transformed as:

$$\begin{aligned} \int\limits_{\{t_i, \phi_i(\mathbf{x})\}}^{\{t_f, \phi_f(\mathbf{x})\}} \mathcal{D}\phi \mathcal{J}[\phi] &= \int \mathcal{D}\phi_m \int\limits_{\{t_m, \phi_m(\mathbf{x})\}}^{\{t_f, \phi_f(\mathbf{x})\}} \mathcal{D}\phi_1 \mathcal{J}[\phi_1] \int\limits_{\{t_i, \phi_i(\mathbf{x})\}}^{\{t_m, \phi_m(\mathbf{x})\}} \mathcal{D}\phi_2 \mathcal{J}[\phi_2] = \\ = \int \mathcal{D}\phi_m \int\limits_{\{t_m, \phi_m(\mathbf{x})\}}^{\{t_f, \phi_f(\mathbf{x})\}} \mathcal{D}\phi_1 \int\limits_{\{t_i, \phi_i(\mathbf{x})\}}^{\{t_m, \phi_m(\mathbf{x})\}} \mathcal{D}\phi_2 \mathcal{J}[\phi_1]\mathcal{J}[\phi_2] &= \int\limits_{\{t_i, \phi_i(\mathbf{x})\}}^{\{t_f, \phi_f(\mathbf{x})\}} \mathcal{D}\phi \mathcal{J}[\phi_1]\mathcal{J}[\phi_2]. \end{aligned} \tag{1.10}$$

In the last equality, the division of paths into three parts was recombined into the same parametrization of the space of functions as in eq. (1.5). The functionals $\mathcal{J}[\phi_1]$ and $\mathcal{J}[\phi_2]$

[†]Throughout this thesis, the points in space-time and in space will be referred to with italic and bold letters respectively.

act only on the part of the path $\phi(x)$ from t_i to t_m and from t_m to t_f respectively. For eq. (1.10) to hold for any t_m and any pair of boundary conditions, one has to demand for all paths ϕ:

$$\mathcal{J}[\phi] = \mathcal{J}[\phi_1]\mathcal{J}[\phi_2]. \tag{1.11}$$

The contribution of each path to the amplitude should be governed by the dynamics of the considered QFT. The functional $\mathcal{J}[\phi]$ must therefore be some function of the action $S[\phi, t_f, t_i]$: $\mathcal{J}[\phi] = J(S[\phi, t_f, t_i])$. The action is additive in time:

$$S[\phi, t_f, t_i] = S[\phi, t_f, t_m] + S[\phi, t_m, t_i], \tag{1.12}$$

and it obeys the boundary condition:

$$S[\phi, t_i, t_i] = 0. \tag{1.13}$$

Combining these properties with eq. (1.11) specifies the functional $\mathcal{J}$ to be an exponential function:

$$\mathcal{J}[\phi] = e^{icS[\phi, t_f, t_i]}. \tag{1.14}$$

The expected dominant part of the integral should come from paths close to the classical trajectory ϕ_{cl}. Indeed, in the classical limit $\hbar \to 0$, it should be the only contribution. This property can now be clearly identified in the form of the path integral:

$$K(\phi_f, t_f, \phi_i, t_i) = \int_{\{t_i, \phi_i(\mathbf{x})\}}^{\{t_f, \phi_f(\mathbf{x})\}} \mathcal{D}\phi e^{icS[\phi, t_f, t_i]}. \tag{1.15}$$

The Euler-Lagrange equation for ϕ_{cl}, $\delta S[\phi_{cl}, t_f, t_i] = 0$, is equivalent to the leading stationary phase approximation. The integral will be more dominated by the classical trajectory as the functional $e^{icS[\phi, t_f, t_i]}$ gets narrower around ϕ_{cl}. This indicates that as the theory becomes classical, i.e. $\hbar$ approaches 0, the coefficient c has to diverge. On dimensional grounds, the only possibility is $c = c'/\hbar$ for some number c'. An application to a simple setup where only a finite amount of paths is viable, such as the double-slit experiment, can be used to fix this coefficient to 1. The transition amplitude in the language of path integrals thus reads

$$K(\phi_f, t_f, \phi_i, t_i) = \int_{\{t_i, \phi_i(\mathbf{x})\}}^{\{t_f, \phi_f(\mathbf{x})\}} \mathcal{D}\phi e^{iS[\phi, t_f, t_i]/\hbar}. \tag{1.16}$$

The above relation provides an interesting interpretation for the Planck constant $\hbar$. From the standpoint of path integrals, it quantifies the amount of allowed paths around the classical trajectory that contribute significantly to transition amplitudes. As $\hbar$ is taken to 0, the stationary phase approximation becomes exact and all other paths cancel out due to the rapid oscillations of the exponent in the integrand.

The formula (1.16) can be formally proven by deriving[†] the differential equation for the right hand side as a function of ϕ_f and t_f. It turns out that it satisfies the Schrödinger equation with the natural boundary condition:

$$\int_{\{t_i, \phi_i(\mathbf{x})\}}^{\{t_f, \phi_f(\mathbf{x})\}} \mathcal{D}\phi e^{iS[\phi, t_f, t_i]} \overset{t_f \to t_i}{\longrightarrow} \delta(\phi_f - \phi_i), \tag{1.17}$$

[†]See for example section 9.2 of ref. [78]

just as the transition amplitude defined in the formalism of operators and vector spaces. Here and below, the factors of $\hbar$ will be consistently suppressed, as one may always recover them by dimensional analysis.

Returning to the n-point Green's functions of eq. (1.1), they may be derived in the path integral formalism. The first step is to relate the QFT vacuum state $|\Omega\rangle$ to the boundary functions of the path integral $\phi_i(\mathbf{x})$ and $\phi_f(\mathbf{x})$. A standard way is to consider state vectors $|\phi_{i(f)}\rangle$ defined as

$$\hat{\phi}^{(S)}(\mathbf{x})\,|\phi_{i(f)}\rangle = \phi_{i(f)}(\mathbf{x})\,|\phi_{i(f)}\rangle\,, \tag{1.18}$$

where $\hat{\phi}^{(S)}(\mathbf{x})$ is the field operator transformed into the Schrödinger picture:

$$\hat{\phi}(x) \equiv \exp(i\hat{H}x^0)\hat{\phi}^{(S)}(\mathbf{x})\exp(-i\hat{H}x^0). \tag{1.19}$$

Let the boundary condition have a non-vanishing overlap with the vacuum $\langle\Omega|\phi_{i(f)}\rangle \neq 0$. Now, one can manipulate the initial vector $|\phi_i\rangle$ evolved into the far future T as follows:

$$\begin{gathered} e^{-i\hat{H}T}\,|\phi_i\rangle = e^{-i\hat{H}T}\sum\!\!\!\!\!\!\int |n\rangle\,\langle n|\phi_i\rangle \quad \overset{T\to(1-i\varepsilon)\infty}{\sim} \quad e^{-iE_0T}\,|\Omega\rangle\,\langle\Omega|\phi_i\rangle \\ \Longrightarrow |\Omega\rangle = \lim_{T\to(1-i\varepsilon)\infty} \frac{e^{-i\hat{H}T}\,|\phi_i\rangle}{e^{-iE_0T}\,\langle\Omega|\phi_i\rangle} \end{gathered} \tag{1.20}$$

and similarly

$$\begin{gathered} \langle\phi_f|\,e^{-i\hat{H}T} = \sum\!\!\!\!\!\!\int \langle\phi_f|n\rangle\,\langle n|\,e^{-i\hat{H}T} \quad \overset{T\to(1-i\varepsilon)\infty}{\sim} \quad \langle\phi_f|\Omega\rangle\,\langle\Omega|\,e^{iE_0T^*} \\ \Longrightarrow \langle\Omega| = \lim_{T\to(1-i\varepsilon)\infty} \frac{\langle\phi_f|\,e^{-i\hat{H}T}}{e^{iE_0T^*}\,\langle\phi_f|\Omega\rangle}. \end{gathered} \tag{1.21}$$

The imaginary shifts of the limiting times are assumed to be infinitesimal and dictate the branch of the analytic continuation of physical quantities. The sum-integrals in the above expressions run over all eigenstates of the Hamiltonian. As E_0 is the smallest energy of the theory, the vacuum terms of sum-integrals vanish the slowest due to the imaginary shift of the far future.

Now consider one of the terms of the expanded time-ordered product (1.2):

$$\langle\Omega|\left(\prod_{k=1}^{n}\hat{\phi}_{\sigma_k}\right)|\Omega\rangle = \lim_{T\to(1-i\varepsilon)\infty}\mathcal{N}^{-1}\,\langle\phi_f|e^{-i\hat{H}T}\left(\prod_{k=1}^{n}\hat{\phi}_{\sigma_k}\right)e^{-i\hat{H}T}|\phi_i\rangle\,, \tag{1.22}$$

where $\mathcal{N} \equiv e^{2E_0\mathrm{Im}T}\,\langle\phi_f|\Omega\rangle\,\langle\Omega|\phi_i\rangle$. For brevity, suppose that there is only one kind of field $\hat{\phi}$ in the Green's function, and label $\hat{\phi}_{\sigma_k} \equiv \hat{\phi}(x_{\sigma_k})$. Each of the Heisenberg picture fields can be written in terms of the Schrödinger picture operator as in eq. (1.19). Therefore:

$$\begin{gathered} \langle\Omega|\left(\prod_{k=1}^{n}\hat{\phi}_{\sigma_k}\right)|\Omega\rangle = \lim_{T\to(1-i\varepsilon)\infty}\mathcal{N}^{-1}\,\langle\phi_f|e^{-i\hat{H}T}\left(\prod_{k=1}^{n}e^{i\hat{H}t_{\sigma_k}}\hat{\phi}^{(S)}_{\sigma_k}e^{-i\hat{H}t_{\sigma_k}}\right)e^{-i\hat{H}T}|\phi_i\rangle = \\ = \lim_{T\to(1-i\varepsilon)\infty}\mathcal{N}^{-1}\,\langle\phi_f|e^{-i\hat{H}(T-t_{\sigma_1})}\hat{\phi}^{(S)}_{\sigma_1}e^{-i\hat{H}(t_{\sigma_1}-t_{\sigma_2})}\hat{\phi}^{(S)}_{\sigma_2}\ldots\hat{\phi}^{(S)}_{\sigma_n}e^{-i\hat{H}(t_{\sigma_n}-(-T))}|\phi_i\rangle\,. \end{gathered} \tag{1.23}$$

Functional integration can now be introduced to the expression sandwiched by boundary states through insertions of the identity operator of the form $\int \mathcal{D}\phi_{\sigma_k} \left|\phi_{\sigma_k}\right\rangle \left\langle\phi_{\sigma_k}\right|$ after each Schrödinger operator:

$$\langle\phi_f|e^{-i\hat{H}(T-t_{\sigma_1})}\hat{\phi}^{(S)}_{\sigma_1}\int \mathcal{D}\phi_{\sigma_1}\left|\phi_{\sigma_1}\right\rangle\left\langle\phi_{\sigma_1}\right|\ldots\hat{\phi}^{(S)}_{\sigma_n}\int \mathcal{D}\phi_{\sigma_n}\left|\phi_{\sigma_n}\right\rangle\left\langle\phi_{\sigma_n}\right|e^{-i\hat{H}(t_{\sigma_n}-(-T))}|\phi_i\rangle\,. \quad (1.24)$$

The integration variables $\phi_{\sigma_k} = \phi_{\sigma_k}(\mathbf{x})$ are functions of space. Using the definition of boundary states in eq. (1.18) and extracting the path integration out of the bra-ket yields

$$\int\left(\prod_{k=1}^{n}\mathcal{D}\phi_{\sigma_k}\phi_{\sigma_k}\right)K(\phi_f,T,\phi_{\sigma_1},t_{\sigma_1})K(\phi_{\sigma_1},t_{\sigma_1},\phi_{\sigma_2},t_{\sigma_2})\ldots K(\phi_{\sigma_n},t_{\sigma_n},\phi_i,-T), \quad (1.25)$$

where each of the bra-kets in eq. (1.24) was recognized as a transition amplitude of eq. (1.7). Now, one can use the result (1.16) to write this expression as

$$\begin{aligned}&\int\left(\prod_{k=1}^{n}\mathcal{D}\phi_{\sigma_k}\phi_{\sigma_k}\right)\int\limits_{\{t_{\sigma_1},\phi_{\sigma_1}\}}^{\{T,\phi_f\}}\mathcal{D}\tilde{\phi}_1 e^{iS[\tilde{\phi}_1,T,t_{\sigma_1}]}\ldots\int\limits_{\{-T,\phi_i\}}^{\{t_{\sigma_n},\phi_{\sigma_n}\}}\mathcal{D}\tilde{\phi}_n e^{iS[\tilde{\phi}_n,t_{\sigma_n},-T]}=\\ &=\int\limits_{\{t_{\sigma_1},\phi_{\sigma_1}\}}^{\{T,\phi_f\}}\mathcal{D}\tilde{\phi}_1\int\mathcal{D}\phi_{\sigma_1}\int\limits_{\{t_{\sigma_2},\phi_{\sigma_2}\}}^{\{t_{\sigma_1},\phi_{\sigma_1}\}}\mathcal{D}\tilde{\phi}_2\int\mathcal{D}\phi_{\sigma_2}\ldots\int\limits_{\{-T,\phi_i\}}^{\{t_{\sigma_n},\phi_{\sigma_n}\}}\mathcal{D}\tilde{\phi}_n\int\mathcal{D}\phi_{\sigma_n}\times\\ &\quad\times\left(\prod_{k=1}^{n}\phi_{\sigma_k}\right)e^{iS[\tilde{\phi}_1,T,t_{\sigma_1}]}\ldots e^{iS[\tilde{\phi}_n,t_{\sigma_n},-T]}.\end{aligned} \quad (1.26)$$

The paths $\tilde{\phi}_k$ are functions of space-time, as opposed to the functions ϕ_{σ_k}. All of the path integrations in the second line can be recombined into a single path integral with the desired boundaries: $\phi(-T,\mathbf{x}) = \phi_i(\mathbf{x})$ and $\phi(T,\mathbf{x}) = \phi_f(\mathbf{x})$. The term of the time-ordered product (1.22) now reads

$$\langle\Omega|\hat{\phi}(x_{\sigma_1})\ldots\hat{\phi}(x_{\sigma_n})|\Omega\rangle = s(\sigma)\lim_{T\to(1-i\varepsilon)\infty}\mathcal{N}^{-1}\int\limits_{\{-T,\phi_i\}}^{\{T,\phi_f\}}\mathcal{D}\phi\;\phi(x_1)\ldots\phi(x_n)e^{iS[\phi,T,-T]}, \quad (1.27)$$

where the path values under the integration were recognized as $\phi_{\sigma_k} = \phi(x_{\sigma_k})$. The exponents were combined using the additive property of the action quoted in eq. (1.12) and the symbol $s(\sigma)$ is the only remnant of commuting the values $\phi(x_k)$ into their canonical order[†]. The overlap factor $\mathcal{N}^{-1}$ does not depend on the specific Green's function, but only on the path integral boundary conditions. It can be evaluated using the above result for the 0-point case:

$$1 = \langle\Omega|\Omega\rangle = \mathcal{N}^{-1}\int\limits_{\{-T,\phi_i\}}^{\{T,\phi_f\}}\mathcal{D}\phi\;e^{iS[\phi,T,-T]}. \quad (1.28)$$

[†]Fermionic fields are described by anticommuting Grassman numbers. Their anticommutation relations also hold for their wavefunctions that appear when the Schrödinger fields act on unity operators in eq. (1.24).

The final result for the n-point Green's function in the language of path integrals reads

$$\langle\Omega|T\hat{\phi}(x_1)\dots\hat{\phi}(x_n)|\Omega\rangle = \lim_{T\to(1-i\varepsilon)\infty} \frac{\int\limits_{\{-T,\phi_i\}}^{\{T,\phi_f\}} \mathcal{D}\phi\ \phi(x_1)\dots\phi(x_n)e^{iS[\phi,T,-T]}}{\int\limits_{\{-T,\phi_i\}}^{\{T,\phi_f\}} \mathcal{D}\phi\ e^{iS[\phi,T,-T]}}. \tag{1.29}$$

As the dependence of the right hand side of eq. (1.29) on the path boundaries cancels in the large T limit between the numerator and the denominator, these boundaries will not be specified below, assuming only that they have a non-zero overlap with the vacuum, as was required in eqs. (1.20) and (1.21).

It is illuminating to reformulate the path integral prescription for Green's functions (1.29) in terms of another object of functional analysis: the functional derivative $\delta/(\delta J)$. For the purposes of this thesis, instead of an involved formal definition, it is sufficient to only specify its necessary characteristics:

$$\begin{aligned}
&(i)\ \frac{\delta}{\delta J(x)}\int dy J(y)\phi(y) = \phi(x),\\
&(ii)\ \frac{\delta}{\delta J(x)}F\left[\int dy J(y)\phi(y)\right] = \phi(x)F'\left[\int dy J(y)\phi(y)\right],\\
&(iii)\ \frac{\delta}{\delta J(x)}\int dy(\partial_y J(y))\phi(y) = -\partial_x\phi(x).
\end{aligned} \tag{1.30}$$

The first property defines the action of the functional derivative on basic integral-based functionals. The second is the functional equivalent of the chain rule of standard derivatives. The test functions will always be assumed to vanish at the integration boundaries, so the third property follows simply from integration by parts.

With this heuristic definition, Green's functions can be calculated by functionally differentiating the following *generating functional* $Z[\mathbf{J}]$:

$$Z[\mathbf{J}] \equiv \int\left(\prod_k \mathcal{D}\phi_k\right)\exp\left[i\int d^D x\left(\mathcal{L} + \sum_k J_k(x)\phi_k(x)\right)\right], \tag{1.31}$$

where D is the space-time dimension, $\mathcal{L}$ is the Lagrangian density, i.e. $S = \int d^D x\mathcal{L}$, the variable $\mathbf{J} \equiv \{J_1, J_2\dots\}$ is the vector of source currents, and the sum and product run over the degrees of freedom of the theory. The boundaries of the path integral are arbitrary, but they are set at the complex-shifted time infinities as in eqs. (1.20) and (1.21). The right hand side of eq. (1.29) can now be written as

$$\langle\Omega|T\hat{\phi}_{j_1}(x_1)\dots\hat{\phi}_{j_n}(x_n)|\Omega\rangle = \frac{1}{Z[\mathbf{J}=\vec{\mathbf{0}}]}\left(\prod_{k=1}^{n}\left(-i\frac{\delta}{\delta J_{j_k}(x_k)}\right)\Big|_{\mathbf{J}=\vec{\mathbf{0}}}\right)Z[\mathbf{J}]. \tag{1.32}$$

Each evaluation of a functional derivative over the source J_{j_k} introduces one factor of $\phi_{j_k}(x_k)$ present in the numerator of the formula (1.29). Setting $\mathbf{J} = \vec{\mathbf{0}}$ after the differentiation recovers the exponent of the action. The denominator is accounted for with the factor of $Z^{-1}[\mathbf{J} = \vec{\mathbf{0}}]$.

To illustrate this formal derivation with a practical example, one may derive the generating functional $Z[\mathbf{J}]$ in the simplest, physically significant model: the Klein-Gordon theory

of a single free real scalar field. The Klein-Gordon action reads:

$$S_0^{(KG)}[\phi, t_f, t_i] = \int_{t_i}^{t_f} dx^0 \int d^{D-1}\mathbf{x} \frac{1}{2}[(\partial_\mu \phi)(\partial^\mu \phi) - m^2\phi] \equiv \int_{t_i}^{t_f} dx^0 \int d^{D-1}\mathbf{x} \mathcal{L}_0. \tag{1.33}$$

In the case of the path integral formula for the Green's function (1.29), the boundary times are $t_{i/f} = \mp(1 - i\varepsilon)\infty$. The clockwise shift of the time integration contour will specify branches of analytic continuations in further calculations but using it in its current form is cumbersome. Instead, it can be moved to the integrand by a variable change: $x^0 \equiv (1 - i\varepsilon)\tilde{t}$. The resulting integral reads:

$$\begin{aligned} &S_0^{(KG)}[\phi, (1 - i\varepsilon)\infty, -(1 - i\varepsilon)\infty] = \\ &\qquad = (1 - i\varepsilon) \int_{-\infty}^{\infty} d\tilde{t} \int d^{D-1}\mathbf{x} \frac{1}{2} \left[(1 + i\varepsilon)(\partial_{\tilde{t}}\phi)^2 - (\partial_{\mathbf{x}}\phi)^2 - m^2\phi^2\right] \end{aligned} \tag{1.34}$$

up to negligible terms $\mathcal{O}(\varepsilon^2)$. The term with ε in front of the integral can be neglected, as it does not impact the direction of analytic continuation and will vanish in the $\varepsilon \to 0$ limit. Because the field ϕ is real valued, the factor $(\partial_{\tilde{t}}\phi)^2$ is non-negative and, when multiplied by ε, can be changed into $\phi^2 \geq 0$ without affecting the analytic continuation. After integrating by parts and neglecting unphysical surface terms, the result is:

$$S_0^{(KG)}[\phi, (1 - i\varepsilon)\infty, -(1 - i\varepsilon)\infty] = \int d^D x \frac{1}{2}\phi \left(-\partial^2 - m^2 + i\varepsilon\right) \phi, \tag{1.35}$$

where $\tilde{t}$ was renamed back as x^0. With the Lagrangian in this form, it is easy to recognize the imaginary time shift as the standard Feynman regulator of propagators. In this formulation, it arises naturally from the definition of Green's functions as vacuum expectation values and the way the vacuum was projected from boundary states in eqs. (1.20) and (1.21).

Turning back to the generating functional of eq. (1.31), the path integration variable can be shifted as

$$\phi \equiv \tilde{\phi} + i \int d^D y \Delta(x - y) J(y), \tag{1.36}$$

for some distribution $\Delta(x - y)$. Then, the exponent reads

$$\begin{aligned} &i \int d^D x \left[\frac{1}{2}\phi(x)\mathscr{L}(x)\phi(x) + J(x)\phi(x)\right] = \\ =&\frac{i}{2} \int d^D x \big[\tilde{\phi}(x)\mathscr{L}(x)\tilde{\phi}(x) \\ &+ \tilde{\phi}(x) i \int d^D y \mathscr{L}(x)\Delta(x - y)J(y) + i \int d^D y \Delta(x - y)J(y)\mathscr{L}(x)\tilde{\phi}(x) + 2J(x)\tilde{\phi}(x) \\ &- \int d^D y_1 d^D y_2 \Delta(x - y_1)J(y_1)\mathscr{L}(x)\Delta(x - y_2)J(y_2) + 2J(x) i \int d^D y \Delta(x - y)J(y)\big], \end{aligned} \tag{1.37}$$

where $\mathscr{L}(x) \equiv -\partial^2 - m^2 + i\varepsilon$ is (-1) times the Klein-Gordon differential operator in variable x. The second term in the third line can be integrated by parts twice with respect to x to turn $\mathscr{L}(x)$ from $\tilde{\phi}(x)$ to $\Delta(x - y)$. Then it becomes clear that by demanding

$$\mathscr{L}(x)\Delta(x - y) = i\delta^{(D)}(x - y), \tag{1.38}$$

all three terms in the third line cancel. This condition fixes $\Delta(x-y)$ to be the Green's function of the classical Klein-Gordon equation:

$$\Delta(x-y) = \tilde{\mathcal{P}}_\phi(x-y) \equiv \int \frac{d^D p}{(2\pi)^D} \frac{i e^{-ip(x-y)}}{p^2 - m^2 + i\varepsilon}, \tag{1.39}$$

where the notation of eq. (1.4) was reintroduced in foreshadowing of the result for the 2-point Green's function. Using eq. (1.38), the two terms in the last line of eq. (1.37) can be recombined to $J(x) i \int d^D y \Delta(x-y) J(y)$. The change of variables introduced in eq. (1.36) is a shift so it does not affect the path integral measure. The generating functional in the free theory thus reads:

$$Z_0[J] = \int \mathcal{D}\phi \exp\left[i \int d^D x \mathcal{L}_0\right] \exp\left[-\frac{1}{2} \int d^D x d^D y J(x) \tilde{\mathcal{P}}_\phi(x-y) J(y)\right], \tag{1.40}$$

where the subscript 0 indicates a non-interacting theory. Note that the second exponent does not depend[†] on ϕ and can be taken outside of the path integral that now simplifies to $Z_0[J=0]$. This is a generic feature of free theories: if the Lagrangian is quadratic in fields, the dependence on the source currents factorizes out of the path integral, and functional derivatives can be taken explicitly to evaluate Green's functions.

Using the above result, the operational formula for computing Green's functions in the free scalar theory is

$$\langle 0|T\hat{\phi}(x_1)\dots\hat{\phi}(x_n)|0\rangle = \left(\prod_{k=1}^{n}\left(-i\frac{\delta}{\delta J(x_k)}\right)\Big|_{J=0}\right)\mathcal{Z}[J], \tag{1.41}$$

with

$$\mathcal{Z}[J] \equiv \exp\left[-\frac{1}{2} \int d^D x d^D y J(x) \tilde{\mathcal{P}}_\phi(x-y) J(y)\right]. \tag{1.42}$$

The free vacuum state was denoted as $|0\rangle$ to distinguish it from the lowest energy state $|\Omega\rangle$ in the interacting theory. Taking a single derivative of $\mathcal{Z}[J]$ yields:

$$\frac{\delta}{\delta J(x_k)}\mathcal{Z}[J] = -\mathscr{I}_k \mathcal{Z}[J], \qquad \mathscr{I}_k \equiv \int d^D z \tilde{\mathcal{P}}_\phi(x_k - z) J(z), \tag{1.43}$$

and

$$\frac{\delta}{\delta J(x_k)}\mathscr{I}_l = \tilde{P}_\phi(x_k - x_l). \tag{1.44}$$

Now, taking higher derivatives is a matter of straightforward combinatorics. In general, one finds

$$\begin{aligned}
&\left(\prod_{k=1}^{N}\left(-i\frac{\delta}{\delta J(x_k)}\right)\right)\mathcal{Z}[J] = \\
&= \begin{cases}
\displaystyle\sum_{j=0}^{n}(-1)^j \sum_{\sigma\in\mathfrak{S}_N} \frac{\prod_{k=1}^{n-j}\tilde{\mathcal{P}}_\phi(x_{\sigma_{2k-1}} - x_{\sigma_{2k}})}{2^{n-j}(n-j)!} \frac{\prod_{k=N-2j+1}^{N}\mathscr{I}_{\sigma_k}}{(2j)!}\mathcal{Z}[J], & N = 2n, \\
\displaystyle i\sum_{j=0}^{n}(-1)^j \sum_{\sigma\in\mathfrak{S}_N} \frac{\prod_{k=1}^{n-j}\tilde{\mathcal{P}}_\phi(x_{\sigma_{2k-1}} - x_{\sigma_{2k}})}{2^{n-j}(n-j)!} \frac{\prod_{k=N-2j}^{N}\mathscr{I}_{\sigma_k}}{(2j+1)!}\mathcal{Z}[J], & N = 2n+1.
\end{cases}
\end{aligned} \tag{1.45}$$

[†]The subscript ϕ in $\tilde{\mathcal{P}}_\phi$ only indicates the type of propagator.

The combinatoric factors $2^{(n-j)}$ and $(n-j)!$ come from swapping the points within each Green's function and permuting Green's functions respectively. Similarly, $(2j)!$ and $(2j+1)!$ cancel out redundant permutations of $\mathscr{I}_k$. Putting $J = 0$ recovers subsequent Green's functions. From the above expression, only the first term of the even case survives, while all odd Green's functions vanish. The result for the $2n$-point function is

$$\langle 0|T\hat{\phi}(x_1)\dots\hat{\phi}(x_{2n})|0\rangle = \frac{1}{n!2^n}\sum_{\sigma\in\mathfrak{S}_{2n}}\prod_{k=1}^{n}\tilde{\mathcal{P}}_\phi(x_{\sigma_{2k-1}}-x_{\sigma_{2k}}). \tag{1.46}$$

The denominator cancels all combinatoric factors, meaning that each term is a product of n different Green's functions with coefficient 1. The structure of this result can be represented with simple graphs. Every term in the $2n$-point Green's function can be depicted as a graph with $2n$ points equivalent to the points x_k and n lines corresponding to the 2-point Green's functions. The graph for the 2-point function is[†]:

$$\langle 0|T\hat{\phi}(x_1)\hat{\phi}(x_2)|0\rangle = \tilde{\mathcal{P}}_\phi(x_1-x_2) = \tag{1.47}$$

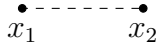

Whenever a diagram refers explicitly to scalar Green's functions, its lines will be depicted with dashed lines, while in more general considerations, the solid lines will be used. In every diagram, factors of $\tilde{\mathcal{P}}_\phi(x-y)$ can be thought of as probability amplitudes for a free particle to propagate between space-time points x and y. Hence, this Green's function is often referred to as the propagator of the theory. At this stage it is important to note an obvious but crucial observation. Since the sum in eq. (1.46) runs over all permutations of points, *all possible graphs with the correct number of lines and vertices contribute to the Green's function.* This fact dictates the first step of every perturbative QFT computation: generate all relevant graphs. From the above expression, the two Feynman rules of the free Klein-Gordon theory follow:

1. Each external point is equal to 1:  $= 1$

2. A line between points x_k and x_l is equal to the propagator $\tilde{\mathcal{P}}_\phi(x_1-x_2)$:
 $= \tilde{\mathcal{P}}_\phi(x_k-x_l)$.

To better illustrate the correspondence between graphs and terms in eq. (1.46), it is instructive to evaluate the next two even Green's functions. The 4-point function reads

$$\begin{aligned}&\langle 0|T\hat{\phi}(x_1)\hat{\phi}(x_2)\hat{\phi}(x_3)\hat{\phi}(x_4)|0\rangle = \\ =&\tilde{\mathcal{P}}_\phi(x_1-x_2)\tilde{\mathcal{P}}_\phi(x_3-x_4)+\tilde{\mathcal{P}}_\phi(x_1-x_3)\tilde{\mathcal{P}}_\phi(x_2-x_4)+\tilde{\mathcal{P}}_\phi(x_1-x_4)\tilde{\mathcal{P}}_\phi(x_2-x_3) = \\ =&\end{aligned} \tag{1.48}$$

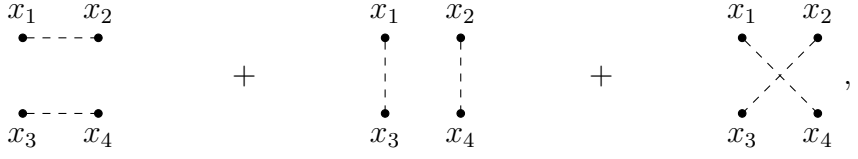

[†]The Feynman diagrams in this thesis were created with the help of the Ti*k*Z-Feynman LaTeX package [90].

and similarly, the 6-point function:

$$\begin{aligned}
&\langle 0|T\hat{\phi}(x_1)\hat{\phi}(x_2)\hat{\phi}(x_3)\hat{\phi}(x_4)\hat{\phi}(x_5)\hat{\phi}(x_6)|0\rangle = \\
&= \tilde{\mathcal{P}}_{12}\tilde{\mathcal{P}}_{34}\tilde{\mathcal{P}}_{56} + \tilde{\mathcal{P}}_{23}\tilde{\mathcal{P}}_{45}\tilde{\mathcal{P}}_{61} + \tilde{\mathcal{P}}_{12}\tilde{\mathcal{P}}_{36}\tilde{\mathcal{P}}_{45} + \tilde{\mathcal{P}}_{14}\tilde{\mathcal{P}}_{23}\tilde{\mathcal{P}}_{56} + \tilde{\mathcal{P}}_{16}\tilde{\mathcal{P}}_{25}\tilde{\mathcal{P}}_{34} + \\
&+ \tilde{\mathcal{P}}_{12}\tilde{\mathcal{P}}_{35}\tilde{\mathcal{P}}_{46} + \tilde{\mathcal{P}}_{13}\tilde{\mathcal{P}}_{26}\tilde{\mathcal{P}}_{45} + \tilde{\mathcal{P}}_{13}\tilde{\mathcal{P}}_{24}\tilde{\mathcal{P}}_{56} + \tilde{\mathcal{P}}_{16}\tilde{\mathcal{P}}_{24}\tilde{\mathcal{P}}_{35} + \tilde{\mathcal{P}}_{15}\tilde{\mathcal{P}}_{23}\tilde{\mathcal{P}}_{46} + \\
&+ \tilde{\mathcal{P}}_{15}\tilde{\mathcal{P}}_{26}\tilde{\mathcal{P}}_{34} + \tilde{\mathcal{P}}_{15}\tilde{\mathcal{P}}_{24}\tilde{\mathcal{P}}_{36} + \tilde{\mathcal{P}}_{14}\tilde{\mathcal{P}}_{26}\tilde{\mathcal{P}}_{35} + \tilde{\mathcal{P}}_{13}\tilde{\mathcal{P}}_{25}\tilde{\mathcal{P}}_{46} + \tilde{\mathcal{P}}_{14}\tilde{\mathcal{P}}_{25}\tilde{\mathcal{P}}_{36} =
\end{aligned}$$

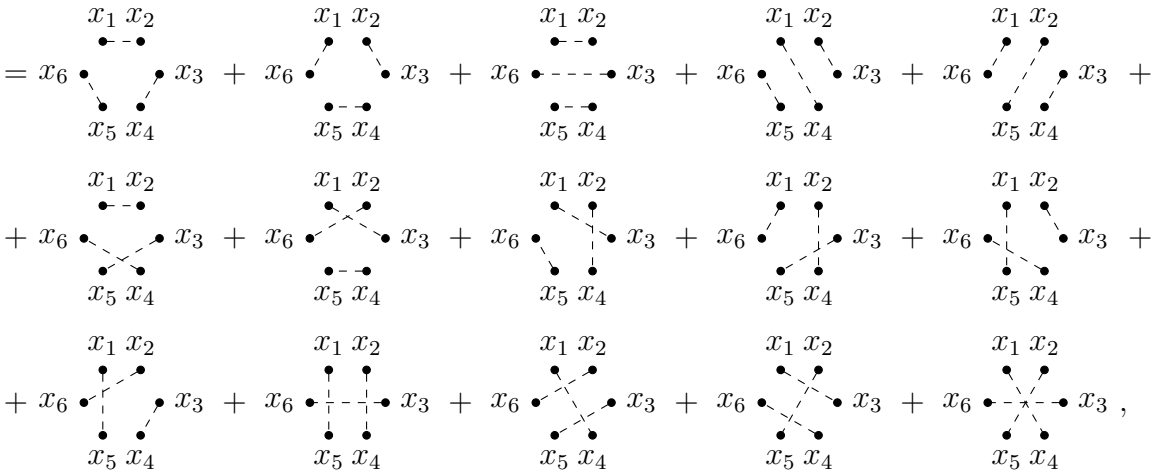

(1.49)

with the abbreviation $\tilde{\mathcal{P}}_{kl} \equiv \tilde{\mathcal{P}}_\phi(x_k - x_l)$. The number of diagrams grows quickly with the number of points. For a $2n$-point Green's function there are $(2n)!/(n!2^n)$ terms, giving 105 and 945 diagrams for 8- and 10-point functions respectively.

Moving on to the simplest interacting theory, one may add a self-coupling term to the free Klein-Gordon Lagrangian:

$$\mathcal{L} = \mathcal{L}_0 - \frac{\lambda}{4!}\phi^4, \tag{1.50}$$

where $\mathcal{L}_0$ was defined in eq. (1.33). The coupling constant λ is assumed to be small, and all arguments below should be understood perturbatively in powers of λ. The new generating functional reads

$$\begin{aligned}
Z[J] &= \int \mathcal{D}\phi \exp\left[i\int (d^D x\mathcal{L} + J\phi)\right] = \\
&= \int \mathcal{D}\phi \exp\left[-i\frac{\lambda}{4!}\int d^D y\phi^4\right] \exp\left[i\int (d^D x\mathcal{L}_0 + J\phi)\right].
\end{aligned} \tag{1.51}$$

Every term of the expansion of the first exponent can be treated as a numerator of a free Green's function from eq. (1.29) with a source term added to the free Lagrangian. Each of those terms can be written as a product of functional derivatives acting on the path integral. All of them can then be recombined into an exponent, yielding

$$Z[J] = \exp\left[-i\frac{\lambda}{4!}\int d^D y\left(\frac{\delta}{\delta J(\tilde{y})}\right)^4\right] Z_0[J]. \tag{1.52}$$

The exponent of the functional derivative should be understood as its Taylor expansion up to the desired precision in λ. Using the result of eq. (1.32), a Green's function in the interacting

theory can be transformed as

$$\begin{aligned}&\langle\Omega|T\hat{\phi}(x_1)\dots\hat{\phi}(x_n)|\Omega\rangle = \\ =&\frac{\frac{1}{Z_0[J=0]}\exp\left[-i\frac{\lambda}{4!}\int d^Dy\left(\frac{\delta}{\delta J(y)}\right)^4\right]\left(\prod_{k=1}^{n}\left(-i\frac{\delta}{\delta J(x_k)}\right)\right)Z_0\Big|_{J=0}}{\frac{1}{Z_0[J=0]}\exp\left[-i\frac{\lambda}{4!}\int d^Dy\left(\frac{\delta}{\delta J(y)}\right)^4\right]Z_0\Big|_{J=0}}.\end{aligned} \tag{1.53}$$

Each term of the λ expansion of the numerator and denominator exponents results in a Green's function of the free theory that can be computed as before but with two important differences. First, these Green's functions can have *internal* points y_k that are not set by the function under computation but have to be integrated over. Second, because of 4 functional derivatives acting at the same point, there is a possibility of lines exiting and entering the same vertex. This can change the combinatorics of the free case, resulting in some numerical factors different than 1 in front of each product of propagators. Moreover, for $D \geq 2$, the equal point Klein-Gordon propagator (1.39) is obviously UV-divergent. Various divergences appearing at different stages are a typical feature of perturbative calculations. This problem will be expanded on later in this chapter, while here treating the factors of $\tilde{\mathcal{P}}_\phi(x-x)$ purely symbolically.

To elucidate the structure of these new Green's functions, it is useful to examine the denominator up to the λ^2 correction. Using the differentiation rules of eqs. (1.43) and (1.44), it is straightforward to compute the necessary functional derivatives:

$$\begin{aligned}\frac{1}{1!4!}\left(\frac{\delta}{\delta J(y_1)}\right)^4\mathcal{Z}\Big|_{J=0} =&\frac{1}{8}\tilde{\mathcal{P}}_\phi^2(y_1-y_1),\\ \frac{1}{2!(4!)^2}\left(\frac{\delta}{\delta J(y_1)}\right)^4\left(\frac{\delta}{\delta J(y_2)}\right)^4\mathcal{Z}\Big|_{J=0} =&\\ \frac{1}{48}\tilde{\mathcal{P}}_\phi^4(y_1-y_2)+\frac{1}{16}\tilde{\mathcal{P}}_\phi(y_1-y_1)\tilde{\mathcal{P}}_\phi^2(y_1-y_2)\tilde{\mathcal{P}}_\phi(y_2-y_1)+&\frac{1}{128}\tilde{\mathcal{P}}_\phi^2(y_1-y_1)\tilde{\mathcal{P}}_\phi^2(y_2-y_2).\end{aligned} \tag{1.54}$$

The denominator can now be rewritten as a sum of diagrams without external points, often referred to as vacuum bubbles:

$$\text{(denominator)} = 1+$$ 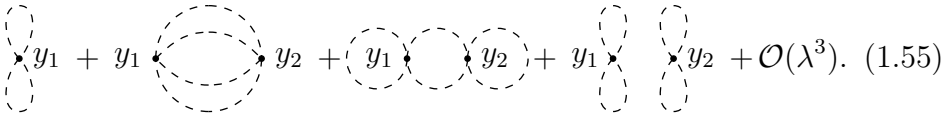 $$+\mathcal{O}(\lambda^3). \tag{1.55}$$

These diagrams, are built using the third and final Feynman rule of the Klein-Gordon theory:

3. Each internal vertex y_k contributes $(-i\lambda)\int d^Dy_k$:  $= (-i\lambda)\int d^Dy_k$.

The numerical factors in front of products of propagators were absorbed into the definition of diagrams. These so called symmetry factors can be systematically read out from the geometry of a particular diagram. The rules for deriving symmetry factors for general diagrams in a real scalar theory are quite involved [91], but simplify significantly in theories without self interactions. In particular, in Quantum Electrodynamics, the symmetry factor of every diagram is 1.

Note that the last diagram in eq. (1.55) can be written as a product of two $\mathcal{O}(\lambda^1)$ diagrams:

$$\text{(denominator)} = 1 + \quad + \quad + \quad + \frac{1}{2!} \quad^2 + \mathcal{O}(\lambda^3), \tag{1.56}$$

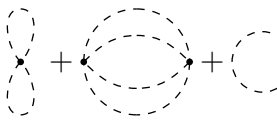

where the symmetry factor of 2! follows from the symmetry of interchanging y_1 and y_2. Moreover, the diagram

$$\frac{1}{n!} \quad^n \tag{1.57}$$

can be found at the $\mathcal{O}(\lambda^n)$ order. This is the leading behavior of a more general phenomenon: even though the denominator is composed of diagrams with possibly disconnected pieces, these pieces can always be rearranged as sums of connected diagrams to a certain power. For example, all terms of the expression

$$\frac{1}{2!} \left(\quad + \quad + \quad \right)^2 \tag{1.58}$$

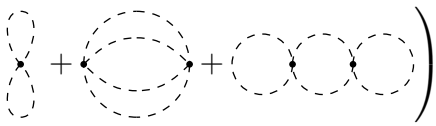

can be found with correct coefficients among terms $\mathcal{O}(\lambda^{2—4})$. Overall, the denominator turns out to be exactly

$$\begin{aligned} \text{(denominator)} &= \exp\left[\quad + \quad + \quad + \ldots \right] = \\ &= \exp[\text{all connected vacuum bubbles}], \end{aligned} \tag{1.59}$$

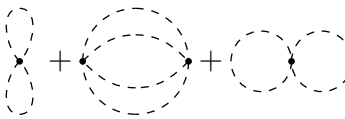

as was foreshadowed by its form in eq. (1.53).

The numerator of eq. (1.53) can also be readily recognized as a combination of free Green's functions with internal vertices. Writing the result for the 2-point function up to $\mathcal{O}(\lambda^2)$ in terms of diagrams yields

$$\begin{aligned} &\text{(numerator)} = \\ &= \quad \left(1 + \quad + \quad + \quad + \frac{1}{2!} \quad^2 + \mathcal{O}(\lambda^3) \right) + \\ &+ \quad \left(1 + \quad + \mathcal{O}(\lambda^2) \right) + \left(\quad + \quad + \quad \right) (1 + \mathcal{O}(\lambda)). \end{aligned} \tag{1.60}$$

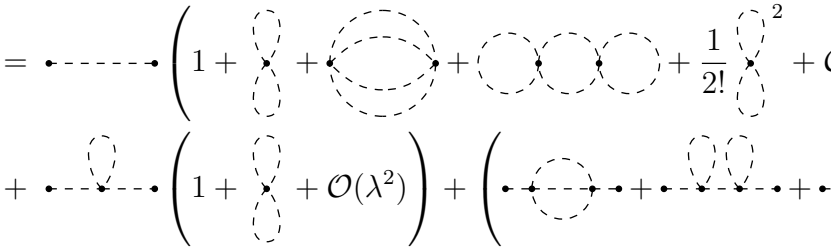

A very particular pattern emerges. Every diagram with external points is multiplied by vacuum bubbles with more and more internal vertices and coefficients of the exponent. Indeed, every diagram connected to external points is multiplied by the exponent of the connected vacuum bubbles from the denominator. After factoring out these vacuum bubble factors and canceling them with the denominator, the 2-point function becomes

$$\begin{aligned} \langle \Omega | T\hat{\phi}(x_1)\hat{\phi}(x_2) | \Omega \rangle &= \quad + \quad + \quad + \quad + \quad = \\ &= \begin{pmatrix} \text{Sum of all diagrams with two connected external points,} \\ \text{without any disconnected vacuum bubbles} \end{pmatrix}. \end{aligned} \tag{1.61}$$

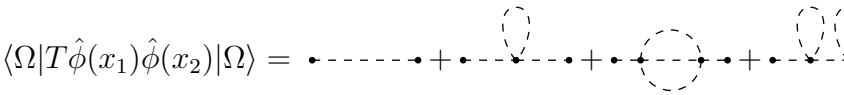

Equivalent expressions hold also for higher Green's functions. The exponentiation of vacuum bubbles described above is a consequence of a more general result:

$$\frac{\delta^n \log Z[J]}{\delta J(y_1)\dots\delta J(y_n)}\Big|_{J=0} = i^n \langle\Omega|T\hat{\phi}(y_1)\dots\hat{\phi}(y_n)|\Omega\rangle_{conn}\,, \tag{1.62}$$

where the subscript *conn* indicates that the Green's function includes only diagrams with a single connected component. This derivative leads to a formal expansion of $\log Z[J]$:

$$\log Z[J] = \sum_{n=0}^{\infty}\frac{i^n}{n!}\int d^Dy_1\dots d^Dy_n\,\langle\Omega|T\hat{\phi}(y_1)\dots\hat{\phi}(y_n)|\Omega\rangle_{conn}\,J(y_1)\dots J(y_n) \tag{1.63}$$

and the equivalent expression for $Z[J]$:

$$Z[J] = \exp\left[\sum_{n=0}^{\infty}\frac{i^n}{n!}\int d^Dy_1\dots d^Dy_n\,\langle\Omega|T\hat{\phi}(y_1)\dots\hat{\phi}(y_n)|\Omega\rangle_{conn}\,J(y_1)\dots J(y_n)\right]. \tag{1.64}$$

The result for the denominator in eq. (1.59) follows immediately from this form, as for $Z[J=0]$ only the $n=0$ term contributes to the series, and it is equivalent to the sum of all connected zero-point Green's functions, i.e. vacuum bubbles:

$$Z[J=0] = e^{\langle\Omega|\Omega\rangle_{conn}}. \tag{1.65}$$

The factoring out of disconnected bubbles from the numerator in eq. (1.60) becomes clear if the necessary partial derivative is written as

$$\begin{aligned}
&-\frac{\delta^2 Z[J]}{\delta J(x_1)J(x_2)}\Big|_{J=0} = -\frac{\delta^2 e^{\log Z[J]}}{\delta J(x_1)J(x_2)}\Big|_{J=0}\\
&= -\left[\frac{\delta^2\log Z}{\delta J(x_1)\delta J(x_2)}\Big|_{J=0} + \frac{\delta\log Z}{\delta J(x_1)}\Big|_{J=0}\frac{\delta\log Z}{\delta J(x_2)}\Big|_{J=0}\right]e^{\log Z[J=0]}\\
&= \left[\langle\Omega|T\hat{\phi}(x_1)\hat{\phi}(x_2)|\Omega\rangle_{conn} + \langle\Omega|T\hat{\phi}(x_1)|\Omega\rangle_{conn}\,\langle\Omega|T\hat{\phi}(x_2)|\Omega\rangle_{conn}\right]Z[J=0].
\end{aligned} \tag{1.66}$$

The one-point Green's functions in the second term vanish, recovering the result of eq. (1.61). Generalization to higher Green's functions is now straightforward. The form of the generating functional given in eq. (1.64) will prove beneficial in the discussion of heavy particle decoupling in section 3.1.

In practical calculations, it is almost always advantageous to evaluate Feynman diagrams in the momentum space. To this end, one needs the momentum space equivalent of the Feynman prescription given by the rules derived above. By convention, every external momentum will be treated as incoming, so the Fourier transform of a Green's function reads

$$G(p_1,\dots,p_n) \equiv \int d^Dx_1\dots d^Dx_n e^{i(p_1x_1+\dots+p_nx_n)}\,\langle\Omega|T\hat{\phi}(x_1)\dots\hat{\phi}(x_2)|\Omega\rangle\,. \tag{1.67}$$

Note that the only dependence on space-time positions in the integrand of any expression coming from a diagram is limited to $\exp[-ip(x-y)]$ in $\tilde{\mathcal{P}}_\phi(x-y)$. Integration over all vertex positions, internal and external, will result in delta functions enforcing momentum conservation. In the case of internal vertices, the sums of all incoming and outgoing momenta have to be equal. The integrations over external positions give overall external momentum conservation in each connected component. If a diagram has closed loops, a number of internal momenta equal to the number of loops will be left unspecified by these delta functions and will have to be integrated over. The procedure of computing the Fourier transform of a diagram contributing to a Green's function is as follows:

1. Treat every external momentum as incoming.

2. Enforce momentum conservation at every internal vertex.

3. Multiply by $(2\pi)^D \delta^{(D)}(\sum p_{external})$ for each connected component.

4. Multiply by $(-i\lambda)$ for every internal vertex:
 $= (-i\lambda)$.

5. Multiply by the propagator $\mathcal{P}_\phi(p)$ for every line with momentum p:
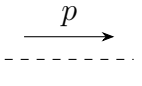 $= \mathcal{P}_\phi(p) = \frac{i}{p^2 - m^2 + i\varepsilon}$.

6. Integrate over loop momenta k with measure $d^D k/(2\pi)^D$.

7. Multiply by the symmetry factor.

The diagram for the $\mathcal{O}(\lambda)$ correction to the 2-point function can serve as an example:

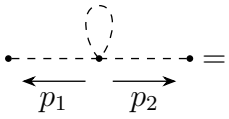

$$= \frac{1}{2}(-i\lambda)(2\pi)^D \delta^{(D)}(p_1 + p_2) \frac{i}{p_1^2 - m^2 + i\varepsilon} \frac{i}{p_2^2 - m^2 + i\varepsilon} \int \frac{d^D p}{(2\pi)^D} \frac{i}{p^2 - m^2 + i\varepsilon}. \tag{1.68}$$

While the technique of computation of simple loop integrals will be discussed in section 1.4, in cutting-edge problems this is the most laborious part of the calculation and requires specialized treatment. The modern approach to computing loop diagrams will be the focus of the next chapter.

In the Dirac and Maxwell theories of free fields with higher spin, the calculation proceeds mostly along similar steps but with some important caveats. In the former case, one has to define the fields using anticommuting variables called Grassmann numbers, which somewhat changes the algebraic properties of Gaussian integrals. Another difference is that the Lagrangian has only a first order derivative present, so the shift in eq. (1.36) required for completing the square is different. In the case of gauge field theories, a naive integral over all possible paths covers physically equivalent field configurations and, as a consequence, turns out to be badly divergent. This issue is overcome by introducing gauge fixing terms in the Lagrangian. In essence, one can reparameterize the space of all paths to separate the integration along the orbits of the gauge group from the integration over physically distinguishable paths. In non-abelian gauge theories, the Jacobian of this change of integration variables introduces additional Grassman-number-valued scalar fields called Faddeev-Popov ghosts [92]. The volume of the orbits then cancels between the numerator and denominator of formula (1.29). For both spin 1/2 and spin 1 theories, the free two-point function turns out to be related to the Green's function of the classical equation of motion just as in eq. (1.47) for the Klein-Gordon field. The results for these propagators will be quoted later in this chapter.

1.2 The LSZ Reduction and Inclusive Rate Formula

This section aims to establish the link between Green's functions described above and quantities measured in particle colliders. For this purpose, one investigates singularities of the Green's function Fourier transform. The famous LSZ formula, named after the authors of ref. [93] where it was first derived, will emerge naturally as a result of this analysis, without the need for the laborious algebraic derivation that is usually presented[†]. Next, one examines the analytic properties of residue matrix of Green's functions that turns out to contain all information on scattering processes described by the theory. The formula for inclusive decays used as the starting point of the computation of the semileptonic q^2 spectrum will follow as a result of this analysis.

First, recall that the 2-point function in the free Klein Gordon theory, derived in eq. (1.47), was given by

$$\langle 0|T\hat{\phi}(x)\hat{\phi}(y)|0\rangle = \tilde{\mathcal{P}}_\phi(x-y) = \int \frac{d^D p}{(2\pi)^D} \frac{ie^{-ip(x-y)}}{p^2 - m_0^2 + i\varepsilon}, \tag{1.69}$$

where the subscript 0 indicates that m_0 is the mass of the free field. This expression clearly has a single isolated pole at $p^2 = m_0^2$. The integral over p^0 can be performed using the Cauchy theorem. The integrand as a function of p^0 has two poles at $\pm\sqrt{\mathbf{p}^2 + m_0^2 - i\varepsilon}$, but only one of those will be inside the integration contour, giving the result

$$\tilde{\mathcal{P}}_\phi(x-y) = \int \frac{d^{D-1}\mathbf{p}}{(2\pi)^{D-1}} \frac{e^{-ip(x-y)}}{2E_\mathbf{p}}\Big|_{p_0=E_\mathbf{p}}, \tag{1.70}$$

with $E_p \equiv \sqrt{\mathbf{p}^2 + m_0^2 - i\varepsilon}$.

The 2-point Green's function in the interacting theory has a much more complicated analytic structure. Without fixing the form of the interaction term, it can be written as

$$\begin{aligned} &\langle\Omega|T\hat{\phi}(x)\hat{\phi}(y)|\Omega\rangle = \\ &= \sum\!\!\!\!\!\!\int_{\alpha_\mathbf{0}} \int \frac{d^{D-1}\mathbf{p}}{(2\pi)^{D-1}} \frac{1}{2E_\mathbf{p}(\alpha)} \big(\Theta(x_0-y_0)\,\langle\Omega|\hat{\phi}(x)|\alpha_\mathbf{p}\rangle\,\langle\alpha_\mathbf{p}|\hat{\phi}(y)|\Omega\rangle + \\ &\qquad + \Theta(y_0-x_0)\,\langle\Omega|\hat{\phi}(y)|\alpha_\mathbf{p}\rangle\,\langle\alpha_\mathbf{p}|\hat{\phi}(x)|\Omega\rangle\,\big), \end{aligned} \tag{1.71}$$

where the identity operator

$$\mathbb{1} = \sum\!\!\!\!\!\!\int_{\alpha_\mathbf{0}} \int \frac{d^{D-1}\mathbf{p}}{(2\pi)^{D-1}} \frac{1}{2E_\mathbf{p}(\alpha)}\, |\alpha_\mathbf{p}\rangle\,\langle\alpha_\mathbf{p}| \tag{1.72}$$

was inserted. The sum-integral runs over all eigenstates $|\alpha_\mathbf{0}\rangle$ of the full Hamiltonian of the theory that have the center-of-mass $(D-1)$-momentum equal to $\mathbf{0}$. The state $|\alpha_\mathbf{p}\rangle$ is defined as the Lorentz boost of the state $|\alpha_\mathbf{0}\rangle$ with $(D-1)$ momentum $\mathbf{p}$. The theory can always be reformulated in terms of a field shifted in such a way that the factor $\langle\Omega|\hat{\phi}(x)|\Omega\rangle$ vanishes. The integral with the Lorentz invariant measure $d^{D-1}\mathbf{p}/[(2\pi)^{D-1}2E_\mathbf{p}(\alpha)]$ covers all D-momenta p on the mass-shell $p_0 = E_p(\alpha)$, with $E_p(\alpha) \equiv \sqrt{m_\alpha^2 + \mathbf{p}^2}$ and m_α the energy of the state $|\alpha_\mathbf{0}\rangle$. Note that m_α are defined as certain eigenvalues of the interacting Hamiltonian and do not

[†]This discussion follows some aspects of the derivation given in chapter 7 of ref. [78].

have to be equal to any mass parameter in the Lagrangian of the theory even for the smallest value of m_α. The relation between m_α and the Lagrangian parameter m_0 is determined in the procedure of mass renormalization[†]. This point is crucial in the proper treatment of UV divergences that appear beyond the leading order in perturbation theory and will be further discussed in section 1.4.

Each of the matrix elements in eq. (1.71) has a simple dependence on $\mathbf{p}$. For example:

$$\langle\Omega|\hat{\phi}(x)|\alpha_{\mathbf{p}}\rangle = \langle\Omega|\hat{\phi}(0)|\alpha_{\mathbf{0}}\rangle\, e^{-ipx}\Big|_{p^0=E_{\mathbf{p}}(\alpha)}. \tag{1.73}$$

The above equation follows from the Poincaré invariance of the vacuum, i.e. $\exp[i\hat{P}x]\,|\Omega\rangle = |\Omega\rangle$, and $U(\Lambda)\,|\Omega\rangle = |\Omega\rangle$, where $U(\Lambda)$ is the operator implementing a Lorentz boost Λ, as well as the transformation of the scalar field under Lorentz boosts

$$U(\Lambda)\hat{\phi}(x)U^{-1}(\Lambda) = \hat{\phi}(\Lambda x). \tag{1.74}$$

The modulus squared of the bra-ket in eq. (1.73) will be denoted as $Z_\phi^{(\alpha)}$. Using eq. (1.70) simplifies the right hand side of eq. (1.71) to

$$\langle\Omega|\hat{\phi}(x)\hat{\phi}(y)|\Omega\rangle = \sum\!\!\!\!\!\!\int_{\alpha_{\mathbf{0}}} \tilde{\mathcal{P}}_\phi^{(\alpha)}(x-y)Z_\phi^{(\alpha)}, \tag{1.75}$$

where $\tilde{\mathcal{P}}_\phi^{(\alpha)}(x-y)$ is the free propagator with m_0 replaced with m_α. The space of states with $(D-1)$ momentum $\mathbf{0}$ can be fully parameterized by the mass m_α, which leads to the Källén-Lehmann representation of the 2-point function:

$$\langle\Omega|T\hat{\phi}(x)\hat{\phi}(y)|\Omega\rangle = \int_0^\infty d\tilde{m}\rho(\tilde{m})\tilde{\mathcal{P}}_\phi^{(\tilde{\alpha})}(x-y)\Big|_{m_\alpha=\tilde{m}}, \tag{1.76}$$

where $\phi^{(\tilde{\alpha})}$ is again the free propagator but with mass $\tilde{m}$. The function $\rho(\tilde{m})$ is referred to as the spectral density of the theory and is given by

$$\rho(\tilde{m}) = \sum_\alpha \delta(\tilde{m}-m_\alpha)Z_\phi^{(\alpha)} = \delta(\tilde{m}-m)Z_\phi + \begin{pmatrix} \text{contributions from bound} \\ \text{and multiparticle states} \end{pmatrix}, \tag{1.77}$$

where m is called the on-shell renormalized mass of the single particle state. The first term is the contribution from the second-lowest energy eigenvector of the Hamiltonian, which is identified as a state of a single particle at rest. As the D-momentum of Lorentz boosts of this state is constrained by the on-shell condition, its rest energy $E_{\mathbf{0}}(1p) = m$ is isolated from the next-lowest energy $|\alpha_{\mathbf{0}}\rangle$ state. This rest energy is identified as the particle mass. In the above equation, the $Z_\phi^{(1p)}$ factor was denoted as Z_ϕ. Note that $Z_\phi = 1$ in the free theory. The second term comes from boosts of higher energy eigenvectors, which correspond to multiparticle states. In these states, the D-momentum of each of the particles is fixed to the $(p_i^0)^2 = m^2 + \mathbf{p}_i^2$ shell but the total D-momentum is unconstrained, resulting in a continuum of possible multiparticle states. The space of possible D-momenta of these states is bound from below by the surface $E_{\mathbf{p}}^2(\alpha) = 4m^2 + \mathbf{p}^2$ and with the lowest energy corresponding to two separated particles at rest. Below the $E_{\mathbf{p}}^2(\alpha) = 4m^2 + \mathbf{p}^2$ surface, there are possible

[†]More specifically, by imposing the on-shell renormalization condition.

bound states, with the binding energy shifting their mass downwards. These states may add a number of poles to the spectral density for $m < \tilde{m} < 2m$.

The Fourier transform of the 2-point function in the Källén-Lehmann representation reads:

$$\begin{aligned}&\int d^D x d^D y e^{ip_1 x} e^{ip_2 x} \langle\Omega|T\hat{\phi}(x)\hat{\phi}(y)|\Omega\rangle = \\ =&(2\pi)^D \delta^{(D)}(p_1+p_2)\frac{iZ_\phi}{p_1^2 - m^2 + i\varepsilon} + \int\limits_{\tilde{m}_{min}}^{\infty} d\tilde{m}\rho(\tilde{m})\frac{i(2\pi)^D\delta^{(D)}(p_1+p_2)}{p_1^2-\tilde{m}^2+i\varepsilon}.\end{aligned} \tag{1.78}$$

where $\tilde{m}_{min}$ is the mass of the lightest multiparticle or bound state. By the above analysis, this expression treated as a function of p^0 and for fixed $\mathbf{p}$ has an isolated pole at $p^0 \to \sqrt{m^2+\mathbf{p}^2} \equiv E_{\mathbf{p}}$, possibly a series of peaks corresponding unstable bound states[†] and a branch cut along the real axis from $2m$ to $+\infty$. The one-particle pole is simply

$$G(p_1,p_2) = \quad \xrightarrow[p_1]{} \quad \xrightarrow[p_2]{} \quad \xrightarrow{p_1^0 \to E_{\mathbf{p}_1}} (2\pi)^D\delta^{(D)}(p_1+p_2)\frac{iZ_\phi}{p_1^2-m^2+i\varepsilon}, \tag{1.79}$$

where the shaded blob denotes all diagrams with two external points and no disconnected vacuum bubbles, as dictated by the result of eq. (1.61). The full 2-point function in this limit reduces to the propagator of the free theory, up to a factor Z_ϕ but with a mass corresponding to the rest energy of a single particle state in the interacting theory. To make this behavior even more apparent, one defines an *on-shell renormalized* field $\hat{\phi}_R \equiv Z_\phi^{-1/2}\hat{\phi}$, so eq. (1.73) for 1-particle states becomes

$$\langle\Omega|\hat{\phi}_R(x)|\mathbf{p}\rangle = e^{-ipx}\Big|_{p_0=E_{\mathbf{p}}}. \tag{1.80}$$

Note that the right hand side is a classical solution to the Klein-Gordon equation. This rescaling has profound consequences for loop computations that will become apparent during the discussion of the treatment of divergences in QFT, but for now, it simply absorbs the factor of Z_ϕ from the numerator of the limit (1.79):

$$\begin{aligned}G_R(p_1,p_2) \xrightarrow{p_1^0\to E_{\mathbf{p}_1}}&(2\pi)^D\delta^{(D)}(p_1+p_2)\frac{i}{p_1^2-m^2+i\varepsilon} \\ =&(2\pi)^D\delta^{(D)}(p_1+p_2)\mathcal{P}_{\phi,m}(p_1),\end{aligned} \tag{1.81}$$

where the subscript R indicates that the momentum-space Green's function is the Fourier transform of a vacuum matrix element of renormalized fields. As only interacting fields are going to be discussed in the remainder of this section, the subscript m will be suppressed in $\mathcal{P}_{\phi,m}$.

The above discussion can be generalized to higher Green's functions for a configuration typical to particle scattering. Theory description of an event in a particle collider is based on an assumption, that the interaction happens on an extremely short time scale when compared with the time particles propagate more or less freely inside the accelerator. This motivates the following picture: incoming particles are prepared as well separated wave packets in the far past $t_i \to -\infty$, collide around $t = 0$ in the lab frame and the products of the collision

[†]Stable bound states are assumed to be absent here and in the remainder of this chapter.

fly away and are measured in the far future $t_f \to +\infty$. To reflect this, at time infinities, the fields should create states with wave functions that are supported on space-time regions well separated from each other. This will allow for treating multi-particle initial and final states as tensor products of single-particle ones. The primary observable measured in a particle detector is the momentum, so momenta of these states should be constrained within narrow distributions. This shaping of the wave packets can be parametrized by some momentum-space envelope functions $f_j(\mathbf{k}_j)$ for each field in the Green's function. Then the starting point for a discussion of wave packet scattering is the smeared Fourier transform of the n-point Green's function:

$$S^{(n)}_{f_1\dots f_n}(p^0_1,\dots,p^0_n) \equiv \left(\prod_{j=1}^{n}\int dx^0_j e^{ip^0_j x^0_j}\int d^{D-1}\mathbf{x}_j \int \frac{d^{D-1}\mathbf{k}_j}{(2\pi)^{D-1}} f_j(\mathbf{k}_j) e^{-i\mathbf{k}_j\mathbf{x}_j}\right) \langle\Omega|T\hat{\phi}_R(x_1)\dots\hat{\phi}_R(x_n)|\Omega\rangle\,. \tag{1.82}$$

The momentum-space Green's function is recovered in the limit

$$S^{(n)}_{f_1\dots f_n}(p^0_1,\dots,p^0_n) \xrightarrow{f_j(\mathbf{k}_j)\to(2\pi)^{D-1}\delta^{(D-1)}(\mathbf{k}_j-\mathbf{p}_j)} G_R(p_1,\dots,p_n). \tag{1.83}$$

This function depends on p^0_j only through the exponent so the possible singularities in p^0_j have to come from the regions of integration over x^0_j near infinities. Consider now one of those regions, where for some $0 \le j_0 \le n$, for $j \le j_0$, $x^0_{\sigma_j}$ are in the far future and for $j > j_0$, $x^0_{\sigma_j}$ are in the far past, for some permutation of n indices σ. The time ordering splits into two parts, with fields in the far future on the left, and those in the far past on the right:

$$\langle\Omega|T\hat{\phi}_R(x_1)\dots\hat{\phi}_R(x_n)|\Omega\rangle = \langle\Omega|\left(T\hat{\phi}_R(x_{\sigma_1})\dots\hat{\phi}_R(x_{\sigma_{j_0}})\right)\left(T\hat{\phi}_R(x_{\sigma_{j_0+1}})\dots\hat{\phi}_R(x_{\sigma_n})\right)|\Omega\rangle\,. \tag{1.84}$$

Next, insert the identity operator of the form given in eq. (1.72) in between the two time orderings:

$$\sum\!\!\!\!\!\!\int_{\alpha_{\mathbf{0}}} \frac{d^{D-1}\mathbf{q}}{(2\pi)^{D-1}}\frac{1}{2E_{\mathbf{q}}(\alpha)} \langle\Omega|T\hat{\phi}_R(x_{\sigma_1})\dots\hat{\phi}_R(x_{\sigma_{j_0}})|\alpha_{\mathbf{q}}\rangle\langle\alpha_{\mathbf{q}}|T\hat{\phi}_R(x_{\sigma_{j_0+1}})\dots\hat{\phi}_R(x_{\sigma_n})|\Omega\rangle \tag{1.85}$$

In order for the first matrix element to not vanish, the image of the inserted state $|\alpha_{\mathbf{q}}\rangle$ under the action of the time-ordered product must have a non-zero overlap with the vacuum. It is important to emphasize here that the sum-integral $\sum\!\!\!\!\!\!\int_{\alpha_{\mathbf{0}}}$ over the vanishing total $(D-1)$-momentum states $|\alpha_{\mathbf{0}}\rangle$ contains contributions from multi-particle configurations were each excitation constrained by the envelope function to some region of space *is in motion* with some momentum $\mathbf{q}_{\sigma_j}$, and only $\sum_j \mathbf{q}_{\sigma_j} = \mathbf{0}$. The integral over all Hamiltonian eigenstates in the case above can be rewritten as

$$\sum\!\!\!\!\!\!\int_{\alpha_{\mathbf{0}}} \frac{d^{D-1}\mathbf{q}}{(2\pi)^{D-1}}\frac{1}{2E_{\mathbf{q}}(\alpha)} = \prod_{j=1}^{j_0} \sum\!\!\!\!\!\!\int_{\alpha_{\sigma_j}} \frac{d^{D-1}\mathbf{q}_{\sigma_j}}{(2\pi)^{D-1}}\frac{1}{2E_{\mathbf{q}_{\sigma_j}}(\alpha^{\sigma_j})}, \tag{1.86}$$

with the wave function of the state $|\alpha^{\sigma_j}_{\mathbf{q}_{\sigma_j}}\rangle$ constrained to the region of space-time where the field $\hat{\phi}_R(x_{\sigma_j})$ is supported. Similarly, out of all generic states $|\alpha_{\mathbf{q}}\rangle$, only those that factorize as

$$|\alpha_{\mathbf{q}}\rangle = \bigotimes_{j}^{j_0} |\alpha^{\sigma_j=1}_{\mathbf{q}_{\sigma_j}}\rangle \tag{1.87}$$

give non-zero contributions when the integral (1.85) is inserted into eq. (1.82). Each spatially constrained field acts only on the vector corresponding to it. The whole "future" matrix element in eq. (1.85) disentangles into the following product:

$$\langle\Omega|\left(T\hat{\phi}_R(x_{\sigma_j})\dots\hat{\phi}_R(x_{\sigma_{j_0}})\right)|\alpha_{\mathbf{q}}\rangle = \prod_{j=1}^{j_0}\langle\Omega|\hat{\phi}_R(x_{\sigma_j})|\alpha^{\sigma_j}_{\mathbf{q}_{\sigma_j}}\rangle = \prod_{j=1}^{j_0}\sqrt{Z_{\phi_R}^{(\alpha^{\sigma_j})}}e^{-iq_{\sigma_j}x_{\sigma_j}}\Big|_{q^0_{\sigma_j}=E_{\mathbf{q}_{\sigma_j}}(\alpha)}, \tag{1.88}$$

with $Z^{(1p)}_{\phi_R}=1$ for one particle states. Such a factorization has been the reason for considering wave packets instead of directly analyzing the Fourier transform of the Green's function. Now, inserting another identity operator in between the $\langle\alpha_q|$ and the second time ordering symbol in eq. (1.85) allows one to follow exactly the same reasoning, and the second matrix element simplifies to

$$\left(\prod_{j=j_0+1}^{n}\sum\!\!\!\!\!\!\int_{\alpha^{\sigma_j}}\frac{d^{D-1}\mathbf{q}_{\sigma_j}}{(2\pi)^{D-1}}\frac{\sqrt{Z_{\phi_R}^{(\alpha^{\sigma_j})*}}}{2E_{\mathbf{q}_{\sigma_j}}(\alpha^{\sigma_j})}e^{iq_{\sigma_j}x_{\sigma_j}}\Big|_{q^0_{\sigma_j}=E_{\mathbf{q}_{\sigma_j}}(\alpha^{\sigma_j})}\right)\langle\alpha^{\sigma_1}_{\mathbf{q}_{\sigma_1}}|\dots\langle\alpha^{\sigma_n}_{\mathbf{q}_{\sigma_{j_0}}}|\alpha^{\sigma_{j_0+1}}_{\mathbf{q}_{\sigma_{j_0+1}}}\rangle\dots|\alpha^{\sigma_n}_{\mathbf{q}_{\sigma_n}}\rangle\,. \tag{1.89}$$

The integration region of the wave packet associated with σ and j_0 becomes

$$\begin{aligned}&\Bigg(\prod_{j=1}^{j_0}\int_T^{\infty}dx^0_{\sigma_j}e^{ip_{\sigma_j}x^0_{\sigma_j}}\int d^{D-1}\mathbf{x}_{\sigma_j}\int\frac{d^{D-1}\mathbf{k}_{\sigma_j}}{(2\pi)^{D-1}}f_{\sigma_j}(\mathbf{k}_{\sigma_j})e^{-i\mathbf{k}_{\sigma_j}\mathbf{x}_{\sigma_j}}\times\\ &\qquad\sum\!\!\!\!\!\!\int_{\alpha^{\sigma_j}}\frac{d^{D-1}\mathbf{q}_{\sigma_j}}{(2\pi)^{D-1}}\frac{\sqrt{Z_{\phi_R}^{\alpha_{\sigma_j}}}}{2E_{\mathbf{q}_{\sigma_j}}(\alpha^{\sigma_j})}e^{-iq_{\sigma_j}x_{\sigma_j}}\Big|_{q^0_{\sigma_j}=E_{\mathbf{q}_{\sigma_j}}(\alpha^{\sigma_j})}\langle\alpha^{\sigma_j}_{\mathbf{q}_{\sigma_j}}|\Bigg)\times\\ &\Bigg(\prod_{j=j_0+1}^{n}\int_{-\infty}^{-T}dx^0_{\sigma_j}e^{ip_{\sigma_j}x^0_{\sigma_j}}\int d^{D-1}\mathbf{x}_{\sigma_j}\int\frac{d^{D-1}\mathbf{k}_{\sigma_j}}{(2\pi)^{D-1}}f_{\sigma_j}(\mathbf{k}_{\sigma_j})e^{-i\mathbf{k}_{\sigma_j}\mathbf{x}_{\sigma_j}}\times\\ &\qquad\sum\!\!\!\!\!\!\int_{\alpha^{\sigma_j}}\frac{d^{D-1}\mathbf{q}_{\sigma_j}}{(2\pi)^{D-1}}\frac{\sqrt{Z_{\phi_R}^{\alpha_{\sigma_j}*}}}{2E_{\mathbf{q}_{\sigma_j}}(\alpha^{\sigma_j})}e^{iq_{\sigma_j}x_{\sigma_j}}\Big|_{q^0_{\sigma_j}=E_{\mathbf{q}_{\sigma_j}}(\alpha^{\sigma_j})}|\alpha^{\sigma_j}_{\mathbf{q}_{\sigma_j}}\rangle\Bigg),\end{aligned} \tag{1.90}$$

where some large boundary time $T>0$ specifies when the wave packets become well separated. The integrations over $\mathbf{x}_{\sigma_j}$, $x^0_{\sigma_j}$, and $\mathbf{q}_{\sigma_j}$ are elementary and yield

$$\begin{aligned}&\left(\prod_{j=1}^{j_0}\int\frac{d^{D-1}\mathbf{k}_{\sigma_j}}{(2\pi)^{D-1}}f_{\sigma_j}(\mathbf{k}_{\sigma_j})\sum\!\!\!\!\!\!\int_{\alpha^{\sigma_j}}\frac{i\sqrt{Z_{\phi_R}^{\alpha_{\sigma_j}}}e^{i(p^0_{\sigma_j}-E_{\mathbf{k}_{\sigma_j}}+i\varepsilon)T}}{2E_{\mathbf{k}_{\sigma_j}}(\alpha^{\sigma_j})(p^0_{\sigma_j}-E_{\mathbf{k}_{\sigma_j}}(\alpha^{\sigma_j})+i\varepsilon)}\langle\alpha^{\sigma_j}_{\mathbf{k}_{\sigma_j}}|\right)\times\\ &\left(\prod_{j=j_0+1}^{n}\int\frac{d^{D-1}\mathbf{k}_{\sigma_j}}{(2\pi)^{D-1}}f_{\sigma_j}(\mathbf{k}_{\sigma_j})\sum\!\!\!\!\!\!\int_{\alpha^{\sigma_j}}\frac{-i\sqrt{Z_{\phi_R}^{\alpha_{\sigma_j}*}}e^{-i(p^0_{\sigma_j}+E_{\mathbf{k}_{\sigma_j}}-i\varepsilon)T}}{2E_{\mathbf{k}_{\sigma_j}}(\alpha^{\sigma_j})(p^0_{\sigma_j}+E_{\mathbf{k}_{\sigma_j}}(\alpha^{\sigma_j})+i\varepsilon)}|\alpha^{\sigma_j}_{-\mathbf{k}_{\sigma_j}}\rangle\right).\end{aligned} \tag{1.91}$$

The last step is to take simultaneous limits:

- $f_{\sigma_j}(\mathbf{k}_{\sigma_j})\to(2\pi)^{D-1}\delta^{(D-1)}(\mathbf{p}_{\sigma_j}-\mathbf{k}_{\sigma_j})$, for $j\le j_0$,
- $f_{\sigma_j}(\mathbf{k}_{\sigma_j})\to(2\pi)^{D-1}\delta^{(D-1)}(\mathbf{p}_{\sigma_j}+\mathbf{k}_{\sigma_j})$, for $j>j_0$,

- $p^0_{\sigma_j} \to E_{\mathbf{p}_{\sigma_j}}$, for $j \leq j_0$,
- $p^0_{\sigma_j} \to -E_{\mathbf{p}_{\sigma_j}}$, for $j > j_0$.

The first two simply replace $\mathbf{k}_{\sigma_j} \to \mathbf{p}_{\sigma_j}$ and $\mathbf{k}_{\sigma_j} \to -\mathbf{p}_{\sigma_j}$ respectively. The sum-integrals in the third and fourth limit become dominated by the contributions of single particle states with definite momenta:

$$\sum\!\!\!\!\!\!\int_{\alpha^{\sigma_j}} F\left[|\alpha^{\sigma_j}_{\pm\mathbf{k}_{\sigma_j}}\rangle\right] \to F\left[|\pm\mathbf{p}_{\sigma_j}\rangle_{out/in}\right], \tag{1.92}$$

as only for these states the denominators $(E_{\mathbf{p}_{\sigma_j}}(\alpha^{\sigma_j}) \pm p^0_{\sigma_j}) = 0$. The subscripts $in(out)$ specify that the state was obtained as a narrow-momentum limit of a state created independently from the others in the far past(future). In these limits it is also possible to replace

$$2E_{\mathbf{p}_{\sigma_j}} \to E_{\mathbf{p}_{\sigma_j}} \pm p^0_{\sigma_j}. \tag{1.93}$$

The momentum space Green's functions thus have the following singular behavior in this limit:

$$\begin{aligned} &G_R(p_1, \ldots, p_n, -\tilde{p}_1, \ldots, -\tilde{p}_m) \\ &\xrightarrow[p^0_j \to E_{\mathbf{p}_j}]{\tilde{p}^0_j \to E_{\tilde{\mathbf{p}}_j}} \left(\prod_{j=1}^{n} \frac{i}{p_j^2 - m^2 + i\varepsilon}\right)\left(\prod_{j=1}^{m} \frac{i}{\tilde{p}_j^2 - m^2 + i\varepsilon}\right) {}_{out}\langle \mathbf{p}_1 \ldots \mathbf{p}_n | \tilde{\mathbf{p}}_1 \ldots \tilde{\mathbf{p}}_m \rangle_{in}. \end{aligned} \tag{1.94}$$

This is the LSZ reduction formula in the on-shell scheme. Its significance stems from the interpretation of the scalar product of states ${}_{out}\langle \mathbf{p}_1 \ldots \mathbf{p}_n | \tilde{\mathbf{p}}_1 \ldots \tilde{\mathbf{p}}_m \rangle_{in}$. It is the probability amplitude for a set of n particles with definite momenta $\mathbf{p}_j$ prepared in the far past to be observed as a different set of particles with definite momenta $\tilde{\mathbf{p}}_j$ in the far future. This is exactly the probability amplitude of the scattering setup described before.

The $in(out)$ states constitute a basis of a subspace consisting of ensembles of particles that were(will be) freely propagating and distinguishable from each other in the far past(future). The states in one of these scattering subspaces have to be in a one-to-one correspondence with their counterparts with the same momentum and discrete quantum numbers in the other subspace. This relation can be described by the action of a linear operator $\hat{S}$:

$$\hat{S}\,|\alpha\rangle_{out} = |\alpha\rangle_{in}\,, \tag{1.95}$$

where α refers to the collection of all quantum numbers defining a scattering state. The matrix of $\hat{S}$ in the *in* or *out* bases is commonly referred to as the S-matrix. Note that this operator is defined only on the scattering subspaces. The probability that after the scattering an *in* state will be found as any one of the *out* states is 1:

$$\forall_{\alpha} \qquad 1 = \sum\!\!\!\!\!\!\int_{\beta} |\,{}_{out}\langle\beta|\alpha\rangle_{in}|^2 = \sum\!\!\!\!\!\!\int_{\beta} \left({}_{out}\langle\alpha|\hat{S}^\dagger|\beta\rangle_{out}\right)\left({}_{out}\langle\beta|\hat{S}|\alpha\rangle_{out}\right) \tag{1.96}$$

The identity operator constrained to the scattering subspaces can be written as

$$\mathbb{1}_{in/out} = \sum\!\!\!\!\!\!\int_{\beta} \left(|\beta\rangle_{in/out}\right)\left({}_{in/out}\langle\beta|\right), \tag{1.97}$$

leading to

$$\underset{\alpha}{\forall} \qquad 1 = {}_{out}\langle\alpha|\hat{S}^\dagger\hat{S}|\alpha\rangle_{out} \qquad \Longrightarrow \qquad \hat{S}^\dagger\hat{S} = \mathbb{1}_{out}, \tag{1.98}$$

and similarly $\hat{S}^\dagger\hat{S} = \mathbb{1}_{in}$. The $\hat{S}$ operator is thus unitary. This fact will turn out to be very important in the discussion of the formula for the particle decay rate.

The S-matrix element can be expanded as follows

$$\begin{aligned} {}_{out}\langle\mathbf{p}_1\dots\mathbf{p}_n|\tilde{\mathbf{p}}_1\dots\tilde{\mathbf{p}}_m\rangle_{in} = {}_{out}\langle\mathbf{p}_1\dots\mathbf{p}_n|\hat{S}|\tilde{\mathbf{p}}_1\dots\tilde{\mathbf{p}}_m\rangle_{out} = \\ = \delta_{\tilde{\mathbf{p}}_1\dots\tilde{\mathbf{p}}_m;\tilde{\mathbf{p}}_1\dots\tilde{\mathbf{p}}_m} + i(2\pi)^D\delta^{(D)}\left(\sum_{k=1}^{n}\mathbf{p}_k - \sum_{k=1}^{m}\tilde{\mathbf{p}}_k\right)\mathcal{M}_{\tilde{\mathbf{p}}_1\dots\tilde{\mathbf{p}}_m\to\mathbf{p}_1\dots\mathbf{p}_n}. \end{aligned} \tag{1.99}$$

The first term corresponds to the amplitude of particles passing through the collision vertex without interacting. Such a scenario is by definition excluded from the calculation of the cross section. The delta function in the second term enforces the overall D momentum conservation. It is clear that the expression for a differential cross section for a $2 \to n$ scattering has to be proportional to the probability of the process happening. This probability is given by the modulus squared of the invariant matrix element $\mathcal{M}_{\tilde{\mathbf{p}}_1\tilde{\mathbf{p}}_2\to\mathbf{p}_1\dots\mathbf{p}_n}$, so

$$\frac{d\sigma_{\tilde{\mathbf{p}}_1\tilde{\mathbf{p}}_2\to\mathbf{p}_1\dots\mathbf{p}_n}}{d^{D-1}\mathbf{p}_1\dots d^{D-1}\mathbf{p}_n} \propto |\mathcal{M}_{\tilde{\mathbf{p}}_1\tilde{\mathbf{p}}_2\to\mathbf{p}_1\dots\mathbf{p}_n}|^2. \tag{1.100}$$

The exact proportionality constant can be derived by considering the kinematics of the particular scattering, but it will not be of importance in this thesis.

The LSZ formula (1.94) specifies that the dynamics of scattering in QFT are described by one-particle residues of Green's functions. It describes how to compute a scattering cross section: one can use the procedure described at the end of the previous section to obtain a Green's function, neglecting the fully disconnected diagrams that correspond to the first term in eq. (1.99), and then extract from the result the poles corresponding to the considered process. One should take into account though that the Green's function in the LSZ formula should be computed for renormalized fields $\hat{\phi}_R$, while the Feynman rules in the previous section were derived for the original, or *bare* ones. Consequences of this fact will be considered later in this chapter.

One may extract the residues from Green's functions in the following procedure. In general, every diagram contributing to a Green's function is composed of several connected components. Each will have a number of external lines with possible loop corrections placed on them. This can be depicted diagrammatically:

$$G_R(p_1,\dots p_n,-\tilde{p}_1,\dots,-\tilde{p}_m) = \prod_{k\in \substack{\text{connected}\\ \text{components}}}$$

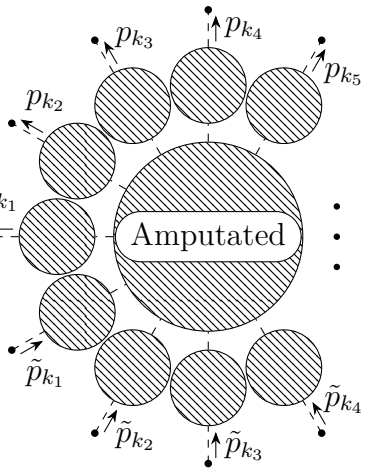

(1.101)

The "amputated" section refers to the part which is obtained by disregarding both the shaded blobs present on the external legs, as well as the lines attaching them to the rest of the diagram. As the external momenta are put on-shell, each of the 2-point functions connected to the amputated part acquires a pole, just as in eq. (1.79). These poles match exactly to the products of denominators in the LSZ formula (1.94):

$$G_R(p_1, \dots p_n, -\tilde{p}_1, \dots, -\tilde{p}_m)$$

$$\xrightarrow[p_j^0 \to E_{\mathbf{p}_j}]{\tilde{p}_j^0 \to E_{\tilde{\mathbf{p}}_j}} \left(\prod_{j=1}^{n} \frac{i}{p_j^2 - m^2 + i\varepsilon}\right)\left(\prod_{j=1}^{m} \frac{i}{\tilde{p}_j^2 - m^2 + i\varepsilon}\right)_{k \in \substack{\text{connected} \\ \text{components}}} \prod$$

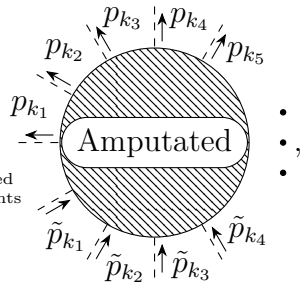

(1.102)

which leads to the formula

$${}_{out}\langle \mathbf{p}_1 \dots \mathbf{p}_n | \tilde{\mathbf{p}}_1 \dots \tilde{\mathbf{p}}_m \rangle_{in} = \prod_{k \in \substack{\text{connected} \\ \text{components}}}$$

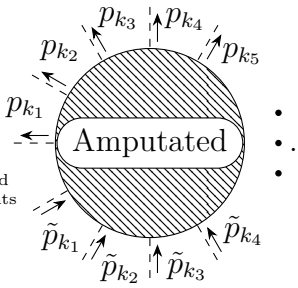

(1.103)

To preserve the dependence on external momenta in the diagrammatic description, the amputated part will be depicted with external lines, even though they do not contribute a factor of the momentum-space propagator. To distinguish the amputated diagrams from the full contributions to the Green's functions, they will be drawn without dots at the external points.

The above equation leads to the LSZ prescription for computing differential cross sections: to find the relevant invariant matrix element $\mathcal{M}$ in eq. (1.99), compute all amputated diagrams with $(n+m)$-external lines with n sources and m sinks of momenta. Disregard any diagrams with connected components that have less than two external lines or are composed only of connected components with 2 external lines[†]. Then use eqs. (1.99) and (1.100).

Returning to the amputated off 2-point functions, these, as mentioned above, encode the shift of particle masses from the Lagrangian parameter to the physical value. The physical masses are given by the poles of the 2-point function, as described by the limit (1.79). The 2-point function itself can be computed using the Feynman diagram formalism. Its basic structure can be depicted as follows:

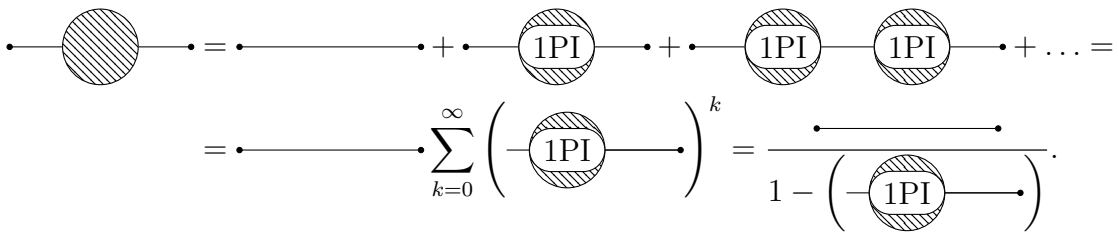

(1.104)

[†]These will contribute to the Kronecker delta term of eq. (1.99).

The principal building block of this expansion is the 1PI, or "one particle irreducible" diagram multiplied by a single free propagator. The 1PI part is defined as the sum of all amputated 2-point diagrams that cannot be separated into two parts by removing a single line. With the abbreviation

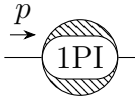

$$\equiv -i\Sigma_{\rm 1PI}(p^2, m^2), \tag{1.105}$$

the momentum-space 2-point function in the scalar theory becomes

$$= (2\pi)^D \delta^{(D)}(p_1+p_2) \frac{\frac{i}{p_1^2-m^2+i\varepsilon}}{1-\frac{\Sigma_{\rm 1PI}(p_1^2)}{p_1^2-m^2+i\varepsilon}} = \frac{i(2\pi)^D\delta^{(D)}(p_1+p_2)}{p_1^2-(m^2+\Sigma_{\rm 1PI}(p_1^2))+i\varepsilon}. \tag{1.106}$$

The pole at the point $p_1^2 = p_{pole}^2 \equiv m^2$ is given by the solution of a relation

$$\Sigma_{\rm 1PI}(p_{pole}^2, m^2) = 0. \tag{1.107}$$

For unstable particles it gets replaced by

$$\mathrm{Re}\Sigma_{\rm 1PI}(p_{pole}^2, m^2) = 0, \tag{1.108}$$

and the propagator denominator becomes $p^2 - m^2 - i\mathrm{Im}\Sigma_{\rm 1PI}(p^2, m^2)$.

To relate the above discussion to decay rates of unstable particles, suppose that such a particle P is created in a scattering of two particles with the center-of-mass energy $E_{cm}^2 \equiv s$ and then decays into a set of stable particles. The total cross section for this process will be a function of s: $\sigma = \sigma(s)$. If s is close to the mass squared of the unstable particle m_P^2, and $|\mathrm{Im}\Sigma_{\rm 1PI}| \ll m_P^2$, any potential loop integrals in the amputated diagrams contributing to $\sigma(s)$ will be dominated by contributions in which the momentum p flowing through the propagator of P carries the entire available energy, i.e. it is in the region where $p^2 \sim m_P^2$. The dominant contribution in this region comes from diagrams of the form

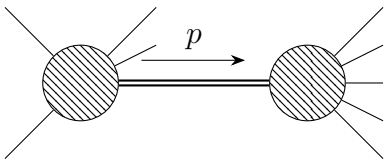

$$\overset{s\to m_P^2}{\propto} \frac{i}{s-m_P^2-i\mathrm{Im}\Sigma_{\rm 1PI}(s, m_P^2)+i\varepsilon}, \tag{1.109}$$

where the double line depicts the unstable particle going close to its mass shell. The cross section contribution computed from the diagram in eq. (1.109) acquires a resonance of the form

$$\sigma(s) \overset{s\to m_P^2}{\propto} \left|\frac{i}{s-m_P^2-i\mathrm{Im}\Sigma_{\rm 1PI}(s)}\right|^2. \tag{1.110}$$

Since $\mathrm{Im}\Sigma_{\rm 1PI}(s, m_P^2)/m_P^2 \ll 1$ for $s \sim m_P^2$, the above expression matches the Breit–Wigner distribution that is used to describe resonances in scattering cross sections due to decaying particles:

$$\sigma_{B-W}(s) \propto \left|\frac{1}{s-M^2+iM\Gamma}\right|^2 \tag{1.111}$$

and the decay rate can be identified as

$$\Gamma = -\frac{1}{m_P}\mathrm{Im}\Sigma_{\rm 1PI}(m_P^2, m_P^2) = -\frac{1}{m_P}\mathrm{Im}\left[i\cdot\right.$$

$$\left.\right]\Big|_{p^2=m_P^2}. \tag{1.112}$$

For B mesons, $\Gamma_B/m_B \approx 10^{-13}$, so this is an extremely good approximation. The appearance of imaginary loop corrections to masses is therefore equivalent with unstable states. This result might be viewed as parallel to the quantum-mechanical behavior of systems with non-hermitian Hamiltonians. There, since the unitarity of evolution is violated, the sum of probabilities decreases exponentially with time, which is interpreted as particle decay.

It is useful to reexamine the "forward $1 \to 1$ scattering" 1PI amplitude appearing in eq. (1.112). To do so, recall that the $\hat{S}$ operator is unitary, as was proven in eq. (1.98). On the other hand, one can expand it as $\hat{S} \equiv \hat{\mathfrak{I}} + i\hat{T}$ for some transition operator $\hat{T}$. The operator $\hat{\mathfrak{I}}$ acts as $\hat{\mathfrak{I}}\,|\alpha\rangle_{out} = |\alpha\rangle_{in}$ and satisfies $\hat{\mathfrak{I}}^\dagger\hat{\mathfrak{I}} = \mathbb{1}_{out}$. From the form of eq. (1.99), it is clear that the matrix elements of $\hat{\mathfrak{I}}^\dagger\hat{T}$ are given by

$$ {}_{out}\langle k|\hat{\mathfrak{I}}^\dagger\hat{T}|l\rangle_{out} = (2\pi)^D\delta^{(D)}(P_k - P_l)\mathcal{M}_{l\to k} \tag{1.113} $$

and analogously

$$ {}_{out}\langle k|\hat{T}^\dagger\hat{\mathfrak{I}}|l\rangle_{out} = (2\pi)^D\delta^{(D)}(P_k - P_l)\mathcal{M}^*_{k\to l}, \tag{1.114} $$

where P_l and P_k are the total momenta of the scattering *out* states. Using this expansion and unitarity of the $\hat{S}$ operator, one obtains

$$ \mathbb{1}_{out} = \hat{S}^\dagger\hat{S} = (\hat{\mathfrak{I}}^\dagger - i\hat{T}^\dagger)(\hat{\mathfrak{I}} + i\hat{T}) \Longrightarrow \hat{T}^\dagger\hat{T} = -i(\hat{\mathfrak{I}}^\dagger\hat{T} - \hat{T}^\dagger\hat{\mathfrak{I}}). \tag{1.115} $$

Any matrix element of the right hand side has to be equal to the corresponding matrix element of the left:

$$ -i\,{}_{out}\langle k|\hat{\mathfrak{I}}^\dagger\hat{T} - \hat{T}^\dagger\hat{\mathfrak{I}}|l\rangle_{out} = {}_{out}\langle k|\hat{T}^\dagger\hat{T}|l\rangle_{out}, \tag{1.116} $$

for any pair of scattering *out* states $|k\rangle_{out}$ and $|l\rangle_{out}$. The left hand side can now be written in terms of the invariant matrix element:

$$ -i\,{}_{out}\langle k|\hat{\mathfrak{I}}^\dagger\hat{T} - \hat{T}^\dagger\hat{\mathfrak{I}}|l\rangle_{out} = -i(2\pi)^D\delta^{(D)}(P_k - P_l)(\mathcal{M}_{l\to k} - \mathcal{M}^*_{k\to l}). \tag{1.117} $$

The right hand side can be turned into a product of matrix elements using the identity operator of eq. (1.97):

$$ {}_{out}\langle k|\hat{T}^\dagger\hat{T}|l\rangle_{out} = \sum\!\!\!\!\!\!\int_f (2\pi)^D\delta^{(D)}(P_k - P_f)\mathcal{M}^*_{k\to f}(2\pi)^D\delta^{(D)}(P_l - P_f)\mathcal{M}_{f\to l}. \tag{1.118} $$

One of the delta functions in the above equation can be equivalently rewritten as $\delta^{(D)}(P_k - P_l)$ and canceled with the delta function in eq. (1.117). Putting $|k\rangle_{out} = |l\rangle_{out}$ results in

$$ 2\mathrm{Im}\mathcal{M}_{k\to k} = \sum_f \int dPS_f |\mathcal{M}_{k\to f}|^2, \tag{1.119} $$

where the intermediate state sum-integral was split into the sum over all particle contents of states $|f\rangle$ and the integral over the allowed phase space of each state $|f\rangle$. This is the QFT optical theorem. Diagrammatically, it can be depicted as

$$ -\mathrm{Im}\left[i\cdot \; k \left\{ \quad \right\} k \right] = \frac{1}{2}\sum_f \int dPS_f \left| \; k \left\{ \quad \right\} f \; \right|^2 . \tag{1.120} $$

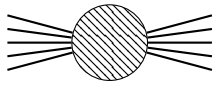

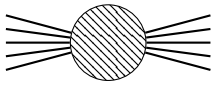

From this picture, the interpretation of the result for the decay rate in eq. (1.112) becomes clear. If the initial state $|k\rangle$ is set to contain only the single decaying particle P, then

the decay rate is proportional to the sum over probabilities of each decay channel $P \to f$. The proportionality constant turns out to be equal to $1/(2m_P)$ in the decaying particle rest frame. In other frames, it will change to $1/(2E_P)$ and account for the necessary Lorentz time dilatation. The optical theorem derived as above applies only to scattering states that become free particles in time infinities. This obviously is not the case for a decaying particle. Nevertheless, the equivalent statement for amplitudes defined by their Feynman diagrams was proven using the formalism of Cutkosky's "cutting" rules [94] and can be applied without modification.

The description of the $B \to X_c l \bar{\nu}_l$ decay relies on generalizing the above results to theories with higher-spin fields. The correct prescription can be obtained along similar lines, as long as the Lorenz transformation properties and the form of the solutions to the classical equations of motion is taken into account. Naturally, the free scalar propagators $\mathcal{P}_\phi$ have to be replaced with $\mathcal{P}_\psi$ or $\mathcal{P}_A$ for the spinor and vector fields respectively. Second, to describe the scattering or decays of fermions, one has to include the following external line Feynman rules [78, 83]:

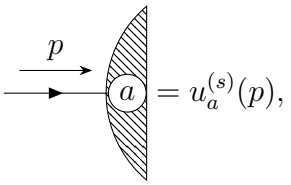

$$= u_a^{(s)}(p), \qquad (1.121)$$

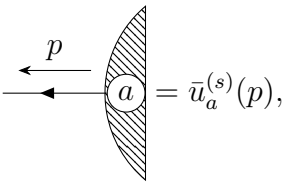

$$= \bar{u}_a^{(s)}(p), \qquad (1.121)$$

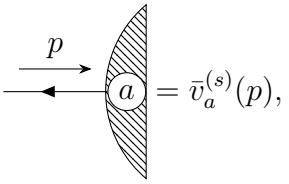

$$= \bar{v}_a^{(s)}(p), \qquad (1.122)$$

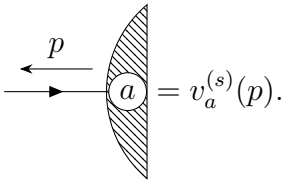

$$= v_a^{(s)}(p). \qquad (1.122)$$

The arrow on the line indicates the flow of the fermionic current. If its direction matches the direction of the momentum, the line depicts a particle, otherwise an antiparticle. The indices a are contracted with Dirac matrix factors coming from vertices attached to external lines. Similarly, the external line Feynman rules for incoming and outgoing vector bosons read [78, 83]:

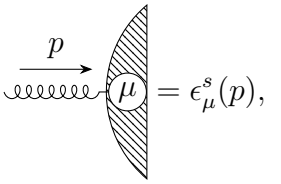

$$= \epsilon_\mu^s(p), \qquad (1.123)$$

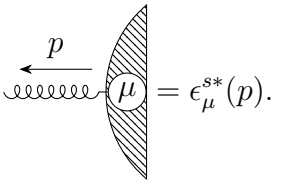

$$= \epsilon_\mu^{s*}(p). \qquad (1.123)$$

The derivation of the LSZ formula assumed wave packets that become well separated far away from the interaction vertex. Such an approach breaks down in theories with long-range interactions, for example in Quantum Electrodynamics. The breakdown of the LSZ formalism manifests itself with infrared and collinear divergences for certain observables in some regions of the phase space. These have to be regularized, for example by introducing small masses to photons, and then systematically canceled out by properly defining observed quantities. Sufficiently inclusive processes, such as the q^2 spectrum in the B meson decay in the leading order in electroweak interactions, are free of such divergences.

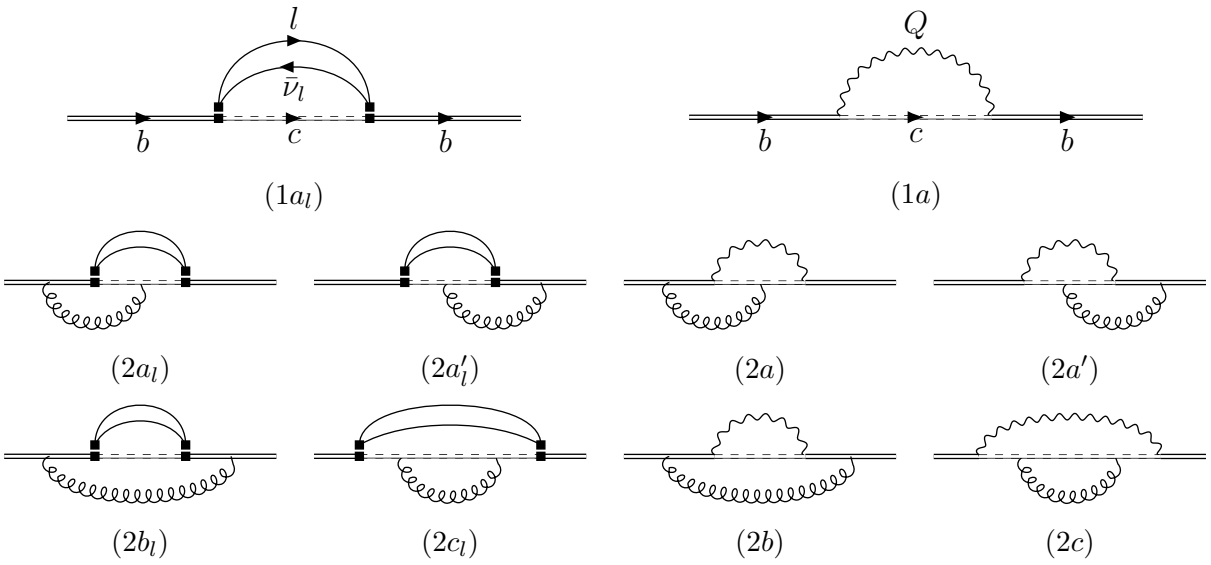

Figure 6: Diagrams contributing to the semileptonic decay at the LO and NLO in QCD. The left panel depicts the standard formulation with the lepton pair. The right uses the auxiliary vector boson approach. For explanation of the elements of diagrams see the text. The diagram $(2a)$ will be examined in greater detail below.

1.3 Sample Calculation - 1

Over the course of chapters 1 and 2, several sections are dedicated to illustrating the described techniques with examples from the calculation of the $\mathcal{O}(\alpha_s^1)$ correction to the q^2 spectrum of the semileptonic b quark decay. Implementing these methods to objects appearing at this level of perturbation theory provides first non-trivial challenges but still can be discussed in detail in the scope of the current chapter and the next one.

Following the formula (1.112) for the inclusive decay rate, one proceeds with generating all necessary connected, 1PI diagrams for the forward "scattering" of the b quark. Note that to describe a semileptonic decay, one should be interested only with contributions that contain both a charm quark and a lepton-neutrino pair as intermediate states. It is therefore justified to doubt whether the process is actually inclusive and is the optical theorem in eq. (1.120) applicable. Fortunately, eq. (1.112) holds order-by-order in G_F and $|V_{cb}|$, so by isolating contributions proportional to $G_F^2|V_{cb}|^2$ on the right hand side, one obtains the desired partonic semileptonic rate in the leading approximation in electroweak interactions. At the leading order in QCD, i.e., with no QCD interactions at all, there is a single diagram contributing to the decay. Diagrams at $\mathcal{O}(\alpha_s^1)$ can be constructed from it by adding a single gluon line in one of the four possible ways. The LO and NLO diagrams are illustrated in the left panel of figure 6. Here and below, the b quarks are depicted with solid double lines, c quarks with solid-dashed double lines, and leptons with single solid lines. Vector bosons and gluons are represented in the standard way with wavy and curly lines respectively. In the NLO diagrams, the fermion arrows have been suppressed. The double-square vertices depict the effective Fermi-like interaction left over after integrating out the W boson from the Standard Model, as will be explained in section 3.1. To obtain the q^2 spectrum, one can replace the lepton-neutrino pair with a vector boson Q^μ with mass $M_Q = \sqrt{q^2}$. This technique will be derived and described in detail in section 3.1. The resulting diagrams are shown in the right panel of figure 6.

This sample calculation follows the evaluation of the contribution to the NLO spectrum coming from the diagram $(2a)$ defined in figure 6. The vertex Feynman rules required to write the algebraic expression corresponding to this diagram are:

(1.124)

while the necessary propagators read

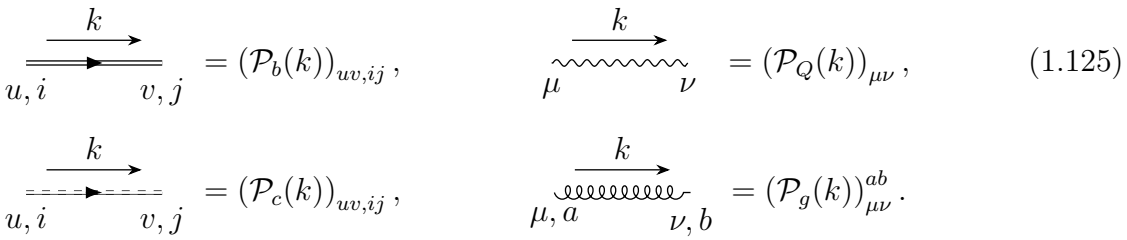

(1.125)

The individual factors are given by

$$
\begin{aligned}
(\mathcal{V}_Q)^{\mu}_{uv,ij} &\equiv -\frac{ig_q}{\sqrt{2}} V_{cb} \left(\gamma^\mu P_L\right)_{uv} \delta_{ij}, \qquad (\mathcal{V}_g)^{\mu,a}_{uv,ij} \equiv -ig_s \gamma^\mu_{uv} T^a_{ij}, \\
\left(\mathcal{P}_b(k)\right)_{uv,ij} &\equiv \frac{i(\not{k} + m_b \mathbb{1}^{(\gamma)})_{uv}\delta_{ij}}{k^2 - m_b^2 + i\varepsilon}, \qquad \left(\mathcal{P}_Q(k)\right)_{\mu\nu} \equiv \frac{-i}{k^2 - q^2 + i\varepsilon}\left[g_{\mu\nu} - \frac{k_\mu k_\nu}{q^2}\right], \\
\left(\mathcal{P}_c(k)\right)_{uv,ij} &\equiv \frac{i(\not{k} + m_c \mathbb{1}^{(\gamma)})_{uv}\delta_{ij}}{k^2 - m_c^2 + i\varepsilon}, \qquad (\mathcal{P}_g(k))^{ab}_{\mu\nu} \equiv \frac{-i\delta^{ab}}{k^2 + i\varepsilon}\left[g_{\mu\nu} - (1-\xi_g)\frac{k_\mu k_\nu}{k^2}\right].
\end{aligned}
\tag{1.126}
$$

These rules can be derived in a similar way to the scalar field Feynman rules, as long as one accounts for the details described at the end of section 1.1. The constant g_q is the $SU(2)$ coupling in the auxiliary SM in which $\Gamma_{b\to X_c Q}$ is computed. It is defined as $g\sqrt{q^2}/M_W$, where g is the $SU(2)$ coupling constant in the regular SM. This relation will be discussed in section 3.1. The $SU(3)$ coupling g_s is unaffected by the shift to the auxiliary SM. The Qcb vertex rule for the reversed ordering of quarks will be denoted by $\mathcal{V}_{\bar{Q}}$. It is equal to $\mathcal{V}_Q$ with the factor of V_{cb} replaced with V^*_{cb}. The algebraic properties of the left projection P_L in the vector boson vertex are described in section 1.5, while its appearance will be explained in section 3.1. In the rule for the quark-gluon vertex, the solid fermion line can correspond to either a bottom or a charm quark. The spin and quark color degrees of freedom were assigned indices uv and ij respectively. The adjoint representation color indices of gluons were represented with a and b. The matrix T^a is a $\mathfrak{su}(3)$ color algebra generator, normalized as $\mathrm{Tr}[T^a T^b] = T_R \delta^{ab}$, with T_R fixed to $1/2$ by convention. Different choices of the normalization constant T_R can be absorbed into the coupling g_s already in the QCD Lagrangian, and thus do not affect the predictions for physical observables. The gluon propagator is written in an arbitrary R_ξ gauge with the gauge parameter ξ_g. The vector boson propagator is taken in the unitary gauge, which is the R_ξ gauge limit with $\xi_Q \to \infty$ (c.f. eq. (21.54) in ref. [78]). This choice eliminates would-be-Goldstone bosons from the calculation of the q^2 spectrum, as will be described in section 3.1.

The inclusive decay rate formula (1.112) specifies that the contribution to the spin and color averaged spectrum should be obtained from:

$$\frac{d\Gamma^{(1)}_{(2a)}}{dq^2} = -\frac{\sqrt{2}G_F}{12\pi^2}\frac{1}{2}\frac{1}{3}\sum_{sc}\mathrm{Im}\left[i\cdot \right.$$

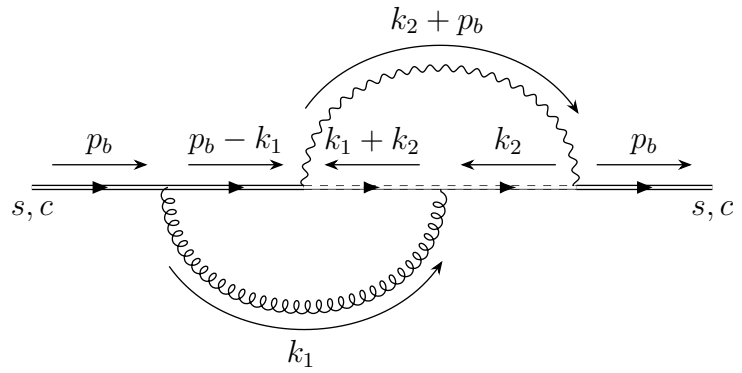

$$\left.\right] \tag{1.127}$$

Using the Feynman rules of eqs. (1.124) and (1.125), together with the rules for external lines for fermions given in eq. (1.121) yields the following expression for the contribution of diagram $(2a)$ to the q^2 spectrum:

$$\begin{aligned}\frac{d\Gamma^{(1)}_{(2a)}}{dq^2} =& \frac{\sqrt{2}G_F}{12\pi^2}\frac{1}{2}\frac{1}{3}\sum_{sc}\mathrm{Im}\, i\int\frac{d^Dk_1}{i(2\pi)^D}\frac{d^Dk_2}{i(2\pi)^D}\Big[\bar{u}^{(s)}_a(p_b)(\mathcal{V}_{\bar{Q}})^{\mu_1}_{ad_1,cc_1}(\mathcal{P}_c(-k_2))_{d_1d_2,c_1c_2}\times \\ & (\mathcal{V}_g)^{\mu_2,c_1'}_{d_2d_3,c_2c_3}(\mathcal{P}_c(-k_1-k_2))_{d_3d_4,c_3c_4}(\mathcal{V}_Q)^{\mu_3}_{d_4d_5,c_4c_5}(\mathcal{P}_b(p_b-k_1))_{d_5d_6,c_5c_6}(\mathcal{V}_g)^{\mu_4,c_2'}_{d_6b,c_6c}u^{(s)}_b(p_b)\Big] \\ & (\mathcal{P}_g(k_1))^{c_1'c_2'}_{\mu_2\mu_4}(\mathcal{P}_Q(k_2+p_b))_{\mu_1\mu_3}\,.\end{aligned} \tag{1.128}$$

The factors of i have been included in the denominators of the loop integration measure for later convenience. The particular momentum routing chosen above will prove beneficial during the IBP reduction step, described in section 2.1. The external momentum is assumed to be on the mass shell $p_b^2 = m_b^2$, as dictated by eq. (1.112). The fraction $\sqrt{2}G_F/(12\pi^2)$ comes from the conversion of the leptons into the vector boson and will be derived in section 3.1. The factors of $1/2$ and $1/3$ account for averaging over the decaying b quark spins s and colors c. The rest of this expression follows directly from eqs. (1.112), (1.121), and (1.126). Note that in order to form a scalar, the Feynman rules on the main fermion line have to be arranged opposite to the flow of the fermion current.

For each of the integrals, the loop momentum dependence comes from two fermion lines and a single boson line. In the region of $k_i \to \infty$, a fermion and boson propagators contribute a suppression factor of $1/k_i$ and $1/k_i^2$ respectively, meaning that the integral behaves as $\int d^Dk_i/k_i^4$. For $D \geq 4$, both loop integrals are at least logarithmically divergent for large loop momenta. It seems like in a 4 dimensional space-time, the prescription for computing the decay rate breaks down. It is saved only after applying a careful, systematic procedure to the whole theory, that first separates the divergences from the finite parts and then absorbs them into the rescaled fields and parameters of the Lagrangian. This procedure is described in the next section.

1.4 Divergences in Quantum Field Theory

The divergence encountered in eq. (1.127) is an example of a typical problem in most QFTs: loop integrals diverge for large loop momenta. The origin of this issue and the resulting

rationale for using the QFT formalism despite apparent unphysical intermediate results is still being debated. One of the more established explanations is as follows. In the UV loop region, the virtual particles have enough energy to spontaneously transform into arbitrary states and any loop correction will be significantly affected by the contributions of these states. But a theory in which the computation is made has been designed only to describe phenomena up to a certain energy scale. The virtual states appearing in the calculation can only be created by the degrees of freedom described by the Lagrangian. The formalism fails to account for effects of possible heavier fields that still contribute to physical processes. In a "true" theory, assuming it exists, these particles would appear in loops even in processes at low energies and cancel the divergent parts. The remaining contributions of the heavy fields on low energy observables will be suppressed by powers of their heavy masses. In this view, the starting theory is just the lowest order effective theory of some unknown higher energy model that is free of divergences. In this leading approximation, the effects of heavy fields can be completely absorbed into the redefined parameters and fields of the low energy theory. Non-leading effects can be accounted for in a "bottom up" Effective Field Theory, such as the SMEFT. In this view, the breakdown of known QFTs is salvaged by a still unknown theory. It is known that some proposed high energy models are free of UV divergences, which seems to support this view, but they fail to describe phenomena observed in current experiments.

Regardless of the physical justification, the formal procedure of removing infinities can be understood as part of the renormalization of the theory, i.e. expressing objects in the Lagrangian by experimentally resolvable quantities. Renormalization is an objective common to all physical theories, but in QFT it has an additional complication: the fields and couplings describing finite, measurable properties of particles turn out to be infinite. The initial, divergent quantities one uses to define the Lagrangian are usually referred to as "bare", while those left after renormalization are called "physical" or "renormalized". In a multiplicative scheme, bare fields ϕ_{j0} and couplings c_{j0} are related to their renormalized counterparts as

$$\phi_{j0} \equiv \sqrt{Z_{\phi_j}(c_k)}\phi_j \qquad\qquad c_{j0} \equiv Z_{c_j}(c_k)c_j, \tag{1.129}$$

with some functions of the renormalized couplings Z called the renormalization constants. The masses are included in the above definition as coupling constants of a $1 \to 1$ self interaction. Note that the above definition mirrors the definition of the renormalized field above eq. (1.80), apart from switching the subscripts R on the right hand side for subscripts 0 on the left. Below, objects not written specifically with this subscript should be understood as renormalized. In principle, one should define independent renormalization constants Z_{c_j} for all linearly independent interaction and mass terms in the Lagrangian. However, in gauge invariant theories, certain relations between those constants can be derived based on the Ward–Takahashi identity or its generalizations. The remaining constants are then fixed by conditions imposed on analytic properties of the Green's functions of renormalized fields: poles (masses) and residues (cross sections or amplitudes). Changing this set of renormalization conditions is equivalent to expressing the Lagrangian with different physical quantities, and no choice is in principle better than others. Nonetheless, in the derivation of the LSZ formula the 2-point Green's functions of renormalized fields had poles at the physical mass of one-particle states, as well as the same residues as in the free theory. This property should be preserved in order to use eq. (1.94) without modifications. The corresponding renormalization condition is called the "On-Shell" (OS) scheme. In the scalar theory, it

states that near the mass shell the propagator can be expanded as:

$$G_R(p_1,p_2) \overset{p_1^2\to m^2}{\sim} (2\pi)^D \delta^{(D)}(p_1+p_2)\left[\frac{i}{p_1^2-m^2+i\varepsilon} + (\text{finite in the } p_1^2\to m^2 \text{ limit})\right]. \tag{1.130}$$

Similar conditions define the OS scheme for fermions and vector bosons, as well. The interaction couplings are fixed by demanding certain values of scattering amplitudes for specific configurations of external momenta. Another choice could be that for some fixed, conventional configuration of external momenta, the scattering amplitude of fields in term j is equal to the tree-level value to all orders in perturbation theory. In any case, one then extracts the value of the coupling by comparing the computed amplitude with the measured cross section. Each choice of a renormalization scheme will obviously result in different value of c_j. The remarkable fact is that even though the renormalization conditions are imposed on a finite number of amplitudes equal to the number of fields and interaction terms, for certain "renormalizable" theories, once the renormalization constants are fixed, *all other amplitudes are finite as well*. This saves the renormalizable QFT formalism as a predictive theory. For the purposes of this discussion, it is enough to state that the Standard Model is renormalizable [95, 96].

Renormalization conditions allow for computing the constants $Z[c_k]$ order-by-order in perturbation theory. Starting with a bare Lagrangian and using the definitions in eq. (1.129), a generic bare kinetic, mass, and interaction terms read

$$\begin{aligned}
&f_j\phi_{j0}^\dagger \mathscr{L}_j(\partial)\phi_{j0} = f_j Z_{\phi_j}\phi_j^\dagger \mathscr{L}_j(\partial)\phi_j = f_j\phi_j^\dagger\mathscr{L}_j(\partial)\phi_j + f_j c^\otimes_{\phi_j}\phi_j^\dagger\mathscr{L}_j(\partial)\phi_j,\\
&s_j f_j\left(\phi_{j0}\right)^\dagger\left(m_{j0}\right)^{p_j}\phi_{j0} = s_j f_j Z^{p_j}_{m_j} Z_{\phi_j}\phi_j^\dagger m_j^{p_j}\phi_j = s_j f_j\phi_j^\dagger m_j^{p_j}\phi_j + s_j f_j c^\otimes_{m_j}\phi_j^\dagger m_j^{p_j}\phi_j,\\
&f_{c_j}c_{j0}\left(\phi_{10}\right)^{p_{j_1}}\ldots\left(\phi_{n0}\right)^{p_{j_n}} = f_{c_j}Z_{c_j}Z_{\phi_1}^{\frac{p_{j_1}}{2}}\phi_1^{p_{j_1}}\ldots Z_{\phi_1}^{\frac{p_{j_n}}{2}}\phi_n^{p_{n_1}} =\\
=&f_{c_j}c_j\phi^{p_{j_1}}\ldots\phi^{p_{j_n}} + f_{c_j}c_j^\otimes c_j\phi^{p_{j_1}}\ldots\phi^{p_{j_n}},
\end{aligned} \tag{1.131}$$

with p_j and p_{j_k} being some non-negative powers determined by the dimensionality of the field and $\mathscr{L}_j(\partial)$ a combination of contractions of partial space-time derivatives. The constants f_j and f_{c_j} are symmetry factors equal to the inverse of the number of permutations of fields that leave a term unchanged, similar to the $1/(4!)$ in the interaction term of the ϕ^4 scalar theory. The factor s_j is equal to $+1$ for bosons and -1 for fermions. The additional terms on the right hand side of these equations can be treated as new interactions in the Lagrangian. Their couplings are related to the renormalization constants as

$$c^\otimes_{\phi_j}\equiv Z_{\phi_j}-1, \qquad c^\otimes_{m_j}\equiv Z^{p_j}_{m_j}Z_{\phi_j}-1, \qquad c^\otimes_j\equiv Z_{c_j}Z_{\phi_1}^{\frac{p_{j_1}}{2}}\ldots Z_{\phi_1}^{\frac{p_{j_n}}{2}}-1. \tag{1.132}$$

In the absence of interactions, Green's functions are finite and all renormalization constants are 1. Consequently, all couplings $c^\otimes_X$ have to be proportional to strictly positive powers of renormalized coupling constants c_j and, as long as $c_j<1$, the new interactions can be treated perturbatively. These so-called "counterterms" yield then the following momentum space Feynman rules:

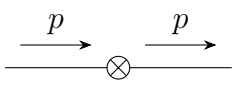

$$= ic^\otimes_{\phi_j}\mathscr{L}_j(-ip) + is_j c^\otimes_{m_j}m_j^{p_j}, \qquad$$

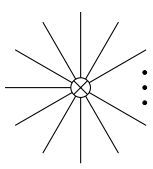

$$= c_j^\otimes$$

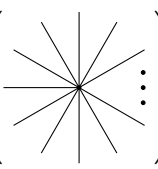

. (1.133)

For scalars and spin 1/2 fermions the first of these can be simplified using the inverse of the propagator:

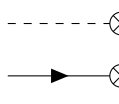

$$= -c_\phi^\otimes \mathcal{P}_\phi^{-1} + i(c_\phi^\otimes - c_{m_\phi}^\otimes) m_\phi^2,$$

$$= -c_\psi^\otimes \mathcal{P}_\psi^{-1} + i(c_\psi^\otimes - c_{m_\psi}^\otimes) m_\psi. \tag{1.134}$$

Using the diagrammatic description, the renormalization conditions at each order in perturbation theory become relations between regular diagrams and diagrams with counterterm insertions. Since the constants $c_X^\otimes$ are suppressed by powers of renormalized couplings, the counterterm diagrams will have strictly less loops than the non-renormalized contribution. For example, to find the renormalized electric charge up to $\mathcal{O}(\alpha_{em})$ in the OS scheme, one demands that

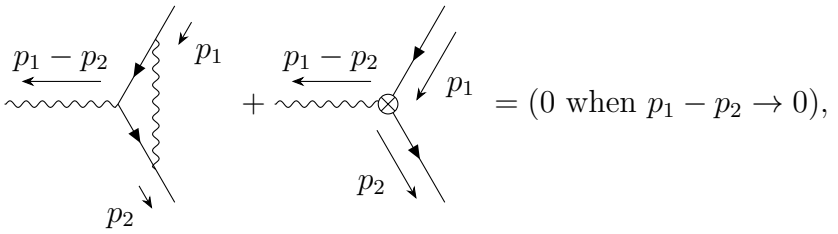

$$= (0 \text{ when } p_1 - p_2 \to 0), \tag{1.135}$$

which fixes $c_e^\otimes$ and in consequence[†] Z_e up to $\mathcal{O}(\alpha_{em})$. In the calculation of the semileptonic decay in the leading order in the HQE, if higher order effects in electroweak interactions are neglected, all divergences can be absorbed into redefinitions of QCD fields, the strong gauge coupling and quark masses. This procedure will be described in sections 3.4 and 3.5.

Before the infinities can be removed, it is important to find the exact divergent parts that need to be canceled out. For this purpose, several techniques have been developed. The most straightforward approach is to limit the range of loop momentum integration range by a hard cutoff, $k^\mu < \Lambda$, compute the desired quantity in 4 space-time dimensions, and expand the result into a Laurent or power-log series in the ratio $r \equiv (\text{masses and external momenta})/\Lambda$. The terms with positive powers and logarithms of Λ in this expansion will constitute the divergent part, clearly separated from the terms finite in the $r \to 0$ limit. This "regularization by cutoff" scheme may be the simplest conceptually, but is quite troublesome in practice, as the integrals have a non-trivial dependence on an additional energy scale Λ. A hard cut-off also breaks the Lorentz invariance of the theory.

Another historically used regularization method is due to Pauli and Villars [97]. The general idea follows the conventional explanation of UV divergences described above: the infinity is canceled by loop contributions of a number of fictitious fields with a very large mass $\Lambda \gg$ (other masses and typical momenta), introduced *ad hoc* to the theory. The result is then expanded in powers of $1/\Lambda$, the poles and logarithms are identified as the divergent parts, the non-zero term left when $\Lambda \to \infty$ is the finite part of the diagram, and all higher powers in $1/\Lambda$ are disregarded. Consider for example the $\mathcal{O}(\alpha_{em})$ correction to the 1PI part of the electron propagator in Quantum Electrodynamics in 4 space-time dimensions. Choosing

[†]The electron field renormalization constants Z_ψ have to be fixed beforehand by computing the renormalized 2-point function up to $\mathcal{O}(\alpha_{em})$.

the Feynman gauge and disregarding the electron mass, the correction is proportional to

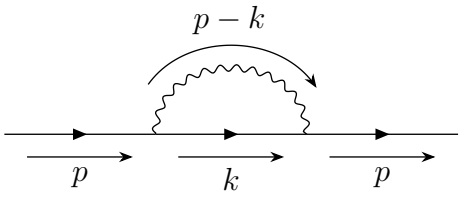

$$= -4\pi i\alpha_{em}\int \frac{d^4k}{i(2\pi)^4}\frac{1}{(p-k)^2+i\varepsilon}\frac{-2\not{k}}{k^2+i\varepsilon}, \tag{1.136}$$

where $\alpha_{em} \equiv e^2/(4\pi)$. The factor of (-2) in the electron propagator follows from the identity $\gamma_\mu \not{k} \gamma^\mu = -2\not{k}$. In the $k^\mu \to \infty$ limit, the integrand behaves as $\sim 1/k^3$ and is not enough to compensate for the divergence in four-dimensional integration. Imagine now a very heavy "photon" coupled to the electron with the electric charge equal to ie. The above integral would be modified as

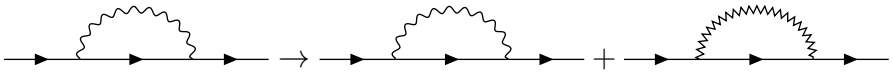

$$\begin{aligned} &= 8\pi i\alpha_{em}\int \frac{d^4k}{(2\pi)^4 i}\left(\frac{1}{(p-k)^2+i\varepsilon} - \frac{1}{(p-k)^2-\Lambda_\gamma^2+i\varepsilon}\right)\frac{\not{k}}{k^2+i\varepsilon} = \\ &= 8\pi i\alpha_{em}\int \frac{d^4k}{(2\pi)^4 i}\frac{-\Lambda_\gamma^2}{\left((p-k)^2+i\varepsilon\right)\left((p-k)^2-\Lambda_\gamma^2+i\varepsilon\right)}\frac{\not{k}}{k^2+i\varepsilon}, \end{aligned} \tag{1.137}$$

where Λ_γ is the mass of the auxiliary photon. For small loop momenta, $k \sim m_e \sim p$, the contribution from the second diagram is negligible due to the large mass in the denominator. This region is well described by regular QED and in the leading approximation in $1/\Lambda_\gamma$, the additional photon does not influence loop effects of this scale. When $k \to \infty$, the integrand vanishes now as $\sim 1/k^5$, sufficiently quickly to eliminate the divergence. The loop integral can be evaluated using two standard tricks. First, the three denominators can be combined into one with the help of Feynman parametrization:

$$\frac{1}{A^\alpha}\frac{1}{B^\beta} = \frac{\Gamma(\alpha+\beta)}{\Gamma(\alpha)\Gamma(\beta)}\int_0^1 dx \frac{x^\alpha(1-x)^\beta}{(xA+(1-x)B)^{\alpha+\beta}}, \tag{1.138}$$

where $\Gamma(x)$ is the Euler gamma function. The resulting expression reads

$$\int_0^1 dx \int_0^1 dy \int \frac{d^4k}{i(2\pi)^4}\frac{-\Lambda_\gamma^2 y\not{k}}{\left(k^2-2y(pk)+yp^2+xy\Lambda_\gamma^2+i\varepsilon\right)^3}. \tag{1.139}$$

Shifting the loop momentum as $k \to k + yp$ and dropping the term odd in k leaves

$$\int_0^1 dx \int_0^1 dy \int \frac{d^4k}{i(2\pi)^4}\frac{-\Lambda_\gamma^2 y^2\not{p}}{\left(k^2+y((1-y)p^2-x\Lambda_\gamma^2)+i\varepsilon\right)^3}. \tag{1.140}$$

The second trick is the change of variables: $k^0 = ik_E^0$, $\mathbf{k} = \mathbf{k}_E$, called the Wick rotation. Now, $k^2 = -k_E^2$, where the latter is a length of a 4-component vector in a Euclidean space. In these variables, an integral of a function of k^2 is transformed as

$$\int \frac{d^4k}{i(2\pi)^4}F(k^2) = \frac{1}{(2\pi)^4}\int d\Omega_3 \int_0^\infty d|k_E||k_E|^3 F(-|k_E|^2) = \frac{2}{(4\pi)^2}\int_0^\infty d|k_E||k_E|^3 F(-|k_E|^2), \tag{1.141}$$

so the considered integral becomes

$$\frac{2i\Lambda_\gamma^2 \not{p}}{(4\pi)^4} \int\limits_0^1 dx \int\limits_0^1 dy y^2 \int\limits_0^\infty d|k_E| \frac{|k_E|^3}{\left(|k_E|^2 + M^2\right)^3}, \tag{1.142}$$

where $M^2 \equiv \Lambda_\gamma^2 y[x - (1-y)r] - i\varepsilon$, and $r \equiv p^2/\Lambda_\gamma^2$. The last integral is simply $1/(2M)^2$, so for the considered example,

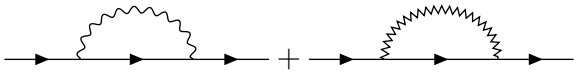

$$= -\frac{\alpha_{em}\not{p}}{4\pi i} \int\limits_0^1 dx \int\limits_0^1 dy \frac{y}{x - (1-y)r - i\varepsilon}. \tag{1.143}$$

The integrals over the Feynman parameters are elementary and in the limit $\varepsilon \to 0^+$ yield

$$\int\limits_0^1 dx \int\limits_0^1 dy \frac{y}{x - (1-y)r - i\varepsilon} = \frac{r - r^2\log(r) + (1-r)^2\log(1-r)}{2r^2} + \frac{i\pi}{2}. \tag{1.144}$$

Expanding around $r = 0$ gives the following result:

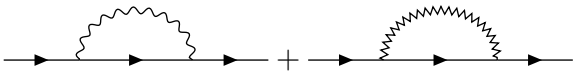

$$= -\frac{\alpha_{em}}{4\pi i}\left(\frac{3}{4} + \frac{i\pi}{2} + \frac{1}{2}\log\left(\frac{\Lambda_\gamma^2}{p^2}\right)\right)\not{p} + \mathcal{O}(r). \tag{1.145}$$

The addition of the heavy "photon" allowed for the integration over the loop momentum and successfully separated the finite and divergent parts of the amplitude. In the decoupling limit of $\Lambda_\gamma^2 \to \infty$, the loop correction becomes infinite, as expected from the simple power counting.

The Pauli-Villars regularization preserves Lorentz invariance, as well as the Ward-Takahashi identities of QED. However, in non-abelian gauge theories, additional finite counterterms are needed to restore the generalization of Ward-Takahashi identities that follows from the BRST symmetry. It also introduces a complicated dependence on the heavy mass Λ, which makes it clearly disadvantageous for modern, automated methods. It turns out that to modify the convergence of loop integrals, instead of changing the integrand, it is much simpler to change the space of integration, but not as sharply as in the hard cutoff scheme. The idea, originally developed by Giambiagi and Bollini in ref. [98] and independently by 't Hooft and Veltman in ref. [99], is to compute all loop integrals in an arbitrary number of dimensions D and later take the limit $D \to 4$. It is based on a simple observation, that the volume of a D-sphere can be analytically continued to arbitrary complex values of D as:

$$\Omega_D \equiv \int d\Omega_D = \frac{2\pi^{\frac{D}{2}}}{\Gamma\left(\frac{D}{2}\right)}, \tag{1.146}$$

so eq. (1.141) can be easily generalized to any value of D:

$$\int \frac{d^D k}{i(2\pi)^D} F(k^2) = \frac{1}{(2\pi)^D} \frac{2\pi^{\frac{D}{2}}}{\Gamma\left(\frac{D}{2}\right)} \int\limits_0^\infty d|k_E| |k_E|^{D-1} F(-|k_E|^2). \tag{1.147}$$

For Feynman integrals, the most relevant case is when $F(k^2) = (k^2 - m^2 + i\varepsilon)^{-\kappa}$, for some arbitrary power κ. After passing to the euclidean momentum space, if $m > 0$ the poles of

the integrand no longer lay close to the integration contour, and one can take the limit $\varepsilon \to 0$ prior to loop integration. Then, the integral over k_E becomes

$$(-1)^\kappa \int_0^\infty d|k_E| \frac{|k_E|^{D-1}}{(|k_E|^2+m^2)^\kappa}. \tag{1.148}$$

This integral can be first computed for $D < \kappa/2$ where it is convergent. Then, its value for arbitrary D is defined by analytic continuation:

$$(-1)^\kappa \int_0^\infty d|k_E| \frac{|k_E|^{D-1}}{(|k_E|^2+m^2)^\kappa} = (-1)^\kappa \frac{\Gamma(2-\epsilon)\Gamma(\kappa-2+\epsilon)}{2\Gamma(\kappa)} \frac{1}{m^{2\kappa-4+2\epsilon}}, \tag{1.149}$$

where $D \equiv 4-2\epsilon$. This result can be used to immediately write the prescription for the simplest Feynman integral, the one loop massive tadpole diagram in a scalar theory:

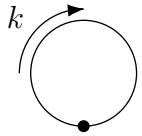

$$\begin{aligned} &= \int \frac{d^D k}{i(2\pi)^D} \frac{1}{(k^2-m^2)^\kappa} = (-1)^\kappa \frac{\Omega_D}{(2\pi)^D} \frac{\Gamma(2-\epsilon)\Gamma(\kappa-2+\epsilon)}{2\Gamma(\kappa)} m^{4-2\epsilon-2\kappa} \\ &= (-1)^\kappa \frac{1}{(4\pi)^{2-\epsilon}} \frac{\Gamma(\kappa-2+\epsilon)}{\Gamma(\kappa)} m^{4-2\epsilon-2\kappa}, \end{aligned} \tag{1.150}$$

where the dependence on κ was preserved for generality.

This dimensional regularization scheme can be formally defined as a functional $\mathcal{F}_D$ that assigns to a function the value of its D-dimensional integral. Such a functional has to coincide with the actual values of integrals in integer dimensions, whenever these are finite. To use it in actual calculations, it should satisfy the basic properties of definite integration over infinite intervals: linearity, proper scaling, and translation symmetry. For all integrands I and J, all complex numbers a and b, and all D-vectors p,

$$\begin{aligned} \mathcal{F}_D[aI(k)+bJ(k)] &\stackrel{!}{=} a\mathcal{F}_D[I(k)] + b\mathcal{F}_D[J(k)], \\ \mathcal{F}_D[I(ak)] &\stackrel{!}{=} \frac{1}{a^D}\mathcal{F}_D[I(k)], \\ \mathcal{F}_D[I(k+p)] &\stackrel{!}{=} \mathcal{F}_D[I(k)], \end{aligned} \tag{1.151}$$

where k is the integration variable. For all D, $a \neq 0$, and κ, by the first and second properties,

$$\mathcal{F}_D\left[(k^2)^\kappa\right] = \mathcal{F}_D\left[\left((ak)^2\right)^\kappa a^{-2\kappa}\right] = a^{-2\kappa}\mathcal{F}_D[\left((ak)^2\right)^\kappa] = a^{-2\kappa-D}\mathcal{F}_D\left[(k^2)^\kappa\right]. \tag{1.152}$$

For this relation to hold for any a, the value of dimensional regularization for all κ has to be defined as zero:

$$\mathcal{F}_D\left[(k^2)^\kappa\right] \stackrel{!}{=} 0. \tag{1.153}$$

This is a very important result for actual calculations. Suppose that a diagram does not depend on any mass or external momentum. By repeated use of the Feynman parametrization of eq. (1.138) and integration variable shifts, its integrand can be brought to a linear combination of terms of the form

$$\frac{1}{(k_j^2+\Delta(k_{i\neq j}))^\kappa}. \tag{1.154}$$

Then all apart from the last k_i D-dimensional integrals can be performed using eq. (1.150). Because there are no other mass scales available, by dimensional analysis, the last one will have to be proportional to

$$\int \frac{d^D k_{\text{last}}}{i(2\pi)^D} \frac{1}{(k_{\text{last}}^2)^\kappa}. \tag{1.155}$$

The result of eq. (1.150) is ill-defined in the limit of $m \to 0$, so it cannot be used in this case. But by eq. (1.153), for dimensional regularization to be self-consistent, this integral has to be set to 0. Thus, all scaleless diagrams vanish in dimensional regularization.

Changing the dimension of space-time affects the dimension of quantities in the Lagrangian. The formula for Green's functions in eq. (1.29) requires taking an exponent of the action, it is thus imperative to keep it dimensionless. As a result, the Lagrangian should have mass-dimension D. Consider the QED Lagrangian:

$$\mathcal{L}_{QED} = -\frac{1}{4}(\partial_\mu A_\nu - \partial_\nu A_\mu)^2 + \bar{\psi}(\not{\partial} + ie\not{A} - m)\psi. \tag{1.156}$$

Since the definition of natural units is unchanged, the derivatives still have mass-dimension 1 as in $D = 4$. This means that the photon field has mass-dimension $D/2 - 1$. The electron mass term dictates that its field has mass-dimension $(D-1)/2$. Combining these results means that the electric charge acquires mass-dimension equal to $2 - D/2 = \epsilon$. As this is supposed to be the small parameter of the perturbative expansion, it must be kept dimensionless. The solution is to rescale e by an arbitrary mass $\tilde{\mu}$ that will absorb its dimension. The new interaction term reads

$$\mathcal{L}_{int} = \tilde{\mu}^\epsilon e \bar{\psi} \not{A} \psi. \tag{1.157}$$

As a result, a factor of $\tilde{\mu}^\epsilon$ will appear in the $\gamma e^+ e^-$ vertex rule. In QED, for a fixed observable, each additional loop order introduces exactly two such vertices, meaning that to take $\tilde{\mu}$ into account it is sufficient to multiply each loop by $\tilde{\mu}^{2\epsilon}$. This result holds also for a generic QFT.

The value of $\tilde{\mu}$ is in principle arbitrary, as it is always raised to a power that vanishes in the limit of $D \to 4$. Choosing a correct value can nonetheless have a large impact on perturbative predictions, as the effects of $\tilde{\mu}$ persist if the perturbation series is truncated at some finite loop level. If all mass scales M_i in the theory are similar in magnitude, $\tilde{\mu}$ should be chosen of the same order. Any other choice will introduce large logarithms of $\tilde{\mu}/M_i$ to perturbatively computed observables that will spoil the behavior of the perturbation series. If the mass scales span many orders of magnitude, there is no "good" choice for $\tilde{\mu}$ and one should successively decouple heavy degrees of freedom to avoid this problem. The $\tilde{\mu}$ dependence of physical quantities will be discussed later in this section.

To conclude the discussion of regularization schemes, it is useful to reexamine the $\mathcal{O}(\alpha_{em})$ correction to the electron propagator in the dimensional regularization. In the Pauli-Villars regularization, taking into account the electron mass makes the computation quite laborious because the integral depends on three independent scales, and is composed of three propagators. In dimensional regularization, it is possible to include it without much difficulty. The corresponding expression is

$$= -4\pi i \alpha_{em} (\tilde{\mu})^{2\epsilon} \int \frac{d^D k}{i(2\pi)^D} \frac{1}{(p-k)^2 + i\varepsilon} \frac{-(2-2\epsilon)\not{k} + (4-2\epsilon)m}{k^2 - m^2 + i\varepsilon}. \tag{1.158}$$

The factors in the numerator of the electron propagator come from D-dimensional identities for products of gamma functions:

$$\gamma_\mu \gamma^\mu = D = 4 - 2\epsilon \qquad \gamma_\mu \not{k} \gamma^\mu = (2-D)\not{k} = -(2-2\epsilon)\not{k}. \tag{1.159}$$

These identities will be proven in the next section. Again, with the help of Feynman parameters and after shifting the loop momentum, it is possible to bring the integrand into the form of eq. (1.150):

$$\begin{aligned} &8\pi i \alpha_{em} (\tilde{\mu})^{2\epsilon} \int \frac{d^D k}{i(2\pi)^D} \int_0^1 dy \frac{y(1-\epsilon)\not{p} - (2-\epsilon)m}{(k^2 - (1-y)(1-y\hat{p}^2)m^2 + i\varepsilon)^2} = \\ =&2\alpha_{em} \frac{1}{(4\pi)^{1-\epsilon}} \left(\frac{\tilde{\mu}}{m}\right)^{2\epsilon} m\Gamma(\epsilon) \int_0^1 dy [y(1-\epsilon)\hat{\not{p}} - 2 + \epsilon][(1-y)(1-y\hat{p}^2 - i\varepsilon)]^{-\epsilon}, \end{aligned} \tag{1.160}$$

where $\hat{p} \equiv p/m$. The result for the y integral can be written in terms of the Gauss hypergeometric function ${}_2F_1$:

$$\begin{aligned} &\int_0^1 dy [y(1-\epsilon)\hat{\not{p}} - 2 + \epsilon][(1-y)(1-y\hat{p}^2 - i\varepsilon)]^{-\epsilon} = \\ =&-\frac{1}{2\hat{p}^2}\left(\hat{\not{p}} - \frac{1}{1-\hat{p}^2}\left((1+\hat{p}^2)\hat{\not{p}} - \frac{4-2\epsilon}{1-\epsilon}\hat{p}^2\right) {}_2F_1\left(\begin{matrix}1, 2-2\epsilon \\ 2-\epsilon\end{matrix}\Big| \frac{\hat{p}^2}{\hat{p}^2 - 1 + i\varepsilon}\right)\right), \end{aligned} \tag{1.161}$$

where all factors of ε that do not affect the branch of the analytic continuation have been neglected. The hypergeometric functions can be expanded around $\epsilon = 0$ using the `Mathematica` package `HypExp` [100, 101] giving the following result for the dimensionaly regularized correction:

$$\begin{aligned} =&\frac{m\alpha_{em}}{4\pi i}\left[\frac{4-\hat{\not{p}}}{\epsilon} + 6 - A_+\hat{\not{p}} - A_-(A_+\hat{\not{p}} - 4)\log(1-\hat{p}^2) + (4-\hat{\not{p}})\log\left(\frac{\mu^2}{m^2}\right)\right] \end{aligned} \tag{1.162}$$

up to terms vanishing in the $\epsilon \to 0$ limit. For $\hat{p}^2 > 1$, the branch of the logarithm should be chosen as $\log(1-\hat{p}^2) \to \log(\hat{p}^2 - 1) - i\pi$. The symbols $A_\pm$ are defined as $A_\pm \equiv 1 \pm 1/\hat{p}^2$. In the limit of $m \to 0$, the above expression reduces to

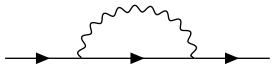

$$= -\frac{\alpha_{em}}{4\pi i}\left(\frac{1}{\epsilon} + 1 + i\pi + \log\left(\frac{\mu^2}{p^2}\right)\right)\not{p}. \tag{1.163}$$

The dimensional regularization scale

$$\mu \equiv \sqrt{4\pi}\exp(-\gamma_{EM}/2)\tilde{\mu}, \tag{1.164}$$

where $\gamma_{EM} \approx 0.577$ is the Euler-Mascheroni constant, was introduced in eq. (1.162) to absorb terms of 4π and γ_{EM} from the expansion in powers of ϵ. As expected, the result is clearly divergent when $D \to 4$. It is also separated into terms that are clearly finite or

infinite in this limit, which is the main goal of regularization. There appeared a logarithmic dependence on the scale μ. For Green's functions, this dependence disappears order-by-order in perturbation theory, i.e. after computing the 2-loop correction, the term $\mathcal{O}(\alpha_{em}\log(\mu/m))$ will cancel, leaving only terms $\mathcal{O}(\alpha_{em}^2\log^2(\mu/m))$.

Even though this computation was much more straightforward than in the Pauli-Villars scheme, and it was possible to compute the m dependence without much additional effort, for multi-loop problems such a direct approach quickly becomes unfeasible. Indeed, the next chapter is dedicated to describing the framework that avoids Feynman parameters, Wick rotations, and complicated momentum shifts altogether. It is also able to tackle hundreds of thousands of Feynman integrals at once, and is quite agnostic to their structure.

The objective of renormalization in dimensional regularization is to absorb the divergent part in the ϵ expansions of S-matrix elements into the renormalization constants Z_{ϕ_j} and Z_{c_j} (see eq. (1.129)). A natural choice of a renormalization scheme is to only absorb the ϵ^n terms for $n < 0$, while preserving the coefficients in the $n \geq 0$ terms unchanged. If one also factorizes the renormalization scale $\tilde{\mu}$ as in eq. (1.164), and rescales all the couplings similarly to eq. (1.157), this scheme is referred to as the Modified Minimal Subtraction, or the $\overline{\text{MS}}$ scheme[†].

1.5 Dirac Algebra

The dimensional regularization provides a definition for the loop momentum k_μ integrals that diverge for $D = 4$. In the conventional computation strategy, one would bring the integrand to the form of eq. (1.150) by repeatedly using the Feynman parametrization of eq. (1.138), shifting loop momenta, completing squares so the numerators cancel with powers of denominators, and eliminating all terms with an odd number of factors of k_μ. Before this can be attempted, the complicated contractions of color, Lorentz, and Dirac indices present in the numerators of propagators and vertex Feynman rules have to be simplified.

This step becomes much more straightforward when one exploits the structure of the specific diagram in question. The discussion below considers only a 1 fermion $\to$ 1 fermion process with external momentum p and mass m, averaged over external spins and colors, just as in the case of the calculation of the unpolarized, inclusive q^2 spectrum of the b quark semileptonic decay width. Moreover, it will be assumed that there are exactly two chirality distinguishing vertices present on the main fermion line, and no such vertices anywhere else, as is the case for the semileptonic decay to all orders in QCD at the leading order in electroweak interactions.

In the formula for the decay rate in eq. (1.112), the discrete quantum numbers of the 2 external lines are exactly the same and, in the unpolarized process, are averaged over. The spinor element of the incoming fermion placed at the end of the chain of gamma matrices contributed by the lines and vertices of the main line can be moved to its beginning. The chain will then be started by a factor

$$\sum_s u_b^{(s)}(p)\bar{u}_a^{(s)}(p) = (\not{p} + m\mathbb{1}^{(\gamma)})_{ba}. \tag{1.165}$$

This identity follows directly from the solution to the free Dirac equation in the chiral

[†]If one instead rescales the couplings with μ, the corresponding renormalization condition is called simply the Minimal Subtraction scheme.

representation, where the positive frequency waves are multiplied by:

$$u^{(s)}(p) = \begin{pmatrix} \sqrt{p \cdot \sigma}\xi^s \\ \sqrt{p \cdot \bar{\sigma}}\xi^s \end{pmatrix}. \tag{1.166}$$

The basis vectors ξ are orthogonal:

$$\sum_s \xi^s \xi^{\dagger s} = \mathbb{1}_{2\times 2}, \tag{1.167}$$

while the gamma matrices in the chiral representation read

$$\gamma^\mu = \begin{pmatrix} 0 & \sigma^\mu \\ \bar{\sigma}^\mu & 0 \end{pmatrix}, \tag{1.168}$$

where $\sigma \equiv (\mathbb{1}_{2\times 2}, \sigma^1, \sigma^2, \sigma^3)$, $\bar{\sigma} \equiv (\mathbb{1}_{2\times 2}, -\sigma^1, -\sigma^2, -\sigma^3)$, and σ^i are the three Pauli matrices. The entire chain of gamma matrices coming from the main line can be written as

$$\begin{aligned} &\sum_s \bar{u}^{(s)}(p)_a (\mathcal{V}_{ff_1})_{aa_1} (\mathcal{P}_{f_1})_{a_1a_2} (\mathcal{V}_{f_1f_2})_{a_2a_3} \dots (\mathcal{V}_{f_nf})_{a_nb} u_b^{(s)}(p) = \\ &= \left(\not{p} + m\mathbb{1}^{(\gamma)}\right)_{ba} (\mathcal{V}_{ff_1})_{aa_1} (\mathcal{P}_{f_1})_{a_1a_2} (\mathcal{V}_{f_1f_2})_{a_2a_3} \dots (\mathcal{V}_{f_nf})_{a_nb} = \mathrm{Tr}[\left(\not{p} + m\mathbb{1}^{(\gamma)}\right) \mathcal{V}_{ff_1} \mathcal{P}_{f_1} \mathcal{V}_{f_1f_2} \dots \mathcal{V}_{f_nf}]. \end{aligned} \tag{1.169}$$

The indices f and f_i indicate the species of fermions, and are not summed over. Closed fermion loops are even simpler. There, gamma matrices of vertices and propagators naturally form a trace, as the chain of indices closes by itself together with the loop[†]. In a diagram with one main line and n closed fermion loops, the entire Dirac algebra comes down to evaluating $n+1$ traces of chains of gamma matrices. For the NNLO calculation of the q^2 spectrum, it is sufficient to only consider cases of $n = 0$ and $n = 1$.

The Dirac algebra proves to be conceptually non-trivial in dimensional regularization [102–117]. When the space-time dimension is changed from an integer to an arbitrary value, the regular definitions of gamma matrices, such as the chiral representation in eq. (1.168), cannot be simply carried over. The objects γ^μ have to be defined purely algebraically, preserving as much of the familiar $D = 4$ structure as possible. It turns out that some property is necessarily violated; one has to give up either the cyclicity of the trace, the normal anticommutation relations of chiral projectors, or the "D-covariant" results for γ traces. If the considered process is unpolarized, and the chiral vertices are limited to a single fermion line, the simplest choice is to keep the cyclicity and the algebraic properties of projectors, as the differences in traces vanish by symmetry arguments. This choice, first introduced in ref. [102], and commonly referred to as the Naive Dimensional Regularization (NDR)[‡] is by far the most straightforward to implement in a computer program. It also has

[†]Due to the anticommuting property of spin 1/2 fields, each closed fermion loop contributes an additional factor of (-1). This is straightforward to see in the formalism of the Wick theorem. A diagram with a fermion loop corresponds to a vacuum expectation value of a contraction of fields $\langle\Omega| \dots \hat{\bar{\psi}}_1 \hat{\psi}_1 \hat{\bar{\psi}}_2 \hat{\psi}_2 \hat{\bar{\psi}}_3 \dots \hat{\psi}_{n-1} \hat{\bar{\psi}}_n \hat{\psi}_n \dots |\Omega\rangle$, where $\hat{\psi}_j \equiv \hat{\psi}(x_j)$ and the ellipses on the left and right stand for contractions of other fields outside of the loop. Each contraction $\hat{\psi}_j \hat{\bar{\psi}}_k = \mathcal{P}_\psi(x_k - x_j)$, so to obtain the algebraic expression for the diagram, the first field has to be anticommuted past all others. As there is an odd number of anticommutations, the diagram acquires a factor of (-1). For an alternative explanation in the formalism of functional analysis see, e.g., section 9.5 of ref. [78].

[‡]I concur with the opinion of the author of ref. [103], that this acronym should more appropriately be read as "Normal Dimensional Regularization".

the additional benefit of preserving the Ward-Takahashi identity, which in other schemes has to be restored "by hand" by an appropriate choice of counterterms that cancel spurious anomalies. The precise algebraic rules for the γ objects in the NDR scheme will be defined below.

In the absence of chirality distinguishing vertices, the traces to be computed in a generic unpolarized diagram can always be expanded into polynomials of

$$\mathrm{Tr}[\gamma^{\mu_1}\gamma^{\mu_2}\dots\gamma^{\mu_n}] \tag{1.170}$$

where each term is fully contracted with some Lorentz tensor with indices $\mu_1\dots\mu_n$. The trace in eq. (1.170) can be computed using the properties of the Clifford algebra in a D dimensional space-time:

$$g^{\mu\nu}g_{\mu\nu} = D, \qquad \mathrm{Tr}[\mathbb{1}^{(\gamma)}] = D^{(\gamma)}, \qquad \{\gamma^\mu,\gamma^\nu\} \equiv \gamma^\mu\gamma^\nu + \gamma^\nu\gamma^\nu = 2g^{\mu\nu}\mathbb{1}^{(\gamma)}. \tag{1.171}$$

For integer dimensions, all irreducible representations of this algebra are $D^{(\gamma)} \equiv 2^{\lfloor D/2\rfloor}$ dimensional[†], where $\lfloor x\rfloor$ is the integer part of x. These rules should be treated as the definition of the algebraic properties of $D^{(\gamma)}$ dimensional objects γ^μ, as the matrices themselves obviously cannot be defined in an arbitrary dimension. It is now possible to compute the simplest traces of gamma matrices. By Lorentz invariance, the trace of a single γ^μ is 0:

$$\mathrm{Tr}[\gamma^\mu] = 0, \tag{1.172}$$

as in any other case it would constitute a process independent, preferred D-vector. The trace of two gammas can be easily obtained with the application of the second and third properties in eq. (1.171):

$$\mathrm{Tr}[\gamma^\mu\gamma^\nu] = \mathrm{Tr}[2g^{\mu\nu}\mathbb{1}^{(\gamma)} - \gamma^\nu\gamma^\mu] = 2g^{\mu\nu}D^{(\gamma)} - \mathrm{Tr}[\gamma^\mu\gamma^\nu] \Longrightarrow \mathrm{Tr}[\gamma^\mu\gamma^\nu] = D^{(\gamma)}g^{\mu\nu}. \tag{1.173}$$

The cyclicity of the trace has been used in the third equality. Computing a trace of a larger but even number of γ^μ can be done recursively. The length of a chain can be lowered by anticommuting the first of the gammas all the way to the right of the trace, and than using the trace cyclicity. Abbreviating $\mathrm{Tr}^{a_1a_2a_3\dots a_n} \equiv \mathrm{Tr}[\gamma^{\mu_{a_1}}\gamma^{\mu_{a_2}}\gamma^{\mu_{a_3}}\dots\gamma^{\mu_{a_n}}]$, such a trace can be expanded as

$$\begin{aligned}
&\mathrm{Tr}^{1234\dots(2n-1)(2n)} = 2g^{\mu_1\mu_2}\mathrm{Tr}^{3456\dots(2n)} - \mathrm{Tr}^{2134\dots(2n)} \\
=&2g^{\mu_1\mu_2}\mathrm{Tr}^{3456\dots(2n)} - 2g^{\mu_1\mu_3}\mathrm{Tr}^{2456\dots(2n)} + \mathrm{Tr}^{2324\dots(2n)} \\
=&\dots = 2g^{\mu_1\mu_2}\mathrm{Tr}^{3456\dots(2n)} - 2g^{\mu_1\mu_3}\mathrm{Tr}^{2456\dots(2n)} + 2^{\mu_1\mu_4}\mathrm{Tr}^{2356\dots(2n)}\dots \\
&- 2g^{\mu_1\mu_{2n-1}}\mathrm{Tr}^{2345\dots(2n-2)(2n)} + 2g^{\mu_1\mu_{2n}}\mathrm{Tr}^{2345\dots(2n-1)} - \mathrm{Tr}^{2345\dots(2n)1}.
\end{aligned} \tag{1.174}$$

Cycling γ^{μ_1} back to the front of the chain and moving the last term to the left hand side yields

$$\mathrm{Tr}[\gamma^{\mu_1}\gamma^{\mu_2}\dots\gamma^{\mu_{2n}}] = \sum_{k=2}^{2n}(-1)^k g^{\mu_1\mu_k}\mathrm{Tr}[\gamma^{\mu_2}\gamma^{\mu_3}\dots\gamma^{\mu_{k-1}}\gamma^{\mu_{k+1}}\dots\gamma^{\mu_{2n}}]. \tag{1.175}$$

[†]If one keeps $D^{(\gamma)}$ arbitrary both during the computation of renormalization constants and of S-matrix elements, it factorizes out of the expressions for renormalized quantities. It is thus conventional to fix $D^{(\gamma)} = 4$ prior to loop integration, which is a part of the definition of the MS and $\overline{MS}$ schemes.

Each γ^μ chain in the sum is shorter by 2 than the one in the initial trace. The recursion ends when $n = 1$ with the result of eq. (1.173). Note that the trace of an even number of γ^μ is given by a combination of products of metric tensors and no other Lorentz structures appear.

In addition to the standard rules in eq. (1.171), the NDR scheme assumes that there exists an object $\tilde{\gamma}_5$ that anticommutes with all γ^μ:

$$\{\tilde{\gamma}_5, \gamma^\mu\} \overset{NDR}{=} 0. \tag{1.176}$$

Consider now the commutator:

$$[\tilde{\gamma}_5^2, \gamma^\mu] = \tilde{\gamma}_5^2\gamma^\mu - \gamma^\mu\tilde{\gamma}_5^2 = \tilde{\gamma}_5^2\gamma^\mu - \tilde{\gamma}_5^2\gamma^\mu = 0. \tag{1.177}$$

Another assumption of the NDR scheme is that the entire algebra of $2^{D/2} \times 2^{D/2}$ matrices can be spanned by γ^μ or their products, so $\tilde{\gamma}_5^2$ commutes with every matrix acting on the spin space. It follows that it has to be proportional to the identity:

$$\tilde{\gamma}_5^2 = \lambda \mathbb{1}^{(\gamma)}, \tag{1.178}$$

for some $\lambda \in \mathbb{C}$. Now it is possible to define

$$\gamma_5 \equiv \frac{1}{\sqrt{\lambda}}\tilde{\gamma}_5, \tag{1.179}$$

so that $\gamma_5^2 = \mathbb{1}^{(\gamma)}$. It is straightforward to show that γ_5 is traceless:

$$\mathrm{Tr}[\gamma^\mu\gamma^\nu\gamma_5] = 2g^{\mu\nu}\mathrm{Tr}[\gamma_5] - \mathrm{Tr}[\gamma^\nu\gamma^\mu\gamma_5] = 2g^{\mu\nu}\mathrm{Tr}[\gamma_5] + \mathrm{Tr}[\gamma^\nu\gamma_5\gamma^\mu]. \tag{1.180}$$

The gammas in the last term can now be cycled back to the original order and cancel the initial trace, which leads to $\mathrm{Tr}[\gamma_5] = 0$. Considering now the first equality in the above derivation, it is clear that $\mathrm{Tr}[\gamma^\mu\gamma^\nu\gamma_5]$ is antisymmetric in the indices $\mu\nu$. As there are no antisymmetric rank-2 Lorentz tensors, this trace must also vanish. Retaining the simple properties of the $D = 4$ dimensional Clifford algebra as assumptions of the NDR scheme thus preserves all of the important algebraic properties of γ_5:

$$\{\gamma_5, \gamma^\mu\} = 0, \qquad \gamma_5^2 = \mathbb{1}^{(\gamma)}, \qquad \mathrm{Tr}[\gamma_5] = 0, \qquad \mathrm{Tr}[\gamma^\mu\gamma^\nu\gamma_5] = 0. \tag{1.181}$$

Another feature of the $D = 4$ Clifford algebra preserved in the NDR scheme is that traces of odd numbers of γ^μ vanish. For a chain without a γ_5 this can be seen as follows:

$$\begin{aligned}\mathrm{Tr}[\gamma^{\mu_1}\gamma^{\mu_2}\dots\gamma^{\mu_{2n}}\gamma^{\mu_{2n+1}}] &= \mathrm{Tr}[\gamma^{\mu_1}\gamma^{\mu_2}\dots\gamma^{\mu_{2n}}\gamma_5\gamma_5\gamma^{\mu_{2n+1}}] = \\ = -\mathrm{Tr}[\gamma_5\gamma^{\mu_1}\gamma^{\mu_2}\dots\gamma^{\mu_{2n}}\gamma^{\mu_{2n+1}}\gamma_5] &= -\mathrm{Tr}[\gamma^{\mu_1}\gamma^{\mu_2}\dots\gamma^{\mu_{2n}}\gamma^{\mu_{2n+1}}].\end{aligned} \tag{1.182}$$

In the second equality, the γ_5 on the right is anticommuted once past the $\gamma^{\mu_{2n+1}}$ while the γ_5 on the left is anticommuted $2n$ times to the beginning of the chain, giving a total of $2n + 1$ anticommutations and a factor of -1. Then, the left γ_5 was recombined with the other using the cyclicity of the trace. The trace of a chain ending with a γ_5 is even simpler:

$$\mathrm{Tr}[\gamma^{\mu_1}\dots\gamma^{\mu_{2n+1}}\gamma_5] = -\mathrm{Tr}[\gamma_5\gamma^{\mu_1}\dots\gamma^{\mu_{2n+1}}] = -\mathrm{Tr}[\gamma^{\mu_1}\dots\gamma^{\mu_{2n+1}}\gamma_5]. \tag{1.183}$$

The price for this simple structure is that for $n > 2$, the NDR scheme fails to recover the correct traces of chains of $2n$ γ^μ matrices with a single γ_5 at the end. This can be seen by manipulating the following trace:

$$\mathrm{Tr}[\gamma^\alpha\gamma^{\mu_0}\gamma^{\mu_1}\gamma^{\mu_2}\gamma^{\mu_3}\gamma^{\mu_4}\gamma_5]. \tag{1.184}$$

The first step is to anticommute γ^α past all other γ^μ to the left of the γ_5. This results in a number of terms:

$$\begin{aligned}&\mathrm{Tr}[\gamma^\alpha\gamma^{\mu_0}\gamma^{\mu_1}\gamma^{\mu_2}\gamma^{\mu_3}\gamma^{\mu_4}\gamma_5] = \\ =&2g^{\alpha\mu_0}\mathrm{Tr}_5^{1234} - 2g^{\alpha\mu_1}\mathrm{Tr}_5^{0234} + 2g^{\alpha\mu_2}\mathrm{Tr}_5^{0134} - 2g^{\alpha\mu_3}\mathrm{Tr}_5^{0124} + 2g^{\alpha\mu_4}\mathrm{Tr}_5^{0123} \\ &- \mathrm{Tr}[\gamma^{\mu_0}\gamma^{\mu_1}\gamma^{\mu_2}\gamma^{\mu_3}\gamma^{\mu_4}\gamma^\alpha\gamma_5],\end{aligned} \tag{1.185}$$

where $\mathrm{Tr}_5^{abcd} \equiv \mathrm{Tr}[\gamma^{\mu_a}\gamma^{\mu_b}\gamma^{\mu_c}\gamma^{\mu_d}\gamma_5]$. The last trace can be moved to the left hand side and γ^α can be cycled to the end of the original trace, giving

$$\mathrm{Tr}[\gamma^{\mu_0}\gamma^{\mu_1}\gamma^{\mu_2}\gamma^{\mu_3}\gamma^{\mu_4}\{\gamma_5,\gamma^\alpha\}] = 2(g^{\alpha\mu_0}\mathrm{Tr}_5^{1234} - g^{\alpha\mu_1}\mathrm{Tr}_5^{0234} + g^{\alpha\mu_2}\mathrm{Tr}_5^{0134} - g^{\alpha\mu_3}\mathrm{Tr}_5^{0124} + g^{\alpha\mu_4}\mathrm{Tr}_5^{0123}). \tag{1.186}$$

By the NDR assumption in eq. (1.176), the left hand side is 0. Contracting both sides with $\gamma_{\mu_0\alpha}$ results in

$$0 = D\mathrm{Tr}_5^{1234} - \mathrm{Tr}_5^{1234} + \mathrm{Tr}_5^{2134} - \mathrm{Tr}_5^{3124} + \mathrm{Tr}_5^{4123}. \tag{1.187}$$

Using the third identity in eq. (1.171) and the fourth result in eq. (1.181), the last three traces can be brought into the canonical ordering of indices, which gives

$$(D-4)\mathrm{Tr}_5^{1234} \equiv (D-4)\mathrm{Tr}[\gamma^{\mu_1}\gamma^{\mu_2}\gamma^{\mu_3}\gamma^{\mu_4}\gamma_5] = 0. \tag{1.188}$$

For $D \neq 4$, the above result cannot be matched in an analytic way to the $D = 4$ identity:

$$\mathrm{Tr}[\gamma^{\mu_1}\gamma^{\mu_2}\gamma^{\mu_3}\gamma^{\mu_4}\gamma_5] = -4i\epsilon^{\mu_1\mu_2\mu_3\mu_4}, \tag{1.189}$$

where $\epsilon^{\mu\nu\rho\sigma}$ is the totally antisymmetric Levi-Civita symbol. This apparent flaw requires a careful treatment in general considerations, but for the present analysis and for the calculation of the semileptonic decay spectra in the leading order in electroweak interactions it can be ignored. The justification of this point will be discussed below.

In handling traces with a γ_5 in $D = 4$ dimensions, the following identity proves convenient:

$$\gamma^\mu\gamma^\nu\gamma^\rho = g^{\mu\nu}\gamma^\rho + g^{\nu\rho}\gamma^\mu - g^{\mu\rho}\gamma^\nu + i\epsilon^{\mu\nu\rho\alpha}\gamma_\alpha\gamma_5. \tag{1.190}$$

It is important to emphasize here that this relation holds only for $D = 4$. To prove it in this case, consider first the case when two indices are equal, while the third can be different. The three possibilities are:

$$\begin{aligned}\gamma^{\bar\mu}\gamma^{\bar\mu}\gamma^\rho &= \frac{1}{2}\{\gamma^{\bar\mu},\gamma^{\bar\mu}\}\gamma^\rho = g^{\bar\mu\bar\mu}\gamma^\rho, \\ \gamma^\mu\gamma^{\bar\nu}\gamma^{\bar\nu} &= \frac{1}{2}\gamma^\mu\{\gamma^{\bar\nu},\gamma^{\bar\nu}\} = g^{\bar\nu\bar\nu}\gamma^\mu, \\ \gamma^{\bar\rho}\gamma^\nu\gamma^{\bar\rho} &= 2g^{\bar\rho\nu}\gamma^{\bar\rho} - \gamma^\nu\gamma^{\bar\rho}\gamma^{\bar\rho} = 2g^{\bar\rho\nu}\gamma^{\bar\rho} - g^{\bar\rho\bar\rho}\gamma^\nu.\end{aligned} \tag{1.191}$$

where a bar over an index indicates that it should not be summed over. The above three equations can be put together as:

$$\gamma^\mu\gamma^\nu\gamma^\rho \overset{\substack{\mu=\nu \text{ or } \nu=\rho \\ \text{or } \rho=\mu}}{=} g^{\mu\nu}\gamma^\rho + g^{\nu\rho}\gamma^\mu - g^{\mu\rho}\gamma^\nu. \tag{1.192}$$

If all three indices are different, by the third identity in eq. (1.171), the three gamma matrices anticommute and the metric tensors on the right hand side are 0. The above equality can thus be extended to a general case by adding some term fully antisymmetric in the indices

$\mu\nu\rho$. The correct choice turns out to be as quoted in eq. (1.190). The last term can be verified case-by-case using the $D = 4$ definition $\gamma_5 \equiv i\gamma^0\gamma^1\gamma^2\gamma^3$. For example:

$$\gamma^0\gamma^1\gamma^2 = \epsilon^{0123}\gamma^0\gamma^1\gamma^2\gamma_3\gamma^3 = -\epsilon^{0123}\gamma_3\gamma^0\gamma^1\gamma^2\gamma^3 = i\epsilon^{0123}\gamma_3\gamma_5 \tag{1.193}$$

and similarly for all other permutations of different indices $\mu\nu\rho$. The first equality utilized the relation $\gamma_\mu = (\gamma^\mu)^{-1}$, which follows directly from the defining properties in eq. (1.171).

Using the identity (1.190) allows for reducing the length of gamma chains in $D = 4$ dimensions with a γ_5 as before in eqs. (1.174) and (1.175). For a generic trace with an even number of γ^μ and a γ_5, an application of eq. (1.190) gives

$$\mathrm{Tr}_5^{1234\ldots(2n)} = g^{\mu_1\mu_2}\mathrm{Tr}_5^{34\ldots(2n)} + g^{\mu_2\mu_3}\mathrm{Tr}_5^{14\ldots(2n)} - g^{\mu_1\mu_3}\mathrm{Tr}_5^{24\ldots(2n)} - i\epsilon^{\mu_1\mu_2\mu_3\alpha}g_{\alpha\beta}\mathrm{Tr}[\gamma^\beta\gamma^{\mu_4}\ldots\gamma^{\mu_{2n}}]. \tag{1.194}$$

In the first three terms, the gamma chain is as desired shorter by two. Each of them can be treated recursively until reaching the length of $2n = 4$. Then, the traces with four γ^μ and a γ_5 can be substituted with the right hand side of eq. (1.189). The last term multiplied by the Levi-Civita symbol and all others of that type appearing in the recursion have traces of an even number of γ^μ without γ_5 and can be reduced with eqs. (1.175) and (1.173). Here, the important point is that in the result, every term will be given by a product of metric tensors and a single Levi-Civita symbol.

The assumed properties of γ_5 allow for defining the following two operators:

$$P_L \equiv \frac{\mathbb{1}^{(\gamma)} - \gamma_5}{2}, \qquad P_R \equiv \mathbb{1}^{(\gamma)} - P_L = \frac{\mathbb{1}^{(\gamma)} + \gamma_5}{2}, \tag{1.195}$$

which satisfy

$$P_{L/R}^2 = P_{L/R}, \qquad P_L P_R = P_R P_L = 0, \qquad P_R + P_L = \mathbb{1}^{(\gamma)}, \qquad P_R - P_L = \gamma_5, \tag{1.196}$$

and inherit the anticommutation relation from the $D = 4$ case:

$$\{P_{L/R}, \gamma^\mu\} = \gamma^\mu \Longleftrightarrow P_{L/R}\gamma^\mu = \gamma^\mu P_{R/L}. \tag{1.197}$$

In any trace coming from a fermion line with chirality distinguishing vertices, all projectors $P_{R/L}$ can be moved to the end of the chain of γ^μ using eq. (1.197), resulting either in 0 when after commuting there are both P_L and P_R present, or a chain of γ^μ with a single factor of P_R or P_L. For diagrams with a single line and exactly two P_L projectors and all other lines without, as is the case in the computation of the q^2 spectrum, all non-vanishing terms will be products of traces of an even number of γ^μ and a single trace with the two P_L separated by an even number of γ^μ. In the latter, the two P_L can be combined into a single projector at the end of the chain. Consider now a term in such a diagram. First, factor out the trace coming from the single line with chirality distinguishing vertices. After the loop integration, the Lorentz tensor left uncontracted due to this factoring out comes entirely from bosonic propagators, uncontracted momenta extracted from fermion traces before integration, and fermion traces from lines without any factors of γ_5. It must be just a linear combination of products of uncontracted external momenta and metric tensors. If the line with the projectors is also the only external line, there is just one external momentum p^μ. Then, each term in the algebraic expression for the diagram will be of the form

$$A(p^2, m_j^2)g^{\mu_1\mu_2}g^{\mu_3\mu_4}\ldots g^{\mu_{n-1}\mu_n}p^{\mu_{n+1}}p^{\mu_{n+2}}\ldots p^{\mu_m}\mathrm{Tr}[\gamma^{\mu_{\sigma_1}}\gamma^{\mu_{\sigma_2}}\ldots\gamma^{\mu_{\sigma_m}}P_L], \tag{1.198}$$

for some permutation of m elements σ. In $D = 4$ dimensions, as was argued below eq. (1.194), the γ_5 term in the trace will result in a combination of terms with a single factor of the Levi-Civita symbol and a number of metric tensors. In the end, the result must be a Lorentz scalar, so the indices of the Levi-Civita symbol have to be contracted either with two metric tensors, four factors of p^μ or a single metric tensor and two factors of p^μ. In any case, the tensor contracted with $\epsilon^{\mu_i\mu_j\mu_k\mu_l}$ must be symmetric in at least two indices, so the entire γ_5 part of the P_L trace vanishes. The other part of the remaining projector is simply $\mathbb{1}^{(\gamma)}/2$ and therefore the correct result for the diagram can be obtained in the following procedure:

1. Expand all traces, separating the mass and momentum terms in fermion propagators,
2. Factor all momenta out of the traces, leaving just chains of γ^μ and P_L inside,
3. Remove all terms where any trace has an odd number of γ^μ inside,
4. Remove all terms in which the two factors of P_L are separated by an odd number of γ^μ,
5. *Remove the two factors of P_L and multiply by $1/2$ instead,*
6. Use eqs. (1.175) and (1.173) to resolve all fermion traces in terms of the metric tensor,
7. Contract all Lorentz indices,
8. Compute the loop integrals.

Even though this reasoning was carried out for $D = 4$ dimensions, thanks to the crucial step 5, the prescription is completely independent of the treatment of γ_5 in dimensional regularization. In the end, the projectors can be simply replaced by a factor of $1/2$, which can be done in any scheme, including the most convenient NDR. The mismatch in Tr_5^{1234} between $D = 4$ and $D \neq 4$ plays no role. The above algorithm is relatively straightforward to automate in a computer program and applies to all orders in QCD.

1.6 Color Algebra

This section is dedicated to the discussion of the basic properties of the $\mathfrak{su}(N)$ Lie algebra that lead to the following four identities for contractions of its generators T^a:

$$\begin{aligned} T^a T^a &= C_F^{(2)} \mathbb{1}^{(c)}, \\ T^a T^b T^a &= -\frac{1}{2N} T^b \\ f^{acd} f^{bcd} T^a T^b &= C_A^{(2)} C_F^{(2)} \mathbb{1}^{(c)}, \\ f^{abc} T^a T^b T^c &= \frac{i}{2} C_A^{(2)} C_F^{(2)} \mathbb{1}^{(c)}. \end{aligned} \tag{1.199}$$

The matrix $\mathbb{1}^{(c)}$ is the identity operator in the color space, satisfying $\mathrm{Tr}[\mathbb{1}^{(c)}] = N$. The symbols f^{abc} are the structure constants of $\mathfrak{su}(N)$ defined by the relation

$$[T^a, T^b] = i f^{abc} T^c. \tag{1.200}$$

The identities in eq. 1.199 were written assuming that the generators are normalized as

$$\mathrm{Tr}[T^a T^b] = T_R \delta^{ab}, \tag{1.201}$$

with $T_R = 1/2$. This is a standard choice found in the literature, and will be adopted throughout the present thesis. The numbers $C_F^{(2)}$ and $C_A^{(2)}$ are referred to as the quadratic Casimir invariants in the fundamental and adjoint representations respectively. In the $\mathfrak{su}(N)$ algebra, they are given by

$$C_F^{(2)} = \frac{N^2-1}{2N}, \qquad C_A^{(2)} = N. \tag{1.202}$$

Although these identities can be easily checked for a particular choice of $\mathfrak{su}(N)$ generators, it is illuminating to sketch their algebraic proofs.

In a Lie algebra, apart from the addition of its elements and their multiplication by real numbers, one defines a two-argument operation called the Lie bracket. In a finite-dimensional matrix representation, this bracket is realized as the regular commutator. From this algebraic standpoint, multiplication of elements is not part of the structure of Lie algebras, but in a matrix representation it can be naturally included. The Lie algebra is closed under the action of the Lie bracket, but not necessarily under matrix multiplication in its representation. This becomes clear in $\mathfrak{su}(N)$ which is defined as the algebra of hermitian, traceless $N \times N$ matrices. A product of two traceless matrices is not necessarily traceless, but their commutator is. This validates eq. (1.200) up to some unknown constants f^{abc}.

The properties of simplicity occur in much of the mathematical theory and physical applications of Lie algebras. To define these, it is first necessary to define an ideal $\mathfrak{i}$ of a Lie algebra $\mathfrak{g}$. A set $\mathfrak{i} \subseteq \mathfrak{g}$ closed under the algebra addition: $\mathfrak{i} + \mathfrak{i} = \mathfrak{i}$ and satisfying $[\mathfrak{g}, \mathfrak{i}] = \mathfrak{i}$ is called the left ideal of $\mathfrak{g}$. Analogously, if $[\mathfrak{i}, \mathfrak{g}] = \mathfrak{i}$, $\mathfrak{i}$ is a right ideal of $\mathfrak{g}$. An algebra $\mathfrak{g}$ is said to be simple if it does not contain any ideals other than $\{\mathbb{0}\}$ and $\mathfrak{g}$. Examples include $\mathbb{R}^3$ with the vector product, $\mathfrak{sl}(N)$ algebra of traceless matrices, and most importantly for QCD, $\mathfrak{su}(N)$.

Another important property of $\mathfrak{su}(N)$ is its dimension. Traceless hermitian $N \times N$ matrices have $N^2 - 1$ free parameters: N real diagonal elements, $2 \cdot N(N-1)/2$ from complex elements in the upper[†] triangle, and -1 from the tracelessness condition. This leads to

$$\delta^{aa} = N^2 - 1, \tag{1.203}$$

where the index a runs over all $\mathfrak{su}(N)$ generators.

The $\mathfrak{su}(N)$ algebra is defined as a subset of $N \times N$ matrices, but its algebraic structure is also realized by a subset of its endomorphisms. Consider for any $A \in \mathfrak{su}(N)$

$$ad_A : \mathfrak{su}(N) \to \mathfrak{su}(N),\ B \mapsto ad_A B \equiv i[A, B]. \tag{1.204}$$

Since the map ad_A was defined for any A, it is also given for commutators of matrices in $\mathfrak{su}(N)$:

$$ad_{[A,B]} C = i[[A, B], C]. \tag{1.205}$$

The commutator of operators ad_A and ad_B is also straightforward to compute:

$$[ad_A, ad_B] C = [A, i[B, C]] - [B, i[A, C]]. \tag{1.206}$$

[†]or lower

Then,

$$\begin{aligned}([ad_A, ad_B] - ad_{[A,B]})C =&[A, i[B, C]] - [B, i[A, C]] - i[[A, B], C] \\ =&i[A, [B, C]] + i[B, [C, A]] + i[C, [A, B]] = 0,\end{aligned} \tag{1.207}$$

where the last equality is the Jacobi identity of commutators. It follows that

$$ad : \mathfrak{su}(N) \to \mathrm{End}[\mathfrak{su}(N)],\ A \mapsto ad_A \tag{1.208}$$

preserves the structure of $\mathfrak{su}(N)$:

$$ad_{[A,B]} = [ad_A, ad_B], \tag{1.209}$$

and is thus a representation. This map is referred to as the adjoint representation of $\mathfrak{su}(N)$ and serves an important role both in the theory of Lie algebras and also in particle physics. Abstract Lie algebras are defined assuming the Jacobi identity and antisymmetry of Lie brackets, so an adjoint representation can be found for any Lie algebra. Fixing the basis of $\mathfrak{su}(N)$ to $T \equiv \{T^a\}$ from eq. (1.200), the matrix elements of adjoint generators ad_{T^a} in this basis are simply $[ad_{T^a}]^{bc}_T = -f^{abc}$.

It is now possible to define the Killing form $\langle \cdot, \cdot \rangle_{\mathfrak{su}(N)}$ as

$$\langle \cdot, \cdot \rangle_{\mathfrak{su}(N)} : \mathfrak{su}(N) \times \mathfrak{su}(N) \to \mathbb{C},\ (A, B) \mapsto \langle A, B \rangle_{\mathfrak{su}(N)} \equiv \mathrm{Tr}[ad_A ad_B]. \tag{1.210}$$

For the T basis vectors, the Killing form reads

$$\langle T^a, T^b \rangle_{\mathfrak{su}(N)} = f^{aij} f^{bji}. \tag{1.211}$$

This result implies that the Killing form is a symmetric bilinear form on $\mathfrak{su}(N)$ and as such can always be diagonalized. For a simple Lie algebra like $\mathfrak{su}(N)$, the Killing form is non-degenerate, which follows from the Cartan criterion [118, 119]. On the other hand, the Lie group $SU(3)$ is a compact manifold, which implies that the Killing form $\mathfrak{su}(N)$ is positive semi-definite. These two facts together mean that there exists a basis of generators T^a, for which

$$\langle T^a, T^b \rangle_{\mathfrak{su}(N)} = f^{aij} f^{bji} = \lambda \delta^{ab}, \tag{1.212}$$

where $\lambda \in \mathbb{C}$ can be freely adjusted by rescaling T^a. Another well known, useful fact[†] states that in a simple Lie algebra, any symmetric, bilinear form $F(A, B)$ satisfying

$$F([A, B], C) = F(A, [B, C]) \tag{1.213}$$

is proportional to the Killing form. An example would be $F(A, B) = \mathrm{Tr}[AB]$, which is symmetric by cyclicity and satisfies the above property as

$$\mathrm{Tr}[A[B, C]] = \mathrm{Tr}[ABC] - \mathrm{Tr}[ACB] = \mathrm{Tr}[ABC] - \mathrm{Tr}[BAC] = \mathrm{Tr}[[A, B]C]. \tag{1.214}$$

In a basis diagonalizing the Killing form,

$$\mathrm{Tr}[T^a T^b] \propto \langle T^a, T^b \rangle_{\mathfrak{su}(N)} = \lambda \delta^{ab} \Longrightarrow \mathrm{Tr}[T^a T^b] = T_R \delta^{ab}, \tag{1.215}$$

The constant T_R on the right hand side can be freely adjusted by rescaling the generators, and is usually chosen by convention as $T_R = 1/2$, as was mentioned above.

[†]A proof can be found for example in ref. [120].

The structure constants defined in eq. (1.200) are obviously antisymmetric in the first two indices. In a simple Lie algebra, they are totally antisymmetric, which can be seen as follows. The value of a structure constant can be obtained as

$$\frac{2}{i}\mathrm{Tr}[T^a[T^b,T^c]] = 2f^{bcd}\mathrm{Tr}[T^a,T^d] = f^{bca} \tag{1.216}$$

by eq. (1.215). On the other hand,

$$\begin{aligned}\frac{2}{i}\mathrm{Tr}[T^a[T^b,T^c]] =& \frac{2}{i}(\mathrm{Tr}[T^aT^bT^c] - \mathrm{Tr}[T^aT^cT^b]) = \frac{2}{i}(\mathrm{Tr}[T^aT^bT^c] - \mathrm{Tr}[T^bT^aT^c]) \\ =& \frac{2}{i}\mathrm{Tr}[[T^a,T^b]T^c] = 2f^{abd}\mathrm{Tr}[T^dT^c] = f^{abc},\end{aligned} \tag{1.217}$$

which leads to $f^{abc} = f^{bca}$. Combining this with the antisymmetry in the first two indices gives

$$f^{abc} = -f^{bac} = -f^{acb}. \tag{1.218}$$

This proves that the structure constants are antisymmetric under a transposition of any pair of indices.

Consider now the matrix on the left hand side of the first identity in eq. (1.199). It commutes with all generators T^b:

$$[T^aT^a,T^b] = T^a[T^a,T^b] + [T^a,T^b]T^a = if^{abc}\{T^a,T^c\} = 0, \tag{1.219}$$

since the structure constants were shown to be totally antisymmetric in eq. (1.218). By the Schur's Lemma [121], T^aT^a is then proportional to the identity:

$$T^aT^a = C_F^{(2)}\mathbb{1}^{(c)}. \tag{1.220}$$

To recover the value of $C_F^{(2)}$, take the trace of both sides of this equation and use eqs. (1.215) and (1.203):

$$\mathrm{Tr}[T^aT^a] = \frac{1}{2}\delta^{aa} = \frac{N^2-1}{2}, \qquad\qquad C_F^{(2)}\mathrm{Tr}[\mathbb{1}^{(c)}] = C_F^{(2)}N, \tag{1.221}$$

so

$$C_F^{(2)} = \frac{N^2-1}{2N}. \tag{1.222}$$

This proves the first result in eq. (1.199).

Any $N \times N$ matrix A with complex valued elements can be written as

$$A = A^0\mathbb{1}^{(c)} + A^aT^a. \tag{1.223}$$

The complex coefficients A^0 and A^a are given by

$$A^0 = \frac{1}{N}\mathrm{Tr}[A], \qquad\qquad A^a = 2\mathrm{Tr}[AT^a], \tag{1.224}$$

which follows from eq. (1.215) and the tracelessness of $\mathfrak{su}(N)$ matrices in the fundamental representation. The elements of the matrix A then satisfy

$$A_{ij} = \frac{1}{N}A_{kk}\delta_{ij} + 2A_{lk}T^a_{kl}T^a_{ij}. \tag{1.225}$$

This relation can be transformed as

$$\left[T^a_{ij}T^a_{kl} - \frac{1}{2}\left(\delta_{il}\delta_{jk} - \frac{1}{N}\delta_{ij}\delta_{kl}\right)\right] A_{lk} = 0. \tag{1.226}$$

Since this equality holds for any matrix A, the expression in the square brackets has to vanish. The second identity in eq. (1.199) follows now immediately by multiplying it by T^b_{jk}:

$$0 = T^a_{ij}T^b_{jk}T^a_{kl} - \frac{1}{2}\delta_{il}T^b_{kk} + \frac{1}{2N}T^b_{il} = \left[T^aT^bT^a + \frac{1}{2N}T^b\right]_{il} \Longrightarrow T^aT^bT^a = -\frac{1}{2N}T^b, \tag{1.227}$$

where the second term vanished by $\mathrm{Tr}[T^b] = 0$.

The decomposition of eqs. (1.223) and (1.224) can be applied to the matrix $A = T^aT^b$:

$$T^aT^b = \frac{1}{N}\mathrm{Tr}[T^aT^b] + 2\mathrm{Tr}[T^aT^bT^c]T^c. \tag{1.228}$$

The coefficient multiplying T^c can also be written as

$$2\mathrm{Tr}[T^aT^bT^c] = \mathrm{Tr}[T^a\{T^b, T^c\}] + \mathrm{Tr}[T^a[T^b, T^c]] = \frac{d^{abc} + if^{abc}}{2}, \tag{1.229}$$

where eq. (1.216) and the antisymmetry of f^{abc} were used in the last equality. The above equation is the definition of a symbol d^{abc}. It is clearly symmetric in the last two indices. The symmetry in the first two indices can easily be derived:

$$\begin{aligned} d^{bac} \equiv& 2\mathrm{Tr}[T^b\{T^a, T^c\}] = 2(\mathrm{Tr}[T^bT^aT^c] + \mathrm{Tr}[T^bT^cT^a]) \\ =& 2(\mathrm{Tr}[T^aT^cT^b] + \mathrm{Tr}[T^aT^bT^c]) = 2\mathrm{Tr}[T^a\{T^b, T^c\}] = d^{abc}, \end{aligned} \tag{1.230}$$

so any contraction of two or three indices of d^{abc} with f^{abc} must vanish. Thus

$$f^{abd}\mathrm{Tr}[T^aT^bT^c] = \frac{i}{4}f^{abd}f^{abc}. \tag{1.231}$$

On the other hand,

$$\begin{aligned} f^{abd}\mathrm{Tr}[T^aT^bT^c] =& -i\mathrm{Tr}[(if^{bda}T^a)T^bT^c] = -i\mathrm{Tr}[[T^b, T^d]T^c] \\ =& -i\mathrm{Tr}[T^bT^dT^bT^c] + i\mathrm{Tr}[T^dT^bT^bT^c]. \end{aligned} \tag{1.232}$$

The first term can be simplified using the second identity in eq. (1.199) while the factor of T^bT^b in the second is equal to $C_F^{(2)}\mathbb{1}^{(c)}$. This leads to

$$f^{abd}\mathrm{Tr}[T^aT^bT^c] = i\left(\frac{1}{2N} + C_F^{(2)}\right)\mathrm{Tr}[T^dT^c] = \frac{i}{2}\left(\frac{1}{2N} + \frac{N^2-1}{2N}\right)\delta^{cd} = \frac{iN}{4}\delta^{cd}. \tag{1.233}$$

Comparing the last expression with eq. (1.231) yields

$$f^{abd}f^{abc} = N\delta^{cd}. \tag{1.234}$$

The form of this result should not be surprising. Since f^{abc} constitute matrix elements of generators ad_{T^a}, this is the analogue of eq. (1.220) for the adjoint representation:

$$f^{abd}f^{abc} = C_A^{(2)}\delta^{dc}, \tag{1.235}$$

with

$$C_A^{(2)} = N. \tag{1.236}$$

The left hand sides of the third and fourth identity in eq. (1.199) can now be simply computed:

$$f^{acd}f^{bcd}T^aT^b = C_A^{(2)}\delta^{ab}T^aT^b = C_A^{(2)}C_F^{(2)}\mathbb{1}^{(c)}, \tag{1.237}$$

and

$$\begin{aligned} f^{abc}T^aT^bT^c =& \frac{f^{abc}}{2}(\{T^a,T^b\}+[T^a,T^b])T^c = \frac{f^{abc}}{2}[T^a,T^b]T^c = \frac{i}{2}f^{abc}f^{abd}T^dT^c \\ =& \frac{i}{2}C_A^{(2)}T^cT^c = \frac{i}{2}C_A^{(2)}C_F^{(2)}\mathbb{1}^{(c)}, \end{aligned} \tag{1.238}$$

where in the second equality of the second equation, the first term vanishes due to the symmetry of the anticommutator and antisymmetry of the structure constants.

The four identities in eq. (1.199) prove to be sufficient to entirely resolve the color algebra in the NLO and NNLO calculation of the q^2 spectrum. To all orders in QCD, in the unpolarized spectrum, the matrix multiplication of $\mathfrak{su}(3)$ generators will result in traces of chains of T^a for the main fermion line and all closed fermion loops, just as in the spin space. Here, there is no additional complication of projector distinguishing between different colors. Whenever two quark lines are connected with a gluon, the adjoint indices ab of the generators T^a and T^b from the vertices of the gluon line are repeated and summed over due to the factor of δ^{ab} from the gluon propagator. This is also the case when a gluon is exchanged between two points on a single line. At the NLO, all diagrams are formed by a single exchange of a gluon attached to the main line (see figure 6), so the color structure comes down to

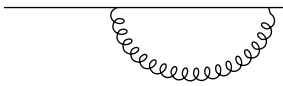

$$\propto \frac{1}{3}\mathrm{Tr}[T^aT^a] = C_F^{(2)} = \frac{3^2-1}{2\cdot 3} = \frac{4}{3}, \tag{1.239}$$

with the factor of $1/3$ due to the averaging over the external b quark color. The color trace was computed by the first identity in eq. (1.199). One may neglect the Qcb vertices, the Q propagator, and the flavors of quarks in the above diagram, as the positioning of these elements does not affect the color algebra.

At the NNLO there are just four additional $\mathfrak{su}(3)$ generator configurations to consider. First, there can be two gluons exchanged between vertices on the main fermion line. In this case, there are three possible structures:

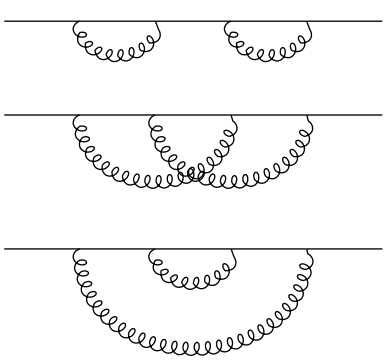

$$\begin{aligned} &\propto \frac{1}{3}\mathrm{Tr}[T^aT^aT^bT^b] = \left(C_F^{(2)}\right)^2 = \frac{16}{9}, \\ &\propto \frac{1}{3}\mathrm{Tr}[T^aT^bT^aT^b] = \frac{1}{3}\left(-\frac{1}{6}\right)3C_F^{(2)} = -\frac{2}{9}, \\ &\propto \frac{1}{3}\mathrm{Tr}[T^aT^bT^bT^a] = \frac{1}{3}\mathrm{Tr}[T^aT^aT^bT^b] = \frac{16}{9}. \end{aligned} \tag{1.240}$$

All three color traces were computed with the first two results of eq. (1.199). The next color structure comes from closed quark loops on gluon lines. At the NNLO, there is only one possibility:

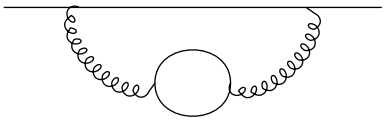

$$\propto \frac{1}{3}\mathrm{Tr}[T^a T^b]\mathrm{Tr}[T^a T^b] = \frac{1}{12}\delta^{ab}\delta^{ab} = \frac{2}{3}. \tag{1.241}$$

Another arrangement of color factors at the NNLO comes from Faddeev-Popov ghost and gluon loops on gluon lines. Both the three-gluon and the ghost-gluon vertices are proportional to the color factor f^{abc}:

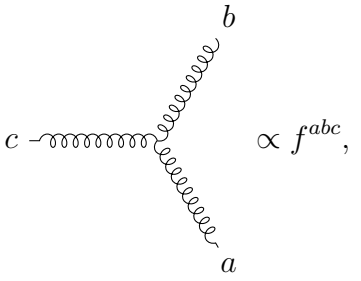

$$\propto f^{abc}, \tag{1.242}$$

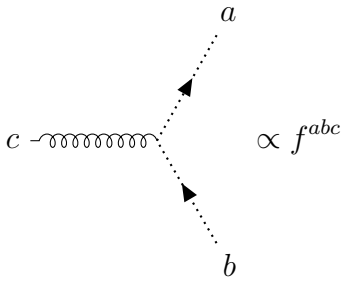

$$\propto f^{abc}$$

while both the gluon and ghost propagators do not change colors and thus are simply multiplied by a color delta. The ambiguity in the overall sign of the three-gluon vertex is resolved by the momentum-dependent factor multiplying the structure constant. These Feynman rules will be further discussed in section 3.1. The ghost lines in such diagrams are arranged as

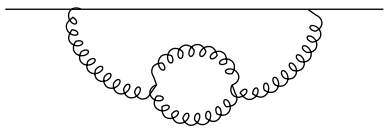

$$\propto \frac{1}{3}f^{acd}f^{bcd}\mathrm{Tr}[T^a T^b] = \frac{1}{3}C_A^{(2)}C_F^{(2)}\mathrm{Tr}[\mathbb{1}^{(c)}] = 4, \tag{1.243}$$

where the contraction of adjoint indices was computed with the third identity in eq. (1.199). Exactly the same result follows for diagrams with a ghost loop. The last color structure comes from diagrams with three gluon lines emitted from the main line and joined at a single three-gluon vertex:

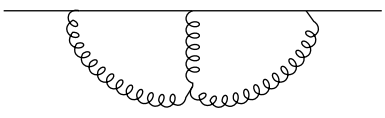

$$\propto \frac{1}{3}f^{abc}\mathrm{Tr}[T^a T^b T^c] = \frac{1}{3}\frac{i}{2}C_A^{(2)}C_F^{(2)}\mathrm{Tr}[\mathbb{1}^{(c)}] = 2i, \tag{1.244}$$

with the contraction obtained using the last identity in eq. (1.199).

1.7 Sample Calculation - 2

I will now return to the computation of the diagram $(2a)$, begun in section 1.3. After extracting all factors of i, numbers and other constants, applying the leading order relation $G_F = \sqrt{2}g_q^2/(8q^2)$ for the effective theory in which the lepton pair is replaced with Q,

resolving the color structure according to the result of eq. (1.239), and recognizing the spin space matrix multiplication as a trace, this diagram's contribution reads:

$$\begin{aligned}\frac{d\Gamma^{(1)}_{(2a)}}{dq^2} = &-\frac{4}{9}\frac{G_F^2|V_{cb}|^2\alpha_s}{\pi}(\tilde{\mu})^{4\epsilon}\mathrm{Im}\Big[\int\frac{d^Dk_1}{i(2\pi)^D}\frac{d^Dk_2}{i(2\pi)^D}\frac{1}{D_1^2D_2D_3D_4D_5}\times\\ &\big(q^2g_{\mu_1\mu_3}-(k_2+p_b)_{\mu_1}(k_2+p_b)_{\mu_3}\big)\big(k_1^2g_{\mu_2\mu_4}-(1-\xi_g)k_{1\mu_2}k_{1\mu_4}\big)\times\\ &\mathrm{Tr}[(\not{p}_b+m_b)\gamma^{\mu_1}P_L(-\not{k}_2+m_c)\gamma^{\mu_2}(-\not{k}_1-\not{k}_2+m_c)\gamma^{\mu_3}P_L(\not{p}_b-\not{k}_1+m_b)\gamma^{\mu_4}]\Big].\end{aligned} \tag{1.245}$$

In the above expression, $\tilde{\mu}$ is the renormalization scale introduced during the discussion of dimensional regularization, and the propagator denominators are defined as

$$\begin{aligned}&\tilde{D}_1\equiv k_1^2, && \tilde{D}_2\equiv k_2^2-m_c^2, && \tilde{D}_3\equiv(k_2+p_b)^2-q^2,\\ &\tilde{D}_4\equiv(k_1-p_b)^2-m_b^2, && && \tilde{D}_5\equiv(k_1+k_2)^2-m_c^2,\end{aligned} \tag{1.246}$$

with $D_a\equiv\tilde{D}_a+i\varepsilon$. In the NDR scheme supplemented with the procedure described at the end of section 1.5, out of the possible 16 terms in the fermion trace, only four are non zero:

$$\begin{aligned}&\mathrm{Tr}[(\not{p}_b+m_b)\gamma^{\mu_1}P_L(-\not{k}_2+m_c)\gamma^{\mu_2}(-\not{k}_1-\not{k}_2+m_c)\gamma^{\mu_3}P_L(\not{p}_b-\not{k}_1+m_b)\gamma^{\mu_4}]\\ =&\frac{1}{2}\Big(-p_{b\mu_5}k_{2\mu_6}(k_1+k_2)_{\mu_7}(k_1-p_b)_{\mu_8}\mathrm{Tr}^{51627384}+m_b^2k_{2\mu_5}(k_1+k_2)_{\mu_6}\mathrm{Tr}^{152634}\\ &-m_c^2p_{b\mu_5}(k_1-p_b)_{\mu_6}\mathrm{Tr}^{512364}+m_b^2m_c^2\mathrm{Tr}^{1234}\Big),\end{aligned} \tag{1.247}$$

where the factor of $1/2$ is the remnant of the chiral projectors. The traces of γ^μ chains can be calculated using eq. (1.175). For the trace of 8 γ^μ there will be $7\cdot5\cdot3=105$ terms with 4 factors of the metric tensor each. Similarly, for the second and third trace, there will be $5\cdot3=15$ terms, and for the last trace only 3. After expanding the parentheses with momenta, the total number of terms will be $4\cdot105+2\cdot15+2\cdot15+3=483$. Each of those terms must then be contracted with $(1+4)\cdot(1+1)=10$ terms coming from the numerators of the gauge boson propagators, resulting in a sum of 4830 Lorentz scalars. After some algebraic manipulations, the contribution can be brought into the following form:

$$\begin{aligned}\frac{d\Gamma^{(1)}_{(2a)}}{dq^2} = &-\frac{4}{9}\frac{G_F^2|V_{cb}|^2\alpha_s}{\pi}(\tilde{\mu})^{4\epsilon}D^{(\gamma)}\mathrm{Im}\Big[\int\frac{d^Dk_1}{i(2\pi)^D}\frac{d^Dk_2}{i(2\pi)^D}\frac{1}{D_1^2D_2D_3D_4D_5}\times\\ &\Big(\frac{1}{0!}(A^{(0)}+\xi_g\tilde{A}^{(0)})+\frac{1}{1!}(A^{(1)}+\xi_g\tilde{A}^{(1)})_aP_a+\frac{1}{2!}(A^{(2)}+\xi_g\tilde{A}^{(2)})_{ab}P_aP_b\\ &+\frac{1}{3!}(A^{(3)}+\xi_g\tilde{A}^{(3)})_{abc}P_aP_bP_c+\frac{1}{4!}(A^{(4)}+\xi_g\tilde{A}^{(4)})_{abcd}P_aP_bP_cP_d\Big)\Big],\end{aligned} \tag{1.248}$$

where $P\equiv(k_1^2,k_2^2,(k_1k_2),(k_1p_b),(k_2p_b))$ constitutes a basis of possible scalar products of momenta[†]. Symbols $A^{(n)}$ are rank-n fully symmetric tensors. By dimensional analysis, their elements are homogeneous polynomials of degree $4-n$ in the possible mass scales: m_b^2, m_c^2,

[†]The external momentum is fixed to $p_b^2=m_b^2$ and need not be included.

and q^2. A direct calculation yields

$$\begin{aligned} A^{(0)} =&0, & \tilde{A}^{(0)} =&0, \\ A^{(1)T} =&-2m_b^2 m_c^2 M_-^2(1,0,0,0,0), & \tilde{A}^{(1)T} =&(0,0,0,0,0), \end{aligned} \tag{1.249}$$

$$A^{(2)} = 2m_b^2 M_2^2 \begin{pmatrix} 0 & 1 & 1 & \frac{(D-1)m_c^2 M_-^2}{2m_b^2 M_2^2} & \frac{-2m_c^2}{M_2^2} \\ & 0 & 0 & 0 & 0 \\ & & 0 & \frac{2m_c^2}{M_2^2} & 0 \\ & & & \frac{2M_+^2}{M_2^2} & 0 \\ & & & & 0 \end{pmatrix}, \quad \tilde{A}^{(2)} = m_c^2 m_b^2 \begin{pmatrix} 0 & 0 & 2 & \frac{M_+^2}{m_b^2} & 0 \\ & 0 & 0 & 0 & 0 \\ & & 0 & -4 & 0 \\ & & & \frac{-4M_+^2}{m_b^2} & 0 \\ & & & & 0 \end{pmatrix}$$

where $M_\pm^2 \equiv m_b^2 \pm (D-2)q^2$, and $M_2^2 \equiv m_b^2 + m_c^2 + (D-2)q^2$. The coefficients $A^{(3)}$ and $\tilde{A}^{(3)}$ read

$$\begin{aligned} A^{(3)}_{112} =&4(D-3)m_b^2, & A^{(3)}_{115} =&2(D-5)(D-2)q^2 + 2(D-3)m_b^2, \\ A^{(3)}_{122} =&A^{(3)}_{123} = A^{(3)}_{125} = -A^{(3)}_{234} = -4m_b^2, & A^{(3)}_{155} =&2A^{(3)}_{244} = -2A^{(3)}_{345} = -8M_2^2, \\ A^{(3)}_{124} =&(D-3)M_3^2, & A^{(3)}_{133} =&-4(D-2)m_b^2, \\ A^{(3)}_{134} =&2(D-2)(2q^2 - m_b^2), & A^{(3)}_{135} =&2M_3^2, \\ A^{(3)}_{145} =&-2m_b^2 + 2(D-2)(m_c^2 - q^2), & & \\ \tilde{A}^{(3)}_{112} =&2\tilde{A}^{(3)}_{123} = -\tilde{A}^{(3)}_{234} = 4m_b^2, & \tilde{A}^{(3)}_{115} =&\tilde{A}^{(3)}_{145} = 2M_+^2, \\ \tilde{A}^{(3)}_{124} =&-\left((D-2)q^2 + 5m_b^2 + m_c^2\right), & \tilde{A}^{(3)}_{244} =&2\tilde{A}^{(3)}_{135} = -\tilde{A}^{(3)}_{345} = 4M_2^2, \end{aligned} \tag{1.250}$$

with all the other values determined by symmetry or vanishing. The constant M_3^2 is defined as $m_c^2 - m_b^2 + (D-2)q^2$. The rank-four tensor coefficients are

$$\begin{aligned} A^{(4)}_{1125} =&2(D-3), & A^{(4)}_{1224} =&-2(D-1), & A^{(4)}_{1234} =&2(2-D), \\ A^{(4)}_{1244} =&4(2-D), & A^{(4)}_{1245} =&2(3-D), & A^{(4)}_{2244} =&8, \\ \tilde{A}^{(4)}_{2244} =&4\tilde{A}^{(4)}_{1245} = -4\tilde{A}^{(4)}_{1125} = -4\tilde{A}^{(4)}_{1224} = -8. & & & & \end{aligned} \tag{1.251}$$

Again, all the other values are either determined by symmetry or vanish.

The next step is to change the basis of scalar products from P_a to D_a. Solving a system of linear equations gives

$$\begin{aligned} k_1^2 =&\tilde{D}_1, & k_2^2 =&\tilde{D}_2 + m_c^2, \\ k_1 k_2 =&\frac{\tilde{D}_5 - \tilde{D}_1 - \tilde{D}_2}{2}, & k_1 p_b =&\frac{\tilde{D}_1 - \tilde{D}_4}{2}, \\ k_2 p_b =&\frac{\tilde{D}_3 - \tilde{D}_2 - m_b^2 - m_c^2 + q^2}{2}. & & \end{aligned} \tag{1.252}$$

The Feynman regulator plays no role in the numerators, so in the above equation one can freely change $\tilde{D}_a \to D_a$. In other diagrams, it is possible that the set of distinct denominators will not constitute a full basis in the space of momentum products. In such cases, it should be enlarged by squares of combinations of loop and external momenta, i.e. inverse massless propagators, until it forms a sufficient set of linearly independent scalar products to form a basis.

$I^{(2a)}_{00110}$	$\epsilon-1$	$I^{(2a)}_{00101}$	$1-\epsilon$
$I^{(2a)}_{1(-1)101}$	$\epsilon-1$	$I^{(2a)}_{101(-1)1}$	$\epsilon-1$
$I^{(2a)}_{2(-1)1(-1)1}$	$\frac{1-\xi_g}{2}$	$I^{(2a)}_{10110}$	$2\epsilon m_b^2-M_+^2$
$I^{(2a)}_{01110}$	$(1-\epsilon)\left(M_{bc-}^2+2q^2\right)$	$I^{(2a)}_{11001}$	M_+^2
$I^{(2a)}_{10101}$	$\epsilon M_{bc+}^2-q^2\left(\left(\frac{1}{2}-\epsilon\right)\xi_g-\frac{3}{2}+2\epsilon^2\right)$	$I^{(2a)}_{01101}$	$(1-\epsilon)\left(2q^2-M_{bc-}^2\right)$
$I^{(2a)}_{2(-1)101}$	$\frac{\xi_g-1}{2}M_3^2$	$I^{(2a)}_{01011}$	$q^2(\epsilon^2+\epsilon-2)-\epsilon M_{bc+}^2$
$I^{(2a)}_{10011}$	$m_c^2-2(\epsilon-1)q^2$	$I^{(2a)}_{11010}$	$m_c^2-2(\epsilon-1)q^2$
$I^{(2a)}_{00111}$	$(1-\epsilon)\left(M_{bc-}^2+2q^2\right)$	$I^{(2a)}_{1(-1)111}$	$(\epsilon-1)m_b^2$
$I^{(2a)}_{111(-1)1}$	$(\epsilon-1)m_c^2$	$I^{(2a)}_{(-1)1111}$	$2(\epsilon-1)q^2$
$I^{(2a)}_{11(-1)11}$	$-M_2^2$	$I^{(2a)}_{201(-1)1}$	$\frac{\xi_g-1}{2}\left(M_+^2-m_c^2\right)$
$I^{(2a)}_{1111(-1)}$	$(\epsilon-1)m_b^2$	$I^{(2a)}_{11110}$	$m_b^4-\left(m_c^2-q^2\right)\left(M_3^2+m_b^2\right)$
$I^{(2a)}_{11101}$	$M_+^2\left(q^2-m_b^2\right)+m_c^4$	$I^{(2a)}_{10111}$	$m_b^4-\left(m_c^2-q^2\right)\left(M_3^2+m_b^2\right)$
$I^{(2a)}_{20101}$	$\frac{\xi_g-1}{2}\left((1-2\epsilon)M_{bc+}^2q^2+M_{bc-}^4+2(\epsilon-1)q^4\right)$		
$I^{(2a)}_{11011}$	$2\left((1-2\epsilon)M_{bc+}^2q^2+m_b^4+m_c^4+2(\epsilon-1)q^4\right)$		
$I^{(2a)}_{01111}$	$(\epsilon-1)M_{bc-}^4+(\epsilon^2+\epsilon-2)(2q^2-M_{bc+}^2)q^2-\epsilon^2q^4$		
$I^{(2a)}_{11111}$	$\left(q^2-M_{bc+}^2\right)\left((1-2\epsilon)M_{bc+}^2q^2+M_{bc-}^4+2q^4(\epsilon-1)\right)$		

Table 2: The scalar integrals and their coefficients contributing to the diagram $(2a)$. The constants $M_{bc\pm}^2$ are equal to $m_b^2\pm m_c^2$.

After another series of elementary simplifications, the result for the diagram can be written as

$$\frac{d\Gamma^{(1)}_{(2a)}}{dq^2}=-\frac{4}{9}\frac{G_F^2|V_{cb}|^2\alpha_s}{\pi}D^{(\gamma)}C_{abcde}\mathrm{Im}[I^{(2a)}_{abcde}]. \tag{1.253}$$

The coefficients C_{abcde} are polynomials in D, m_b^2, m_c^2, q^2, and the gauge fixing parameter ξ_g. The scalar Feynman Integrals $I^{(2a)}_{abcde}$ are defined as

$$I^{(2a)}_{abcde}\equiv\tilde{\mu}^{4\epsilon}\int\frac{d^Dk_1}{i(2\pi)^D}\frac{d^Dk_2}{i(2\pi)^D}\frac{1}{D_1^aD_2^bD_3^cD_4^dD_5^e}. \tag{1.254}$$

After changing the basis of scalar products, in addition to non-zero scalar integrals that have to be computed, there also appear 7 additional integrals:

$$I^{(2a)}_{10100},\quad I^{(2a)}_{10001},\quad I^{(2a)}_{21000},\quad I^{(2a)}_{20100},\quad I^{(2a)}_{11100},\quad I^{(2a)}_{20001},\quad I^{(2a)}_{21100}, \tag{1.255}$$

in which the k_1- and k_2-loop integrals factorize, and the k_1 part is scaleless, thus vanishing in dimensional regularization.

There are 28 non-vanishing scalar integrals for this diagram, listed together with their corresponding coefficients C_{abcde} in table 2. Computing each of them using the direct technique described for the one loop diagram in section 1.4 is unfeasible, as even a single arbitrary 2-loop integral with three independent mass scales constitutes a considerable challenge. Considering that there are two[†] more diagrams at this level, and 8275 non-zero, unique, and significantly more complicated 3 loop integrals at the NNLO, it is necessary to approach the calculation with a completely different method. The next chapter is dedicated to its description.

[†]The diagram $(2a')$ gives the same result as $(2a)$ due to mirror symmetry.

Chapter 2:

The IBP Reduction and its Applications

At the end of the previous chapter, it has been illustrated how a significant number of scalar integrals emerges at intermediate steps of a typical multiloop calculation. The discussion focused on the simplest case of "$1 \to 1$" diagrams, as these are the most relevant to the computation of inclusive decay widths and spectra, but this conclusion holds also for a perturbative description of scattering. Indeed, the problem becomes even more exacerbated for diagrams with more than two external legs. The only modification to the arguments of section 1.7 is that the integral coefficients $C_{a_1 \ldots a_n}$ will additionally depend on some basis of generalized Mandelstam variables, increasing the number of terms remaining after computing fermion traces and contracting the Lorentz indices. If the process is polarized in spins, one can construct a set of projectors that isolate Lorentz scalars multiplying each spinor in the final result. Then, the procedure presented in the previous chapter calculations from applies to each of those scalars separately.

The amount of scalar integrals grows rapidly with the complexity of a diagram. For cutting edge calculations, their number can easily reach hundreds of thousands and even several million. The origin of this issue was already apparent in section 1.7. Each of the boson propagators in an arbitrary gauge multiplies the number of terms by at least a factor of 2. In the absence of chirality distinguishing vertices, after expanding the parenthesis in the numerators of massive fermion propagators, the number of individual, non-vanishing traces coming from each closed fermion loop and external fermion line with n vertices is 2^{n-1} and 2^n respectively. The contributions of each fermion line are then multiplied by each other. Finally, the number of terms coming from a fermion trace with m gamma matrices is $(m-1)!! \equiv (m-1)(m-3)\ldots 3 \cdot 1$. Many of the terms are linearly dependent in the algebra spanned by scalar products of loop and external momenta but still several others persist. If a diagram depends on any additional mass scales, such as arbitrary external momenta or Mandelstam variables, some of the linear relations among various terms are broken, further increasing the number of integrals.

Fortunately, the scalar integrals in this large family inherited from a given diagram differ only by their indices, i.e. integer powers of the propagator denominators. It is therefore natural to suspect that they are somehow connected with each other. A study of functional relations between scalar integrals can indeed reduce their number by orders of magnitude, but a more careful examination also provides powerful tools for their evaluation. Using these, one can evade altogether the laborious calculation of loop integrals with the direct method presented in section 1.4. This chapter provides a review of the results of this analysis that were directly relevant to the completion of this project. It does not constitute an exhaustive survey, as this is an extensive and still very active field.

2.1 Integration-By-Parts Identities

The simplest type of relations between scalar integrals follows from the symmetry under loop momentum shifts. Consider, for example, the first perturbative correction to the photon propagator in QED, called the vacuum polarization contribution:

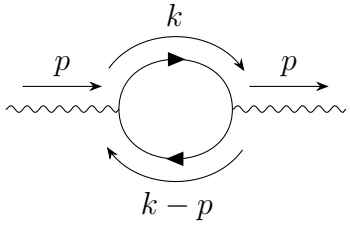

$$= C_{ab}^{VP} \int \frac{d^D k}{i(2\pi)^D} \frac{1}{\left(k^2 - \tilde{m}_e^2\right)^a \left((k-p)^2 - \tilde{m}_e^2\right)^b} \equiv C_{ab}^{VP} I_{ab}^{VP}, \quad (2.1)$$

where $\tilde{m}_e^2 \equiv m_e^2 - i\varepsilon$, and the indices a and b are bound within some range that will not be relevant for the current discussion. Changing the integration variable as $k \equiv p - \tilde{k}$ must not affect the result but it swaps the indices a and b. The scalar integrals are thus symmetric under their interchange:

$$I_{ab}^{VP} = I_{ba}^{VP}. \quad (2.2)$$

Such relations only hold true if in a considered graph two lines with equal masses can be freely interchanged without changing the graph.

A much larger class of relations comes from an observation[†], that scalar integrals in regularization schemes that do not restrict the loop integration range are invariant under a general linear variable change $k^\mu \to ak^\mu + l^\mu$, where a is a non-zero number, and l^μ is some D-momentum independent of k. The first set of relations can be obtained by taking $a = 1$ and $l^\mu = \delta p^\mu$, with some finite D-vector p^μ and δ infinitesimal. Expanding in δ gives

$$\begin{aligned} I =& \int \frac{d^D k}{i(2\pi)^D} J(k) = \int \frac{d^D k}{i(2\pi)^D} J(k+\delta p) = \int \frac{d^D k}{i(2\pi)^D} \left[J(k) + \delta p^\mu \partial_{k^\mu} J(k)\right] + \mathcal{O}(\delta^2) \\ =& I + \delta \int \frac{d^D k}{i(2\pi)^D} \partial_{k^\mu}\left(p^\mu J(k)\right) + \mathcal{O}(\delta^2), \end{aligned} \quad (2.3)$$

where $J(k)$ is the integrand of a scalar integral. The invariance under loop momentum shifts implies that the integral in the last line must vanish. Next, setting $l^\mu = 0$ and $a = (1+\delta)$ gives

$$\begin{aligned} I =& \int \frac{d^D k}{i(2\pi)^D} J(k) = (1+\delta)^D \int \frac{d^D k}{i(2\pi)^D} J\big((1+\delta)k\big) \\ =& (1 + D\delta) \int \frac{d^D k}{i(2\pi)^D} \left[J(k) + \delta k^\mu \left(\partial_{k^\mu} J(k)\right)\right] + \mathcal{O}(\delta^2) \\ =& I + \delta \int \frac{d^D k}{i(2\pi)^D} \left[J(k)(\partial_{k^\mu} k^\mu) + k^\mu \left(\partial_{k^\mu} J(k)\right)\right] + \mathcal{O}(\delta^2) \\ =& I + \delta \int \frac{d^D k}{i(2\pi)^D} \partial_{k^\mu}\left(k^\mu J(k)\right) + \mathcal{O}(\delta^2), \end{aligned} \quad (2.4)$$

where, in the third equality, $D = \partial_{k^\mu} k^\mu$ was recognized. The symmetry thus leads to the following two types of equations:

$$\int \frac{d^D k_i}{i(2\pi)^D} \partial_{k_i^\mu}\left(p_j^\mu J\right) = 0, \qquad \int \frac{d^D k_i}{i(2\pi)^D} \partial_{k_i^\mu}\left(k_j^\mu J\right) = 0, \quad (2.5)$$

[†]This derivation essentially follows the proof given in ref. [122].

that hold for all loop momenta k_i^μ and all external momenta p_i^μ in a multi-loop integral.

The next observation is that the application of a partial derivative with respect to a loop momentum to an integrand produces terms in which a single index is increased by one and the original integrand is multiplied by some D-momentum. After contracting with either k^μ in the first or p^μ in the second equation and expressing the scalar product as a linear combination of denominators, one obtains a homogeneous linear relation between scalar integrals with indices shifted by ± 1. These are the IBP identities between scalar integrals, that have been already mentioned in the Introduction. They were first applied in refs. [123, 124], and have since been of paramount importance in most multi-loop calculations.

Integrals with more than two external legs satisfy another set of so-called Lorentz Invariance (LI) recurrence equations [125]. In contrast to the IBP relations, LI equations are a consequence of a symmetry under changes of external momenta p_i^μ. When an integral is treated as a function of p_i^μ, $I = I(p_i^\mu)$, it should be invariant under a simultaneous Lorentz transformation of all its external momenta:

$$I(p_i^\mu) = I(p_i^\mu + \delta[T_j]^\mu{}_\nu p_i^\nu), \tag{2.6}$$

where δ again is infinitesimal, and $T_j^{\mu\nu} = -T_j^{\nu\mu} \in \mathfrak{so}(1,3)$, are generators of the Lorentz group. Expanding in δ and using the antisymmetry of T_j gives

$$\sum_i \left(p_i^\nu \partial_{p_i^\mu} - p_i^\mu \partial_{p_i^\nu} \right) I = 0. \tag{2.7}$$

Contracting the above equation with antisymmetric tensors of the form $p_{i\mu}p_{j\nu} - p_{i\nu}p_{j\mu}$ yields the desired set of recurrence relations. Even though the LI equations were derived using a different symmetry, and are obtained by differentiating over the external rather than loop momenta, they can be reduced to linear combinations of IBP relations [126].

The calculation of the one-loop vacuum polarization diagram of eq. (2.1) can again serve as an example. There is a single external momentum p^μ and a single loop momentum k^μ, so the integrals I_{ab}^{VP} satisfy two general IBP relations. After explicitly computing the derivatives and changing the basis of scalar products to the propagator denominators, these become

$$\begin{aligned} (D-2a-b)I_{ab}^{VP} - bI_{(a-1)(b+1)}^{VP} + b(p^2 - 2m_e^2)I_{a(b+1)}^{VP} - 2am_e^2 I_{(a+1)b}^{VP} = 0, \\ (a-b)I_{ab}^{VP} + bI_{(a-1)(b+1)}^{VP} - bp^2 I_{a(b+1)}^{VP} - aI_{(a+1)(b-1)}^{VP} + ap^2 I_{(a+1)b}^{VP} = 0. \end{aligned} \tag{2.8}$$

One way to use these equations would be to find some set of ladder operators that transform integrals with higher indices into those with lower [127–132]. This would effectively "solve" the integral family up to some integrals serving as initial conditions for the recurrence. In general, finding such a solution is very difficult, and even harder to automatize.

In another approach due to Laporta [133], one generates IBP relations for a large set of values of integral indices, and treats it as a system of linear equations for the unknown scalar integrals. The region of the infinite lattice of scalar integrals for which the relations are generated must be specified beforehand, and should cover all integrals that appear in the computation of the considered diagram. Enlarging this region further can yield additional independent equations which can serve to eliminate further integrals. The rank of the system of equations is always smaller than their number, so it can only be used to express some integrals as linear combinations of others. Nevertheless, a sufficiently large set of IBP relations with numerical indices can be used to eliminate the vast majority of integrals.

Continuing the one loop vacuum polarization example and setting $a = 1$ and $b = 0$ in eq. (2.8) together with using the symmetry relation from eq. (2.2) results in

$$(D-2)I_{01}^{VP} - 2m_e^2 I_{02}^{VP} = 0, \qquad I_{01}^{VP} + p^2 I_{02}^{VP} - I_{(-1)2}^{VP} = 0. \tag{2.9}$$

Similarly, for $a = 0$ and $b = 1$ one gets

$$(D-1)I_{01}^{VP} + (p^2 - 2m_e^2)I_{02}^{VP} - I_{(-1)2}^{VP} = 0, \qquad I_{(-1)2}^{VP} - I_{01}^{VP} - p^2 I_{02}^{VP} = 0. \tag{2.10}$$

The last equation is clearly linearly dependent with the second one in eq. (2.9). The other three can be row-reduced, giving

$$\begin{pmatrix} 1 & 0 & -\left(1 + \frac{(D-2)p^2}{2m_e^2}\right) \\ 0 & 1 & -\frac{D-2}{2m_e^2} \\ 0 & 0 & 0 \end{pmatrix} \begin{pmatrix} I_{(-1)2}^{VP} \\ I_{02}^{VP} \\ I_{01}^{VP} \end{pmatrix} = \begin{pmatrix} 0 \\ 0 \\ 0 \end{pmatrix}. \tag{2.11}$$

As expected, the rank of the system is lower than the number of different integrals that appeared in the generated IBP relations. Still, two integrals can be eliminated from the calculation. It is natural to leave I_{01}^{VP}, as it is the simplest one to compute. Indeed, its result can be read out of eq. (1.150).

In an automated approach, after generating all IBP relations for a set of seed integrals, it is necessary to specify some ordering on all n integrals appearing in the generated equations that arranges them from what one considers most to least complicated:

$$I_{\bar{a}_1} \succeq I_{\bar{a}_2} \succeq I_{\bar{a}_3} \succeq \ldots \succeq I_{\bar{a}_{n-1}} \succeq I_{\bar{a}_n}, \tag{2.12}$$

where $\bar{a}_k$ is a vector of indices. Common ordering criteria are:

- by largest sum of positive indices r,
- by largest sum of negative indices s,
- by largest number of strictly positive indices,
- by largest number of strictly negative indices,
- by largest sector ID S,

or some combination of these. The sector ID, defined as

$$S[I_{a_1 \ldots a_d}] \equiv \sum_{k=1}^{d} \Theta\left(a_k - \frac{1}{2}\right) 2^{k-1}, \tag{2.13}$$

specifies which lines of the original diagram are kept as scalar propagators in the considered integral and which become terms in the numerator or are shrunk to a point in the case when $a_k = 0$. The number of preserved lines is a natural measure of complexity of an integral and is often the primary ordering criterion. The number of sectors in an integral family with d indices is 2^d. It is advantageous to order the denominators in the original diagram from least to most complicated. In this way, S is also a measure of how computationally costly the algebraic manipulations of IBP relations are for a given integral. Note that the IBP relations can never change any index from non-positive to positive. Consequently, an

IBP relation generated from a given integral can only involve integrals with smaller or equal S. If any integral in a sector is scaleless, all other integrals in this sector are also scaleless. It is thus sufficient to check scalelessness sector by sector, and only for an integral with all indices either 1 or 0. If a sector with ID S is found to be scaleless, all sectors with lines belonging only to a subset of lines of sector S must also be scaleless. All integrals belonging to scaleless sectors can be set to 0 prior to any row operations.

Once the IBP relations are generated and an ordering of integrals is established, one can proceed with the reduction. This procedure follows the standard Gaussian elimination method. The system of equations E is ordered into groups E_k according to the most complicated integral $I_{\bar{a}_k}$ in the sense of eq. (2.12) appearing in each equation. The first equation in each group E_k is then used to eliminate $I_{\bar{a}_k}$ from all others in its group. After that, a new grouping of equations is established, with the first group containing only one equation. This part of the algorithm terminates when all groups contain a single equation and the upper triangular form is reached. Next, one performs back substitutions, each time expressing the most complicated integral in terms of linear combinations of less complicated ones.

The choice of integrals to preserve after utilizing the IBP relations in the Laporta approach, commonly referred to as Master Integrals (MIs), is in principle arbitrary, and follows directly from the ordering of all integrals. If in the generated IBP relations there were n different non-zero integrals, and the rank of the system was m, the MIs will constitute the least complicated $n-m$ independent integrals in the ordering. As will be discussed in section 2.3, it can be advantageous to specify a set of independent integrals as a priori least complicated on top of any ordering criteria to designate them as MIs by hand. This definition of MIs is also dependent on the system of generated IBP relations. In principle, by enlarging the region of the lattice of integrals under reduction, some MIs may be eliminated while new ones can appear. It was proven in ref. [134] that the integral families inherited from any diagram (with arbitrary indices) form a finite-dimensional vector space. Thus, at some point, enlarging the reduction region becomes superfluous.

In the Laporta approach, the most demanding step in terms of computation time is the row reduction. Depending on the problem, both back substitution and achieving a triangular form can become a bottleneck. To aid the algebraic manipulations of large expressions appearing when rows are added together or rescaled, one can substitute unique random integers for all variables such as Mandelstam variables, masses and the space-time dimension and perform the reduction modulo some large prime number. This substitution can either be performed to eliminate linearly dependent IBP relations from the system prior to the main reduction [135], or in the main reduction itself [136]. In the latter case, after substitutions of several different choices of integers, the result in terms of symbolic values of variables can be reconstructed using one of the variety of probabilistic methods [137–141]. Performing many reductions with integer valued variables as well as consistency checks and error correction turn out to be less demanding than performing a single symbolic reduction. Additionally, it is straightforward to parallelize the reductions for different choices of integer substitutions.

Several competitive implementations of the Laporta algorithm are publicly available. These include `AIR` [142], `Reduze` [143, 144], `LiteRED` [145, 146], `Fire` [147–150], `Kira` [151–157], `NeatIBP` [158, 159], and `Blade` [160]. Throughout the preparation of this thesis, I utilized version 2.3 of the `C++` program `Kira` for all IBP reductions.

2.2 Sample Calculation - 3

The Laporta method described in the previous section can be applied to the scalar integrals encountered in the calculation of the diagram $(2a)$ in section 1.7. With one external and two loop momenta, an integral $I^{(2a)}_{abcde}$ satisfies six IBP relations. Three of them come from differentiating with respect to k_1^μ. They read,

$$(D-2a-b-e)I^{(2a)}_{abcde} - e\left(I^{(2a)}_{(a-1)bcd(e+1)} - I^{(2a)}_{a(b-1)cd(e+1)}\right) - dI^{(2a)}_{(a-1)bc(d+1)e} = 0, \tag{2.14}$$

$$\begin{aligned}&(a-e)I^{(2a)}_{abcde} + a\left(I^{(2a)}_{(a+1)(b-1)cde} - I^{(2a)}_{(a+1)bcd(e-1)}\right) + \\ &+d\left(I^{(2a)}_{(a-1)bc(d+1)e} + I^{(2a)}_{ab(c-1)(d+1)e} - I^{(2a)}_{abc(d+1)(e-1)} - (M_{bc+}-q^2)I^{(2a)}_{abc(d+1)e}\right) + \\ &+e\left(I^{(2a)}_{(a-1)bcd(e+1)} - I^{(2a)}_{a(b-1)cd(e+1)} - 2m_c^2 I^{(2a)}_{abcd(e+1)}\right) = 0,\end{aligned} \tag{2.15}$$

$$\begin{aligned}&(d-a)I^{(2a)}_{abcde} + d\left(2m_b^2 I^{(2a)}_{abc(d+1)e} - I^{(2a)}_{(a-1)bc(d+1)e}\right) + aI^{(2a)}_{(a+1)bc(d-1)e} + \\ &+e\left((M^2_{bc+}-q^2)I^{(2a)}_{abcd(e+1)} - I^{(2a)}_{(a-1)bcd(e+1)} + I^{(2a)}_{a(b-1)cd(e+1)} - I^{(2a)}_{ab(c-1)d(e+1)} + I^{(2a)}_{abc(d-1)(e+1)}\right) = 0.\end{aligned} \tag{2.16}$$

The remaining three follow from differentiating with respect to k_2^μ:

$$\begin{aligned}&(D-2b-c-e)I^{(2a)}_{abcde} - 2em_c^2 I^{(2a)}_{abcd(e+1)} - c(q^2-M^2_{bc-})I^{(2a)}_{ab(c+1)de} - 2bm_c^2 I^{(2a)}_{a(b+1)cde} + \\ &+eI^{(2a)}_{(a-1)bcd(e+1)} - eI^{(2a)}_{a(b-1)cd(e+1)} - cI^{(2a)}_{a(b-1)(c+1)de} = 0,\end{aligned} \tag{2.17}$$

$$\begin{aligned}&(b-e)I^{(2a)}_{abcde} - eI^{(2a)}_{(a-1)bcd(e+1)} + bI^{(2a)}_{(a-1)(b+1)cde} + eI^{(2a)}_{a(b-1)cd(e+1)} + \\ &+c\left(I^{(2a)}_{a(b-1)(c+1)de} + I^{(2a)}_{ab(c+1)(d-1)e} - I^{(2a)}_{ab(c+1)d(e-1)}\right) - bI^{(2a)}_{a(b+1)cd(e-1)} = 0,\end{aligned} \tag{2.18}$$

$$\begin{aligned}&(b-c)I^{(2a)}_{abcde} + b\left((M^2_{bc+}-q^2)I^{(2a)}_{a(b+1)cde} - I^{(2a)}_{a(b+1)(c-1)de}\right) + \\ &+c\left(I^{(2a)}_{a(b-1)(c+1)de} - (M^2_{bc-}+q^2)I^{(2a)}_{ab(c+1)d,e}\right) + \\ &+e\left((M^2_{bc+}-q^2)I^{(2a)}_{abcd(e+1)} - I^{(2a)}_{ab(c-1)d(e+1)} + I^{(2a)}_{abc(d-1)(e+1)} - I^{(2a)}_{(a-1)bcd(e+1)} + I^{(2a)}_{a(b-1)cd(e+1)}\right) = 0.\end{aligned} \tag{2.19}$$

The integrals to be reduced have indices bounded by $r = 5$ and $s = 2$, with r and s being sums of positive and negative indices defined above eq. (2.13). As the reduction is quite small, it does not require much memory to generate all the IBP relations for integrals with r and s up to 10 and 5 respectively. Thanks to this offset, one can be practically sure that no relations were missed, and the obtained MIs do not turn out to be linearly dependent in higher IBP relations. Indeed, a reduction bounded by $(r, s) = (5, 2)$ produces the same result, so in this case such a precaution is not necessary.

For maximal $(r, s) = (10, 5)$, `Kira` 2.3 generates 142412 IBP relations for this family and finds 70910 of them to be linearly independent. On an AMD Ryzen 5950x CPU utilizing 16 threads in parallel and with DDR4 1800MHz RAM, the total reduction time is $6.7s$ and requires 117.8MB of memory. Turning on the numerical reduction followed by reconstruction of the algebraic result changes these numbers to $2.4s$ and 122.3MB. By comparison, for (r, s)

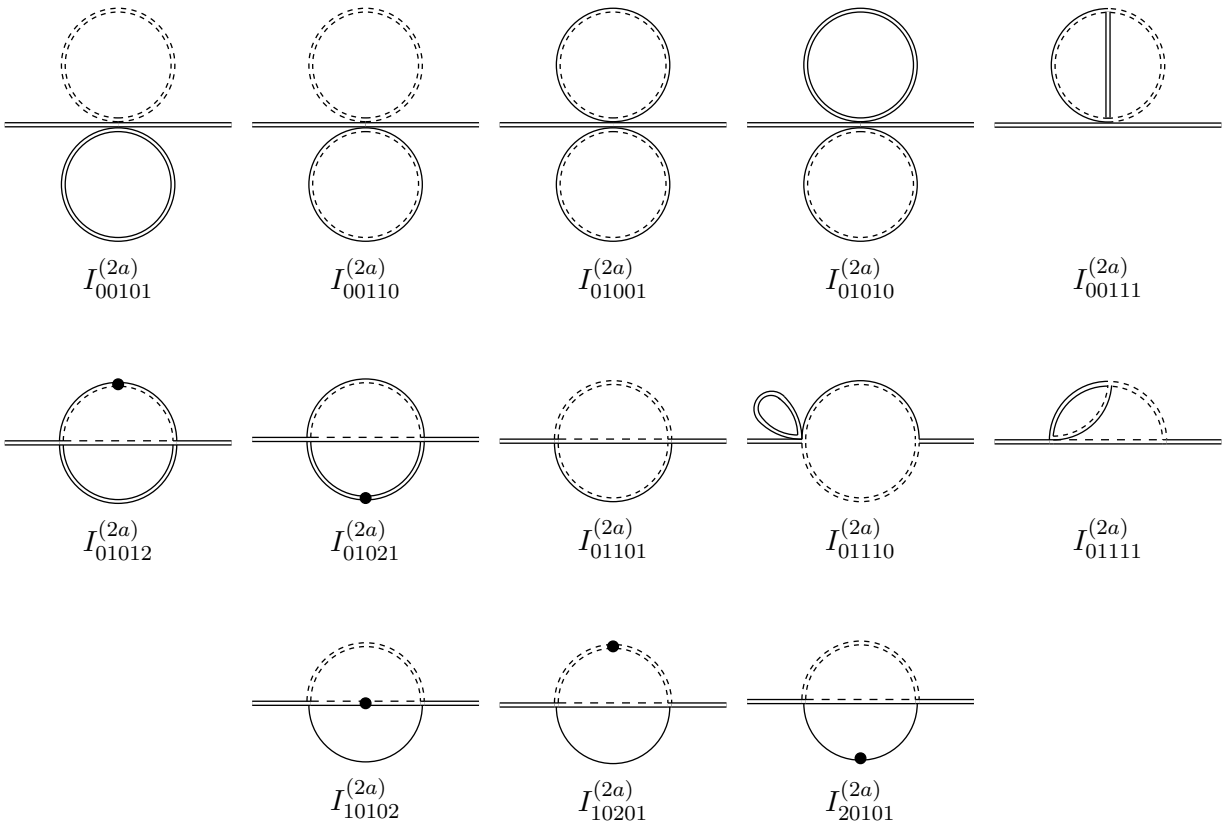

Figure 7: The 13 Master Integrals of the $(2a)$ topology. For the explanation of the different elements see the text.

set to the minimal required values $(5, 2)$ there are 5096 total and 2988 independent IBP relations. The reduction time and memory consumption are $5.7s$ and 30.5MB for the fully algebraic method while in the numerical + reconstruction case these are $2.0s$ and 30.1MB. It is important to note that the performance of the `Kira` algorithm is heavily dependent on the chosen basis and ordering of denominators. If possible, one should avoid denominators with more than 2 different momenta. Massless denominators should always precede massive ones, and those with less symbolic momenta in the squares should be earlier than those with more. If some lines appear only with non-positive indices, they should be relegated to the end of the basis. This is the origin of the momentum routing chosen for the diagram $(2a)$ in eq. (1.127), and the ordering in eq. (1.246).

If in each sector, the total number of negative indices is chosen to be the most important complexity criterion, followed by the number of indices larger than 1, then the following set of 13 MIs is obtained:

$$M^{(2a)} \equiv$$
$$[I^{(2a)}_{00101}, I^{(2a)}_{00110}, I^{(2a)}_{01001}, I^{(2a)}_{01010}, I^{(2a)}_{00111}, I^{(2a)}_{01012}, I^{(2a)}_{01021}, I^{(2a)}_{01101}, I^{(2a)}_{01110}, I^{(2a)}_{01111}, I^{(2a)}_{10102}, I^{(2a)}_{10201}, I^{(2a)}_{20101}]^T. \tag{2.20}$$

The above integrals are presented in figure 7. The different propagators of these diagrams

are defined as:

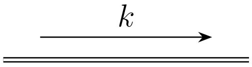 $= \dfrac{1}{k^2 - m_b^2 + i\varepsilon}$, 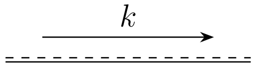 $= \dfrac{1}{k^2 - m_c^2 + i\varepsilon}$,

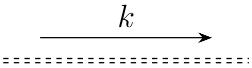 $= \dfrac{1}{k^2 - q^2 + i\varepsilon}$, 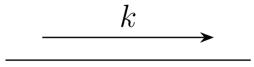 $= \dfrac{1}{k^2 + i\varepsilon}$, (2.21)

while dots on lines indicate that a propagator is squared. The Cutkosky rules rules mentioned in section 1.2 specify that an integral can have a non-vanishing imaginary part only if there exists a cut through that integral which crosses the lines of particles that can simultaneously be put on-shell. The first five MIs above do not have any cuts that can be associated with the creation of real intermediate particles. The 6th and 7th MIs do not have a cut that would be allowed kinematically, since it has to cross through a propagator with mass m_b. As a result, only the last six MIs can give a non-zero contribution to the spectrum. An example scalar integral $I^{(2a)}_{2(-1)101}$ appearing in section 1.7 was reduced to

$$\begin{aligned} I^{(2a)}_{2(-1)101} = \frac{2}{(2-3\epsilon)(M^2_{bc-} - q^2)} \Big[&(1-\epsilon)^2, 0, 0, 0, 0, 0, 0, 0, 0, 0, \\ m_c^2 \left((1-\epsilon) M^2_{bc-} - (2-3\epsilon) q^2 \right), &-q^2(m_b^2 - q^2)(1-2\epsilon), -\frac{\epsilon}{2} \lambda(m_b^2, m_c^2, q^2) \Big] M^{(2a)}, \end{aligned} \tag{2.22}$$

where $\lambda(x, y, z) \equiv x^2 + y^2 + z^2 - 2xy - 2xz - 2yz$ is the Källén function. The calculation now comes down to computing the imaginary parts of the last six MIs shown in figure 7.

2.3 The Differential Equations Method

The IBP relations originate from the fact that partial derivatives with respect to momenta contracted with other momenta are linear operators on the vector space spanned by scalar integrals. This is also true for derivatives with respect to masses and Mandelstam variables. The mass derivatives are most relevant to the investigation of inclusive decays, and the discussion below will focus on their case. Suppose that only the denominators $D_{k_1}, D_{k_2}, \ldots, D_{k_{n_m}}$ of a scalar integral $I_{a_1 a_2 \ldots a_N}$ have mass m, with some $\{k_1, k_2, \ldots, k_{n_m}\} \subseteq \overline{1, N}$. The derivative over m^2 can be readily computed:

$$\partial_{m^2} I_{a_1 a_2 \ldots a_{k_1} \ldots a_{k_2} \ldots a_{k_{n_m}} \ldots a_N} = \sum_{j=1}^{n_m} a_{k_j} I_{a_1 a_2 \ldots a_{k_j - 1} (a_{k_j} + 1) a_{k_j + 1} \ldots a_N}. \tag{2.23}$$

If an integral has more than one mass present, the above result applies for each disjoint subset of denominators with each mass separately. In the equation above, it is assumed that there is no external momentum p with p^2 set to m^2 or any other function of m. This assumption has to be lifted when one wishes to compute derivatives over Mandelstam variables and the structure of the right-hand side becomes more complicated. Consider now a basis of MIs $M = (M_1, M_2, \ldots, M_r)$ through which one can express all scalar integrals present in the calculation of a Feynman diagram that depends on two or more masses m_1, m_2, $\ldots$, m_{n+1}, $n > 0$. The mass dependence of each of the MIs can be written as

$$M_k(m_1, m_2, \ldots, m_{n+1}) = m_{n+1}^{2\rho_k} \hat{M}_k(\hat{m}_1^2, \hat{m}_2^2, \ldots, \hat{m}_n^2), \tag{2.24}$$

with $\hat{m}_l \equiv m_l/m_{n+1}$, and the power ρ_k depending on the number of loops and the sum of indices of M_k. The functions $\hat{M}_k$ and M_k will be referred to as MIs interchangeably, as these are in a one-to-one correspondence. The integrals $\hat{M}_k$ form a basis $\hat{M}$ and are obtained from the MIs M_k by simply replacing $m_{n+1} \to 1$, $m_l \to \hat{m}_l$, and $k_l \to \hat{k}_l \equiv k_l/m_{n+1}$, where k_l can be either an external or a loop momentum. Derivatives over $\hat{m}_l^2$ of functions $\hat{M}_k$ are given by the same expression as in eq. (2.23). Applying this equation for all normalized squared masses to all normalized MIs $\hat{M}_k$ in $\hat{M}$ produces a set of normalized scalar integrals that can be IBP reduced[†] back to the same basis $\hat{M}$. Using the freedom of choosing an ordering of scalar integrals in the Laporta algorithm, the original MIs can be chosen as the least complicated. In consequence they remain preserved throughout the reduction. It is possible and common that during this reduction some additional MIs have to be introduced. If that is the case, the basis $\hat{M}$ should be enlarged by these new MIs. This step should be repeated until all $\hat{m}_l^2$ derivatives of all MIs $\hat{M}_k$ are expressed with the same MIs. This procedure produces a system of partial, linear first-order homogeneous DEs for the functions $\hat{M}_k(\hat{m}_1^2, \hat{m}_2^2, \ldots, \hat{m}_n^2)$:

$$\partial_{\hat{m}_1^2}\hat{M} = A_1\hat{M},\ \partial_{\hat{m}_2^2}\hat{M} = A_2\hat{M},\ \ \ldots,\ \partial_{\hat{m}_n^2}\hat{M} = A_n\hat{M}, \tag{2.25}$$

with some matrices A_k. Their elements are simply the coefficients in the results of the IBP reduction of normalized-mass-squared derivatives of the MIs. As these are computed in a row reduction algorithm, they have to be rational functions of $\hat{m}_l$ and the space-time dimension D. Once the system of DEs is established, one can choose any of the various analytical, semi-analytical or numerical methods of solving linear first-order equations. The above method, first introduced in ref. [161] over 30 years ago, remains to this day a primary tool for computing multi-scale Feynman integrals.

Note that the above procedure could have been applied for unnormalized MIs and masses $m_1, \ldots, m_{n+1}$, resulting in a system of $n+1$ rather than n equations. The equivalent system presented above should be understood as being in free variables $\hat{m}_1, \ldots, \hat{m}_n, m_{n+1}$ and, to describe the original MIs M_k, is technically subject to a set of trivial equations:

$$\partial_{m_{n+1}^2} M_k = \frac{\rho_k}{m_{n+1}^2} M_k. \tag{2.26}$$

The introduction of normalized quantities effectively diagonalized the matrix A_{n+1} and removed the dependence on m_{n+1} from all other equations. This is also the reason why one cannot obtain non-trivial information on single mass-scale integrals with this approach.

The remainder of this section describes a method first proposed in ref. [162] of obtaining an analytic solution for the system of DEs (2.25) as an expansion in some small parameter ϵ present in the matrix elements of A_k. In the context of scalar Feynman integrals, this is simply the dimensional regularization parameter ϵ. First, the generic system of DEs in eq. (2.25) can be neatly written in the language of differential forms and the exterior derivative

$$d\hat{M} = \mathfrak{A}\hat{M}, \tag{2.27}$$

where

$$d\hat{M} = \sum_{k=1}^{n} d\hat{m}_k^2 \partial_{\hat{m}_k^2}\hat{M}, \qquad \mathfrak{A} \equiv \sum_{k=1}^{n} d\hat{m}_k^2 A_k. \tag{2.28}$$

[†]This operation is normally performed for unnormalized MIs but since these are in a one-to-one correspondence with their normalized counterparts, this is not a complication.

The formal general solution of eq. (2.27) reads

$$\hat{M}(\hat{m}_1^2,\ldots,\hat{m}_n^2) = \mathscr{P}_C\; e^{\int_C \mathfrak{A}}\; \hat{M}(\hat{m}_{1(0)}^2,\ldots,\hat{m}_{n(0)}^2), \tag{2.29}$$

where $(\hat{m}_{1(0)}^2,\ldots,\hat{m}_{n(0)}^2)$ is some point in the parameter space where all MIs are regular, and a boundary condition can be computed. The integration contour C connects this point with $(\hat{m}_1^2,\ldots,\hat{m}_n^2)$, without intersecting any singularities of the DEs. The symbol $\mathscr{P}_C$ establishes path ordering along the contour C of integrals in each term of the exponent similarly to the time ordering introduced in eq. (1.2).

Next, one can always change the basis of the unknown functions subject to the system of DEs with some invertible linear transformation T:

$$\hat{M} = T\hat{M}'. \tag{2.30}$$

The DEs for these new functions transform to

$$d\hat{M}' = T^{-1}(\mathfrak{A}T - dT)\hat{M}' \equiv \mathfrak{A}_T\hat{M}'. \tag{2.31}$$

Even though T can in principle be any function of D and $\hat{m}_k$, in practice it is important to constrain its elements to be rational in these variables, so the new DE matrices do not introduce any more complicated dependence. One can also change the set of free variables from $\hat{m}_k$ to some v_j such that $\hat{m}_k^2 = \hat{m}_k^2(v_1,\ldots,v_n)$ is a rational function. The DEs in these variables can be readily established:

$$d\hat{M} = \sum_{j,k=1}^{n} dv_j\left(\partial_{v_j}\hat{m}_k^2\right)\partial_{\hat{m}_k^2}\hat{M} = \left(\sum_{j,k=1}^{n} dv_j\left(\partial_{v_j}\hat{m}_k^2\right)A_k\right)\hat{M} \equiv \mathfrak{A}^{(v)}\hat{M}. \tag{2.32}$$

Suppose now that there exists a set of variables v_j and an invertible linear transformation $\mathfrak{T}$, such that

$$\mathfrak{T}^{-1}(\mathfrak{A}^{(v)}\mathfrak{T} - d\mathfrak{T}) = \epsilon\mathfrak{C}, \tag{2.33}$$

resulting in a system of DEs:

$$d\hat{M}' = \epsilon\mathfrak{C}\hat{M}', \tag{2.34}$$

which is usually referred to as the canonical or the ϵ-form of the original DEs. The 1-form $\mathfrak{C}$ is assumed to be independent of ϵ, so the general solution in eq. (2.29) can be easily expanded in ϵ:

$$\hat{M}'(v_k) = \mathscr{P}_C\left(\mathbb{1}_{r\times r} + \epsilon\int_C\mathfrak{C} + \frac{\epsilon^2}{2}\int_C\mathfrak{C}\int_C\mathfrak{C} + \mathcal{O}(\epsilon^3)\right)\hat{M}'\left(v_{k(0)}\right) \tag{2.35}$$

An additional assumption on $\mathfrak{C}$ is that it can be written as

$$\mathfrak{C} = \sum_{l=1}^{L}\mathcal{C}_l d\log\alpha_{l_1} \tag{2.36}$$

for some matrices $\mathcal{C}_l$ with numerical elements. The functions $\alpha_l(v_1,\ldots,v_n)$ are referred to as the letters, and their collection as the alphabet of the system of DEs. Below, they are assumed to be linear in each variable v_k separately, i.e. $\partial_{v_k}^2\alpha_l = 0$. Adopting a Cartesian integration contour is conceptually the simplest. It is going to be done in the following. The

boundary condition is computed for $v_{k(0)} = 0$, and each of the MIs is evolved in each of the variables v_k separately in a sequence:

$$(0,0,0,\ldots,0) \xrightarrow{C_1} (v_1,0,0,\ldots,0) \xrightarrow{C_2} (v_1,v_2,0,\ldots,0) \xrightarrow{C_3} \ldots \xrightarrow{C_n} (v_1,v_2,v_3,\ldots,v_n). \tag{2.37}$$

Then, the general solution in eq. (2.35) becomes

$$\begin{aligned}\hat{M}'(v_1,\ldots v_n) = \\ &= \left[\prod_{k=0}^{n-1} \mathscr{P}_{C_{n-k}}\left(\mathbb{1}_{r\times r} + \epsilon\sum_{l=1}^{L}\mathcal{C}_l \int\limits_{C_{n-k}} d\log\alpha_{l_1}\right.\right. \\ &\quad \left.\left. + \frac{\epsilon^2}{2}\sum_{l_1 l_2}^{L}\mathcal{C}_{l_1}\mathcal{C}_{l_2}\int\limits_{C_{n-k}} d\log\alpha_{l_1}\int\limits_{C_{n-k}} d\log\alpha_{l_2} + \mathcal{O}(\epsilon^3)\right)\right]\hat{M}'(0,\ldots,0).\end{aligned} \tag{2.38}$$

Each term in the product can be rewritten as

$$\mathbb{1}_{r\times r} + \epsilon\sum_{l=1}^{L}\mathcal{C}_l\int_0^{v_k} d\tilde{v}_k W[\alpha_l,\tilde{v}_k] + \epsilon^2\sum_{l_1,l_2=1}^{L}\mathcal{C}_{l_1}\mathcal{C}_{l_2}\int_0^{v_k} d\tilde{v}_k^{(1)} W[\alpha_{l_1},\tilde{v}_k^{(1)}]\int_0^{\tilde{v}_k^{(1)}} d\tilde{v}_k^{(2)} W[\alpha_{l_2},\tilde{v}_k^{(2)}] + \mathcal{O}(\epsilon^3). \tag{2.39}$$

The integrands $W[\alpha_l,\tilde{v}_k]$ are defined as

$$W[\alpha_l,\tilde{v}_k] \equiv \partial_{\tilde{v}_k}\log[\alpha_l(v_1,v_2,\ldots,v_{k-1},\tilde{v}_k,0,0,\ldots,0)], \tag{2.40}$$

and come from the change of the integration variable from $\log\alpha_l$ to $\tilde{v}_k$. If $W[\alpha_l,\tilde{v}_k] = 0$, the corresponding term in the sum over the letters of the alphabet vanishes. If it is nonzero, it can be transformed as

$$W[\alpha_l,\tilde{v}_k] = \frac{1}{\tilde{v}_k - \left[\tilde{v}_k - \frac{1}{W[\alpha_l,\tilde{v}_k]}\right]} \equiv \frac{1}{\tilde{v}_k - \nu_k^{(l)}}. \tag{2.41}$$

Note that such $\nu_k^{(l)}$ is independent of $\tilde{v}_k$ thanks to the condition $\partial_{v_k}^2\alpha_l = 0$. Substituting $\nu_k^{(l)}$ into eq. (2.39) results in

$$\mathbb{1}_{r\times r} + \epsilon\sum_{l=1}^{L}\mathcal{C}_l G\left(\nu_k^{(l)}\middle|v_k\right) + \epsilon^2\sum_{l_1,l_2=1}^{L}\mathcal{C}_{l_1}\mathcal{C}_{l_2}G\left(\nu_k^{(l_1)},\nu_k^{(l_2)}\middle|v_k\right) + \mathcal{O}(\epsilon^3), \tag{2.42}$$

where the sums are assumed to run only over the letters of the alphabet that depend on v_k. The function $G(\nu_1,\ldots,\nu_n|z)$ is the Goncharov polylogarithm (GPL) [163], given recursively as

$$G(\nu_1,\nu_2,\nu_3,\ldots,\nu_n|z) = \int_0^z \frac{d\tilde{z}}{\tilde{z}-\nu_1}G(\nu_2,\nu_3,\ldots,\nu_n|\tilde{z}), \tag{2.43}$$

where ν_1 is independent of $\tilde{z}$, with the initial normalization

$$G(|z) = 1. \tag{2.44}$$

The GPL function with all indices $\nu_k = 0$ is instead defined as

$$G(\underbrace{0,\ldots,0}_{n \text{ times}}|z) = \frac{1}{n!}\log^n z. \tag{2.45}$$

With a single evolution operator written as in eq. (2.42), the result for $\hat{M}'$ reads

$$\hat{M}'(v_1,\ldots,v_n) = \left[\mathbb{1}_{r\times r} + \epsilon\sum_{l=1}^{L}\mathcal{C}_l\sum_{k=1}^{n}G\left(\nu_k^{(l)}\middle|v_k\right) + \epsilon^2\left[\sum_{l_1,l_2=1}^{L}\mathcal{C}_{l_1}\mathcal{C}_{l_2}\times\right.\right.$$
$$\left.\left.\left(\sum_{k_1,k_2=1}^{n}G\left(\nu_{k_1}^{(l_1)}\middle|v_{k_1}\right)G\left(\nu_{k_2}^{(l_2)}\middle|v_{k_2}\right) + \sum_{k=1}^{n}G\left(\nu_k^{(l_1)},\nu_k^{(l_2)}\middle|v_k\right)\right)\right] + \mathcal{O}(\epsilon^3)\right]\hat{M}'(0,\ldots,0). \tag{2.46}$$

Again, the terms in the sums over k for which $\partial_{v_k}\alpha_l = 0$ are implicitly set to 0, or equivalently $G(\ldots,\infty,\ldots|z) \equiv 0$. The above equation, together with the relations $\hat{M} = \mathfrak{T}\hat{M}'$, $v_k = v_k(\hat{m}_1^2,\ldots,\hat{m}_n^2)$, and eq. (2.24), give the result for the MIs up to the boundary condition $\hat{M}'(0,\ldots,0)$. For most free variable sets v_k, this boundary condition should be understood as a limit of $v_k \to 0$ from some direction specified by the Feynman prescription for analytical continuations of scalar integrals, as $v_k = 0$ is usually a branch point of the MIs. Higher orders in ϵ can be obtained in an analogous way.

The constraints placed in the above derivation on the canonical 1-form $\mathfrak{C}$ were of course very stringent, and the change of basis $\mathfrak{T}$ may not exist for a generic linear first-order system of DEs. It is thus at first surprising that it does exist for a large class of scalar Feynman integrals, and can be assembled in an algorithmic way. The construction method due to Lee [164–166] relies on a careful analysis and manipulation of the poles of the matrices A_k in eq. (2.25). The algorithm described below assumes that the system is reduced to the ϵ-form for each variable consecutively while fixing all others as constants. The reduction in one variable v_k achieved with a transformation matrix $T^{(k)}$ will not be spoiled by reductions in any later variable v_l, as long as the transformation $T^{(l)}$ does not depend on v_k for $k < l$. Hence, it is sufficient to focus on the case of a system depending on a single variable v:

$$\partial_v\hat{M}(v,\epsilon) = A(v,\epsilon)\hat{M}(v,\epsilon). \tag{2.47}$$

Since the elements of the matrix A are rational functions of v, they can always be expanded into a Laurent series around any point $v = v_0$ including infinities. The expansion around infinities is defined as the expansion of a DE system obtained from the original after changing the variable to $\tilde{v} = 1/v$ and expanding around $\tilde{v} = 0$. Only for a finite number of points a these expansions will have negative power terms:

$$A = \sum_{j=-p_a^{(A)}-1}^{\infty}(v-a)^j\,A_a^{(j)}, \tag{2.48}$$

where $p_a^{(A)} \geq 0$ is called the Poincaré rank of the matrix A at point a. In the Lee algorithm, the transformation matrix $\mathfrak{T}$ that reduces the system to the ϵ-form is split into three parts:

$$\mathfrak{T} = T_F T_N T_E. \tag{2.49}$$

The first matrix T_F transforms the system into $A_F \equiv T_F^{-1}(AT_F - \partial_v T_F)$ in the Fuchsian form, i.e. with $p_a^{(A_F)} = 0$ for all singular points a including infinity. This corresponds precisely to

the condition (2.36), which is essential for the solution to be expressible in terms of GPLs. The second matrix T_N "normalizes" the system, that is it changes the eigenvalues of the residue matrices $A_F^{(-1)}$ to be proportional to ϵ. If the original DE describes the evolution of an actual basis of MIs, finding T_N is the most likely point at which the algorithm may fail. The last step is to construct the matrix T_E that is independent of v, and factorizes ϵ out of $A_N \equiv T_N^{-1}(A_F T_N - \partial_v T_N) = \epsilon \mathfrak{C}$, achieving the ϵ-form.

To find T_F, one considers a chain of balance operators $\mathcal{B}(P, a, b|v)$, where P is a projection operator, while a and b are singular points of the original DE. It can be proven [166] that for a projection operator P satisfying

$$\begin{aligned} &A_a^{\left(-p_a^{(A)}-1\right)} \mathrm{Im}P = 0, \\ &A_a^{\left(-p_a^{(A)}\right)} \mathrm{Im}P \subseteq \mathrm{Im}A_a^{\left(-p_a^{(A)}-1\right)} + \mathrm{Im}P, \\ &\dim\left[\mathrm{Im}P \cap \mathrm{Im}A_a^{\left(-p_a^{(A)}-1\right)}\right] > 0, \end{aligned} \tag{2.50}$$

transforming the matrix A with a balance operator

$$\mathcal{B}(P, a, b|v) \equiv \mathbb{1}_{r\times r} - P + \frac{v-b}{v-a} P \tag{2.51}$$

strictly lowers the rank of $A_a^{\left(-p_a^{(A)}-1\right)}$. If, in addition, P satisfies

$$\mathrm{coIm}P A_b^{\left(-p_b^{(A)}-1\right)} \subseteq \mathrm{coIm}P, \tag{2.52}$$

where

$$\mathrm{coIm}X \equiv \{I^T | \exists \tilde{I}^T : I^T = \tilde{I}^T X\}, \tag{2.53}$$

the Poincaré rank at point b is not affected by the transformation $\mathcal{B}(P, a, b|v)$. Applying a finite number of such balance transformations reduces $A_a^{\left(-p_a^{(A)}-1\right)}$ to 0, lowering the Poincaré rank at point a by 1 and not affecting Poincaré ranks at any other point. As long as the projection operators satisfying the conditions (2.50) and (2.52) can be found, after a finite number of steps, a Fuchsian form of the system of DEs is reached. For a system with only rational matrix elements, a projector satisfying all the three conditions in eq. (2.50) exists if, and only if [166]

$$\dim\ker \begin{pmatrix} A_a^{\left(-p_a^{(A)}-1\right)} & A_a^{\left(-p_a^{(A)}\right)} - \lambda \mathbb{1}_{r\times r} \\ \mathbb{0}_r & A_a^{\left(-p_a^{(A)}-1\right)} \end{pmatrix} > \dim\ker A_a^{\left(-p_a^{(A)}-1\right)}. \tag{2.54}$$

A projection operator is defined uniquely by its image and coimage. Having specified a subspace[†] $K \subseteq \mathrm{span}(\hat{M})$ and an equal-dimension subspace $L^T \subseteq \mathrm{span}(\hat{M}^T)$, a projector can be constructed as

$$P_{KL} \equiv \bar{K}(\bar{L}^T \bar{K})^{-1} \bar{L}^T, \tag{2.55}$$

where $\bar{K}(\bar{L}^T)$ denotes a matrix of columns(rows) equal to some basis of $K(L^T)$. The image and coimage of P_{KL} are equal to K and L^T respectively. This implies that for any choice

[†]Here, $\hat{M}$ is treated as a basis of a vector space of scalar integrals.

of ImP satisfying (2.50), one has to choose coImP that satisfies both eq. (2.52) and that $\overline{\text{coIm}P}$ $\overline{\text{Im}P}$ forms an invertible matrix. If that is not possible, even if eq. (2.54) holds, the DE cannot be brought into an ϵ-form.

If a transformation T_F can be found, the necessary projectors in $\mathcal{B}(P, a, b|v)$ can be constructed from generalized[†] eigenvectors of $A_{a/b}^{\left(-p_{a/b}^{(A)}-1\right)}$, as described in the original work in ref. [164]. Then, the DE matrix can be transformed into

$$A_F(v, \epsilon) = \sum_k \frac{A_F^{(k)}(\epsilon)}{v - a_k}, \tag{2.56}$$

where the sum runs over all singular points of A_F and the matrices $A_F^{(k)}$ are independent[‡] of v.

The second part of the Lee algorithm finds the normalizing transformation T_N. It is known that rational transformations can only shift the eigenvalues of matrix residues by integers. Another set of balance transformations with projectors built out of generalized eigenvectors of $A_F^{(k)}$ was shown in ref. [164] to shift the eigenvalues of these matrices by ± 1. This means that for a DE to be normalizable by rational transformations, its eigenvalues must be of the form

$$\alpha\epsilon + n, \tag{2.57}$$

for some $n \in \mathbb{Z}$ and $\alpha \in \mathbb{C}$. That is not the case for systems describing elliptic-like integrals, such as the massive "sunrise" diagrams. There, some eigenvalues of $A_F^{(k)}$ turn out to be of the form $\alpha\epsilon + n + 1/2$ and the ϵ-form is not achievable by a rational transformation. This behavior appears also for integrals that can be normalized after changing the free variable to $\tilde{v}$ with $v = v(\tilde{v})$ being some rational function. Note that such a variable change is in general not equivalent to a rational transformation, since the inverse function $\tilde{v} = \tilde{v}(v)$ might contain a square root or higher roots. In other words, given a rational transformation $T(v)$, there is no rational transformation $\tilde{T}$ such that $\tilde{T}(v) = V^{-1} \circ T(\tilde{v}) \circ V$, where V denotes the operation of changing the free variables from v to $\tilde{v}$. Properly chosen transformations belonging to this extension of the class of allowed changes of the DEs can sometimes shift eigenvalues by a half-integer. The analysis of different cases and corresponding proper variable changes was given in ref. [165]. One of the conclusions was that if there are four or more distinct points at which the residue has $\alpha\epsilon + n + 1/2$ eigenvalues, there is no variable change that can remove all of them, and the ϵ-form cannot be reached, even with this extended class of transformations. For three or less points, the authors specify the changes of variables that may shift the eigenvalues to the form in eq. (2.57), and prove that if these do not help, there is no other rational variable change that can.

If all eigenvalues of all matrices $A_F^{(k)}$ are of the form in eq. (2.57), the matrices can always be normalized at all but one singular point. The balance transformations adjusting residue eigenvalues always change them at two separate singular points. One special point can be chosen as a "sink" of all balance transformations, absorbing the unwanted eigenvalue changes, while all others are adjusted to be proportional to ϵ. Suppose that this point is first chosen at infinity, and then moved by a rational transformation $T_{\infty\to 0}$ to 0. The sufficient conditions for the existence of T_N given in ref. [165] state that

[†]These matrices are not diagonalizable, so generalized eigenvectors refer to a basis in which a matrix assumes the Jordan form.

[‡]Note that any constant term in the above sum, or any dependence of the numerators on v spoils the Fuchsian form at $v = \infty$.

1. $\det T_{\infty\to 0}$ is independent of v,
2. both $T_{\infty\to 0}$ and $T^{-1}_{\infty\to 0}$ are given by finite degree polynomials in v and $1/v$,
3. $T_{\infty\to 0}(v) = Q(v)R(1/v)$, where both $Q(x)$ and $R(x)$ are polynomial in x.

Then, the matrix $Q(v)$ is the transformation T_N that takes a system normalized everywhere but at infinity to a system normalized everywhere.

The last step of the algorithm is finding the matrix T_E. Once a system is of the form of eq. (2.56), and all eigenvalues of matrices $A^{(k)}_F(\epsilon)$ are proportional to ϵ, it suffices to solve a system of linear equations:

$$\frac{A_N(v,\epsilon)}{\epsilon} T(\epsilon,\mu) = T(\epsilon,\mu)\frac{A_N(v,\mu)}{\mu} \tag{2.58}$$

for $T(\epsilon,\mu)$, with μ treated as a parameter. If the solution $T(\epsilon,\mu)$ is invertible and independent of v, the transformation $T_E = T(\epsilon,\mu)$ factorizes the ϵ dependence, and completes the construction of $\mathfrak{T}$. If no invertible solution exists for any μ, the ϵ-form cannot be found.

The case of more than 2 masses can now be briefly reexamined. Applying an exterior derivative to eq. (2.34) gives

$$0 = d(\mathfrak{C}\hat{M}) = (d\mathfrak{C})\hat{M} - \mathfrak{C}\wedge d\hat{M} = (d\mathfrak{C} - \epsilon\mathfrak{C}\wedge\mathfrak{C})\hat{M}. \tag{2.59}$$

As this equation has to hold for any ϵ, both terms in the parenthesis have to vanish independently. The vanishing of the former implies that $\mathfrak{C} = dC$ for some matrix $C(v_1,\ldots,v_n)$. Since in the ϵ-form each of the matrices A_k is assumed to be Fuchsian at all singular points, the only possibility is that C is of the form

$$C = \sum_l^L \mathcal{C}_l \log\alpha_l. \tag{2.60}$$

The numerical coefficient matrices $\mathcal{C}_l$ can be simply read out of A_k transformed to the ϵ-form. The condition $dS = 0$ ensures that there will be no conflicts between coefficients coming from different matrices A_k. Then, the assumed form of $\mathfrak{C}$ in eq. (2.36) follows. The second term in eq. (2.59) being 0 gives a useful consistency check for the matrices $\mathcal{C}_l$, once the ϵ-form is reached:

$$[\mathcal{C}_l, \mathcal{C}_{l'}] = 0 \tag{2.61}$$

for all l and l'. In a multivariate problem, as in a reduction with just one mass ratio, the most likely point of failure of the algorithm is the normalization. To my best knowledge, a comprehensive analysis of variable changes removing half integer eigenvalues[†] of matrix residues similar to that of ref. [165] is still missing. Quoting Roman Lee, when there are more than two masses, choosing free variables in which the ϵ-form can be reached "mostly remains a matter of art and luck".

Numerous implementations of the algorithm described in this section are publicly available. These include a C++ program `epsilon` [167], a Python program `Fuchsia` [168], and a `Mathematica` package `Canonica` [169]. Another `Mathematica` package published by the author of the original algorithm himself, `Libra` [170], is the latest and by far the most complete. Among many other features, it provides the user with an intelligible manual tool for

[†] in the limit of $\epsilon \to 0$.

constructing each of the matrices constituting the canonical transformation $\mathfrak{T}$, permitting a directed search for the transformation in cases where other programs fail outright. The release of `Libra` enabled using the method of the ϵ-form in much more complicated cases than before, and opened a path towards analytical solutions of truly nontrivial problems [67, 171–179].

The construction of a general solution to DEs in terms of GPLs defined in eq. (2.43) is motivated by two advantages of using this family of functions. First, the numerical values of GPLs can be computed very efficiently and to any desired precision limited only by the available hardware. One of the standard algorithms for this purpose has been implemented in the `GiNaC` computer algebra library for C++ [180]. It allows for obtaining hundreds of significant digits of GPLs on modern personal computers in negligible time. There also exists a convenient `Mathematica` interface specialized in the algebra of polylogarithms, hyperpolylogarithms and GPLs called `PolyLogTools` [181], that greatly facilitates the numerical evaluation and algebraic manipulations of GPLs. Second, this class of functions admits a rich mathematical structure[†]. For instance, the GPLs can be used to express the elementary logarithm,

$$G(\nu, z) \equiv \int_0^z \frac{d\tilde{z}}{\tilde{z} - \nu} = \log\left(1 - \frac{z}{\nu}\right), \ \nu \neq 0, \tag{2.62}$$

its powers,

$$G(\underbrace{\nu, \ldots, \nu}_{n \text{ times}}|z) = \frac{1}{n!}\log^n\left(1 - \frac{z}{\nu}\right), \tag{2.63}$$

and classical polylogarithms,

$$G(\underbrace{0, \ldots, 0}_{(n-1) \text{ times}}, 1|z) = -\mathrm{Li}_n(z) \equiv -\int_0^z \frac{d\tilde{z}}{\tilde{z}}\mathrm{Li}_{n-1}(\tilde{z}), \ \mathrm{Li}_1(z) = -\log(1-z) = -G(1|z). \tag{2.64}$$

The family of GPLs as functions of both their last argument and their indices, satisfies a large number of functional relations. For example, if $\nu_n \neq 0$, the GPLs are invariant under a simultaneous rescaling of all arguments:

$$G(k\nu_1, \ldots, k\nu_n|kz) = G(\nu_1, \ldots, \nu_n|z), \tag{2.65}$$

where $k \in \mathbb{C} \setminus \{0\}$. This equation can be proven by induction in n. Suppose that it holds for the GPLs of rank $n-1$. Changing the integration variable as $\tilde{z} = k\tilde{z}'$, the definition in eq. (2.43) yields

$$\begin{aligned} G(k\nu_1, \ldots, k\nu_n|kz) &\equiv \int_0^{kz} \frac{d\tilde{z}}{\tilde{z} - k\nu_1} G(k\nu_2, \ldots, k\nu_n|\tilde{z}) = \int_0^z \frac{d\tilde{z}'}{\tilde{z}' - \nu_1} G(k\nu_2, \ldots, k\nu_n|k\tilde{z}') \\ &= \int_0^z \frac{d\tilde{z}'}{\tilde{z}' - \nu_1} G(\nu_2, \ldots, \nu_n|\tilde{z}') \equiv G(\nu_1, \ldots, \nu_n|z), \end{aligned} \tag{2.66}$$

where the second to last equality follows immediately from the induction assumption. The initial case for $n = 0$ is satisfied because of eq. (2.44). As the GPL definition in eq. (2.43)

[†]For a comprehensive review, see ref. [182].

does not hold for the case of all indices equal to 0, the inductive recursion breaks if one chooses $\nu_n = 0$ at the first step $n = 1$, hence the assumption $\nu_n \neq 0$.

Another important property of GPLs is their shuffle algebra. Consider a product of two rank 1 GPLs evaluated at the same point z:

$$G(\nu_1|z)G(\nu_2|z) = \int_0^z \frac{d\tilde{z}_1}{\tilde{z}_1 - \nu_1} \int_0^z \frac{d\tilde{z}_2}{\tilde{z}_2 - \nu_2} = \int_\square \frac{d^2\tilde{z}}{(\tilde{z}_1 - \nu_1)(\tilde{z}_2 - \nu_2)}, \tag{2.67}$$

where $\square$ refers to integrating over a square with side length z placed in the first quadrant of the $\tilde{z}_1 \times \tilde{z}_2$ space and aligned with the coordinate axes. The last integral can be split as

$$\begin{aligned} G(\nu_1|z)G(\nu_2|z) &= \left(\int_{\triangle} + \int_{\triangledown} \right) \frac{d^2\tilde{z}}{(\tilde{z}_1 - \nu_1)(\tilde{z}_2 - \nu_2)} \\ &= \int_0^z \frac{d\tilde{z}_1}{\tilde{z}_1 - \nu_1} \int_0^{\tilde{z}_1} \frac{d\tilde{z}_2}{\tilde{z}_2 - \nu_2} + \int_0^z \frac{d\tilde{z}_2}{\tilde{z}_2 - \nu_2} \int_0^{\tilde{z}_2} \frac{d\tilde{z}_1}{\tilde{z}_1 - \nu_1} \equiv G(\nu_1, \nu_2|z) + G(\nu_2, \nu_1|z). \end{aligned} \tag{2.68}$$

Equivalent relations can be derived for products of two higher rank GPLs at the same point, but only the above result will be relevant for the discussion below. The shuffle identity for $\nu_1 = \nu_2 \equiv \nu \neq 0$ can be used to evaluate:

$$G(\nu, \nu|z) = \frac{1}{2} G^2(\nu|z) = \frac{1}{2} \log^2 \left(1 - \frac{z}{\nu}\right), \tag{2.69}$$

which confirms eq. (2.63) for rank 2 GPLs. On the other hand, for $\nu_1 \equiv \nu \neq \nu_2 = 0$, eq. (2.68) reads:

$$G(\nu, 0|z) = G(\nu|z)G(0, z) - G(0, \nu|z) = \log \left(1 - \frac{z}{\nu}\right) \log z + \mathrm{Li}_2 \left(\frac{z}{\nu}\right), \tag{2.70}$$

where the results of eqs. (2.62), (2.64), and (2.65) were used.

Consider now a GPL of rank two evaluated at 1. For each choice of a number r, the integration region can be divided into three parts:

$$G(a, b, 1) = \int_{\triangle} d^2\tilde{z} \frac{1}{\tilde{z}_1 - \nu_1} \frac{1}{\tilde{z}_2 - \nu_2} = \left(\int_{\mathrm{I}} + \int_{\mathrm{II}} + \int_{\mathrm{III}} \right) d^2\tilde{z} \frac{1}{\tilde{z}_1 - a} \frac{1}{\tilde{z}_2 - b} \tag{2.71}$$

shown in figure 8. The geometric interpretation of r relies on the inequalities $0 < r < 1$, but the results hold for any $r \in \mathbb{C}$. The three regions can be parameterized as

$$\begin{aligned} G(a, b, 1) &= \left(\int_0^{1-r} d\tilde{z}_1 \int_0^{\tilde{z}_1} d\tilde{z}_2 + \int_{1-r}^1 d\tilde{z}_1 \int_0^{1-r} d\tilde{z}_2 + \int_{1-r}^1 d\tilde{z}_2 \int_{\tilde{z}_2}^1 d\tilde{z}_1 \right) \frac{1}{\tilde{z}_1 - a} \frac{1}{\tilde{z}_2 - b} \\ &= \left(\int_0^{1-r} d\tilde{z}_1 \int_0^{\tilde{z}_1} d\tilde{z}_2 + \int_0^r d\tilde{z}_1' \int_0^{1-r} d\tilde{z}_2 + \int_0^r d\tilde{z}_2' \int_0^{\tilde{z}_2'} d\tilde{z}_1' \right) \frac{1}{\tilde{z}_1 - a} \frac{1}{\tilde{z}_2 - b} \\ &= G(a, b|1 - r) - G(1 - a|r)G(b|1 - r) + G(1 - b, 1 - a|r), \end{aligned} \tag{2.72}$$

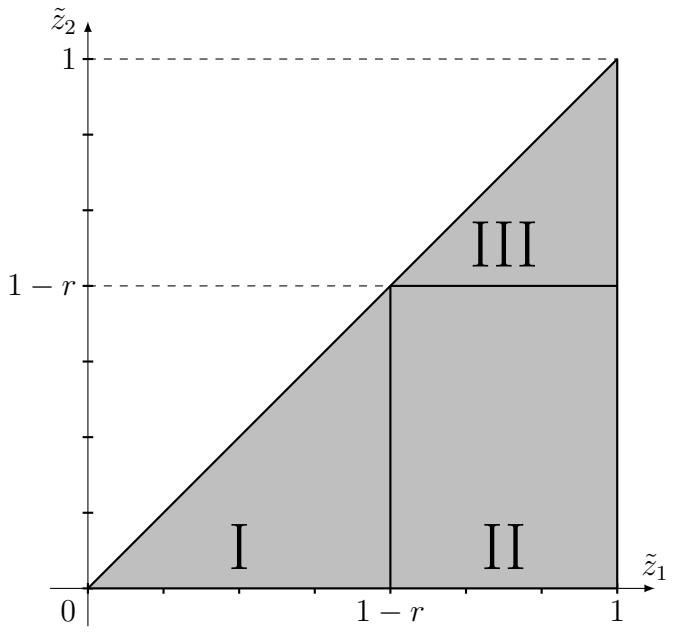

Figure 8: The three integration regions of eq. (2.71)

where the variable change $\tilde{r}'_j \equiv 1 - \tilde{r}_j$ was applied in the second line. This result is the rank 2 case of a more general identity called Hölder convolution:

$$G(a_1, \ldots, a_n|1) = \sum_{k=0}^{n} (-1)^k G(a_{k+1}, \ldots, a_n|1-r) G(1-a_k, \ldots, 1-a_1|r), \tag{2.73}$$

which can be proven in a similar way by dividing the integration over an n-dimensional triangle into $n+1$ parts [183].

Applying the result of eq. (2.72) to $G(0, 1-\nu_1/\nu_2, 1)$ and choosing $r = z/\nu_2$ for $\nu_2 \neq 0$ yields

$$G\left(0, 1-\frac{\nu_1}{\nu_2}\middle|1\right) = G\left(0, 1-\frac{\nu_1}{\nu_2}\middle|1-\frac{z}{\nu_2}\right) - G\left(1\middle|\frac{z}{\nu_2}\right) G\left(1-\frac{\nu_1}{\nu_2}\middle|1-\frac{z}{\nu_2}\right) + G\left(\frac{\nu_1}{\nu_2}, 1\middle|\frac{z}{\nu_2}\right), \tag{2.74}$$

or, if $\nu_1 \neq \nu_2$ and using eq. (2.65)

$$\begin{aligned} G(\nu_1, \nu_2, z) =& G\left(0, 1\middle|\frac{\nu_2}{\nu_2-\nu_1}\right) - G\left(0, 1\middle|\frac{\nu_2-z}{\nu_2-\nu_1}\right) + G(\nu_2|z) G(\nu_2-\nu_1|\nu_2-z) \\ =& \mathrm{Li}_2\left(\frac{\nu_2-z}{\nu_2-\nu_1}\right) - \mathrm{Li}_2\left(\frac{\nu_2}{\nu_2-\nu_1}\right) + \log\left(1-\frac{z}{\nu_2}\right) \log\left(\frac{z-\nu_1}{\nu_2-\nu_1}\right), \end{aligned} \tag{2.75}$$

where eqs. (2.62) and (2.64) were used in the last equality. The last equation, together with eqs. (2.45), (2.62), (2.64), (2.69), and (2.70), complete the evaluation of rank 1 and 2 GPLs in terms of logarithms and dilogarithms.

2.4 Sample Calculation - 4

Using the results of the previous section, all master integrals of the diagram ($2a$) found in section 2.2 (c.f. figure 7 on page 75) can be computed analytically up to and including

$\mathcal{O}(\epsilon^1)$, which is the required order of the expansion in ϵ due to ϵ-divergent coefficients of the IBP reduction. Treating m_b as the mass m_{n+1} that was factorized out of the MIs in eq. (2.24) results in a basis of normalized MIs $\hat{M}^{(2a)}$. Taking derivatives over $\hat{m}_c^2$ and $\hat{q}^2$ is straightforward:

$$\partial_{\hat{m}_c^2} I^{(2a)}_{abcde} = b I^{(2a)}_{a(b+1)cde} + e I^{(2a)}_{abcd(e+1)}, \qquad \partial_{\hat{q}^2} I^{(2a)}_{abcde} = c I^{(2a)}_{ab(c+1)de}, \tag{2.76}$$

so, for example:

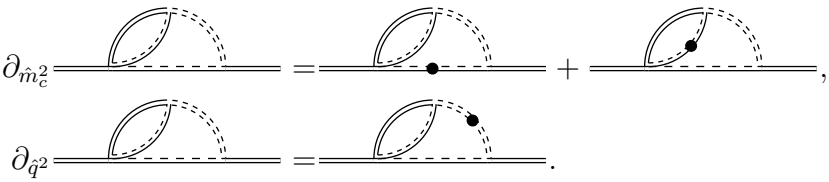

(2.77)

Computing the $\partial_{\hat{m}_c^2}$ and $\partial_{\hat{q}^2}$ derivatives of all the MIs, and reducing the resulting scalar integrals back to the same basis of MIs, produces a system of DEs. In this case, the basis $\hat{M}^{(2a)}$ already encompasses all necessary integrals and need not be enlarged. The obtained system takes the form

$$\partial_x \hat{M}^{(2a)} = A_x \hat{M}^{(2a)} = \frac{1-\epsilon}{x\hat{\lambda}} \begin{pmatrix} D_x^{(0)} & & & \\ E_x^{(1)} & D_x^{(1)} & & \\ E_x^{(2)} & F_x^{(2)} & D_x^{(2)} & \\ E_x^{(3)} & \mathbb{0} & \mathbb{0} & D_x^{(3)} \end{pmatrix} \hat{M}^{(2a)}, \tag{2.78}$$

with $x \in \{\hat{q}^2, \hat{m}_c^2\}$ and $\hat{\lambda} \equiv \lambda(m_b^2, m_c^2, q^2)/m_b^4$, (c.f. eq. (2.22) and the text below). Both matrices A_x assume a block-triangular form with $D_x^{(0)}$ being a lower-triangular 5×5 matrix, and the dimensions of the remaining diagonal blocks $D_x^{(1)}$, $D_x^{(2)}$, and $D_x^{(3)}$ being 2×2, 3×3, and 3×3 respectively. Recall that only the last six MIs contribute a non-zero imaginary part to the spectrum correction. Thanks to this fact and to the block-triangular form of the above matrix, to compute these imaginary parts it is sufficient restrict the above system to the last two diagonal blocks. The necessary submatrices are given by:

$$D^{(2)}_{\hat{q}^2} = \begin{pmatrix} \frac{\hat{q}^2(\omega-2)(2\epsilon-1)}{\epsilon-1} & 0 & 0 \\ 0 & \frac{\hat{q}^2(\omega-2)(2\epsilon-1)}{\epsilon-1} & 0 \\ -\omega & \delta & \frac{2\hat{q}^2(\omega-2)(2\epsilon-1)}{\epsilon-1} - \hat{\lambda} \end{pmatrix}, \tag{2.79}$$

$$D^{(2)}_{\hat{m}_c^2} = \begin{pmatrix} \frac{\omega(1-2\epsilon)\hat{m}_c^2}{\epsilon-1} + \hat{\lambda} & 0 & 0 \\ 0 & \frac{\omega(1-2\epsilon)\hat{m}_c^2}{\epsilon-1} & 0 \\ \omega-2 & 2\hat{m}_c^2 & \frac{2\omega(1-2\epsilon)\hat{m}_c^2}{\epsilon-1} \end{pmatrix}, \tag{2.80}$$

$$D^{(3)}_{\hat{q}^2} = \begin{pmatrix} \frac{\hat{\lambda}\hat{q}^2(1-2\epsilon)}{\delta(\epsilon-1)} & \frac{\hat{\lambda}\hat{q}^2(1-2\epsilon)}{\delta(\epsilon-1)} & \frac{2\hat{\lambda}\hat{q}^2\epsilon}{\delta-\delta\epsilon} \\ 0 & \frac{\hat{\lambda}\epsilon}{\epsilon-1} & \frac{\hat{\lambda}\epsilon}{1-\epsilon} \\ \frac{4\hat{q}^2(2\epsilon-1)\hat{m}_c^2(\hat{m}_c^2-1)}{\delta(\epsilon-1)} & -\frac{\hat{q}^2(2\epsilon-1)\left(2\hat{m}_c^2(2\hat{q}^2+\omega)+\hat{\lambda}\right)}{\delta(\epsilon-1)} & \frac{\hat{q}^2\left(\delta(\omega-2)(6\epsilon-1)+2\hat{\lambda}\epsilon\right)}{\delta(\epsilon-1)} \end{pmatrix}, \tag{2.81}$$

$$D^{(3)}_{\hat{m}_c^2} = \begin{pmatrix} \frac{\hat{\lambda}\epsilon}{\epsilon-1} & 0 & \frac{\hat{\lambda}\epsilon}{1-\epsilon} \\ \frac{\hat{\lambda}(1-2\epsilon)\hat{m}_c^2}{\delta(\epsilon-1)} & \frac{\hat{\lambda}(1-2\epsilon)\hat{m}_c^2}{\delta(\epsilon-1)} & \frac{2\hat{\lambda}\epsilon\hat{m}_c^2}{\delta-\delta\epsilon} \\ \frac{(2\epsilon-1)\hat{m}_c^2\left(4\hat{q}^2\hat{m}_c^2+(\hat{m}_c^2-1)^2-\hat{q}^4\right)}{\delta-\delta\epsilon} & \frac{4\hat{q}^2\left(\hat{q}^2-1\right)(2\epsilon-1)\hat{m}_c^2}{\delta(\epsilon-1)} & \frac{\hat{m}_c^2\left(\delta\omega(1-6\epsilon)+2\hat{\lambda}\epsilon\right)}{\delta(\epsilon-1)} \end{pmatrix}, \tag{2.82}$$

The symbols appearing in the above result are defined as

$$\delta \equiv 1-\hat{m}_c^2-\hat{q}^2, \qquad \omega \equiv 1-\hat{m}_c^2+\hat{q}^2. \tag{2.83}$$

The key to finding the ϵ-form of the above DEs is a correct change of free variables. Here, it is sufficient to apply the well known substitution:

$$\hat{q}^2 \equiv (1-uv)\left(1-\frac{v}{u}\right), \qquad \hat{m}_c \equiv v. \tag{2.84}$$

The DEs in the new variables read

$$\begin{aligned} &\left[\partial_u - \frac{(1-u^2)v}{u^2} A_{\hat{q}^2}\Big|_{\substack{\hat{q}^2=(1-uv)\left(1-\frac{v}{u}\right)\\ \hat{m}_c=v}}\right]\hat{M}^{(2a)} = 0, \\ &\left[\partial_v - \left(\left(2v-u-\frac{1}{u}\right)A_{\hat{q}^2} + 2vA_{\hat{m}_c^2}\right)\Big|_{\substack{\hat{q}^2=(1-uv)\left(1-\frac{v}{u}\right)\\ \hat{m}_c=v}}\right]\hat{M}^{(2a)} = 0. \end{aligned} \tag{2.85}$$

The kinematically allowed ranges $0 \leq m_c \leq m_b$ and $0 \leq q^2 \leq (m_b-m_c)^2$ are mapped onto $0 \leq v \leq 1$ and $v \leq u \leq 1$, with $u = v$ corresponding to $q^2 = 0$ and $u = 1$ to the phase space endpoint $q^2 = (m_b - m_c)^2$. As a result, the limit defining the boundary conditions for the ϵ-form solution in eq. (2.46) should be taken first as $v \to 0^+$ and only then $u \to 0^+$, as the reverse ordering would cross a branch cut. The definitions (2.84) can be inverted to express u and v in terms of $\hat{m}_c^2$ and $\hat{q}^2$. There are four possible solutions but only one of them gives u and v in the described ranges for $\hat{m}_c^2$ and $\hat{q}^2$ in the kinematically allowed region:

$$u = \frac{2-\omega-\sqrt{\hat{\lambda}}}{2\hat{m}_c}, \qquad v = \hat{m}_c. \tag{2.86}$$

Clearly, such a change of variables results in rational DE matrices but is not equivalent to any rational linear transformation of the MIs, thus extending the class of allowed transformations of the DEs, as described in the previous section.

After elementary algebraic simplifications, the denominators present in the DE matrices in eq. (2.85) can be expressed as products of the following letters:

$$\begin{aligned} \alpha_1 &\equiv u, & \alpha_2 &\equiv u-1, & \alpha_3 &\equiv u+1, \\ \alpha_4 &\equiv v, & \alpha_5 &\equiv v-1, & \alpha_6 &\equiv v+1, \\ \alpha_7 &\equiv u-v, & \alpha_8 &\equiv uv-1, & \tilde{\alpha} &\equiv \alpha_7^2-\alpha_5\alpha_6. \end{aligned} \tag{2.87}$$

The last letter $\tilde{\alpha}$ turns out to correspond to a spurious singularity, and is removed from the denominators by the Fuchsifying transformation T_F.

Using the package `Libra` [170], it is possible to construct each of the three transformations defined in eq. (2.49). The final result for $\mathfrak{T}$ reads

$$\mathfrak{T}(u,v) = \begin{pmatrix} D^{(0)}_{\mathfrak{T}} & \mathbb{0} \\ \mathbb{0} & D^{(1)}_{\mathfrak{T}} \end{pmatrix}, \tag{2.88}$$

with the diagonal blocks

$$D_{\mathfrak{T}}^{(0)} = \frac{(u^2-1)\,v^2(\epsilon-1)}{u(2\epsilon-1)(uv-1)} \begin{pmatrix} -\frac{v(2\epsilon-1)(uv-1)}{\epsilon-1} & 0 & 0 \\ 0 & -\frac{(2\epsilon-1)(uv-1)}{v(\epsilon-1)} & 0 \\ \frac{uv-1}{u-v} & \frac{1}{v} & -\frac{3(u^2-1)}{u-v} \end{pmatrix} \tag{2.89}$$

and

$$D_{\mathfrak{T}}^{(1)} = -\frac{1-2\epsilon}{u(1+\epsilon)}\times \begin{pmatrix} \frac{u^2v(1+2\epsilon)+u\left((1+v^2)(4\epsilon-1)-1\right)+v(1-6\epsilon)}{2\epsilon-1} & \frac{v\left(u^2+(uv-1)(4\epsilon-1)-4\epsilon\right)}{2\epsilon-1} & \frac{2u(v^2+1)(4\epsilon-1)-4u\epsilon-2\left(u^2+1\right)v(3\epsilon-1)}{6\epsilon-3} \\ \frac{5u^2v\epsilon+u\left(v^2-2\right)(4\epsilon-1)-3v\epsilon}{2\epsilon-1} & \frac{\epsilon v\left(3u^2+4uv-5\right)-uv^2}{2\epsilon-1} & \frac{2u\left(v^2-1\right)(4\epsilon-1)}{6\epsilon-3} \\ 3v-u\left(5uv+v^2-2\right) & -v(3u^2+uv-5) & -\frac{2}{3}u\left(v^2-1\right) \end{pmatrix}. \tag{2.90}$$

Applying this transformation reduces the DEs for the imaginary parts of the last six MIs to the ϵ-form:

$$d\mathrm{Im}\hat{M}^{(2a)'} = \epsilon dC \mathrm{Im}\hat{M}^{(2a)'} \qquad\qquad \mathrm{Im}\hat{M}^{(2a)} \equiv \mathfrak{T} \qquad \mathrm{Im}\hat{M}^{(2a)'}, \tag{2.91}$$

where

$$C = \sum_{l=1}^{8} \mathcal{C}_l \log \alpha_l. \tag{2.92}$$

The coefficient matrices $\mathcal{C}_5$ and $\mathcal{C}_6$ vanish while the other six read

$$\mathcal{C}_1 = \begin{pmatrix} 2 & 0 & 0 & 0 & 0 & 0 \\ 0 & 2 & 0 & 0 & 0 & 0 \\ -\frac{1}{3} & -\frac{1}{3} & 3 & 0 & 0 & 0 \\ 0 & 0 & 0 & \frac{49}{8} & \frac{55}{8} & 0 \\ 0 & 0 & 0 & -\frac{15}{8} & -\frac{9}{8} & 0 \\ 0 & 0 & 0 & -\frac{63}{8} & -\frac{105}{8} & 2 \end{pmatrix}, \quad \mathcal{C}_2 = \mathcal{C}_3 = \begin{pmatrix} -2 & 0 & 0 & 0 & 0 & 0 \\ 0 & -2 & 0 & 0 & 0 & 0 \\ \frac{1}{3} & \frac{1}{3} & -4 & 0 & 0 & 0 \\ 0 & 0 & 0 & -3 & -3 & 0 \\ 0 & 0 & 0 & -3 & -3 & 0 \\ 0 & 0 & 0 & 9 & 9 & 0 \end{pmatrix}, \tag{2.93}$$

$$\mathcal{C}_4 = \begin{pmatrix} -4 & 0 & 0 & 0 & 0 & 0 \\ 0 & -2 & 0 & 0 & 0 & 0 \\ 0 & \frac{1}{3} & -4 & 0 & 0 & 0 \\ 0 & 0 & 0 & -2 & 0 & \frac{2}{3} \\ 0 & 0 & 0 & -2 & -4 & -\frac{2}{3} \\ 0 & 0 & 0 & 6 & 0 & -2 \end{pmatrix}, \qquad \mathcal{C}_7 = \begin{pmatrix} 0 & 0 & 0 & 0 & 0 & 0 \\ 0 & 0 & 0 & 0 & 0 & 0 \\ -\frac{1}{3} & 0 & 1 & 0 & 0 & 0 \\ 0 & 0 & 0 & \frac{7}{8} & \frac{5}{8} & \frac{1}{6} \\ 0 & 0 & 0 & \frac{7}{8} & \frac{5}{8} & \frac{1}{6} \\ 0 & 0 & 0 & -\frac{105}{8} & -\frac{75}{8} & -\frac{5}{2} \end{pmatrix}, \tag{2.94}$$

$$\mathcal{C}_8 = \begin{pmatrix} 0 & 0 & 0 & 0 & 0 & 0 \\ 0 & 0 & 0 & 0 & 0 & 0 \\ 0 & -\frac{1}{3} & 1 & 0 & 0 & 0 \\ 0 & 0 & 0 & \frac{1}{8} & \frac{3}{8} & -\frac{1}{6} \\ 0 & 0 & 0 & \frac{1}{8} & \frac{3}{8} & -\frac{1}{6} \\ 0 & 0 & 0 & \frac{9}{8} & \frac{27}{8} & -\frac{3}{2} \end{pmatrix}. \tag{2.95}$$

With the above result and eq. (2.46), it is straightforward to build the general solution for $\mathrm{Im}\hat{M}^{(2a)}$:

$$\begin{aligned}\mathrm{Im}\hat{M}^{(2a)}(u,v) =&\mathfrak{T}(u,v)\Big[\mathbb{1}+\epsilon\Big((\mathcal{C}_1+\mathcal{C}_7)\log u+\mathcal{C}_2\log(1-u^2)+\mathcal{C}_4\log v+\mathcal{C}_7\log\left(1-\frac{v}{u}\right)\\ &+\mathcal{C}_8\log(1-uv)\Big)+\mathcal{O}(\epsilon^2)\Big]\lim_{u\to 0^+}\lim_{v\to 0^+}\mathrm{Im}\hat{M}^{(2a)'}(u,v)\\ \equiv&\mathfrak{T}(u,v)P(u,v)\lim_{u\to 0^+}\lim_{v\to 0^+}\mathrm{Im}\hat{M}^{(2a)'}(u,v).\end{aligned} \tag{2.96}$$

In the last line, $P(u,v)$ has been introduced to denote all the terms in the square bracket, namely the evolution operator of the imaginary parts of the MIs. The term $\mathcal{O}(\epsilon^2)$ involves dilogarithms arising from the results for the GPLs of rank two derived in the previous section. These have to be analytically continued to the physical region using the Euler's formula:

$$\mathrm{Li}_2(z)+\mathrm{Li}_2(1-z)+\log(z)\log(1-z)=\frac{\pi^2}{6}, \tag{2.97}$$

which follows directly from the Hölder convolution of eq. (2.72) for $G(0,1|1)$, and the identity $\mathrm{Li}_2(1)=\pi^2/6$. The branch of the logarithms can be resolved using the Feynman prescription for the variables $v=v-i\varepsilon$ and $u=u-i\varepsilon$. The latter can be derived from its equivalents $m_c^2=m_c^2-i\varepsilon$ and $q^2=q^2-i\varepsilon$ and the definition of u. Now, the only remaining non-trivial step in the calculation of the contribution $(2a)$ is the determination of the boundary condition $\lim_{u\to 0^+}\lim_{v\to 0^+}\mathrm{Im}\hat{M}^{(2a)'}(u,v)$.

2.5 The Auxiliary Mass Flow

The general solutions to the DEs given in eqs. (2.29), (2.35), or (2.46) specify the functional dependence of the MIs on the mass scales of the problem, up to a boundary condition. When one uses the ϵ-form approach, this boundary has to be computed at the point where all the free variables v_k are set to 0. This is usually a branch point of the original diagrams, and the calculation here has to be performed via a careful asymptotic expansion [184–188]. An alternative would be to compute the MIs at a regular point, evolve them to $v_k=0$ and use the result as the boundary condition. This method often avoids nuances of asymptotic expansions and analytic continuation, as one can choose the regular point in the same branch of the MIs as the physical region[†]. Unfortunately, obtaining an analytic result for the MIs by a direct calculation, even for a single regular point, is usually unfeasible. This section describes a recently developed algorithm that can circumvent this problem by computing very precise numerical approximations to the MIs at any regular point. Even for the frontier computations, the solution can be made precise enough to reconstruct the exact transcendental constants appearing after its evolution to $v_k=0$. This is a qualitative improvement over previous numerical methods that were many orders of magnitude less efficient. It also allows for a completely numerical treatment of multi-scale problems with dense scans of parameter spaces. The latter approach has been used in the present thesis for evaluation of the q^2 spectrum including the triple-charm contributions, as will be described in the next chapter.

The method described below was first presented by Liu, Ma, and Wang in ref. [189]. Their initial idea is quite similar to the DE method for computing MIs with more than one

[†]Usually in the physical region itself.

mass scale. The difference is that the DEs are constructed specifically to have the simplest possible boundary condition. For this purpose, the Feynman regulator ε, referred to in this approach as the Auxiliary Mass, can be treated as a free variable, while the MIs in a basis M as limits

$$M(\varepsilon) \xrightarrow{\varepsilon\to 0^+} M \tag{2.98}$$

of functions $M(\varepsilon)$ constructed by removing the limit $\varepsilon \to 0^+$ from the definition of M. One can then construct a system of DEs for $M(\varepsilon)$ in exactly the same way as was described at the beginning of section 2.3. Instead of describing some actual evolution of integrals as functions of masses and kinematical variables, they can be used to evolve the functions $M(\varepsilon)$ from a conveniently chosen boundary condition down to the physical limit (2.98). The original role of ε as a limit parameter plays no role in the IBP reduction or computing mass derivatives, so from the standpoint of these operations, it can be treated as yet another mass. Note that in this approach, all other, physical scales, i.e. masses, external momenta lengths, and Mandelstam variables are fixed to some chosen numerical values. The functions $M(\varepsilon)$ are treated as depending on a single free variable – ε, resulting in a system of *ordinary* DEs. As it is constructed in the same way, it has the same form as previously:

$$\frac{d}{d\varepsilon}M(\varepsilon) = A(\varepsilon)M(\varepsilon), \tag{2.99}$$

with $A(\varepsilon)$ being some matrix of rational functions of ε. As the mathematical theory of ordinary DEs is much simpler than that of the partial ones, there exists a plethora of possible solution methods. It is important to emphasize that the IBP reduction performed to establish above DEs will introduce a number of new MIs that vanish in the limit $\varepsilon \to 0^+$. In essence, treating ε as a free variable introduces an additional mass scale to the problem, which is bound to substantially complicate the IBP reduction and the DEs. One advantage of this approach is in the simplicity of the necessary boundary conditions. In practical applications, the IBP reduction can usually be expected to be efficiently achievable if all mass scales apart from ε are substituted by some numerical values.

Before describing the particular solution procedure applied to eq. (2.99), one should consider the limit of functions $M(\varepsilon)$ as ε approaches positive infinity. A generic function $M_n(\varepsilon)$ is an integral

$$\begin{aligned} M_n(\varepsilon) =& \int \left(\prod_{l=1}^{L} \frac{d^D k_l}{i(2\pi)^D}\right) \prod_j \frac{1}{\left((\hat{k}_j + \hat{p}_j)^2 - m_j^2 + i\varepsilon\right)^{a_j}} \\ =& \varepsilon^{\frac{DL}{2}-a_n} \int \left(\prod_{l=1}^{L} \frac{d^D \tilde{k}_l}{i(2\pi)^D}\right) \prod_j \frac{1}{\left((\hat{\tilde{k}}_j + \hat{\tilde{p}}_j)^2 - \tilde{m}_j^2 + i\right)^{a_j}}, \end{aligned} \tag{2.100}$$

where $\hat{k}_j$ and $\hat{p}_j$ are some combinations of loop and external momenta respectively, $a_n \equiv \sum_j a_j$, and $\tilde{x} \equiv x/\sqrt{\varepsilon}$. In the $\varepsilon \to \infty^+$ limit, $\tilde{m}_j^2$ and $\hat{\tilde{p}}_j$ vanish. The interchange of the loop integration and the limit can be understood in the framework of the expansion by regions [185, 186], where only regions with large loop momenta matter when ε is sufficiently large when compared with kinematical invariants. The function $M_n(\varepsilon)$ simplifies then as follows:

$$\varepsilon^{a_n - \frac{DL}{2}} M_n(\varepsilon) \xrightarrow{\varepsilon\to\infty} \int \left(\prod_{l=1}^{L} \frac{d^D k_l}{i(2\pi)^D}\right) \prod_j \frac{1}{\left(\hat{k}_j^2 - \left(\sqrt{-i}\right)^2\right)^{a_j}} \equiv V_n\left(\sqrt{-i}\right). \tag{2.101}$$

The factor of $1/\sqrt{\varepsilon}$ in $\hat{\tilde{k}}_l$ was absorbed by a rescaling variable change. The integral $V_n\left(\sqrt{-i}\right)$ is obtained from the M_n by setting all external momenta to 0 and replacing the mass in all propagators with $\sqrt{-i}$, including the massless ones. In the diagrammatic picture, it can be seen as the original MI with external legs removed and all masses equal[†]. This class of so-called equal mass tadpole integrals was analyzed extensively over the years and the analytic results for deep expansions in ϵ are known up to three loops [133, 190–193]. Deep ϵ expansions of four [194] and five [195] loop equal mass tadpoles are known numerically with hundreds of digits of precision. These integrals can also be IBP reduced to a small set of MIs. Up to three loops, the MI basis can be chosen as:

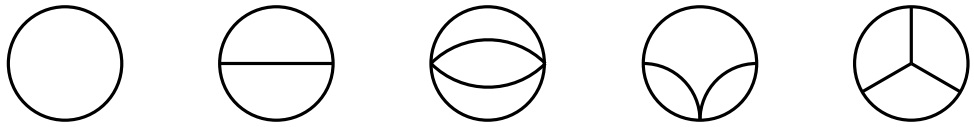

(2.102)

and products of the first two. Their numerical results are gathered in a convention independent manner in ref. [196]. The authors of ref. [189] prove that the expression in the parenthesis in eq. (2.101) is an analytic function of ε near infinity. This provides an ansatz for the asymptotic expansion of $M(\varepsilon)$ around infinity:

$$M_n(\varepsilon) = \varepsilon^{\frac{DL}{2}-a_n} \sum_{j=0}^{\infty} M_{n,j}^{(\infty)} \varepsilon^{-j}, \tag{2.103}$$

with $M_{n,0}^{(\infty)} = V_n\left(\sqrt{-i}\right)$ being IBP reducible to known results up to five loops. This series converges for all ε such that $|\varepsilon| > \max\{|\varepsilon_j^{(pole)}|\}$, where $\{\varepsilon_j^{(pole)}\}$ is the set of singular points of $M_n(\varepsilon)$.

The numerical solution of the DE system in eq. (2.99) specifies the Auxiliary Mass Flow (AMF) from the boundary at infinity that was discussed above to the physical limit $\varepsilon \to 0^+$. It can be done in a variant of the "expand-and-match" approach. First, all mass scales present in the matrix $A(\varepsilon)$ should be substituted with numbers for which the MIs are to be computed. One uses eq. (2.99) and the ansatz (2.103) to derive recurrence relations between consecutive $M_{n,j}^{(\infty)}$. These can be recursively solved for $M_{n,j}^{(\infty)}$, $j > 0$, using the result $M_{n,0}^{(\infty)} = V_n\left(\sqrt{-i}\right)$. This produces a deep expansion of $M_n(\varepsilon)$ in powers of $1/\varepsilon$. One then chooses a point ε_1 inside the convergence region of the series in eq. (2.103). The singularities of $M_n(\varepsilon)$ are a subset of poles of the AMF DE in eq. (2.99), so the region of convergence can be read out of the matrix $A(\varepsilon)$. A typical analytic structure of $A(\varepsilon)$ is presented in figure 9. As long as the point ε_1 is chosen to be outside of the red circle, the values of $M_n(\varepsilon_1)$ can be approximated using the previously obtained asymptotic expansion around infinity:

$$M_n(\varepsilon_1) \simeq \varepsilon_1^{\frac{DL}{2}-a_n} \sum_{j=0}^{N} M_{n,j}^{(\infty)} \varepsilon_1^{-j}, \tag{2.104}$$

for some integer N large enough to reach the desired precision of $M_n(\varepsilon_1)$.

The above procedure can now be repeated for another point ε_2 that is closer to $\varepsilon = 0$. As ε_1 is a regular point of $M_n(\varepsilon)$, MIs have a standard Taylor expansion around it:

$$M_n(\varepsilon) = \sum_{j=0}^{\infty} M_{n,j}^{(1)} (\varepsilon - \varepsilon_1)^j, \tag{2.105}$$

[†]Note that the lack of ε prescription plays no role for these integrals, as they never possess any intermediate cuts that could produce branch ambiguities.

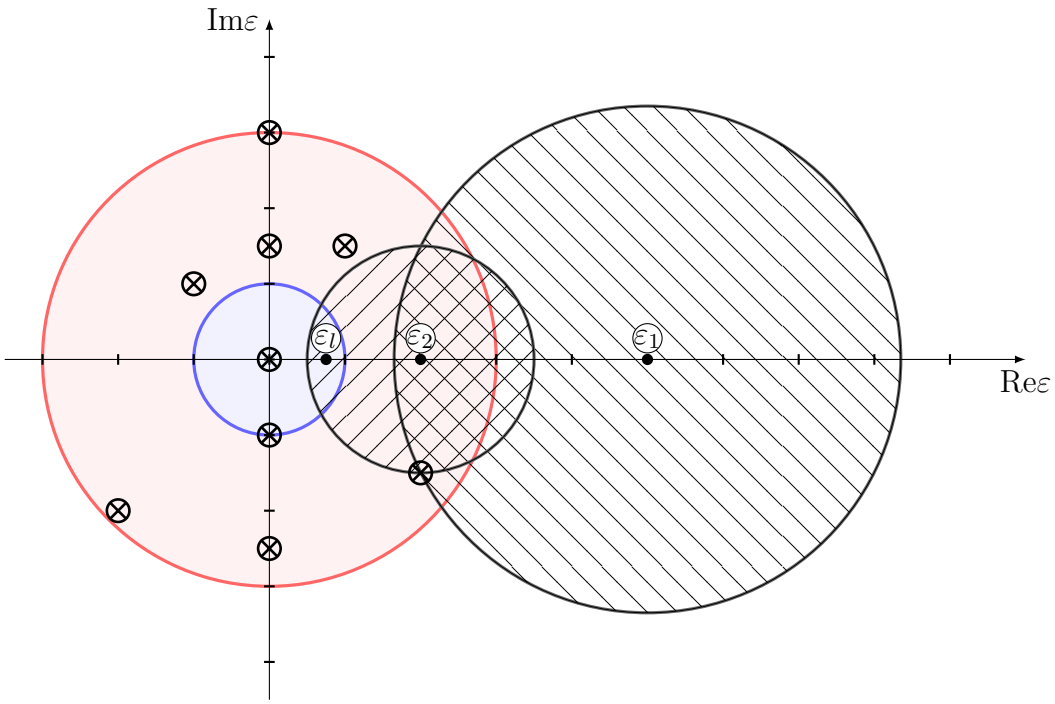

Figure 9: An example illustrating the Auxiliary Mass Flow [189, 197]. The poles of the AMF DEs are indicated with the small crossed circles. The red circle depicts the region in the complex ε plane where the expansion of the MIs around infinity is not convergent. The blue circle is the region of convergence of the expansion around $\varepsilon = 0$. The points chosen for the intermediate expansions are indicated with ε_1 and ε_2 with the regions of convergence drawn as striped circles. The point ε_l is both inside the blue circle and inside the region of convergence of the expansion around ε_2 so it can be used to fix the coefficients of the expansion around $\varepsilon = 0$.

with $M^{(1)}_{n,0} = M_n(\varepsilon_1)$ obtained in eq. (2.104). The AMF DEs again provide relations between consecutive coefficients $M^{(1)}_{n,j}$ that can be used to recursively calculate $M^{(1)}_{n,j}$ using $M^{(1)}_{n,0} = M_n(\varepsilon_1)$. The convergence region of this expansion extends from ε_1 to the closest singularity, which again can be read out of the AMF DE matrix. It has some non zero overlap with the region in which the expansion at infinity is divergent (the red circle in figure 9), and one can choose ε_2 to be inside that overlap. The series in eq. (2.105) can now be used to obtain an arbitrarily precise approximation of $M_n(\varepsilon_2)$:

$$M_n(\varepsilon_2) \simeq \sum_{j=0}^{N} M^{(1)}_{n,j}(\varepsilon_2 - \varepsilon_1)^j. \tag{2.106}$$

This step is then iterated until one obtains an approximation of the value of $M_n(\varepsilon)$ at a point ε_l that is inside the convergence region of the asymptotic expansion of $M_n(\varepsilon)$ around 0 (the blue circle in figure 9), i.e. $|\varepsilon_l| < \min\left(\{|\varepsilon_j^{(pole)}|\} \setminus \{0\}\right)$.

To obtain the physical limit $\lim_{\varepsilon\to 0^+} M_n(\varepsilon)$, one needs to derive the correct ansatz for the asymptotic expansion of $M_n(\varepsilon)$ around 0. Below, it is assumed that the Poincaré rank $p_0^{(A(\varepsilon))}$ can be lowered to 0 by a rational transformation $T(\varepsilon)$. If it can, the transformed AMF DE

matrix can be expanded as

$$\tilde{A}(\varepsilon) = \sum_{k=-1}^{\infty} \tilde{A}_k \varepsilon^k. \tag{2.107}$$

The general solution of the AMF DE in eq. (2.99) can then be written as

$$\tilde{M}(\varepsilon) = T^{-1}(\varepsilon) M(\varepsilon) = e^{\log \varepsilon \tilde{A}_{-1}} v(\varepsilon), \tag{2.108}$$

where $v(\varepsilon)$ is analytic around $\varepsilon = 0$:

$$v(\varepsilon) = \sum_{n=0}^{\infty} v_n \varepsilon^n, \ \varepsilon < \min\left(\{|\varepsilon_j^{(pole)}|\} \setminus \{0\}\right). \tag{2.109}$$

Substituting this ansatz into the transformed AMF DE:

$$\partial_\varepsilon \tilde{M} = \tilde{A} \tilde{M} \tag{2.110}$$

results in a recurrence relation for the coefficient vectors v_k:

$$k v_k = \sum_{j=0}^{k-1} \tilde{A}_j v_{k-j-1}, \tag{2.111}$$

which can be solved up to the unknown v_0 for arbitrarily high v_k. The boundary vector v_0 is fixed by the approximation:

$$M(\varepsilon_l) = T(\varepsilon_l) \tilde{M}(\varepsilon_l) \simeq T(\varepsilon_l) e^{\log \varepsilon_l \tilde{A}_{-1}} \sum_{n=0}^{N} v_n \varepsilon_l^n, \tag{2.112}$$

where $M(\varepsilon_l)$ was obtained in the last step of the chain of Taylor expansions around regular finite points. The physical value of the MIs obtained in the AMF finally reads

$$M = \lim_{\varepsilon \to 0^+} M(\varepsilon) = \left(\lim_{\varepsilon \to 0^+} T(\varepsilon) e^{\log \varepsilon \tilde{A}_{-1}} \right) v_0. \tag{2.113}$$

An implementation of the AMF algorithm was published by two of its original authors in a `Mathematica` package `AMFlow` [198]. It features two major improvements beyond the procedure described above. First, `AMFlow` performs the AMF evolution for various numerical probe values of the dimensional ϵ. In that approach, the only symbolic quantity left is the Auxiliary Mass ε. The result for the expansion of the MIs in ϵ can then be reconstructed from the separate probe calculations and the error of the reconstruction can be suppressed by considering enough values of ϵ. Second, the package uses an iterative strategy [197] of introducing the Auxiliary Mass parameter ε to propagators of MIs. Instead of treating all Feynman regulators as equal, only some of them are taken to ∞ to compute boundary conditions while the rest is left near 0^+. This can drastically lower the number of MIs present in the ε dependent IBP reduction for the price of more complicated boundary conditions at $\varepsilon \to \infty$. In the expansion by regions, diagrams with a very heavy mass present in some of the lines can be written as combinations of diagrams factorized into tadpoles and the original graphs with some of the heavy lines shrunk to a point. To obtain the boundary condition, one can compute the latter using the AMF method, again introducing large ε only to some lines. This results in an iterative pattern. Each consecutive introduction of large ε into a subset of lines of a diagram simplifies it further in the $\varepsilon \to \infty$ limit. The procedure closes in a finite number of steps. Again one only has to provide the results for tadpoles, but the first DE established for the MIs with free ε present in only some of the lines is much simpler than in the basic case discussed above.

2.6 Sample Calculation - 5

The boundary condition for the general solution in eq. (2.96) can be computed by using the properties of the evolution operator $P(u,v)$ written in the square bracket of that equation. More specifically, one can realize that this boundary condition can be obtained by evolving the values of MIs in the transformed basis from any generic point (u_0, v_0) in the physical region down to $u = v = 0$. This general idea can be formulated as

$$\lim_{u\to 0^+}\lim_{v\to 0^+} \mathrm{Im}\hat{M}^{(2a)'}(u,v) = P^{-1}(u_0,v_0)\mathfrak{T}^{-1}(u_0,v_0)\mathrm{Im}\hat{M}^{(2a)}(u_0,v_0), \tag{2.114}$$

where the canonical transformation $\mathfrak{T}$ was used to transform $\mathrm{Im}\hat{M}^{(2a)'}(u_0,v_0)$ back to the original MI basis. The last factor can be obtained using the AMF technique. A naive choice would be to take $(u_0,v_0) = (0,0)$ with $P(0,0) = \mathbb{1}$. However, a direct computation of the MIs at this point cannot be transformed to the ϵ basis, as the elements of $\mathfrak{T}$ become singular in the limit of $(u,v) \to (0,0)$. This is an expected behavior since this is a branch point of the GPLs appearing in the general solution. Instead, one can take for example $(u_0,v_0) = (0.02, 0.01)$, which is inside the kinematically allowed phase space and corresponds to $(\hat{q}^2, \hat{m}_c^2) = (0.4999, 0.0001)$. Using the package `AMFlow` [198], both the real and imaginary parts of all 13 MIs of the diagram $(2a)$ can be computed at this point in a single run of the AMF algorithm. The results up to $\mathcal{O}(\epsilon)$ inclusive were obtained with 100 significant digits on the same computer as for the IBP reduction in section 2.2 in 216 seconds. After rounding to 4 digits, they read

$$\left(\frac{m_b}{\mu}\right)^{4\epsilon} \mathrm{Im}\left[\text{ 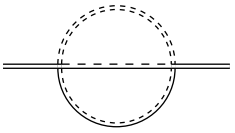 }\right]\Big|_{u=2v=0.02} = \frac{6.297\times10^{-9}}{\epsilon} + 8.562\times10^{-8} + 5.875\times10^{-7}\epsilon,$$

$$\left(\frac{m_b}{\mu}\right)^{4\epsilon} \mathrm{Im}\left[\text{ 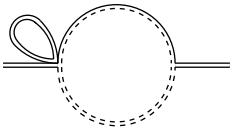 }\right]\Big|_{u=2v=0.02} = \frac{6.297\times10^{-5}}{\epsilon} + 2.762\times10^{-4} + 6.598\times10^{-4}\epsilon,$$

$$\left(\frac{m_b}{\mu}\right)^{4\epsilon} \mathrm{Im}\left[\text{ 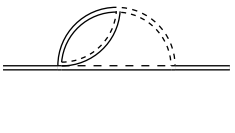 }\right]\Big|_{u=2v=0.02} = \frac{6.297\times10^{-5}}{\epsilon} + 2.955\times10^{-4} + 7.589\times10^{-4}\epsilon,$$

$$\left(\frac{m_b}{\mu}\right)^{4\epsilon} \mathrm{Im}\left[\text{ 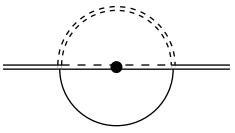 }\right]\Big|_{u=2v=0.02} = 3.863\times10^{-4} + 3.926\times10^{-3}\epsilon, \tag{2.115}$$

$$\left(\frac{m_b}{\mu}\right)^{4\epsilon} \mathrm{Im}\left[\text{ 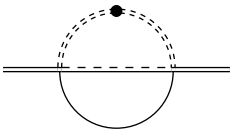 }\right]\Big|_{u=2v=0.02} = 2.423\times10^{-5} + 2.063\times10^{-4}\epsilon,$$

$$\left(\frac{m_b}{\mu}\right)^{4\epsilon} \mathrm{Im}\left[\text{ 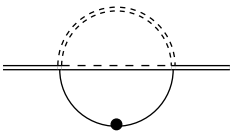 }\right]\Big|_{u=2v=0.02} = \frac{-6.297\times10^{-5}}{\epsilon} - 4.076\times10^{-4} - 1.098\times10^{-3}\epsilon,$$

where the overall factors of m_b to an ϵ-dependent power were suppressed, together with the uncomputed terms $\mathcal{O}(\epsilon^2)$. Using eq. (2.114), the boundary condition becomes

$$\begin{aligned}\left(\frac{m_b}{\mu}\right)^{4\epsilon} \lim_{u\to 0^+}\lim_{v\to 0^+} \mathrm{Im}\hat{M}^{(2a)'} = \frac{1}{256\pi^3}\Big[&\frac{1}{\epsilon}+3+\left(7-\frac{\pi^2}{6}\right)\epsilon, \frac{1}{\epsilon}+3+\left(7-\frac{\pi^2}{6}\right)\epsilon,\\ &\frac{1}{3\epsilon}+1+\frac{1}{9}\left(21-\pi^2\right)\epsilon, \frac{1}{8\epsilon}+\frac{3}{4}+\frac{1}{48}\left(144-37\pi^2\right)\epsilon,\\ &\frac{1}{8\epsilon}+\frac{3}{4}+\frac{1}{48}\left(144+11\pi^2\right)\epsilon, -\frac{3}{8\epsilon}-\frac{9}{4}+\frac{1}{16}\left(-144+37\pi^2\right)\epsilon\Big]^T + \mathcal{O}(\epsilon^2).\end{aligned} \tag{2.116}$$

The exact expressions for both the $\mathcal{O}(\epsilon^{-1})$ and $\mathcal{O}(\epsilon^0)$ terms can be obtained by first guessing the overall factor of $1/(256\pi^3)$ that is common for two-loop calculations. The analytical values for the $\mathcal{O}(\epsilon)$ term can be reconstructed using the `Mathematica` implementation of the PSLQ algorithm [199, 200] fitted to just two constants: $\{1, \pi^2\}$. In all three terms, the result agrees with all 100 digits obtained from `AMFlow`.

The only remaining thing to do now is to recombine all the intermediate results as specified by eq. (1.253), table 2, and the results of the IBP reduction into the final formula for the $d\Gamma^{(1)}_{(2a)}/dq^2$ contribution (c.f. I.20):

$$\begin{aligned}\frac{d\Gamma^{(1)}_{(2a)}}{dq^2} =&\frac{G_F^2|V_{cb}|^2 m_b^3}{144\pi^3 u^3}\frac{\alpha_s}{\pi}\left(\frac{\mu}{m_b}\right)^{4\epsilon}\Bigg[\left(\frac{\xi_g}{\epsilon}+\frac{3}{2}+\frac{10\xi_g}{3}\right)H_1+\frac{uv(u^2-1)}{4}\left(H_2-\xi_g H_2^{(\xi)}\right)\\ &+(4-6\xi_g)H_1\log(1-u^2)+(F_1-4\xi_g H_1)\log v+(F_2+\xi_g F_2^{(\xi)})\log u\\ &+(F_3+\xi_g F_3^{(\xi)})\log(1-uv)+(F_4+\xi_g F_4^{(\xi)})\log\left(1-\frac{v}{u}\right)\\ &+4\frac{u^2+1}{u^2-1}H_1\left(\overline{\mathrm{Li}}_2\left(1-\frac{v}{u}\right)-\overline{\mathrm{Li}}_2\left(1-uv\right)-2\overline{\mathrm{Li}}_2\left(u^2\right)\right)\Bigg],\end{aligned} \tag{2.117}$$

where

$$\begin{aligned}H_1(u,v) \equiv&\left(u^2-1\right)v^2\left(\left(u^4+4u^2+1\right)v-\frac{3}{2}u\left(u^2+1\right)\left(v^2+1\right)\right),\\ H_2(u,v) \equiv&3v\left(v^2+1\right)\left(u^2+1\right)+4u\left(v^4-5v^2+1\right),\\ F_1(u,v) \equiv&(u^2-1)v^3\left(u^4+4u^2+1-3uv(1+u^2)\right),\\ F_2(u,v) \equiv&v^2\Big(12u^3\left(1+u^2\right)+v\left(1-11u^2-35u^4-7u^6\right)\\ &+v^2\left(13u^5+20u^3+u\right)-4v^3\left(u^2+u^4\right)+2v^4u^3\Big),\\ F_3(u,v) \equiv&(1-uv)\Big(u^3-vu^2\left(u^2+2\right)+v^2u\left(u^4+2u^2-1\right)\\ &-v^3\left(u^4-2u^2-1\right)-v^4u\left(2u^2+1\right)+v^5u^2\Big),\\ F_4(u,v) \equiv&(v-u)\Big(u^2-u\left(2u^2+1\right)v+\left(-u^4+2u^2+1\right)v^2\\ &+v^3u\left(u^4+2u^2-1\right)-v^4u^2\left(u^2+2\right)+v^5u^3\Big).\end{aligned} \tag{2.118}$$

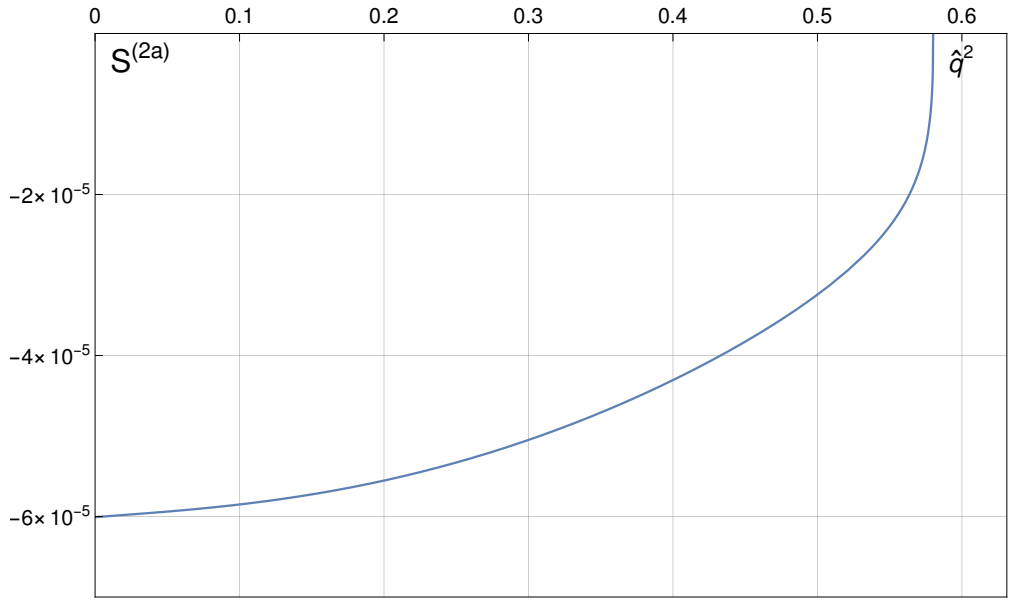

Figure 10: The function $S^{(2a)}$ from eq. (2.121) after changing the variables back to $\hat{q}^2$ and $\hat{m}_c^2$, for $\hat{m}_c = 0.2384$. The latter value corresponds to the ratio of the $\overline{\text{MS}}$ renormalized charm quark mass at $\mu = 2\text{GeV}$, and the bottom quark mass in the kinetic scheme [23–26] renormalized at the kinetic scale of 1GeV. These parameters were taken from ref. [35].

The terms proportional to ξ_g are specified by the polynomials:

$$\begin{aligned}
H_2^{(\xi)}(u,v) \equiv& 5v\left(v^2+1\right)\left(u^2+1\right) - 2u\left(v^4+6v^2+1\right), \\
F_2^{(\xi)}(u,v) \equiv& v^2\left(6\left(1-2u^4\right)u\left(v^2+1\right) + u^3v^2\left(v^2-3\right) + 4\left(2u^4+6u^2-3\right)u^2v - 4v\right), \\
F_3^{(\xi)}(u,v) \equiv& \frac{1}{2}(1-uv)^2\left(u^3(2uv+1) + 3\left(1-u^2\right)uv^2 - v^3(uv+2)\right), \\
F_4^{(\xi)}(u,v) \equiv& \frac{1}{2}(v-u)^2\left(u^3v^3(2u+v) + 3u\left(1-u^2\right)v^2 - u - 2v\right).
\end{aligned} \tag{2.119}$$

The function $\overline{\text{Li}}_2(x)$ is defined as a combination of two dilogarithms:

$$\overline{\text{Li}}_2(x) \equiv \text{Li}_2(x) - \text{Li}_2(1-x). \tag{2.120}$$

To illustrate the functional dependence of this result on $\hat{q}^2$, it is convenient to define a function $S^{(2a)}(\hat{q}^2, \hat{m}_c^2)$ through the equation:

$$\lim_{\epsilon\to 0}\left[\frac{d\Gamma^{(1)}_{(2a)}}{dq^2}\Big|_{\xi=0,\mu=m_b}\right] = G_F^2|V_{cb}|^2 m_b^3 S^{(2a)}(\hat{q}^2, \hat{m}_c^2). \tag{2.121}$$

This function is shown in figure 10. The value of $\alpha_s = \alpha_s(m_b) \approx 0.2183$ used in this figure was obtained with the package `RunDec` [201–203]. The running of α_s with the renormalization scale μ will be described in section 3.2.

The result in eq. (2.117) depends on ξ_g and diverges for $D \to 4$. The first of these issues is resolved after combining this correction with the contributions of the other 3 diagrams at the NLO[†]. The result becomes convergent after the full bare NLO correction is combined

[†]This becomes apparent already after the combined IBP reduction of all four diagrams, before calculating the MIs.

with results for the one loop counterterm diagrams. An interesting feature of eq. (10) is that the divergent term can be set to 0 by choosing the Landau gauge $\xi_g = 0$. The result for the finite, non-vanishing part in this gauge after changing the variables back to $\hat{q}^2$ and $\hat{m}_c^2$ for a reference value of $\hat{m}_c^2$ is presented in figure 10.

This concludes the sample calculation of the diagram $(2a)$ begun in section 1.3. It is important to emphasize here that because the contributions to $\mathrm{Im}\Sigma_{\mathrm{1PI}}$ coming from the three remaining diagrams can be IBP reduced to the imaginary parts of the same 6 MIs computed in this section, the calculation outlined above constitutes the vast majority of the work required to obtain the NLO correction to the spectrum. I will return to this point in section 3.4.

Chapter 3:

Semileptonic Decay of the B Meson

In the remainder of this thesis, I am going to apply the computational framework and tools developed in the previous chapters to the leading term in the HQE of the q^2 spectrum of the inclusive semileptonic decay up to NNLO in QCD. To this end, it is first important to argue the form of the Feynman rules quoted in eqs. (1.124), (1.125) (1.126), and (1.242). Most of them follow from the standard quantization procedure of non-Abelian gauge theories supplemented with the Faddeev-Popov prescription for path integrals involving gauge bosons. The only exception is the appearance of the auxiliary boson Q and the vertex factors $\mathcal{V}_Q$ and $\mathcal{V}_{\bar{Q}}$ in place of respectively the lepton pair and the four-fermion operators present in the vertices of diagrams in the left panel of figure 6. These replacements are only possible in the leading order in electroweak interactions because only in this approximation the q^2 spectrum factorizes into a contraction of leptonic and hadronic tensors (see eqs. (3.40) to (3.56)). At higher orders, photon exchanges between quarks and leptons spoil this simple behavior and introduce additional collinear singularities to the calculation.

The Q boson and its interactions with quarks can be derived from the SM Lagrangian in two steps. First, the degrees of freedom heavier than the b quark are integrated out of the path integrals for the full SM Green's functions. In general, this results in a description of SM particles below the electroweak scale called the Low-energy Effective Field Theory. In the case of the semileptonic transition at the leading order in electroweak interactions, this theory simplifies to QCD with five quark flavors, free leptons, and a single additional Fermi-like vertex involving the quark and lepton currents. In this approximation, it is possible to prove that the q^2 spectrum to all orders in QCD is equal (up to a constant factor) to the width of the process $B \to X_c Q$, where Q is the W boson in the SM with parameters tuned such that its mass is equal to $\sqrt{q^2}$. These steps will be described in section 3.1.

The other subject that needs to be addressed is the quantitative treatment of the hadronic structure of the B meson in the framework of the Heavy Quark Expansion. Parameterizing the B meson hadronic structure effects in a systematic way, and identifying the leading HQE term as given by the perturbatively calculable decay of the b quark is a highly non-trivial step. It is possible only because the considered process is inclusive. It is also phenomenologically viable thanks to $\hat{\Lambda} \approx (M_B - m_b)/m_b$ being small. Terms in the HQE factorize into parts coming from the hard and soft regions of parton momenta. Since the b quark mass is much larger than the QCD confinement scale, the hard factors can be computed perturbatively in powers of α_s. The contributions of the soft region can then be analyzed numerically using lattice QCD or fixed in a global fit to experimental data. One begins with deriving a basis of operators and computing their Wilson coefficients. At the leading order, the matrix elements of the operator describing the soft contribution are exactly the same, irrespectively whether one considers the full B meson or the perturbative b quark states. This allows for a completely perturbative treatment of the inclusive decay up to corrections suppressed by $\hat{\Lambda}^2$. The section 3.3 is dedicated to a more thorough discussion of these results. Still, a subject as extensive as the HQE and the underlying HQET could only be outlined within

the present thesis. A classic course covering many more aspects of these formalisms, such as the relations between the masses of heavy hadrons, the treatment of exclusive decays, and the Chiral Perturbation Theory can be found in ref. [204].

The calculation of the q^2 spectrum in the leading order in the HQE proceeds along the lines described in the previous two chapters. Section 3.4 describes the computation of the LO QCD term and the NLO correction using the DE method. The NLO term can be assembled from the MIs obtained in the sample calculation of the diagram $(2a)$ introduced in figure 6 on page 41. The NNLO term is not as straightforward because some of its MIs are not given by GPLs and thus cannot be obtained using the ϵ-form method described in the previous chapter. This motivated us to determine it in a numerical manner using the `AMFlow` package. This procedure is described in section 3.5. Our results are presented in section 3.6 as fits to a power-log ansatz.

3.1 Semileptonic Transition at the Leading Order

The analysis of the semileptonic decay in this thesis is limited to the SM prediction. It is therefore important to outline the structure of SM interactions that induce the underlying quark flavor-changing transition within the decaying B meson. The discussion below will focus only on the aspects relevant to the calculation of the semileptonic decay of the B meson in the leading approximation in electroweak interactions. This is certainly only a small fragment of the much richer Glashow-Weinberg-Salam theory [205–208], which in turn is only an example (although a crucial one for our current understanding of particle physics) of the broadly studied field of gauge invariant quantum theories. The interested reader may be referred to many classic textbooks on the subject, such as refs. [78, 80, 81, 84].

The SM Lagrangian density is built out of several terms:

$$\mathcal{L}_{SM} = \mathcal{L}_\psi + \mathcal{L}_g + \mathcal{L}_H + \mathcal{L}_Y + \mathcal{L}_{gf} + \mathcal{L}_{FP} + \mathcal{L}_\otimes. \tag{3.1}$$

The first two terms, $\mathcal{L}_\psi$ and $\mathcal{L}_g$, contain the kinetic and gauge-interaction terms for the fermions and gauge bosons, respectively. The third one, $\mathcal{L}_H$, includes the kinetic, gauge-interaction and self-interaction terms of the Higgs doublet. The fourth one, $\mathcal{L}_Y$, describes interactions between this doublet and fermions. The next two follow from the gauge fixing procedure in Yang-Mills theories, as mentioned at the end of section (1.1). The first of these terms introduces the gauge fixing parameter ξ into the vector boson propagators, while the second describes the Faddeev-Popov ghosts. The last term combines all counterterms that appear when the bare quantities in the original Lagrangian density are replaced with renormalized ones.

The quark flavor-changing transitions in question arise due to flavor non-diagonal Yukawa interactions between the quark fields and the Higgs doublet. The corresponding term in the SM Lagrangian reads[†]

$$\mathcal{L}_Y \supset \mathcal{L}_{q\text{-}Y} = -\bar{\psi}_Q \Gamma^{(d)} \psi_D H - \bar{\psi}_Q \Gamma^{(u)} \psi_U \tilde{H} + h.c. \tag{3.2}$$

The vector $\psi_Q \equiv (\psi_{Q1}, \psi_{Q2}, \psi_{Q3})^T$ combines the three generations of left-handed quark doublets introduced on page 2. Similarly, the vectors ψ_U and ψ_D combine the right-handed $SU(2)$ quark singlets. The Higgs doublet is denoted as $H = (H_1, H_2)^T$, while its hypercharge conjugate is $\tilde{H} = (H_2^*, -H_1^*)^T$. The matrices $\Gamma^{(x)}$ specify the Yukawa couplings. The

[†]The glossary presented in ref. [209] can be of great help whenever the discussion of the SM structure is needed.

terms in eq. (3.2) constitute the most general renormalizable interaction of the fermions with H that is Lorentz- and $SU(3)\otimes SU(2)\otimes U(1)$-invariant.

In the BEH mechanism [210, 211], the Higgs doublet is assigned a tree-level potential $V(H)$ with a gauge group orbit of lowest energy configurations H_0 different from $(0,0)^T$. A conventional choice is $H_0=(0,v)^T/\sqrt{2}$, where the parameter v is the vacuum expectation value of H. One then parameterizes the Higgs doublet as

$$H(x)=H_0+\begin{pmatrix}\chi^+(x)\\ \frac{h(x)+i\chi^0(x)}{\sqrt{2}}\end{pmatrix},\ \chi^+(x)\in\mathbb{C},\ h(x),\chi^0(x)\in\mathbb{R}. \tag{3.3}$$

With such a decomposition, the potential terms for the Higgs doublet become

$$\mathcal{L}_H\supset -V(H)=\frac{1}{2}M_h^2\left(H^\dagger H\right)-\frac{M_h^2}{2v^2}\left(H^\dagger H\right)^2=\frac{M_h^2v^2}{8}-\frac{M_h^2}{2}h^2+\ldots, \tag{3.4}$$

where the ellipsis denotes terms with at least three powers of the dynamical fields h, χ^+, and χ^0. The field h acquires a mass M_h, and is recognized as the physical Higgs boson. The other three dynamical fields are referred to as would-be Goldstone bosons. They can be removed from the theory with an $SU(2)$ gauge transformation as follows:

$$\exp\left[i\alpha^a(x)\tau^a\right]H(x)=\exp\left[i\alpha^a(x)\tau^a\right]\begin{pmatrix}H_1(x)\\ H_2(x)\end{pmatrix}=\begin{pmatrix}0\\ \frac{v+h(x)}{\sqrt{2}}\end{pmatrix}, \tag{3.5}$$

and thus do not belong to the spectrum of physical states of the SM. The symmetry generators are defined as $\tau^a\equiv\sigma^a/2$, with σ^a being the Pauli matrices. They are normalized as $\mathrm{Tr}(\tau^a\tau^b)=T_R^{\mathfrak{su}(2)}\delta^{ab}$, with $T_R^{\mathfrak{su}(2)}$ fixed by convention to $1/2$, the same as in the case of the QCD gauge group.

The part of $\mathcal{L}_{q\text{-}Y}$ in eq. (3.2) proportional to v gives rise to the bare quark mass parameters in the SM:

$$\begin{aligned}\mathcal{L}_{q\text{-}Y}\supset\mathcal{L}_{q\text{-mass}}&=-\bar{\psi}_Q\Gamma^{(d)}\psi_DH_0-\bar{\psi}_Q\Gamma^{(u)}\psi_U\tilde{H}_0+h.c\\&=-\frac{v}{\sqrt{2}}\left(\bar{\psi}_Q^{(1)}\Gamma^{(u)}\psi_U+\bar{\psi}_Q^{(2)}\Gamma^{(d)}\psi_D\right)+h.c.,\end{aligned} \tag{3.6}$$

where $\psi_Q^{(j)}\equiv\left(\psi_{Q1}^{(j)},\psi_{Q2}^{(j)},\psi_{Q3}^{(j)}\right)^T$, and $\psi_{Qk}^{(j)}$ is the j-th component of the $SU(2)$ doublet ψ_{Qk}. The coupling matrices $\Gamma^{(x)}$ can be singular-value-decomposed into products of unitary transformations and diagonal matrices $M^{(x)}$ with non-negative elements:

$$\Gamma^{(u)}=\frac{\sqrt{2}}{v}\mathcal{U}_QM^{(u)}\mathcal{U}_U^\dagger,\qquad\qquad\Gamma^{(d)}=\frac{\sqrt{2}}{v}\mathcal{U}_QVM^{(d)}\mathcal{U}_D^\dagger. \tag{3.7}$$

The unitary matrix V accounts for the fact that the left-diagonalizing transformation is different for $\Gamma^{(u)}$ and $\Gamma^{(d)}$. It turns out to be exactly the CKM matrix introduced in the Feynman rules in eq. (I.1), as will be discussed below. With the above form of $\Gamma^{(x)}$, $\mathcal{L}_{q\text{-mass}}$ becomes

$$\mathcal{L}_{q\text{-mass}}=-\bar{\psi}_Q^{(1)}\mathcal{U}_QM^{(u)}\mathcal{U}_U^\dagger\psi_U+\bar{\psi}_Q^{(2)}\mathcal{U}_QVM^{(d)}\mathcal{U}_D^\dagger\psi_D+h.c. \tag{3.8}$$

The diagonal elements of matrices $M^{(x)}$ are denoted as

$$M^{(u)}=\begin{pmatrix}m_u&&\\&m_c&\\&&m_t\end{pmatrix},\qquad\qquad M^{(d)}=\begin{pmatrix}m_d&&\\&m_s&\\&&m_b\end{pmatrix}. \tag{3.9}$$

This term simplifies with the following field redefinitions

$$\psi_Q^{(1)} \equiv \mathcal{U}_Q \mathfrak{u}_L, \qquad \psi_Q^{(2)} \equiv \mathcal{U}_Q V \mathfrak{d}_L, \qquad \psi_U \equiv \mathcal{U}_U \mathfrak{u}_R, \qquad \psi_D \equiv \mathcal{U}_D \mathfrak{d}_R, \tag{3.10}$$

and

$$\mathfrak{u} \equiv \mathfrak{u}_L + \mathfrak{u}_R \equiv (u, c, t)^T, \qquad \mathfrak{d} \equiv \mathfrak{d}_L + \mathfrak{d}_R \equiv (d, s, b)^T. \tag{3.11}$$

All unitary transformations in eq. (3.8) cancel and the quark mass Lagrangian reads

$$\mathcal{L}_{q\text{-mass}} = -\sum_{q\in\{u,d,c,s,t,b\}} m_q \bar{q}_L q_R + h.c. = -\sum_{q\in\{u,d,c,s,t,b\}} m_q \bar{q} q, . \tag{3.12}$$

The last equality utilized the fact that for all Dirac spinors ψ, $\bar{\psi}_{L/R}\psi_{L/R} = 0$, as well as that after the singular value decomposition, the diagonal elements $m_q \in \mathbb{R}$. The rotated fields $\mathfrak{u}$ and $\mathfrak{d}$ annihilate free quark mass eigenstates that define the flavor quantum numbers of hadrons. The structure of flavor changing interactions in the SM becomes clear once these fields are used consistently throughout the SM Lagrangian. The price is that this choice obfuscates the electroweak gauge invariance.

Just as the Yukawa interactions induce the quark masses, parts of the interaction between the Higgs doublet and the $SU(2)\otimes U(1)$ gauge bosons proportional to v give rise to the masses of W and Z. The gauge invariant kinetic term for H reads

$$\begin{aligned} \mathcal{L}_H \supset \mathcal{L}_{H\text{-kin}} &= \left[D_\mu H\right]^\dagger \left[D^\mu H\right] \\ &= \left[\left(\partial_\mu + igW_\mu^a \tau^a + ig' B_\mu Y_H\right) H\right]^\dagger \left[\left(\partial^\mu + igW_\mu^a \tau^a + ig' B^\mu Y_H\right) H\right], \end{aligned} \tag{3.13}$$

where g and g' are the gauge couplings of $SU(2)$ and $U(1)$ respectively and W^a and B are the corresponding real valued gauge boson fields. The 2×2 identity matrix multiplying the partial derivative and the B^μ term is implicit. The part proportional to v is

$$\begin{aligned} \mathcal{L}_{H\text{-kin}} \supset \mathcal{L}_{\text{gauge-mass}} &= \left[\left(igW_\mu^a \frac{\sigma^a}{2} + ig' B_\mu Y_H\right) H_0\right]^\dagger \left[\left(igW^{\mu,b} \frac{\sigma^b}{2} + ig' B^\mu Y_H\right) H_0\right] \\ &= \frac{v^2 g^2}{8} \begin{pmatrix} W_\mu^1 + iW_\mu^2 \\ \frac{g'}{g} B_\mu - W_\mu^3 \end{pmatrix}^T \begin{pmatrix} W^{1\,\mu} - iW^{2\,\mu} \\ \frac{g'}{g} B^\mu - W^{3\,\mu} \end{pmatrix}. \end{aligned} \tag{3.14}$$

The gauge field mass- and electric-charge-eigenstates are denoted by $W_\mu^\pm$, Z_μ and A_μ. They are related to the original fields as follows

$$\begin{aligned} W_\mu^1 &= \frac{1}{\sqrt{2}}\left(W_\mu^+ + W_\mu^-\right), & W_\mu^2 &= \frac{i}{\sqrt{2}}\left(W_\mu^+ - W_\mu^-\right), \\ W_\mu^3 &= \cos\theta_W Z_\mu + \sin\theta_W A_\mu, & B_\mu &= -\sin\theta_W Z_\mu + \cos\theta_W A_\mu, \end{aligned} \tag{3.15}$$

where θ_W is the Weinberg angle, $\cos\theta_W \equiv g/\sqrt{g^2+g'^2}$, and $\sin\theta_W \equiv g'/\sqrt{g^2+g'^2}$. The gauge mass term written using these fields is

$$\mathcal{L}_{\text{gauge-mass}} = M_W^2 W_\mu^+ W^{-\,\mu} + \frac{M_Z^2}{2} Z_\mu Z^\mu, \tag{3.16}$$

with $M_W = vg/2$ and $M_Z = M_W/\cos\theta_W$. The photon field A_μ remains massless.

With the quark and gauge boson fields transformed into the mass eigenbasis, the flavor-changing interactions can be readily derived. These follow from the gauge-invariant kinetic terms of quarks

$$\mathcal{L}_{SM} \supset \mathcal{L}_{q\text{-kin}} = \bar{\psi}_Q i\not{D}\psi_Q + \bar{\psi}_U i\not{D}\psi_U + \bar{\psi}_D i\not{D}\psi_D. \tag{3.17}$$

The part that is non-diagonal in flavor stems from the first term. Apart from the QCD quark-gluon interaction which does not induce flavor transitions, the electroweak covariant derivative acting on ψ_Q is the same as the one for H in eq. (3.13) but with Y_H replaced by Y_Q. The relevant term is

$$\mathcal{L}_{q\text{-kin}} \supset \mathcal{L}_{\bar{q}qW} = -g\bar{\psi}_Q \left(\not{W}^1\tau^1 + \not{W}^2\tau^2\right)\psi_Q = -\frac{g}{\sqrt{2}}\bar{\psi}^1_Q \not{W}^+ \psi^2_Q + h.c. \tag{3.18}$$

Writing the above expression in terms of the mass-eigenstate quark fields introduced in eq. (3.10) yields

$$\mathcal{L}_{\bar{q}qW} = -\frac{g}{\sqrt{2}}\bar{\mathfrak{u}}_L V \not{W}^+ \mathfrak{d}_L + h.c. = -\frac{g}{\sqrt{2}}\bar{\mathfrak{u}} V \not{W}^+ P_L \mathfrak{d} + h.c. \tag{3.19}$$

These two terms induce the vertex Feynman rules quoted in eq. (I.1). In all others, there is either no ψ^2_Q field whose redefinition introduces the CKM matrix, or the CKM matrix cancels with its hermitian conjugate, and the corresponding vertices are diagonal in flavor.

The only other SM Lagrangian term that can induce a change of flavor comes from the Yukawa interactions of quarks with the would-be-Goldstone bosons $\chi^\pm$ introduced in eq. (3.3). The propagator of $\chi^\pm$ reads

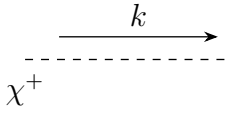

$$= \frac{i}{k^2 - \xi_W M_W^2 + i\varepsilon}, \tag{3.20}$$

where ξ_W is the R_ξ gauge parameter of the W boson. Contributions of these bosons can be removed by performing all calculations in the unitary gauge $\xi_W \to \infty$, which is related to the observation made in eq. (3.5). Such a choice will always be assumed below.

The $Wl\nu_l$ vertex Feynman rule can be obtained in a similar way. In the limit of massless neutrinos, assumed throughout the present thesis, the PMNS matrix, which is the lepton-sector equivalent of the CKM matrix, becomes $\mathbb{1}_{3\times3}$. Apart from this simplification, the derivation is exactly the same, and the resulting vertices are

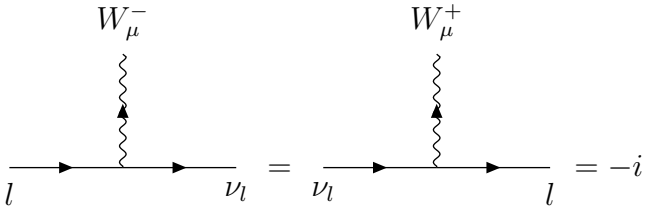

$$= -i\frac{g}{\sqrt{2}}\gamma_\mu P_L. \tag{3.21}$$

The observed masses of the $W^\pm$ and Z bosons, as well as the mass of the Higgs boson h and the top quark are much larger than any external mass scale present in the center-of-mass frame of the semileptonic B-meson decay. The scattering and decays mediated by fields that are much heavier than particles appearing on external legs are most conveniently described in a "top-down" Effective Field Theory. In such a description, the heavy degrees of freedom are decoupled, leaving in their place an infinite tower of local operators built out of the light

fields and with matrix elements between light states suppressed by powers of E_l/M_H, where E_l can be a light mass or a product of soft momenta and M_H is one of the heavy masses. The discussion below is limited to the outline of the general formalism of decoupling the heavy fields and its application to the Fermi-like interactions. A more thorough analysis of the procedure can be found in section 7.7 of ref. [80]. Consider a Green's function of k light fields in a theory describing some number n of light particles L_j and a single heavy particle H. Using the path integral description discussed in section 1.1, it can be written as

$$\langle L_{a_1}(p_1)L_{a_2}(p_2)\dots L_{a_k}(p_k)\rangle = \frac{1}{N}\int (\mathcal{D}L_1\mathcal{D}L_2\dots\mathcal{D}L_n\mathcal{D}H)\, L_{a_1}(p_1)L_{a_2}(p_2)\dots L_{a_k}(p_k)e^{iS}, \tag{3.22}$$

where $N \equiv \int (\mathcal{D}L_1\mathcal{D}L_2\dots\mathcal{D}L_n\mathcal{D}H)\exp(iS)$, and $\langle\mathcal{O}\rangle$ denotes the Fourier transform of $\langle\Omega|T\hat{\mathcal{O}}|\Omega\rangle$. This Green's function is generated by the functional

$$Z_L[J] = \int (\mathcal{D}L_1\mathcal{D}L_2\dots\mathcal{D}L_n\mathcal{D}H)\exp\left[i\int d^Dx\left(\mathcal{L}+\sum_{j=1}^{n}L_jJ_j\right)\right]. \tag{3.23}$$

The Lagrangian density $\mathcal{L}$ can be divided as

$$\mathcal{L} = \mathcal{L}_L + \mathcal{L}_{LH} + \mathcal{L}_H, \tag{3.24}$$

with $\mathcal{L}_L$ containing only the light fields, $\mathcal{L}_H$ containing only H, and $\mathcal{L}_{LH}$ describing light-heavy interactions. This interaction Lagrangian density will be assumed as linear in H:

$$\mathcal{L}_{LH} = H\tilde{\mathcal{L}}, \tag{3.25}$$

with $\tilde{\mathcal{L}}$ independent of H, as is the case for the interactions relevant to the $b\to c$ transition at the leading order in electroweak interactions. Then, the generating functional in eq. (3.23) can be written as

$$Z_L[J] = \int (\mathcal{D}L_1\mathcal{D}L_2\dots\mathcal{D}L_n)\, e^{i\int d^Dx\left(\mathcal{L}_L+\sum_{j=1}^{n}L_jJ_j\right)}\int \mathcal{D}H e^{i\int d^Dx\left(\mathcal{L}_H+H\tilde{\mathcal{L}}\right)}. \tag{3.26}$$

The second path integral can be recognized as the generating functional of the theory of the heavy field H with sources replaced with $\tilde{\mathcal{L}}$. Then, using the representation of eq. (1.64), it can be rewritten as

$$\int \mathcal{D}H e^{i\int d^Dx\left(\mathcal{L}_H+H\tilde{\mathcal{L}}\right)} = Z_H[\tilde{\mathcal{L}}] = e^{\sum_{j=0}^{\infty}\frac{i^j}{j!}\int d^Dy_1\dots d^Dy_j\langle H(y_1)\dots H(y_j)\rangle_{conn}\tilde{\mathcal{L}}(y_1)\dots\tilde{\mathcal{L}}(y_j)}. \tag{3.27}$$

The light Green's functions of eq. (3.22) are thus the same in the full theory and in a theory where only the light fields are dynamical, described by the following effective non-local action:

$$S_{eff}[L_k] \equiv \int d^Dx\mathcal{L}_L + \sum_{j=0}^{\infty}\frac{i^{j-1}}{j!}\int d^Dy_1\dots d^Dy_j\,\langle H(y_1)\dots H(y_j)\rangle_{conn}\,\tilde{\mathcal{L}}(y_1)\dots\tilde{\mathcal{L}}(y_j). \tag{3.28}$$

Naively, the connected Green's functions $\langle H(y_1)\dots H(y_j)\rangle_{conn}$ can be expanded as

$$\begin{aligned}
&\langle H(y_1)\dots H(y_j)\rangle_{conn}\\
&= \int \frac{d^Dq_1}{(2\pi)^D}\dots\frac{d^Dq_j}{(2\pi)^D}e^{i(q_1y_1+\dots+q_jy_j)}\,\langle H(q_1)\dots H(q_j)\rangle_{conn}\,\delta^{(D)}(q_1+\dots+q_j)\\
&= \int \frac{d^Dq_1}{(2\pi)^D}\dots\frac{d^Dq_{j-1}}{(2\pi)^D}e^{i[q_1(y_1-y_n)+\dots+q_{j-1}(y_{j-1}-y_j)]}\left(c_0^{(j)}+c_1^{(j),ab}\frac{q_aq_b}{M_H^2}+\mathcal{O}\left[\frac{1}{M_H^4}\right]\right),
\end{aligned} \tag{3.29}$$

as long as the momenta flowing through the effective non-local vertices are small when compared with the heavy mass. In the above equation, the overall momentum conservation delta appears because the Green's function is connected. Then, the $d^D y_k$ integrals can be performed, resulting in

$$\langle H(y_1)\dots H(y_j)\rangle_{conn} = \left(c_0^{(j)} + c_1^{(j),ab}\frac{\partial_{y_a^\mu}\partial_{y_{b,\mu}}}{i^2 M_H^2} + \mathcal{O}\left[\frac{1}{M_H^4}\right]\right)\delta^{(D)}(y_1-y_n)\dots\delta^{(D)}(y_{n-1}-y_n), \tag{3.30}$$

and the light Green's functions in eq. (3.22) can be calculated using an effective *local* action

$$S_{eff} = \int d^D x \left(\mathcal{L}_L(x) + \sum_n \frac{C_n O_n(x)}{M_H^{p(n)}}\right). \tag{3.31}$$

The operators $O_n(x)$ are built out of the light fields and their derivatives.

The assumption $q_a q_b / M_H^2 \ll 1$ in eq. (3.29) holds for the tree-level Green's functions, but is broken by the high-momentum modes of the light fields present in loops. To obtain a local effective action that describes the light Green's functions, one must first integrate the high momentum modes of the light fields out of the full theory generating functional. To obtain the Wilson coefficients C_n, the light Green's functions computed in the effective theory are equated with their counterparts in the full theory described by the non-local action (3.28) and with the high momentum modes integrated out. To reflect the latter step on the effective theory side, one may regularize it with a cutoff $\Lambda_c \ll M_H$, and only change the regularization scheme to dimensional after the matching is performed, restoring the momentum integration region to the full D-dimensional Minkowski space. Nevertheless, such issues matter for the semileptonic decay only at higher orders in electroweak interactions, which is beyond the scope of the present thesis. In our case, the connected Green's functions in eq. (3.28) can be expanded as in eq. (3.29).

Instead of explicitly computing the Wilson coefficients C_n from the expansion of $\langle H(q_1)\dots H(q_j)\rangle_{conn}$, one can first guess[†] the form of the local operators O_n, and then calculate C_n from the condition that *all* momentum space Green's functions obtained with this action must be equal to their counterparts in the full theory. One can thus chose a convenient, off-shell configuration of external momenta for this matching condition, and the obtained coefficients will also hold for the Green's functions relevant to physical processes. After moving to dimensional regularization, one may also expand all diagrams in external momenta and light masses on both sides of the matching condition, prior to loop integration. The effective theory Green's function used for the matching can then be expressed with just tree diagrams.

The above construction can be performed for t, h, Z, and $W^\pm$, decoupling them simultaneously from the SM description of flavor-changing processes at scales much smaller than M_W. The resulting Low-energy Effective Field Theory is governed by the Lagrangian density

$$\mathcal{L}_{LEFT} = \mathcal{L}_{\substack{QCD\times QED \\ udcsb+\text{leptons}}} + \sum_n \frac{C_n O_n}{M_W^{p(n)}}. \tag{3.32}$$

The decoupling of $W^\pm$ bosons is particularly relevant for the present discussion. The analysis is only slightly different from the case of a real H field considered above because the $W^\pm$ field is complex. At the leading order in electroweak interactions, the effective operators

[†]That is, construct all the operators needed for the successful matching between the full and effective theories.

pertinent to the $b \to c$ semileptonic transition must be built out of the b, c, l, and ν_l fields only. The relevant factors multiplying $W_\mu^\pm$ in the SM Lagrangian are

$$\begin{aligned}\tilde{\mathcal{L}}_+^\mu &= -\frac{g}{\sqrt{2}}\left[V_{cb}\bar{c}\gamma^\mu P_L b + \bar{l}\gamma^\mu P_L \nu_l\right], \\ \tilde{\mathcal{L}}_-^\mu &= -\frac{g}{\sqrt{2}}\left[V_{cb}^*\bar{b}\gamma^\mu P_L c + \bar{\nu}_l\gamma^\mu P_L l\right],\end{aligned} \tag{3.33}$$

with the necessary connected momentum space Green's functions given by the $W^\pm$ propagators:

$$\begin{aligned}&\langle W_\mu^+(p_1)W_\nu^-(p_2)\rangle_{conn} = \langle W_\mu^-(p_1)W_\nu^+(p_2)\rangle_{conn} \\ =&\frac{-i}{p_1^2 - M_W^2 + i\varepsilon}\left[g_{\mu\nu} - \frac{p_{1,\mu}p_{1,\nu}}{M_W^2}\right]\delta^{(D)}(p_1+p_2) + \mathcal{O}(g^2) \\ =&\frac{ig_{\mu\nu}}{M_W^2}\delta^{(D)}(p_1+p_2) + \mathcal{O}\left(\frac{1}{M_W^4}, g^2\right).\end{aligned} \tag{3.34}$$

The last expression was written in the unitary gauge ($\xi_W \to \infty$). Once transformed into the position space, it reads

$$\langle W_\mu^+(y_1)W_\nu^-(y_2)\rangle_{conn} = \frac{ig_{\mu\nu}}{M_W^2}\delta^{(D)}(y_1 - y_2) + \mathcal{O}\left(\frac{1}{M_W^4}, g^2\right). \tag{3.35}$$

The effective action can be now constructed with the use of eqs. (3.28). In the considered approximation, only the $j = 2$ term is relevant and reads

$$\begin{aligned}\frac{i}{2!}\int d^D y_1 d^D y_2 \Big(&\langle W_\mu^+(y_1)W_\nu^-(y_2)\rangle\, \tilde{\mathcal{L}}_+^\mu(y_1)\tilde{\mathcal{L}}_-^\nu(y_2) \\ &+ \langle W_\mu^-(y_1)W_\nu^+(y_2)\rangle\, \tilde{\mathcal{L}}_-^\mu(y_1)\tilde{\mathcal{L}}_+^\nu(y_2)\Big) + \mathcal{O}(g^4),\end{aligned} \tag{3.36}$$

which, after neglecting the two non-semileptonic terms, leads to a Fermi-like effective interaction

$$\mathcal{L}_{b\to c}^F = -\frac{4G_F}{\sqrt{2}}\left[V_{cb}(\bar{c}\gamma^\mu P_L b)(\bar{\nu}_l\gamma_\mu P_L l) + h.c.\right] + \mathcal{O}\left(G_F^2\right) \tag{3.37}$$

The Fermi constant is defined as

$$G_F \equiv \frac{g^2}{4\sqrt{2}M_W^2} = \frac{1}{\sqrt{2}v^2}, \tag{3.38}$$

up to non-leading corrections in electroweak interaction. The $b \to c$ semileptonic transition in the leading order in electroweak interactions and for vanishing lepton masses is therefore described by the following effective Lagrangian density:

$$\mathcal{L} = \underset{udcsb}{\mathcal{L}_{QCD}} + i\bar{l}\partial\!\!\!/ l + i\bar{\nu}_l\partial\!\!\!/\nu_l + \mathcal{L}_{b\to c}^F. \tag{3.39}$$

The first term cannot be perturbatively treated. Instead, for the moment, one may assume that the theory described by the Lagrangian without the last term has been solved: the Hamiltonian eigenstates have been found together with the energy spectrum. The states $|B\rangle$ and $|X_c l\bar{\nu}_l\rangle$ belong to this basis, describe stable particles, and one may construct the corresponding asymptotic scattering states. Then, the last term $\mathcal{L}_{b\to c}^F$ can be treated as a

small perturbation. In this picture, at the leading order in this perturbation, the $\hat{S}$ operator matrix elements corresponding to the semileptonic decay that vanish in unperturbed QCD are modified by matrix elements of $\mathcal{L}^F_{b\to c}$. Using the result of eqs. (1.112) and (1.120), the differential rate of the inclusive semileptonic decay can be written as

$$\begin{aligned} d\Gamma_{sl} =& \frac{1}{2M_B}\sum_{X_c,\text{spins}} dPS_{B\to X_c l\bar{\nu}_l} \left|i\mathcal{M}_{B\to X_c l\bar{\nu}_l}\right|^2 \\ =& \frac{1}{2M_B}\sum_{X_c,\text{spins}} dPS_{B\to X_c l\bar{\nu}_l} 8G_F^2|V_{cb}|^2 \left|\langle X_c|J^\mu(0)|B\rangle \langle l\bar{\nu}_l|J_{l,\mu}(0)|0\rangle\right|^2 \\ =& \frac{4G_F^2|V_{cb}|^2}{M_B}\sum_{X_c,\text{spins}} dPS_{B\to X_c l\bar{\nu}_l} \left|\langle X_c|J^\mu(0)|B\rangle \left(\bar{u}_l^{(s_l)}\gamma_\mu P_L v_{\bar{\nu}_l}^{(s_{\bar{\nu}_l})}\right)\right|^2. \end{aligned} \tag{3.40}$$

where $|0\rangle$ is the unperturbed vacuum. The definitions of the quark and lepton currents $J^\mu(x)$ and $J^\mu_l(x)$ follow from the interaction term in eq. (3.37):

$$J^\mu(x) \equiv \bar{c}(x)\gamma^\mu P_L b(x) \qquad\qquad J^\mu_l(x) \equiv \bar{\nu}_l(x)\gamma_\mu P_L l(x). \tag{3.41}$$

In the decay rate, they can be evaluated at $x = 0$ due to translational invariance. The necessary integrals over x reduce to momentum conservation delta functions that are included in the phase space measure. The leptonic part of the modulus squared in eq. (3.40) can be readily computed using the completeness relation of eq. (1.165)[†]. It reads

$$\begin{aligned} &\sum_{\substack{\text{lepton}\\ \text{spins}}} \bar{u}_l\gamma_\alpha P_L v_{\bar{\nu}_l} v^\dagger_{\bar{\nu}_l} P_L\gamma^\dagger_\beta\gamma_0 u_l = \text{Tr}\left[\not{p}_l\gamma_\alpha P_L \not{p}_{\bar{\nu}_l}\gamma_0 P_L\gamma^\dagger_\beta\gamma_0\right] = \text{Tr}\left[\not{p}_l\gamma_\alpha\not{p}_{\bar{\nu}_l}\gamma_\beta P_L\right] \\ =& 2p_l^\mu p_{\bar{\nu}_l}^\nu \left[g_{\mu\alpha}g_{\nu\beta} - g_{\mu\nu}g_{\alpha\beta} + g_{\mu\beta}g_{\nu\alpha} - i\epsilon_{\mu\alpha\nu\beta}\right] \equiv 2L_{\alpha\beta}. \end{aligned} \tag{3.42}$$

The form of the antisymmetric term is only true in $D = 4$ dimensions, but it does not affect the q^2 spectrum, as will be shown below. The leptonic tensor defined above satisfies the following relations:

$$q^\alpha L_{\alpha\beta} = q^\beta L_{\alpha\beta} = 0. \tag{3.43}$$

The phase space element of the inclusive semileptonic decay will now be discussed. In $D = 4$ dimensions it is given by

$$\begin{aligned} &dPS_{p_B\to p_l p_{\bar{\nu}_l}\{p_j\}} = \\ =& \frac{d^4p_l}{(2\pi)^3}\delta_+\left(p_l^2\right)\frac{d^4p_{\bar{\nu}_l}}{(2\pi)^3}\delta_+\left(p_{\bar{\nu}_l}^2\right)\left(\prod_{j=1}^n \frac{d^4p_j}{(2\pi)^3}\delta_+\left(p_j^2\right)\right)(2\pi)^4\delta^{(4)}\left(p_B - p_l - p_{\bar{\nu}_l} - \sum_{j=1}^n p_j\right), \end{aligned} \tag{3.44}$$

where $\delta_+(p_x^2) \equiv \Theta\left(p_x^0\right)\delta\left(p_x^2 - m_x^2\right)$ and p_j are the four-momenta of the n particles contained in the X_c final state. This expression can be factorized as

$$dPS_{p_B\to p_l p_{\bar{\nu}_l}\{p_j\}} = \frac{dq^2}{2\pi}\frac{dr^2}{2\pi} dPS_{p_B\to qr} dPS_{q\to p_l p_{\bar{\nu}_l}} dPS_{r\to\{p_j\}}, \tag{3.45}$$

which is a simple consequence of a more general phase space decomposition

$$dPS_{p\to k_1 k_2\{l_j\}} = \frac{dk^2}{2\pi} dPS_{p\to k\{l_j\}} dPS_{k\to k_1 k_2}. \tag{3.46}$$

[†]For massless fermions, the same relation holds also for spinors v.

The latter form can be proven by multiplying the left hand side by 1 written as

$$1 = 1 \cdot 1 = \left(\frac{dk^2}{2\pi}(2\pi)\delta(k^2 - m_k^2)\right)\left(\frac{d^4k}{(2\pi)^4}(2\pi)^4\delta^{(4)}(k - k_1 - k_2)\Theta\left(k^0\right)\right). \tag{3.47}$$

The point selected by the delta function $\delta(k^0 - k_1^0 - k_2^0)$ lays at a positive value of k^0 because of the Heaviside step functions for the energies of k_1 and k_2 in the phase space element $dPS_{p\to k_1 k_2\{l_j\}}$. Applying the condition enforced by the delta function in the second factor of the above equation, it is now straightforward to show the identity (3.46). The first two measures of eq. (3.45) can be simplified in the rest frame of the B meson. For a fixed q^2 and r^2, the first element can be written as

$$\begin{aligned} dPS_{p_B\to qr} =& \frac{d^4q}{(2\pi)^3}\frac{d^4r}{(2\pi)^3}\delta_+(q^2)\delta_+(r^2)(2\pi)^4\delta^{(D)}\left(p_B - q - r\right) = \frac{d^4q}{(2\pi)^2}\delta_+\left(q^2\right)\delta_+\left((p_B - q)^2\right) \\ =& \frac{dq^0 d|\mathbf{q}|^2 d\Phi_q}{8\pi^2}|\mathbf{q}|\delta_+\left(\left(q^0\right)^2 - |\mathbf{q}|^2\right)\delta_+\left(2M_B q^0 - M_B^2\right) = \frac{d\Phi_q}{16\pi^2}\frac{|\mathbf{q}|}{M_B}. \end{aligned} \tag{3.48}$$

where $d\Phi_q$ is the solid angle element containing the direction of q. The length $|\mathbf{q}|$ and energy q^0 are fixed by the 4-momentum conservation and on-shell conditions

$$|\mathbf{q}| = \frac{\sqrt{\lambda\left(M_B^2, q^2, r^2\right)}}{2M_B}, \qquad\qquad q^0 = \frac{M_B^2 + q^2 - r^2}{2M_B}. \tag{3.49}$$

The range of kinematically allowed values of E_l can be established from the condition $-1 \leq \cos\theta_l \leq 1$ and reads

$$\frac{q^0 - |\mathbf{q}|}{2} \equiv E_l^- \leq E_l \leq E_l^+ \equiv \frac{q^0 + |\mathbf{q}|}{2}. \tag{3.50}$$

The decay is isotropic in the rest frame of the B meson, so one may integrate over Φ_q, which is equivalent to replacing

$$dPS_{p_B\to qr} \to \frac{1}{4\pi}\frac{|\mathbf{q}|}{M_B}. \tag{3.51}$$

A similar calculation leads to the following form for the second phase space element in eq. (3.45):

$$dPS_{q\to p_l p_{\bar{\nu}_l}} = \frac{dE_l|\mathbf{p}_l|d\cos\theta_l d\phi_l}{8\pi^2}\delta_+\left(q^2 - 2q^0E_l + 2|\mathbf{q}||\mathbf{p}_l|\cos\theta_l\right) = \frac{dE_l d\phi_l}{16\pi^2|\mathbf{q}|}, \tag{3.52}$$

where θ_l and ϕ_l are the polar and azimuthal coordinates of $\mathbf{p}_l$ in the coordinate system specified by $\mathbf{q} = |\mathbf{q}|\hat{e}_z$ and any spatial direction $\hat{e}_x$ orthogonal to $\hat{e}_z$. The decay is invariant under changes of ϕ_l, so one may again integrate over ϕ_l and replace

$$dPS_{q\to p_l p_{\bar{\nu}_l}} \to \frac{1}{8\pi}\frac{dE_l}{|\mathbf{q}|}. \tag{3.53}$$

Combining the results of eqs. (3.45), (3.51), and (3.53) gives the following result for the phase space element (3.44) integrated over the blind angles of the semileptonic decay:

$$dPS_{p_B\to p_l p_{\bar{\nu}_l}\{p_j\}} \to \frac{dE_l dq^2 dr^2}{128\pi^4 M_B}dPS_{r\to\{p_j\}}. \tag{3.54}$$

The differential rate in eq. (3.40) now reads

$$d\Gamma_{sl} = \frac{G_F^2|V_{cb}|^2}{16\pi^4 M_B^2} dW_{\mu\nu} L^{\mu\nu} dE_l dq^2 dr^2, \tag{3.55}$$

with $L^{\mu\nu}$ given by eq. (3.42) and the hadronic tensor $dW_{\mu\nu}$ defined as

$$dW_{\mu\nu} \equiv \sum_{X_c,\ \substack{\text{hadron}\\ \text{spins}}} dPS_{r\to\{p_j\}} \langle B|J_\mu^\dagger(0)|X_c\rangle \langle X_c|J_\nu(0)|B\rangle . \tag{3.56}$$

This is a Lorentz tensor that can depend only on $p_B \equiv M_B v$ and the total leptonic momentum q but not on the individual outgoing momenta p_l, $p_{\bar{\nu}_l}$, and in particular not on E_l. One can therefore write its most general decomposition as

$$\begin{aligned} dW_{\mu\nu}(v,\hat{q}) = &- g_{\mu\nu} dW_1(r^2,q^2) + v_\mu v_\nu dW_2(r^2,q^2) + \epsilon_{\mu\nu\alpha\beta} v^\alpha \hat{q}^\beta dW_3(r^2,q^2) \\ &+ \hat{q}_\mu v_\nu dW_4(r^2,q^2) + \hat{q}_\nu v_\mu dW_5(r^2,q^2) + \hat{q}_\mu \hat{q}_\nu dW_6(r^2,q^2). \end{aligned} \tag{3.57}$$

Note that the symbol $\hat{q}^2$ refers to the notation defined under eq. (2.24), i.e. q^2/m_b^2. The contraction $dW_{\mu\nu}L^{\mu\nu}$ reads

$$dW_{\mu\nu}L^{\mu\nu} = dW_1 q^2 + dW_2 \left(2E_l\left(q^0 - E_l\right) - \frac{q^2}{2}\right) + i dW_3 q^2 \left(2E_l - q^0\right), \tag{3.58}$$

where eq. (3.43) was used to eliminate the contributions of the $dW_{4,\mu}$, $dW_{5,\mu}$, and $dW_{6,\mu}$ terms.

With the above results, the q^2 spectrum may now be discussed. The differential rate of eq. (3.55) leads to

$$\frac{d\Gamma_{sl}}{dq^2} = \frac{G_F^2|V_{cb}|^2}{16\pi^4 M_B^2} \int dr^2 \int dE_l W_{\mu\nu} L^{\mu\nu}, \tag{3.59}$$

with $W_{\mu\nu} \equiv \int dW_{\mu\nu}$. The contraction obtained in eq. (3.58) can be integrated over the allowed range of E_l given in eq. (3.50)

$$\int_{E_l^-}^{E_l^+} dE_l W_{\mu\nu} L^{\mu\nu} = |\mathbf{q}| \left(q^2 W_1 + \frac{|\mathbf{q}|^2}{3} W_2\right), \tag{3.60}$$

which simplifies eq. (3.59) as

$$\frac{d\Gamma_{sl}}{dq^2} = \frac{G_F^2|V_{cb}|^2}{16\pi^4 M_B^2} \int dr^2 |\mathbf{q}| \left(q^2 W_1(r^2,q^2) + \frac{|\mathbf{q}|^2}{3} W_2(r^2,q^2)\right). \tag{3.61}$$

The calculation of the spectrum thus comes down to obtaining the hadronic from factors $W_{1/2}$.

It is important to note that $W_{\mu\nu}$ is related to the inclusive rate of the decay $B \to X_c W^-$ if W^- was light enough. The mass of W^- can be decreased by making the electroweak coupling g smaller and keeping all other SM parameters the same. Considering the decay $B \to X_c W^-$ in the SM with the appropriate value of g leads to the replacement of the lepton pair by the auxiliary Q boson, introduced in figure 6 on page 41. This process can indeed be thought of as fully inclusive if one chooses the unitary gauge for the $W^\pm$ bosons, setting

their propagators to the form of eq. (3.34). With this choice, the would-be Goldstone bosons $\chi^{\pm}$ are no longer dynamical (c.f. the $\chi^{\pm}$ propagator in eq. (3.20) for $\xi_W \to \infty$), and this is the only decay channel of the B meson with its width proportional to g^2 and $|V_{cb}|^2$:

$$\Gamma_{B\to X_c W^-} = \frac{1}{2M_B} \sum_{X_c,\ \substack{\text{hadron}\\ \text{spins}}} \sum_{s_W} \int dPS_{p_B \to p_W \{p_j\}} \frac{|V_{cb}|^2 g^2}{2} \left| \langle X_c | J_\mu(0) | B \rangle \, \epsilon^\mu_{s_W} \right|^2 + \mathcal{O}(g^4), \quad (3.62)$$

where s_W indexes the polarization of the outgoing W boson and $\epsilon^\mu_{s_W}$ is the corresponding polarization vector. Using the result of eq. (3.51), one may decompose the phase space measure as

$$dPS_{p_B \to p_W \{p_j\}} = \frac{dr^2}{8\pi^2} \frac{|\mathbf{p}_W|}{M_B} dPS_{r \to \{p_j\}}, \quad (3.63)$$

which leads to

$$\Gamma_{B\to X_c W^-} = \frac{|V_{cb}|^2 G_F M_W^2}{4\sqrt{2}\pi^2 M_B^2} \int dr^2 |\mathbf{p}_W| W_{\mu\nu}(r^2, p_W^2) \sum_{s_W} \epsilon^\mu_{s_W} \epsilon^{\nu *}_{s_W} + \mathcal{O}(G_F^2). \quad (3.64)$$

The sum over polarization vectors can be read out of the W propagator. The result has to be exactly equal to $-i$ times the numerator of this propagator, and reads

$$\sum_{s_W} \epsilon^\mu_{s_W} \epsilon^{\nu *}_{s_W} = -g^{\mu\nu} + \frac{p_W^\mu p_W^\nu}{M_W^2}. \quad (3.65)$$

After contracting it with the integral of the decomposition of eq. (3.57), the formula for the decay width becomes

$$\Gamma_{B\to X_c W^-} = \frac{3|V_{cb}|^2 G_F}{4\sqrt{2}\pi^2 M_B^2} \int dr^2 |\mathbf{p}_W| \left(M_W^2 W_1 + \frac{|\mathbf{p}_W|^2}{3} W_2 \right) + \mathcal{O}(G_F^2). \quad (3.66)$$

Identifying p_W with q yields the most important result of this section. The q^2 spectrum in eq. (3.61) and the above width $\Gamma_{B\to X_c W^-}$ become proportional to each other if in the latter, M_W is set to $\sqrt{q^2}$. This can be achieved by considering the decay $\Gamma_{B\to X_c Q}$ in the SM with g replaced with g_q defined as

$$g_q \equiv g \frac{\sqrt{q^2}}{M_W} \quad (3.67)$$

and all other free parameters left unaltered. This change affects neither the quark masses, nor the CKM matrix elements, nor the Fermi constant, as the latter is given by v alone (cf. eq. (3.38)). The electroweak perturbation series convergence is not affected, as the coupling becomes smaller. From the point of view of the $B \to X_c W^-$ decay, the only change is that the W^- boson is replaced by the lighter Q boson with $M_Q^2 = q^2$. The proportionality constant can be established immediately by comparing eqs. (3.61) and (3.66):

$$\frac{d\Gamma_{sl}}{dq^2} = \frac{\sqrt{2} G_F}{12\pi^2} \Gamma_{B\to X_c Q}. \quad (3.68)$$

Note that this result holds to all orders in QCD, and has been derived for the decay of the B meson bound state. Therefore, can be applied to all orders in the HQE. Since the q^2 spectrum can be identified with a physical, fully inclusive decay width, it has to be free of any infrared and collinear divergences. This is no longer true if one considers QED to the semileptonic decay.

3.2 Quantum Chromodynamics

The analysis in this section returns to the chromodynamic effects that previously were treated as solved. These are governed by the first term in the effective Lagrangian density of eq. (3.39)

$$\mathcal{L}_{\substack{QCD\\udcsb}} = \mathcal{L}_{g\text{-kin}} + \mathcal{L}_{gf} + \mathcal{L}_{FP} + \mathcal{L}_q + \mathcal{L}_\otimes, \tag{3.69}$$

with

$$\begin{aligned} \mathcal{L}_{g\text{-kin}} &= -\frac{1}{4} G^a_{\mu\nu} G^{\mu\nu,a}, & \mathcal{L}_{gf} &= -\frac{1}{2\xi_g} \left(\partial^\mu A^a_\mu\right) \left(\partial^\nu A^a_\nu\right), \\ \mathcal{L}_{FP} &= \left(\partial^\mu \eta^{a*}\right) \left(D^\mu \eta\right)^a, & \mathcal{L}_q &= \sum_{\psi\in\{u,d,c,s,b\}} \bar{\psi}(i\not{D} - m_\psi)\psi, \end{aligned} \tag{3.70}$$

and the last term, $\mathcal{L}_\otimes$, containing all of the counterterms stemming from replacing the bare fields, masses and the strong coupling with the renormalized ones. The dynamical fields of this theory are gluons A^a_μ, quarks ψ, and the Faddeev-Popov ghosts η^a. The gluon field strength tensor is defined as

$$G^a_{\mu\nu} \equiv \partial_\mu A^a_\nu - \partial_\nu A^a_\mu - g_s f^{abc} A^b_\mu A^c_\nu \equiv G^{(\partial),a}_{\mu\nu} - g_s f^{abc} A^b_\mu A^c_\nu, \tag{3.71}$$

where f^{abc} are the structure constants of $\mathfrak{su}(3)$. The second and third terms arise in the Faddeev-Popov procedure of evaluating path integrals in gauge invariant theories. The form of $\mathcal{L}_{gf}$ is valid for a particular choice of parameterizing the space of paths called the R_ξ gauge. The parameter ξ_g can be chosen freely, and does not affect physical quantities. It is helpful to keep it arbitrary, and treat its cancellation in physical quantities as a crosscheck. The contraction $G^{(\partial),a}_{\mu\nu} G^{(\partial),\mu\nu,a}$ in the first term of eq. (3.69) together with the gauge fixing term $\mathcal{L}_{gf}$ are the only terms quadratic in A^a_μ. These can be rewritten as

$$G^{(\partial),a}_{\mu\nu} G^{(\partial),\mu\nu,a} + \mathcal{L}_{gf} = \frac{1}{2} A^a_\mu \left[\partial_\alpha \partial^\alpha g^{\mu\nu} + \overleftarrow{\partial}^\nu \left(1 - \frac{1}{\xi_g}\right) \partial^\mu\right] A^a_\mu, \tag{3.72}$$

up to a total derivative that does not affect physical amplitudes. The Fourier transform of the Green's function of the Euler-Lagrange equation derived from this Lagrangian density gives the Feynman rule for the gluon propagator quoted in eq. (1.126) on page 42.

Contractions of the last term in eq. (3.71) give rise to three- and four-gluon self-interaction terms that are absent in the abelian case. The term with three gluon fields reads

$$\frac{1}{2} g_s f^{abc} G^{(\partial),a}_{\mu\nu} A^{\mu,b} A^{\nu,c} = \frac{g_s}{3!} \left[f^{abc} G^{(\partial),a}_{\mu\nu} A^{\mu,b} A^{\nu,c} + f^{bca} G^{(\partial),b}_{\mu\nu} A^{\mu,c} A^{\nu,a} + f^{cab} G^{(\partial),c}_{\mu\nu} A^{\mu,a} A^{\nu,b}\right] \tag{3.73}$$

and corresponds to the Feynman rule

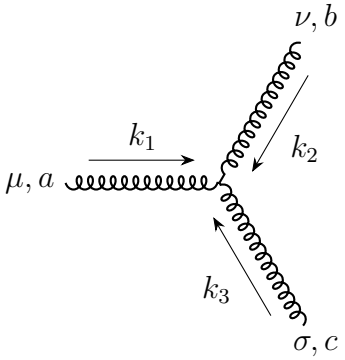

$$= g_s f^{abc} \left[g^{\mu\nu}(k_1 - k_2)^\sigma + g^{\nu\sigma}(k_2 - k_3)^\mu + g^{\sigma\nu}(k_3 - k_1)^\nu\right]. \tag{3.74}$$

The quartic gluon interaction begins to affect the semileptonic decay only at $\mathcal{O}(\alpha_s^3)$, and therefore is not relevant to this thesis.

The Faddeev-Popov ghosts η^a are absent in the physical spectrum of QCD but must be included in calculations of loop corrections. The fields η^a are Grassmann-number-valued Lorentz scalars, and their covariant derivative reads

$$(D^\mu \eta)^a = \partial^\mu \eta^a + g_s f^{abc} \eta^b A^c_\mu. \tag{3.75}$$

The ghost propagator can again be obtained from the Green's function of the free Euler-Lagrange equation. It takes the form

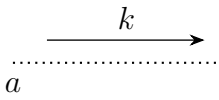

$$= \frac{i\delta^{ab}}{k^2 + i\varepsilon}. \tag{3.76}$$

The Feynman rule for the ghost-gluon interaction follows from the second term of the covariant derivative (3.75), and reads

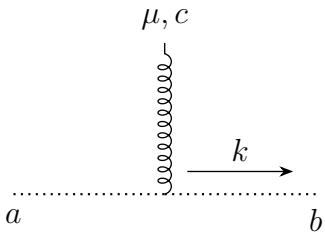

$$= -g_s f^{abc} k^\mu. \tag{3.77}$$

The dynamics of quarks are described by the last term in eq. (3.69). The covariant derivative is given by

$$D_\mu \equiv \partial_\mu + i g_s A^a_\mu T^a. \tag{3.78}$$

The algebra of the fundamental generators T^a was described in section 1.6. It will be assumed that $m_u = m_d = m_s = 0$. The quark propagators once more follow from the Euler Lagrange equations and quark-gluon vertex Feynman rules from the second term of the above equation. The results were quoted in eq. (1.126).

The above analysis does not take into account modifications induced by loop corrections. Once they are included, one necessarily encounters UV divergences discussed in section 1.4. Dimensionally regulated Feynman diagrams depend on the renormalization scale μ through the logarithm $\log(\mu/m_b)$. For physical quantities, this dependence has to cancel order-by-order in their perturbative expansion in powers of α_s. This cancellation does not simply happen between the diagrams proportional to a certain power of α_s. Rather, the μ dependence of their sum is exactly compensated by the dependence of α_s, up to higher terms in the perturbative series. To derive the function $\alpha_s(\mu)$, one first observes that the bare coupling in the original Lagrangian density (3.69) is μ-independent, i.e.

$$\mu \frac{d g_s^{(0)}}{d\mu} = 0, \tag{3.79}$$

where the first factor of μ is introduced for later convenience. This condition is equivalent to a differential equation for the renormalized α_s

$$\mu \frac{d}{d\mu} \left[\mu^{2\epsilon} Z_g^2 \alpha_s \right] = 0 \Longleftrightarrow \mu \frac{d\alpha_s}{d\mu} = -\frac{2\epsilon Z_g^2 \alpha_s}{Z_g^2 + \alpha_s \frac{dZ_g^2}{d\alpha_s}}. \tag{3.80}$$

The factor of $\mu^{2\epsilon}$ appears due to the rescaling of coupling constants in dimensional regularization discussed in section 1.4. The renormalization constant of the $SU(3)$ coupling, Z_g, can be computed perturbatively in powers of α_s, after a renormalization condition is chosen for the vertex amplitudes. In the $\overline{\text{MS}}$ scheme[†], it reads

$$Z_g^{\overline{\text{MS}}} = 1 - \frac{\alpha_s}{4\pi\epsilon}\frac{11 - \frac{2n_f}{3}}{2} + \mathcal{O}(\alpha_s^2), \tag{3.81}$$

where n_f is the number of quark flavors in the theory. One should set $n_f = 5$ in the effective theory of the semileptonic decay given by the Lagrangian density in eq. (3.39). This leads to the following Renormalization Group Equation (RGE) for α_s:

$$\mu\frac{d\alpha_s}{d\mu} = -\left(11 - \frac{2n_f}{3}\right)\frac{\alpha_s^2}{2\pi} + \mathcal{O}(\alpha_s^3) \equiv \beta(\alpha_s). \tag{3.82}$$

The most important qualitative conclusion one may draw from this result is that for $n_f \leq 16$, the right hand side of the above equation is negative, and the coupling of the strong interactions becomes weaker for larger choices of μ. On the other hand, the behavior of the QCD perturbative series is heavily dependent on the choice of μ in the calculation of Feynman diagrams, due to the appearance of potentially large logarithms $\log(\mu/\Lambda)$, where Λ is a mass scale describing the considered process. To obtain reliable theoretical predictions despite truncating the expansion in α_s after a finite number of terms, one should choose μ close to Λ. Such a choice also affects the value of the expansion parameter $\alpha_s(\mu)$. Combining these two effects implies that QCD is not perturbative for processes involving only small scales. When a sufficiently large Λ is available, there exists a value of μ for which including more and more terms in the perturbative expansion gives more and more accurate predictions[‡]. This behavior is referred to as the asymptotic freedom of QCD, as first described in refs. [212, 213]. The function $\beta(\alpha_s)$ has been extensively studied over the recent decades, and is now known up to five loops [214–220]. The numerical solution for the running of α_s with μ described by the RGE (3.82) is implemented in particular in the `Mathematica` package `RunDec` [201–203].

The knowledge of the β function allows one to construct a μ-independent mass scale:

$$\Lambda_{QCD} \equiv \mu \exp\left[-\int \frac{d\alpha_s}{\beta(\alpha_s)}\right], \qquad \frac{d\Lambda_{QCD}}{d\mu} = 0. \tag{3.83}$$

This scale arises dynamically from QCD loop effects, as opposed to being introduced by hand into the Lagrangian. It inherits the dependence on the choice of the renormalization scheme from the β function. For QCD with $n_f = 5$ quark flavors the value of $\Lambda_{QCD}^{\overline{\text{MS}}}$ amounts to around 200 MeV. Neglecting higher-loop corrections to the Z_g renormalization constant in eq. (3.81), the integral in the definition of Λ_{QCD} can be computed giving

$$\Lambda_{QCD} \approx \mu \exp\left[-\frac{1}{\beta_0\alpha_s(\mu)}\right], \qquad \beta_0 \equiv \frac{11 - \frac{2n_f}{3}}{2\pi}, \tag{3.84}$$

which can be solved for $\alpha_s(\mu)$, yielding

$$\alpha_s(\mu) \approx \frac{2\pi}{\left(11 - \frac{2n_f}{3}\right)\log\left(\frac{\mu}{\Lambda_{QCD}}\right)}. \tag{3.85}$$

[†]Recall that in the definition of the $\overline{MS}$ scheme adopted in this thesis, the loop integrals are normalized to powers of $\tilde{\mu}$ defined in eq. (1.164) and the counterterms have only terms with inverse powers of ϵ.

[‡]However, the perturbative series in QFT are believed to be asymptotic rather than convergent.

The above relation was obtained by neglecting higher loop terms in the expression for the β function; an approximation that is clearly invalid in the region where $\mu \sim \Lambda_{QCD}$. Still, this result gives a physical interpretation for Λ_{QCD}: it is a scale at which the QCD coupling becomes large. Its value obtained with the 5-loop β function with $n_f = 5$, and the experimentally measured $\alpha_s(M_Z) \approx 0.1179$ is 207.5 MeV. Using the same experimental input and the 5-loop RGE, the value of $\alpha_s(m_b)$ is approximately 0.2153. This indicates that the perturbative approach is applicable to the partonic decays of the b quark, which is an important fact for the analysis of the q^2 spectrum in the present thesis.

Substituting the renormalized quantities into the bare Lagrangian density introduces counterterm interactions, as was described in eqs. (1.132), (1.133), and (1.134) on page 45. For the quark-gluon vertex, the part dependent on the renormalization constants reads

$$-g_s^{\otimes,\psi}\bar{\psi}\not{A}^a T^a\psi = -(Z_g Z_\psi \sqrt{Z_A} - 1) g_s \bar{\psi}\not{A}^a T^a \psi = -\left(\delta_\psi + \frac{\delta_A}{2} + \delta_g\right) g_s \bar{\psi}\not{A}^a T^a \psi + \mathcal{O}(g_s^5), \tag{3.86}$$

where the renormalization factors δ are defined as

$$Z_x \equiv 1 + \delta_x = 1 + \alpha_s \delta_x^{(1)} + \alpha_s^2 \delta_x^{(2)} + \mathcal{O}(\alpha_s^3). \tag{3.87}$$

The counterterm (3.86) introduces an additional vertex with the Feynman rule

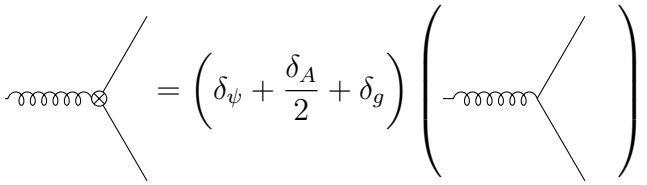

$$= \left(\delta_\psi + \frac{\delta_A}{2} + \delta_g\right)$$

, (3.88)

where only the $\mathcal{O}(\alpha_s)$ terms have been retained. The quark line counterterms follow from eq. (1.134), and read

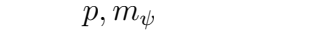

$$p, m_\psi \qquad = -\delta_\psi \mathcal{P}_\psi^{-1} - i\left(\delta_{m_\psi} + \delta_\psi \delta_{m_\psi}\right) m_\psi. \tag{3.89}$$

The last QCD counterterm needed for the renormalization of the q^2 spectrum up to the NNLO comes from the gluon line. When one includes counterterms, the term quadratic in A_μ^a in eq. (3.72) changes to

$$-\frac{Z_A}{4} G_{\mu\nu}^{(\partial),a} G^{(\partial),a,\mu\nu} - \frac{Z_A Z_\xi^{-1}}{2\xi_g} \left(\partial^\mu A_\mu^a\right)\left(\partial^\nu A_\nu^a\right). \tag{3.90}$$

The renormalization constant Z_ξ is equal to Z_A to all orders in perturbation theory due to the BRST symmetry (see chapter 12.2.5 of ref. [221]). The gluon line counterterm is thus

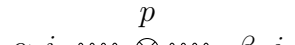

$$\alpha, i \qquad p \qquad \beta, j \quad = -i\delta_A \delta^{ij}\left(p^2 g^{\alpha\beta} - p^\alpha p^\beta\right). \tag{3.91}$$

This counterterm always appears with two gluon lines on each side. Such a line contributes a factor

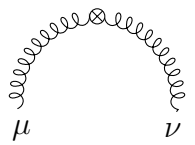

$$\mu \qquad \nu \quad = -i\delta_A \mathcal{P}_{A,\mu\alpha}\left(p^2 g^{\alpha\beta} - p^\alpha p^\beta\right)\mathcal{P}_{A,\beta\nu} = \frac{i}{p^2}\delta_A\left(g_{\mu\nu} - \frac{p_\mu p_\nu}{p^2}\right) = -\delta_A \mathcal{P}_{A,\mu\nu}\Big|_{\xi_g=0}. \tag{3.92}$$

If one fixes the QCD gauge to $\xi_g = 0$ (Landau gauge), the contributions from diagrams with counterterms on gluon lines directly connecting two quark-gluon vertices cancel the δ_A terms from the quark-gluon vertex counterterms:

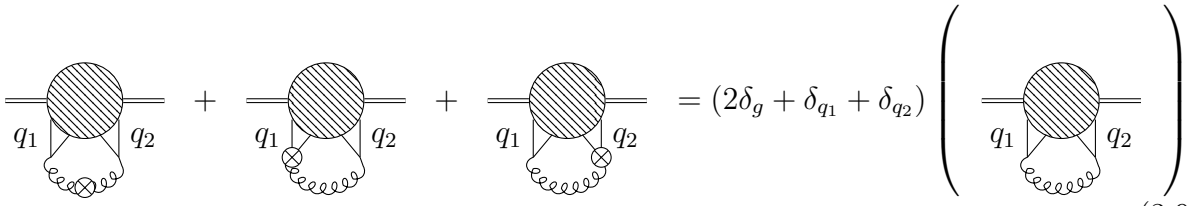

(3.93)

In the calculation of the NNLO correction to the q^2 spectrum, all diagrams with counterterm insertions on the gluon line can be compensated in this way. The renormalization of the spectrum will be discussed further in sections 3.4 and 3.5.

3.3 Heavy Quark Expansion

The first step in the analysis of the effects of the hadronic structure in inclusive decays of the B meson is to find a more convenient form of the product of matrix elements that enters the definition of the hadronic tensor $dW_{\mu\nu}$ in eq. (3.56). To this end, one conventionally defines a forward scattering matrix element $T_{\mu\nu}$ as

$$T_{\mu\nu}(q^2, qv) \equiv i \int d^4x e^{-iqx} \langle B|T J_\mu^\dagger(x) J_\nu(0)|B\rangle \,, \tag{3.94}$$

with $J_\mu(x) \equiv \bar{c}(x)\gamma_\mu P_L b(x)$ and $q \equiv p_l + p_{\bar{\nu}_l}$ as before. To evaluate the space-time integral, one can split the time ordering into the two constituent terms, and use the identity

$$\Theta(t) = -\frac{1}{2\pi i} \int\limits_{-\infty}^{\infty} d\omega \frac{e^{-i\omega t}}{\omega + i\varepsilon}, \tag{3.95}$$

which yields

$$T_{\mu\nu} = -\frac{1}{2\pi} \int d^4x e^{-iqx} \int\limits_{-\infty}^{\infty} d\omega \left[\frac{e^{-i\omega x^0}}{\omega + i\varepsilon} \langle B|J_\mu^\dagger(x) J_\nu(0)|B\rangle + \frac{e^{i\omega x^0}}{\omega + i\varepsilon} \langle B|J_\nu(0) J_\mu^\dagger(x)|B\rangle \right]. \tag{3.96}$$

The next step is to insert the identity operator

$$\sum\!\!\!\!\!\!\int_{X_c} |X_c\rangle \langle X_c| \tag{3.97}$$

in between the currents in both terms. The sum integral runs over all possible scattering states and covers both their particle content and the possible on-shell momenta. The x-dependence of the quark current can be extracted with the translation operator:

$$J_\mu^\dagger(x) = e^{i\hat{P}x} J_\mu^\dagger(0) e^{-i\hat{P}x}, \tag{3.98}$$

which leads to

$$T_{\mu\nu} = -\frac{1}{2\pi}\int d^4x \int_{-\infty}^{\infty} d\omega \sum\!\!\!\!\!\!\int_{X_c} \Bigg[\frac{e^{i(p_B - r - q)x - i\omega x^0}}{\omega + i\varepsilon} \langle B|J_\mu^\dagger|X_c\rangle \langle X_c|J_\nu|B\rangle + \frac{e^{i(r - p_B - q)x + i\omega x^0}}{\omega + i\varepsilon} \langle B|J_\nu|X_c\rangle \langle X_c|J_\mu^\dagger|B\rangle \Bigg], \tag{3.99}$$

with r denoting the total momentum of the state $|X_c\rangle$, and all currents evaluated at $x = 0$. The space-time and the ω integrals can now be evaluated. In the rest frame of the B meson, the original matrix element reads

$$T_{\mu\nu} = -(2\pi)^3 \sum\!\!\!\!\!\!\int_{X_c} \left[\frac{\langle B|J_\mu^\dagger|X_c\rangle \langle X_c|J_\nu|B\rangle}{M_B - r^0 - q^0 + i\varepsilon} \delta^{(3)}(\mathbf{q} + \mathbf{r}) + \frac{\langle B|J_\nu|X_c\rangle \langle X_c|J_\mu^\dagger|B\rangle}{M_B - r^0 + q^0 + i\varepsilon} \delta^{(3)}(\mathbf{q} - \mathbf{r}) \right]. \tag{3.100}$$

The imaginary part of the above expression is of physical importance. It can be obtained using the Sochocki-Plemelj formula

$$\lim_{\varepsilon \to 0^+} \frac{1}{\alpha + i\varepsilon} = -i\pi\delta(\alpha) + \mathcal{P}\left(\frac{1}{\alpha}\right), \tag{3.101}$$

where $\mathcal{P}$ is the Cauchy principal value. Applying it to the denominators in eq. (3.100) yields

$$\frac{1}{\pi}\mathrm{Im}T_{\mu\nu} = (2\pi)^3 \sum\!\!\!\!\!\!\int_{X_c} \big[\langle B|J_\mu^\dagger|X_c\rangle \langle X_c|J_\nu|B\rangle \, \delta^{(4)}(p_B - r - q) + \langle B|J_\nu|X_c\rangle \langle X_c|J_\mu^\dagger|B\rangle \, \delta^{(4)}(p_B - r + q) \big]. \tag{3.102}$$

The condition for the momenta enforced by the delta function in the second term can never be satisfied for the values of p_B and q considered in the q^2 spectrum of the $B \to X_c l \bar{\nu}_l$ or equivalently $B \to X_c Q$ decay width. The sum-integral with the momentum conservation condition enforced by the first delta function acts on a test function f as

$$\sum\!\!\!\!\!\!\int_{X_c} \delta^{(4)}(p_B - r - q) f(r^2, q^2) = \sum_{X_c,\ \substack{\text{hadron} \\ \text{spins}}} \int dr^2 dPS_{r \to \{p_j\}} f(r^2, q^2). \tag{3.103}$$

Thus,

$$\frac{1}{\pi}\mathrm{Im}T_{\mu\nu}(q^2, qv) = (2\pi)^3 \int dr^2 W_{\mu\nu}(r^2, q^2), \tag{3.104}$$

for the kinematically allowed values of q^2. Here, as before, $v \equiv p_B/M_B$ is the velocity of the B meson. The double differential semileptonic decay rate therefore reads

$$\frac{d\Gamma_{sl}}{dE_l dq^2} = \frac{G_F^2 |V_{cb}|^2 \pi}{(2\pi)^7 M_B^2} \mathrm{Im}T_{\mu\nu} L^{\mu\nu}. \tag{3.105}$$

The tensor $T_{\mu\nu}$ can be analyzed using the Operator Product Expansion(OPE) [222, 223]. A product of operators separated in space-time is assumed [224] to be expressible as an

infinite series of local operators. In the case of the product of currents defining $T_{\mu\nu}$, this assumption is referred to as the Heavy Quark Expansion, and reads

$$TJ_\mu^\dagger(x)J_\nu(0) = \sum_n C_n(x)\mathcal{O}_n(0), \tag{3.106}$$

with the dependence on the separation limited to the Wilson coefficients $C_n(x)$. The basis of operators $\mathcal{O}_n$ and the values of C_n have to be established by demanding that the two sides of the above equation match for all matrix elements. The OPE for the product of quark currents defining the tensor $T_{\mu\nu}$ can be established for partonic matrix elements, and then extended to the full B meson states. The simplest of such matching equations reads

$$\int d^4x e^{-iqx}\,\langle b_{\sigma'}(p_b')|TJ_\mu^\dagger(x)J_\nu(0)|b_\sigma(p_b)\rangle = \sum_n C_{n,\mu\nu}(q^2,qv)\,\langle b_{\sigma'}(p_b')|\mathcal{O}_n|b_\sigma(p_b)\rangle\,, \tag{3.107}$$

where σ indexes the b quark spin. The left hand side can be computed in perturbative QCD. At $\mathcal{O}(\alpha_s^0)$, it corresponds to a single Feynman diagram

$$\begin{aligned}
&\int d^4x e^{-iqx}\,\langle b_{\sigma'}(p_b')|TJ_\mu^\dagger(x)J_\nu(0)|b_\sigma(p_b)\rangle = \\
&= i\frac{\bar{u}_b(p_b)\gamma_\mu P_L(\not{p}_b - \not{q} + m_c)\gamma_\nu P_L u_b(p_b')}{(p_b-q)^2 - m_c^2 + i\varepsilon} + \mathcal{O}(\alpha_s) = i\frac{\bar{u}(p_b)_b\gamma_\mu(\not{p}_b - \not{q})\gamma_\nu P_L u_b(p_b')}{(p_b-q)^2 - m_c^2 + i\varepsilon} + \mathcal{O}(\alpha_s) \\
&= i(p_b-q)^\alpha \frac{\bar{u}_b(p_b)\left[g_{\mu\alpha}\gamma_\nu + g_{\alpha\nu}\gamma_\mu - g_{\mu\nu}\gamma_\alpha\right]P_L u_b(p_b')}{(p_b-q)^2 - m_c^2 + i\varepsilon} + \mathcal{O}(\alpha_s).
\end{aligned} \tag{3.108}$$

The last equality utilizes the γ matrix identity of eq. (1.190). In the kinematical configuration of the B meson, the valence b quark carries most of the momentum. It can deviate from the B momentum $p_B = M_B v$ only by momentum transfers from light partons k that can be of order of the QCD confinement scale

$$p_b = M_B v + k, \qquad k \sim \overline{\Lambda} \sim M_B - m_b. \tag{3.109}$$

Expanding eq. (3.108) in k to the leading order gives

$$i(M_B v - q)^\alpha \frac{g_{\mu\alpha}g_{\nu\rho} + g_{\alpha\nu}g_{\mu\rho} - g_{\mu\nu}g_{\alpha\rho}}{M_B^2 - 2M_B q^0 + q^2 - m_c^2 + i\varepsilon}\,\langle b_{\sigma'}(p_b')|\bar{b}\gamma^\rho P_L b|b_\sigma(p_b)\rangle + \mathcal{O}(\alpha_s, k). \tag{3.110}$$

Higher order terms of the expansion in k can only be expressed as matrix elements of operators of higher mass-dimension and will necessarily be suppressed by powers of $\overline{\Lambda}/M_B$. The only two operators with mass-dimension = 3 that can contribute a non-vanishing imaginary part to $T^{\mu\nu}$ are

$$\mathcal{O}_0^\rho \equiv \bar{b}\gamma^\rho b, \qquad\qquad \mathcal{O}_0^{(5),\rho} \equiv \bar{b}\gamma^\rho\gamma_5 b. \tag{3.111}$$

Consequently,

$$T_{\mu\nu} = C_{0,\mu\nu\rho}\,\langle B|\mathcal{O}_0^\rho|B\rangle + C_{0,\mu\nu\rho}^{(5)}\,\langle B|\mathcal{O}_0^{(5),\rho}|B\rangle + \mathcal{O}(k). \tag{3.112}$$

The Wilson coefficients $C_{0,\mu\nu\rho}$ and $C_{0,\mu\nu\rho}^{(5)}$ at the leading order in α_s can be read out of eq. (3.110). At higher orders, they follow from diagrams obtained from the one in eq. (3.108)

by adding a number of gluon and quark internal lines, but with the same configuration of external particles. The operator $\mathcal{O}_0$ generates a $U(1)$ symmetry of QCD with a conserved charge $Q_b = \int d^3\mathbf{x} b^\dagger b(x)$, called "bottomness". The B meson states have unit bottomness, i.e.

$$Q_b \left|B\right\rangle = \left|B\right\rangle . \tag{3.113}$$

The standard normalization of meson states,

$$\langle B(p)|B(q)\rangle = 2M_B(2\pi)^3\delta^{(3)}(\mathbf{p}-\mathbf{q}), \tag{3.114}$$

and Lorentz invariance imply that the matrix element $\langle B(p_B)|\mathcal{O}_0^\rho|B(p_B)\rangle$ satisfies

$$\langle B(p_B)|\mathcal{O}_0^\rho|B(p_B)\rangle = 2p_B^\rho. \tag{3.115}$$

The matrix element of $\mathcal{O}_0^{(5)\rho}$ vanishes due to its parity transformation properties. This can be seen by first considering the most general form of the result. Since the only available vector is p_B, the matrix element reads

$$\langle B(p_B^\mu)|\mathcal{O}_0^{(5)\rho}|B(p_B^\mu)\rangle = f(p_B^2)p_B^\rho, \tag{3.116}$$

for some function f. The meson state is a pseudoscalar and transforms under parity $\mathcal{P}$ as

$$\left|B(p_B^\mu)\right\rangle = -\left|B(p_B^{\bar\mu})\right\rangle , \tag{3.117}$$

where $k^{\bar\mu} \equiv (k^0, -\mathbf{k})$. The left hand side of eq. (3.116) transforms under parity as

$$\begin{aligned}\langle B(p_B^\mu)|\mathcal{O}_0^{(5)\rho}|B(p_B^\mu)\rangle &\to \langle B(p_B^\mu)|\mathcal{P}^\dagger\mathcal{O}_0^{(5)\rho}\mathcal{P}|B(p_B^\mu)\rangle \\ &= -\langle B(p_B^\mu)|\mathcal{O}_0^{(5)\bar\rho}|B(p_B^\mu)\rangle = -f(p^2)p_B^{\bar\rho},\end{aligned} \tag{3.118}$$

where the transformation property of the relevant Dirac bilinear,

$$\mathcal{P}^\dagger\bar\psi\gamma^\mu\gamma_5\psi\mathcal{P} = -\bar\psi\gamma^{\bar\mu}\gamma_5\psi, \tag{3.119}$$

was used. The right hand side of eq. (3.116) transforms as

$$f(p_B^2)p_B^\rho \to f(p_B^2)p_B^{\bar\rho}. \tag{3.120}$$

Thus, the requirement that eq. (3.116) holds after the parity transformation implies that $f(p^2) = 0$, and

$$\langle B(p_B^\mu)|\mathcal{O}_0^{(5)\rho}|B(p_B^\mu)\rangle = 0. \tag{3.121}$$

These results allow for calculating the leading term in the HQE purely perturbatively. Indeed, it is straightforward to see that

$$\frac{1}{2}\sum_\sigma\frac{1}{3}\sum_c \langle b_{c,\sigma}(p_B)|\mathcal{O}_0|b_{c,\sigma}(p_B)\rangle = 2p_B^\rho \tag{3.122}$$

and

$$\frac{1}{2}\sum_\sigma\frac{1}{3}\sum_c \langle b_{c,\sigma}(p_B)|\mathcal{O}_0^{(5)}|b_{c,\sigma}(p_B)\rangle = 0, \tag{3.123}$$

where c and σ index the color and spin of the b quark. The above two equations justify the partonic treatment of the inclusive semileptonic decay in the leading order of the HQE. The

matrix elements of $\mathcal{O}_0^\rho$ and $\mathcal{O}_0^{(5)\rho}$ are exactly equal for the B meson and averaged b quark states. At the leading order in the OPE, but to all orders in α_s, $T^{\mu\nu}$, and consequently $\Gamma_{B\to X_cQ}$ and $d\Gamma_{sl}/dq^2$, can be obtained by replacing the full B meson state with a b quark averaged over its spins and colors. One may thus avoid matching the HQE as in eqs. (3.108) and (3.110) but simply compute the spin and color averaged $\Gamma_{b\to X_cQ}$ in perturbative QCD.

Even though a detailed analysis of higher order terms in the HQE is beyond the scope of the present thesis, in the context of the q^2 spectrum it is important to discuss some aspects of their general structure. To obtain these non-leading terms, it is convenient to pass to the HQET, which provides an equivalent description of the dynamics of hadrons with a single heavy valence quark. As the first step in the construction of this theory, one decomposes the b-quark field as

$$b(x) = P_+ b(x) + P_- b(x) \equiv e^{-im_b vx} b_v(x) + e^{-im_b vx} \beth_v(x), \tag{3.124}$$

where

$$P_\pm \equiv \frac{\mathbb{1}_{4\times4} \pm \not{v}}{2}, \qquad P_\pm^2 = P_\pm. \tag{3.125}$$

In the rest frame of the B meson, $\not{v} = \gamma^0$. If the b quark was at rest in this frame, the operators $P_+(P_-)$ would project onto the particle(antiparticle) components of its Dirac spinor. One can check it using the chiral representation for the γ matrices:

$$P_\pm \xrightarrow{v\to(1,0,0,0)^T} \frac{1}{2}\begin{pmatrix} \mathbb{1}_{2\times2} & \pm\mathbb{1}_{2\times2} \\ \pm\mathbb{1}_{2\times2} & \mathbb{1}_{2\times2} \end{pmatrix}. \tag{3.126}$$

Applying P_+ in this limit to a zero-momentum solution of the free Dirac equation yields

$$\frac{1}{2}\begin{pmatrix} \mathbb{1}_{2\times2} & \mathbb{1}_{2\times2} \\ \mathbb{1}_{2\times2} & \mathbb{1}_{2\times2} \end{pmatrix} \sum_\sigma \left[a_\sigma \begin{pmatrix} \xi^\sigma \\ \xi^\sigma \end{pmatrix} + b_\sigma \begin{pmatrix} \eta^\sigma \\ -\eta^\sigma \end{pmatrix} \right] = \sum_\sigma a_\sigma \begin{pmatrix} \xi^\sigma \\ \xi^\sigma \end{pmatrix}, \tag{3.127}$$

where ξ^σ and η^σ stand for the normalized two-dimensional basis vectors. An analogous relation holds for P_-. This gives an interpretation of the fields b_v and $\beth_v$. In the rest frame of the b quark, they would be the b and anti-b fields with momenta shifted by $-m_b v$. Consequently, the typical momenta of the b quark in the matrix element $T^{\mu\nu}$ with the b field replaced with b_v are $\mathcal{O}(\overline{\Lambda})$.

The QCD Lagrangian density (3.69) can be expressed in terms of the fields b_v and $\beth_v$:

$$\mathcal{L}_{\substack{QCD \\ udcsb}} = \mathcal{L}_{\substack{QCD \\ udcs}} + \bar{b}_v(ivD)b_v - \bar{\beth}_v(ivD + 2m_b)\beth_v + \bar{b}_v(i\not{D}_\perp)\beth_v + \bar{\beth}_v(i\not{D}_\perp)b_v, \tag{3.128}$$

with

$$D_\perp^\mu \equiv D^\mu - (vD)v^\mu. \tag{3.129}$$

The QCD Green's functions that do not involve anti-b quarks on external lines can be computed in an effective theory with the field $\beth_v$ integrated out of the full QCD generating functional. This effective theory is obtained in the same manner as in the heavy particle decoupling described in section 3.1. The result is the HQET Lagrangian density:

$$\mathcal{L}_{HQET} = \mathcal{L}_{\substack{QCD \\ udcs}} + \bar{b}_v(ivD)b_v + \sum_n C_n \frac{\mathcal{O}_n}{m_b^{p(n)}}. \tag{3.130}$$

The effective operators $\mathcal{O}_n$ are finite-rank polynomials in the field b_v, lighter quarks, gluons, ghosts, as well as derivatives of these fields. They are constrained by symmetries of the full

QCD, such as gauge invariance, parity and flavor conservation. The Wilson coefficients C_n are assumed to be dimensionless, which means that the powers $p(n) \geq 1$ are fixed by the mass-dimension of the effective operators.

Since the matrix element $T^{\mu\nu}$ has to be the same when computed in the full QCD or in HQET, one can match the corresponding product of quark currents to the full basis of effective operators $\mathcal{O}_n$ in eq. (3.130). At mass-dimension = 4, again there are only two operators that can contribute a non-vanishing imaginary part to $T^{\mu\nu}$:

$$\tilde{\mathcal{O}}_v^{\rho\alpha} \equiv \bar{b}_v \gamma^\rho (iD^\alpha) b_v, \qquad \tilde{\mathcal{O}}_v^{(5)\rho\alpha} \equiv \bar{b}_v \gamma^\rho \gamma_5 (iD^\alpha) b_v. \tag{3.131}$$

The B meson matrix elements of the second one vanish by a similar argument to the mass-dimension = 3 case. The first can be simplified using the identities

$$P_+ b_v = b_v, \qquad \bar{b}_v P_+ = \bar{b}_v, \qquad P_+ \gamma_\alpha P_+ = v_\alpha P_+. \tag{3.132}$$

The latter can be proven be explicitly computing the left hand side as follows:

$$\begin{aligned} P_+ \gamma_\alpha P_+ =& \frac{1}{4}(\gamma_\alpha + \gamma_\alpha \not{v} + \not{v}\gamma_\alpha + \not{v}\gamma_\alpha \not{v}) \\ =& \frac{1}{4}\left[\gamma_\alpha + \gamma_\alpha \not{v} + (2v_\alpha - \gamma_\alpha \not{v}) + (2v_\alpha - \gamma_\alpha \not{v})\not{v}\right] \\ =& \frac{1}{4}(2v_\alpha + 2v_\alpha \not{v}) = v_\alpha P_+, \end{aligned} \tag{3.133}$$

where in the second equality, $\not{v}$ was anticommuted past γ_α using the defining anticommutation relation of the Clifford algebra, and the third equality follows from $\not{v}\not{v} = v^2 = 1$. The operator $\mathcal{O}_v^{\rho\alpha}$ can now be written as

$$\tilde{\mathcal{O}}_v^{\rho\alpha} = \bar{b}_v \gamma^\rho (iD^\alpha) b_v = \bar{b}_v P_+ \gamma^\rho (iD^\alpha) P_+ b_v = v^\rho \bar{b}_v (iD^\alpha) b_v. \tag{3.134}$$

At this order of the HQE, it is therefore sufficient to consider a single operator:

$$\mathcal{O}_v^\alpha \equiv \bar{b}_v (iD^\alpha) b_v \tag{3.135}$$

and its B meson matrix element:

$$\langle B | \mathcal{O}_v^\alpha | B \rangle = A v^\alpha, \tag{3.136}$$

where A is a number. The Euler-Lagrange equation for the field b_v that follows from eq. (3.130) reads

$$(ivD) b_v = \mathcal{O}\left(\frac{1}{m_b}\right). \tag{3.137}$$

The operator $v_\alpha \mathcal{O}_v^\alpha$ thus vanishes by classical equations of motion up to corrections proportional to higher mass-dimension operators:

$$v_\alpha \mathcal{O}_v^\alpha = \mathcal{O}\left(\frac{1}{m_b}\right). \tag{3.138}$$

This fact, together with the contraction of eq. (3.136) with v_α implies that the matrix element $\langle B | \mathcal{O}_v^\alpha | B \rangle$ vanishes up to higher order corrections in the HQE.

The remainder of this section is devoted to discussing the impact of reparametrization invariance on the Wilson coefficients of the HQE. This discussion follows the original reasoning

presented in ref. [34], where the RP symmetry was employed to eliminate some of the terms in the HQE for the inclusive semileptonic rate. The RPI properties can be utilized in full QCD, without integrating out the $\sqsupset$ component of the b field. To this end, one introduces a rescaled b-quark field[†]

$$\beta_v(x) \equiv e^{im_b vx} b(x) \tag{3.139}$$

and inserts this definition into the QCD Lagrangian. One may relax the assumption that v is the four-velocity of the B meson and vary it over a range of time-like vectors normalized as $v^2 = 1$, as long as $M_B v - p_B \sim \overline{\Lambda}$. Note that

$$\beta_v(0) = b(0). \tag{3.140}$$

All QCD observables defined without a specific reference of v must be independent of the choice of v as the definition (3.139) is a trivial notation change. Consider a shift transformation $v \to v + \delta v$ for infinitesimal δv. The condition $v^2 = (v + \delta v)^2 = 1$ implies that

$$v^\mu \delta v_\mu = 0. \tag{3.141}$$

Under this shift, the field β_v transforms as

$$\beta_v(x) \to \beta_v(x) + \delta\beta_v(x) = [1 + im(x\delta v)]\beta_v(x), \tag{3.142}$$

which follows immediately from the definition (3.139) and the invariance of $b(x)$ under the considered transformation. Again, note that

$$\beta_v(0) \to \beta_v(0). \tag{3.143}$$

The Euler-Lagrange equation for β_v follows from the gluon-coupled Dirac equation for b and reads

$$[i\not{D} + m_b(1 - \not{v})]\beta_v = 0. \tag{3.144}$$

This equation must still hold after the shift $v \to v + \delta_v$, which leads to

$$[i\not{D} + m_b(1 - \not{v})]\delta\beta_v + (i\delta\not{D} + m_b\delta\not{v})\beta_v = 0, \tag{3.145}$$

where δD_μ denotes the shift of the covariant derivative in the transformation. For $\beta_v(0)$, this equation is satisfied if an additional transformation condition is imposed on the covariant derivative:

$$iD_\mu \to iD_\mu - m_b\delta v_\mu. \tag{3.146}$$

The prescription (3.104) and the expansion (3.106) allow for setting up a HQE for the kinematic moments of the differential decay rate defined in the Introduction in eq. (I.10). For the width $\Gamma_{B\to X_c Q}$, the HQE is of the form

$$M = \sum_{n=0}^{\infty} \sum_{\Gamma} c^{(n,\Gamma)}_{\mu_1\ldots\mu_n} \bar{\beta}_v(0)(iD^{\mu_1})\ldots(iD^{\mu_n})\Gamma\beta_v(0), \tag{3.147}$$

up to loop corrections $\mathcal{O}(\alpha_s)$. The rate is obtained as

$$\Gamma_{B\to X_c Q} = \langle B|M|B\rangle\,. \tag{3.148}$$

[†]Note that this field is defined without the projector P_+.

The Wilson coefficients depend on the mass $\sqrt{q^2}$ and on the components v^μ. The symbol Γ denotes an element of the basis spanning the algebra of 4×4 matrices acting in the spin space. The HQE (3.147) is RPI, that is, it does not transform under the shift $v \to v + \delta v$:

$$\begin{aligned} 0 = \delta M = \sum_{n=0}^{\infty} \sum_{\Gamma} \Big[& \delta c^{(n,\Gamma)}_{\mu_1 \dots \mu_n} \bar{\beta}_v(0) (iD^{\mu_1}) \dots (iD^{\mu_n}) \Gamma \beta_v(0) \\ & - m_b c^{(n,\Gamma)}_{\mu_1 \dots \mu_n} \sum_{k=1}^{n} \delta v^{\mu_k} \bar{\beta}_v(0) (iD^{\mu_1}) \dots (iD^{\mu_{k-1}}) (iD^{\mu_{k+1}}) \dots (iD^{\mu_n}) \Gamma \beta_v(0) \Big], \end{aligned} \tag{3.149}$$

where eqs. (3.143) and (3.146) were used to transform the fields and covariant derivatives. Including only the $n = 0$, $n = 1$, and $n = 2$ terms leads to

$$0 = \sum_{\Gamma} \left[\left(\delta c^{(0,\Gamma)} - m_b \delta v^{\mu_1} c^{(1,\Gamma)}_{\mu_1} \right) \bar{\beta}_v \Gamma \beta_v + \left(\delta c^{(1,\Gamma)}_{\mu} - m_b \delta v^{\nu} (c^{(2,\Gamma)}_{\mu\nu} + c^{(2,\Gamma)}_{\nu\mu}) \right) \bar{\beta}_v i D^{\mu} \Gamma \beta_v \right]. \tag{3.150}$$

The most general Lorentz invariant ansatz for the Wilson coefficients that can be built only with v_μ is

$$\begin{aligned} \sum_{\Gamma} c^{(0,\Gamma)} \Gamma &= a_0 + \hat{a}_0 \not{v}, \\ \sum_{\Gamma} c^{(1,\Gamma)}_{\mu} \Gamma &= v_\mu (a_1 + \hat{a}_1 \not{v}) + \gamma_\mu (b_1 + \hat{b}_1 \not{v}), \\ \sum_{\Gamma} c^{(2,\Gamma)}_{\mu\nu} \Gamma &= v_\mu v_\nu (a_2 + \hat{a}_2 \not{v}) + g_{\mu\nu} (b_1 + \hat{b}_1 \not{v}) + (v_\mu \gamma_\nu + v_\nu \gamma_\mu)(g_2 + \hat{g}_2) + [\gamma_\mu, \gamma_\nu] h_2. \end{aligned} \tag{3.151}$$

where a_i, $\hat{a}_i$, b_i, $\hat{b}_i$, g_2, $\hat{g}_2$, and h_2 are scalar functions of q^2, m_c^2, and m_b^2. The RPI condition (3.150) enforces a set of relations between these functions. The vanishing of the first parenthesis implies

$$\sum_{\Gamma} \delta c^{(0,\Gamma)} \Gamma = \hat{a}_0 \delta \not{v} \stackrel{!}{=} m_b \delta \not{v} (b_1 + \hat{b}_1 \not{v}) = \sum_{\Gamma} m_b \delta v^{\mu} c^{(1,\Gamma)}_{\mu} \Gamma, \tag{3.152}$$

where the term involving a_1 and $\hat{a}_1$ vanishes due to eq. (3.141). The second equality has to hold for any vector v, and therefore

$$b_1 = \frac{\hat{a}_0}{m_b}, \qquad \hat{b}_1 = 0. \tag{3.153}$$

The second parenthesis in eq. (3.150) vanishes independently of the first, and thus

$$\delta v_\mu (a_1 + \hat{a}_1 \not{v}) + (\hat{a}_1 v_\mu + \hat{b}_1 \gamma_\mu) \delta \not{v} \stackrel{!}{=} m_b \delta v^{\nu} \Big(2 g_{\mu\nu} (b_2 + \hat{b}_2 \not{v}) + 2 \gamma_\nu v_\mu (g_2 + \hat{g}_2 \not{v}) \Big). \tag{3.154}$$

This relation can be used to also eliminate the functions a_1 and $\hat{a}_1$, as well as g_2 and $\hat{g}_2$:

$$a_1 = 2 m_b b_2, \qquad \hat{a}_1 = 2 m_b \hat{b}_2 = 2 m_b g_2, \qquad \hat{g}_2 = 0. \tag{3.155}$$

This confirms the conclusion obtained using the HQET, that the contributions of all operators with mass-dimension = 4 relevant for the computation of the semileptonic decay can be written in terms of operators of other dimensionalities.

A discussion of similar RPI relations between Wilson coefficients of higher mass-dimension operators and the generalization to all orders in perturbative QCD can be found in ref. [34]. In particular, the RP invariance can be used to eliminate from the HQE one operator at mass-dimension = 5, another one at mass-dimension = 6, and 4 operators at mass-dimension = 7. As the q^2 spectrum and its moments are RP invariant (see eq. (I.11) on page 7), the fit used to extract the value of V_{cb} from their measurements thus has less free parameters. This is the primary motivation for considering these quantities in addition to the lepton-energy and hadronic-invariant-mass moments that were utilized in the previous fits.

3.4 The q^2 Spectrum at the LO and NLO in QCD

The present section is devoted to the analysis of the leading term and the NLO correction of the expansion in powers of α_s. As discussed above, to obtain these quantities at the leading order in HQE (neglecting $\mathcal{O}(\hat{\Lambda}^2)$ corrections), it is sufficient to calculate the spin and color averaged decay width $\bar{\Gamma}_{b\to X_c Q}$ in perturbative QCD. At the LO, it is given by a single diagram:

$$\bar{\Gamma}_{b\to X_c Q} = -\frac{1}{m_b}\frac{1}{2}\sum_s \frac{1}{3}\sum_c \mathrm{Im}\left[i\cdot \left(\right.\right. \quad + \mathcal{O}(\alpha_s^1), \tag{3.156}$$

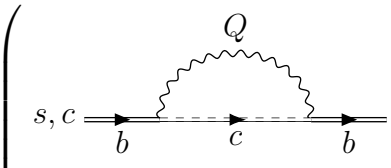

with the Feynman rules given in eqs. (1.124), (1.125) and (1.126). For the purpose of renormalizing the NLO QCD correction, one must compute this expression up to and including the $\mathcal{O}(\epsilon^2)$ term. In the following, only the $\mathcal{O}(\epsilon^0)$ and $\mathcal{O}(\epsilon^1)$ terms are going to be determined analytically, while the $\mathcal{O}(\epsilon^2)$ will be computed numerically, together with the 2- and 3-loop diagrams. It is straightforward to obtain the leading order in the ϵ expansion by using eq. (1.120), thus avoiding the loop integration altogether. Calculating subsequent terms using this approach becomes difficult due to the necessary $D-$dimensional phase space integral and non-trivial analytical continuations. Therefore, it is simpler to proceed with the general method outlined in the Sample Calculation sections in the previous two chapters. The process is diagonal in color at this order in QCD, so one may replace $\sum_c \to 3$. Within the NDR prescription defined on page 58, one can apply the γ-matrix identity

$$\mathrm{Tr}[\gamma^\mu\gamma^\nu\gamma^\rho\gamma^\sigma] = 4(g^{\mu\rho}g^{\nu\sigma} - g^{\mu\nu}g^{\rho\sigma} + g^{\mu\sigma}g^{\nu\rho}), \tag{3.157}$$

which is a simple consequence of eqs. (1.175) and (1.173), with $D^{(\gamma)}$ fixed to 4. After elementary algebraic simplifications, the contribution of this diagram gives

$$\bar{\Gamma}_{b\to X_c Q} = \sqrt{2}G_F|V_{cb}|^2 m_b^3 \left[(D-1)\hat{q}^2(1+\hat{m}_c^2-\hat{q}^2) + \lambda(1,\hat{m}_c^2,\hat{q}^2)\right] \mathrm{Im}\left[I_{11}^{(1a)}\right] + \mathcal{O}(\alpha_s^1), \tag{3.158}$$

where

$$I_{ab}^{(1a)} \equiv \tilde{\mu}^{2\epsilon}\int \frac{d^Dk}{i(2\pi)^D}\frac{1}{D_1^a D_2^b} \tag{3.159}$$

and

$$D_1 \equiv (k+p_b)^2 - m_c^2 + i\varepsilon, \qquad D_2 \equiv k^2 - q^2 + i\varepsilon. \tag{3.160}$$

The contributions of scalar integrals with non-positive indices a or b were neglected in eq. (3.158) due to their vanishing imaginary parts.

Next, one may derive a DE for the integral $\mathrm{Im}\left[I_{11}^{(1a)}\right]$ as a a function of $\hat{m}_c^2$ and $\hat{q}^2$. Computing the derivatives is straightforward:

$$\partial_{\hat{m}_c^2}\mathrm{Im}\left[I_{11}^{(1a)}\right] = m_b^2\mathrm{Im}\left[I_{21}^{(1a)}\right], \qquad \partial_{\hat{q}^2}\mathrm{Im}\left[I_{11}^{(1a)}\right] = m_b^2\mathrm{Im}\left[I_{21}^{(1a)}\right]. \tag{3.161}$$

The necessary IBP relations read

$$\begin{aligned}
0 &= \tilde{\mu}^{2\epsilon}\int \frac{d^Dk}{i(2\pi)^D}\partial_{k^\mu}\frac{p_b^\mu}{D_1^aD_2^b}\\
&=(b-a)I_{ab}^{(1a)} + b(m_b^2 - m_c^2 + q^2)I_{a(b+1)}^{(1a)} - a(m_b^2 + m_c^2 - q^2)I_{(a+1)b}^{(1a)} + aI_{(a+1)(b-1)}^{(1a)} - bI_{(a-1)(b+1)}^{(1a)},\\
0 &= \tilde{\mu}^{2\epsilon}\int \frac{d^Dk}{i(2\pi)^D}\partial_{k^\mu}\frac{k^\mu}{D_1^aD_2^b}\\
&=(D-a-2b)I_{ab}^{(1a)} - 2bq^2I_{a(b+1)}^{(1a)} + a(m_b^2 - m_c^2 - q^2)I_{(a+1)b}^{(1a)} - aI_{(a+1)(b-1)}^{(1a)},
\end{aligned} \tag{3.162}$$

which for $a = b = 1$ can be transformed as

$$\begin{aligned}
\partial_{\hat{m}_c^2}\mathrm{Im}\left[I_{11}^{(1a)}\right] &= m_b^2\mathrm{Im}\left[I_{21}^{(1a)}\right] = (3-D)\frac{1-\hat{m}_c^2+\hat{q}^2}{\lambda(1,\hat{m}_c^2,\hat{q}^2)}\mathrm{Im}\left[I_{11}^{(1a)}\right],\\
\partial_{\hat{q}^2}\mathrm{Im}\left[I_{11}^{(1a)}\right] &= m_b^2\mathrm{Im}\left[I_{12}^{(1a)}\right] = (3-D)\frac{1+\hat{m}_c^2-\hat{q}^2}{\lambda(1,\hat{m}_c^2,\hat{q}^2)}\mathrm{Im}\left[I_{11}^{(1a)}\right].
\end{aligned} \tag{3.163}$$

Changing the variables to u and v defined in eq. (2.84) results in two separated equations

$$\begin{aligned}
\partial_u\mathrm{Im}\left[I_{11}^{(1a)}\right] &= \frac{D-3}{u}\frac{u^2+1}{u^2-1}\mathrm{Im}\left[I_{11}^{(1a)}\right],\\
\partial_v\mathrm{Im}\left[I_{11}^{(1a)}\right] &= \frac{D-3}{v}\mathrm{Im}\left[I_{11}^{(1a)}\right].
\end{aligned} \tag{3.164}$$

These can be brought to the ϵ-form with a transformation

$$\mathrm{Im}\left[I_{11}^{(1a)}\right] = T(u,v)X(u,v), \qquad T(u,v) \equiv \frac{v}{u} - uv = \frac{|\mathbf{q}|}{m_b}, \tag{3.165}$$

where the rescaling factor can be recognized as the length of the momentum $\mathbf{q}$ that is fixed by eq. (3.49) with M_B replaced by m_b. The function $X(u,v)$ satisfies the transformed DE

$$dX = \epsilon dCX. \tag{3.166}$$

The coefficient C is given by

$$C = \sum_{l=1}^{4}\mathcal{C}_l\log\alpha_l, \tag{3.167}$$

with the four letters α_l defined in eq. (2.87) and the constants

$$\mathcal{C}_1 = 2, \qquad \mathcal{C}_2 = -2, \qquad \mathcal{C}_3 = -2, \qquad \mathcal{C}_4 = -2. \tag{3.168}$$

The general solution for $X(u, v)$ can be constructed as described in section 2.3. It takes a simple form

$$X(u, v) = \left(1 - 2\epsilon \log T + \mathcal{O}(\epsilon^2)\right) \lim_{u\to 0} \lim_{v\to 0} X(u, v). \tag{3.169}$$

Using the `AMFlow` package, one can compute a boundary condition $\mathrm{Im}[I_{11}^{(1a)}](u = 0.02, v = 0.01)$, rescale it with $T^{-1}(u = 0.02, v = 0.01)$, and evolve to the limit given by $\lim_{u\to 0} \lim_{v\to 0}$ using the above equation to obtain

$$\left(\frac{m_b}{\mu}\right)^{2\epsilon} \lim_{u\to 0} \lim_{v\to 0} X(u, v) = \frac{1}{16\pi} \left[1 + 2\epsilon\right] + \mathcal{O}(\epsilon^2). \tag{3.170}$$

Rescaling this solution back, the imaginary part of the considered MI reads

$$\left(\frac{m_b}{\mu}\right)^{2\epsilon} \mathrm{Im}[I_{11}^{(1a)}] = \frac{T}{16\pi} \left[1 + 2\epsilon(1 - \log T)\right] + \mathcal{O}(\epsilon^2). \tag{3.171}$$

Using eq. (3.158), as well as the relation between the auxiliary width and the q^2 spectrum (3.68) yields the result

$$\frac{d\Gamma_{sl}^{(0)}}{dq^2} = \frac{G_F^2 |V_{cb}|^2 m_b^3}{96\pi^3} \frac{Tv}{u^2} \left[P_1 + \epsilon \left(P_1(L_\mu - 2\log T) + \frac{P_2}{2}\right)\right] + \mathcal{O}(\epsilon^2). \tag{3.172}$$

The polynomials P_i are given by

$$\begin{aligned} P_1(u, v) =& 3u \left(u^2 + 1\right) \left(v^2 + 1\right) - 2 \left(u^4 + 4u^2 + 1\right) v, \\ P_2(u, v) =& 5u \left(u^2 + 1\right) \left(v^2 + 1\right) - 2 \left(u^4 + 8u^2 + 1\right) v, \end{aligned} \tag{3.173}$$

and the symbol L_μ denotes $\log(\mu^2/m_b^2)$. Note that the leading term in eq. (3.172) is finite in the limit $\epsilon \to 0$. This should not be surprising, as the same quantity can be obtained from tree-level diagrams. Consequently, the spectrum in this approximation is independent of the renormalization scale μ. To assess the uncertainty from higher order terms without computing the $\mathcal{O}(\alpha_s^1)$ correction, one can assume a relative error $\mathcal{O}(\pm\alpha_s(m_b)/\pi)$. As it will become apparent, this is a very conservative estimate.

The computation of the NLO QCD correction proceeds along the lines outlined in the "Sample Calculation" sections of this thesis. Aside from the analyzed diagram $(2a)$, this correction receives contributions from the three remaining diagrams presented in the right panel of figure 6. The analytic expression stemming from the diagram $(2a')$ is exactly equal to the one from the diagram $(2a)$ due to the γ matrix identity

$$\mathrm{Tr}^{1234\ldots n} = \mathrm{Tr}^{n(n-1)\ldots 21} \tag{3.174}$$

in the notation introduced above eq. (1.174).

With the routing of momenta depicted in the left panel of figure 11, the expression for the diagram $(2b)$ can be written as a linear combination of the imaginary parts of scalar integrals of the form

$$I_{abcde}^{(2b)} \equiv \tilde{\mu}^{4\epsilon} \int \frac{d^D k_1}{i(2\pi)^D} \frac{d^D k_2}{i(2\pi)^D} \frac{D_2^e}{D_1^a D_3^b D_4^c D_5^d}, \tag{3.175}$$

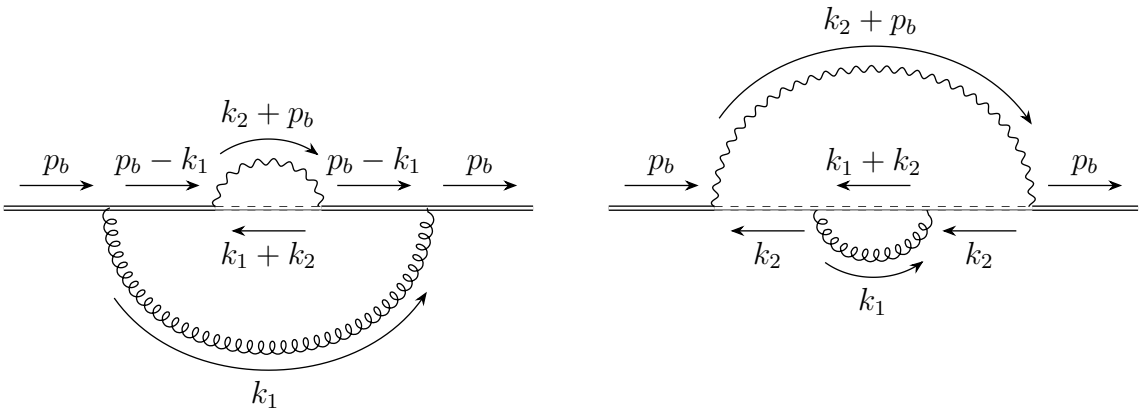

Figure 11: The routing of momenta in diagrams $(2b)$ and $(2c)$ that defines integral families reducible to $I^{(2a)}_{abcde}$.

with the denominators D_i defined as in eq. (1.246). The integer index e is greater or equal zero, as the corresponding line does not appear in the diagram $(2b)$. The factor D_2^a, which in this case is referred to as an irreducible numerator, must be included in the definition of $I^{(2b)}$ because the chosen denominators must form a basis in the space of scalar products (possibly shifted by masses) in order for the numerator of the integrand to be expressible as a linear combination of products of integer powers of D_a. These integrals satisfy an obvious relation

$$I^{(2b)}_{abcde} = I^{(2a)}_{a(-e)bcd}. \tag{3.176}$$

Therefore, the considered diagram can be written as a linear combination of MIs already computed in the "Sample Calculation" sections. One only needs to find the coefficients of all integrals $I^{(2b)}_{abcde}$, which is done in the same way as described in section 1.7. The same reasoning holds for scalar integrals contributing to the expression for the diagram $(2c)$. With the momenta routed as depicted in the right panel of figure 11, they read

$$I^{(2c)}_{abcde} \equiv \tilde{\mu}^{4\epsilon} \int \frac{d^D k_1}{i(2\pi)^D} \frac{d^D k_2}{i(2\pi)^D} \frac{D_4^e}{D_1^a D_2^b D_3^c D_5^d} = I^{(2a)}_{abc(-e)d}. \tag{3.177}$$

Again, the expression for the diagram $(2c)$ reduces to a linear combination of the imaginary parts of previously computed MIs.

The IBP reduction program `Kira` [151] can automatically find relations like the one in eq. (3.176) among various diagrams. This allows for simultaneous reductions to a basis of MIs belonging to integral families inherited only from a subset of diagrams. The number of MIs obtained in this way can be much smaller than if each diagram was independently reduced. However, as the IBP relations for all seed integrals are generated at the same time, the size of the system of equations can be significantly larger, and the computer memory demand much more significant. This was not a problem for the IBP reductions for the NLO and NNLO corrections to the q^2 spectrum, but a simultaneous reduction at the NNNLO does not seam feasible at present.

The expressions originating from the four two-loop diagrams at the NLO are divergent in the limit $\epsilon \to 0$, as was observed in the case of the diagram $(2a)$ in eq. (2.117). This divergence is canceled by the contributions of one-loop diagrams with a single counterterm insertion. At this order in perturbation theory, aside from the quark line counterterm expression found in eq. (3.89), one also needs the counterterm coming from the Qcb vertex. The renormalization

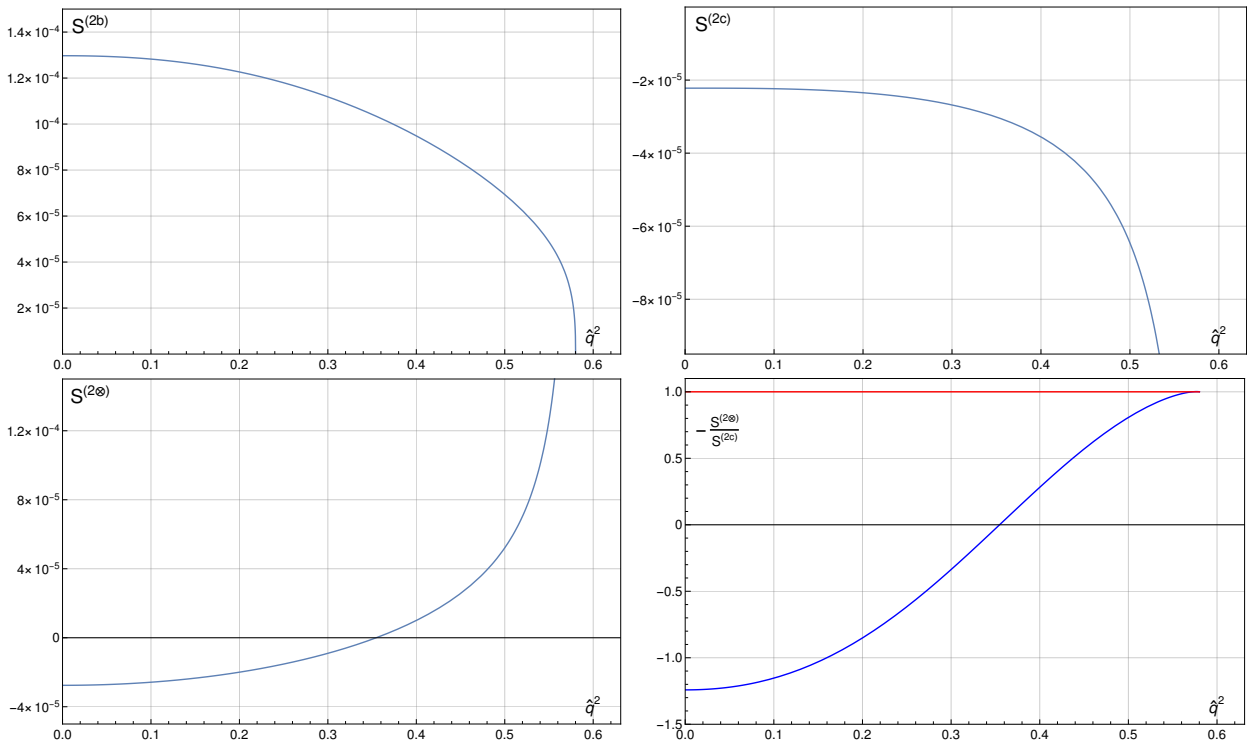

Figure 12: The functions $S^{(2b)}$, $S^{(2c)}$, $S^{(2\otimes)}$, and the ratio $-S^{(2b)}/S^{(2c)}$ for $\hat{m}_c = 0.2384$. The function $S^{(2b)}$ vanishes in the $q^2 \to (m_b - m_c)^2$ limit, while $S^{(2c)}$ and $S^{(2\otimes)}$ diverge, with their ratio approaching -1.

constants of the Q field, its mass, and the weak effective coupling g_q begin contributing only at the non-leading order in electroweak interactions: $Z_Q, Z_{g_q} = 1 + \mathcal{O}(g_q^2)$, which is not considered here. The counterterm for the Qcb vertex can thus be written as

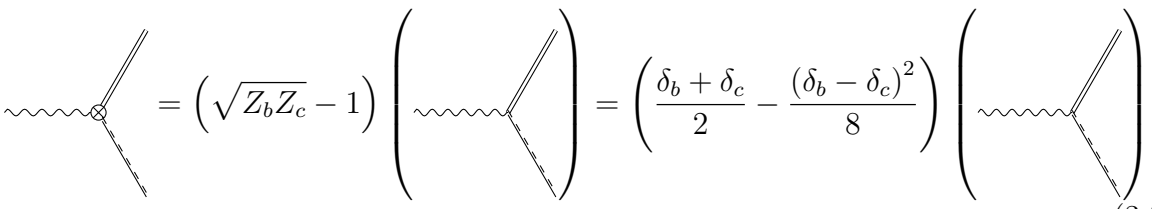

$$= \left(\sqrt{Z_b Z_c} - 1\right)$$

$$= \left(\frac{\delta_b + \delta_c}{2} - \frac{(\delta_b - \delta_c)^2}{8}\right)$$

, (3.178)

where the $\mathcal{O}(\alpha_s^3)$ terms have been neglected. The renormalization factors δ_X and their α_s expansion coefficients $\delta_X^{(n)}$ were defined in eq. (3.87) on page 114.

With the above results, it is straightforward to construct the counterterm contribution to the NLO correction. There are three one-loop diagrams with a non-vanishing α_s^1 term:

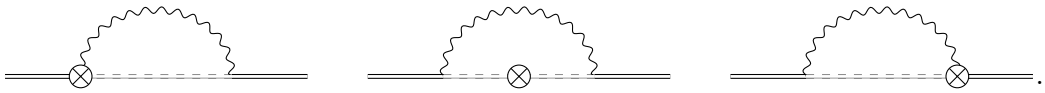

. (3.179)

The first and third are proportional to the LO diagram

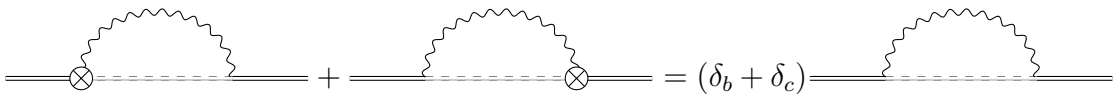

$= (\delta_b + \delta_c)$

. (3.180)

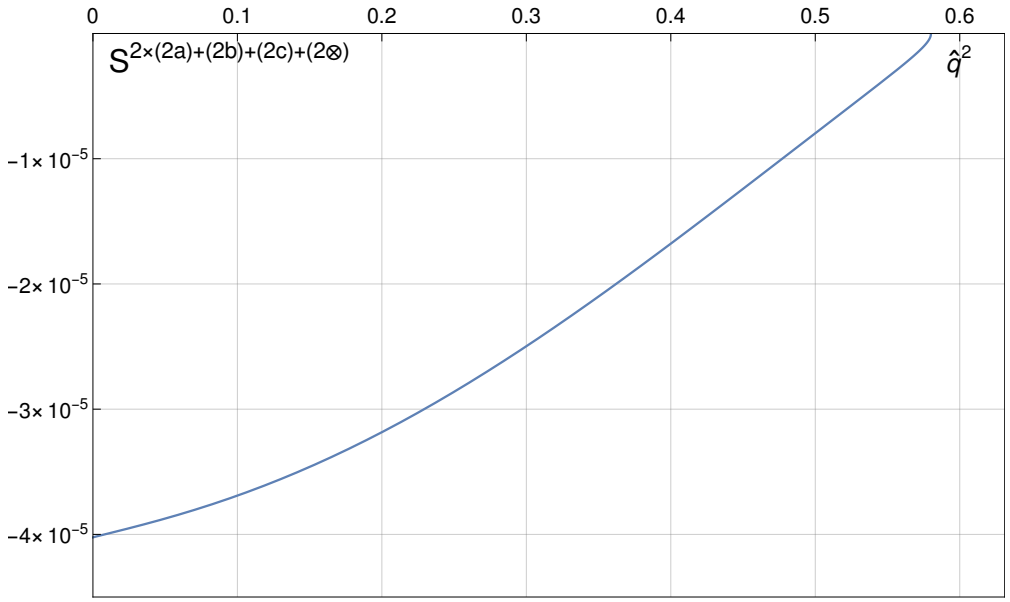

Figure 13: The sum of the functions $S^{(2b)}$, $S^{(2c)}$, $S^{(2\otimes)}$, and twice $S^{(2a)}$ for $\hat{m}_c = 0.2384$.

In the second one, the c-quark lines together with the counterterm yield

$$\begin{aligned}&\mathcal{P}_c\left(-\delta_c\mathcal{P}_c^{-1} - i\left(\delta_{m_c} + \delta_c\delta_{m_c}\right)m_c\right)\mathcal{P}_c = -\delta_c\mathcal{P}_c - im_c\left(\delta_{m_c} + \delta_c\delta_{m_c}\right)\mathcal{P}_c^2\\ &= -\delta_c\mathcal{P}_c + \left(\delta_{m_c} + \delta_c\delta_{m_c}\right)2\hat{m}_c^2\partial_{\hat{m}_c^2}\mathcal{P}_c,\end{aligned} \tag{3.181}$$

where the last equality follows from the identity

$$\mathcal{P}_\psi^2 = 2im_\psi\partial_{m_\psi^2}\mathcal{P}_\psi. \tag{3.182}$$

Hence, the second diagram in eq. (3.179) can be written as

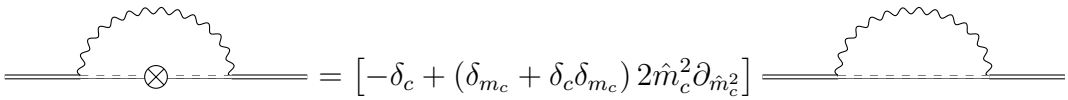

(3.183)

At this level in perturbation theory, the last term can be neglected. Combining the results of eqs. (3.180) and (3.183) yields the following formula for the counterterm part of the NLO correction:

$$\frac{d\Gamma_{sl}^{(1,\otimes)}}{dq^2} = \alpha_s\left(\delta_b^{(1)} + 2\delta_{m_c}^{(1)}\hat{m}_c^2\partial_{\hat{m}_c^2}\right)\frac{d\Gamma_{sl}^{(0)}}{dq^2}. \tag{3.184}$$

The necessary OS-scheme renormalization factors δ_b and δ_{m_c} can be obtained up to the $\mathcal{O}(\alpha_s^3)$ term from refs. [225, 226]. The result of eq. (3.172) can thus be utilized to readily compute the counterterm part of the NLO term of the q^2 spectrum.

After combining the contributions of all relevant diagrams, the final result reads

$$\begin{aligned}\frac{d\Gamma^{(1)}}{dq^2} =& \frac{G_F^2|V_{cb}|^2m_b^3}{144\pi^3u^3}\frac{\alpha_s}{\pi}\Big[3H_1 + uv(u^2-1)A\\ &+ 16H_1\log(1-u^2) + B_1\log v + B_2\log u + B_3\log(1-uv) + B_4\log\left(1-\frac{v}{u}\right)\\ &+ 8\frac{u^2+1}{u^2-1}\left(\overline{\mathrm{Li}}_2\left(1-\frac{v}{u}\right) - \overline{\mathrm{Li}}_2\left(1-uv\right) - 2\overline{\mathrm{Li}}_2\left(u^2\right)\right)H_1\Big].\end{aligned} \tag{3.185}$$

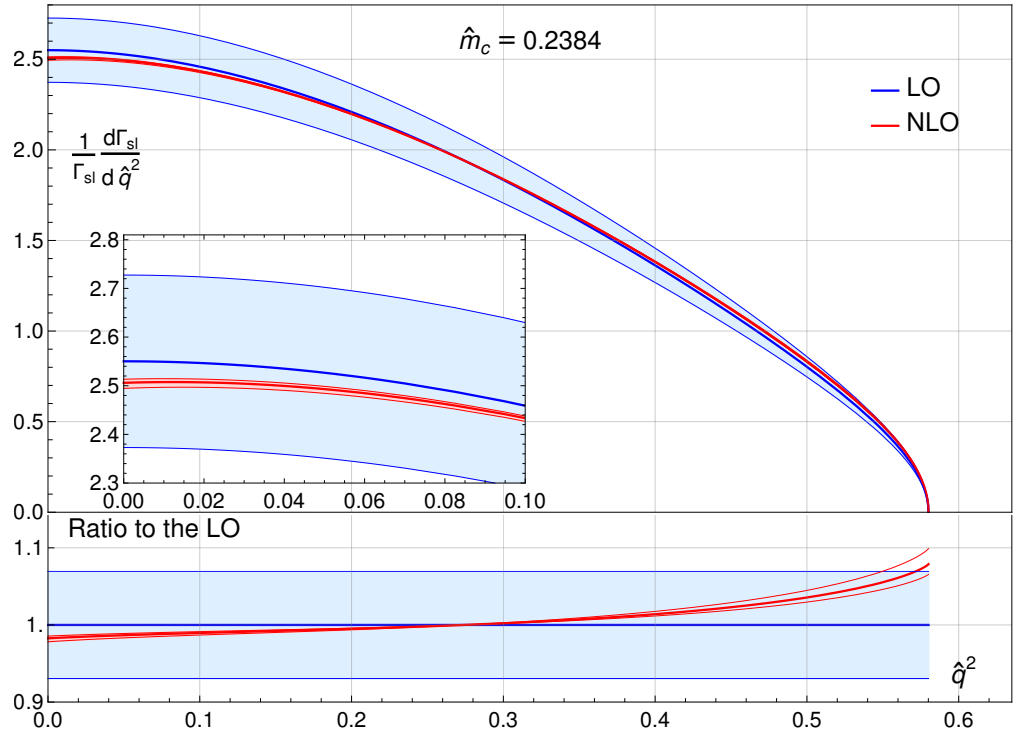

Figure 14: The semileptonic q^2 spectrum including the NLO QCD correction. The panel on the left shows the spectrum behavior in the small $\hat{q}^2$ region. The bottom panel depicts the ratio of the spectrum including the NLO correction to the LO approximation. For the explanation of the uncertainties see the text.

The function $\overline{\mathrm{Li}}_2(x)$ has been defined in eq. (2.120) on page 97. The polynomial $H_1(u,v)$ has been defined in eq. (2.118) on page 96. The other polynomials appearing in this result read

$$\begin{aligned}
A(u,v) =& 3v\left(v^2+1\right)\left(u^2+1\right) - 2u\left(2v^4-v^2+2\right),\\
B_1(u,v) =& 4\left(u^2-1\right)v^2\left(\left(u^4+4u^2+1\right)v - \frac{3}{4}u\left(u^2+1\right)\left(v^2+3\right)\right),\\
B_2(u,v) =& v^2\Big(3u\left(13u^4+4u^2-3\right) - 4v\left(7u^6+23u^4-u^2-1\right),\\
&+ uv^2\left(55u^4+68u^2+7\right) - 28v^3\left(u^4+u^2\right) + 8u^3v^4\Big),
\end{aligned} \tag{3.186}$$

and

$$\begin{aligned}
B_3(u,v) =& 2(1-uv)\Big(2u^3 - v\left(5u^4+7u^2\right) + v^2\left(2u^5+7u^3+u\right),\\
&+ v^3\left(u^4+7u^2+2\right) - v^4\left(7u^3+5u\right) + 2v^5u^2\Big),\\
B_4(u,v) =& 2(v-u)\Big(2u^2 - v\left(7u^3+5u\right) + v^2\left(u^4+7u^2+2\right),\\
&+ v^3\left(2u^5+7u^3+u\right) - v^4\left(5u^4+7u^2\right) + 2v^5u^3\Big).
\end{aligned} \tag{3.187}$$

Note that at this order, the μ dependence coming from loop integrations cancels out exactly in the linear combination of the MIs. The only residual running is due to $\alpha_s(\mu)$, which formally is an $\mathcal{O}(\alpha_s^2)$ effect. The μ dependence of the spectrum at the NLO thus cancels out up to neglected corrections as expected.

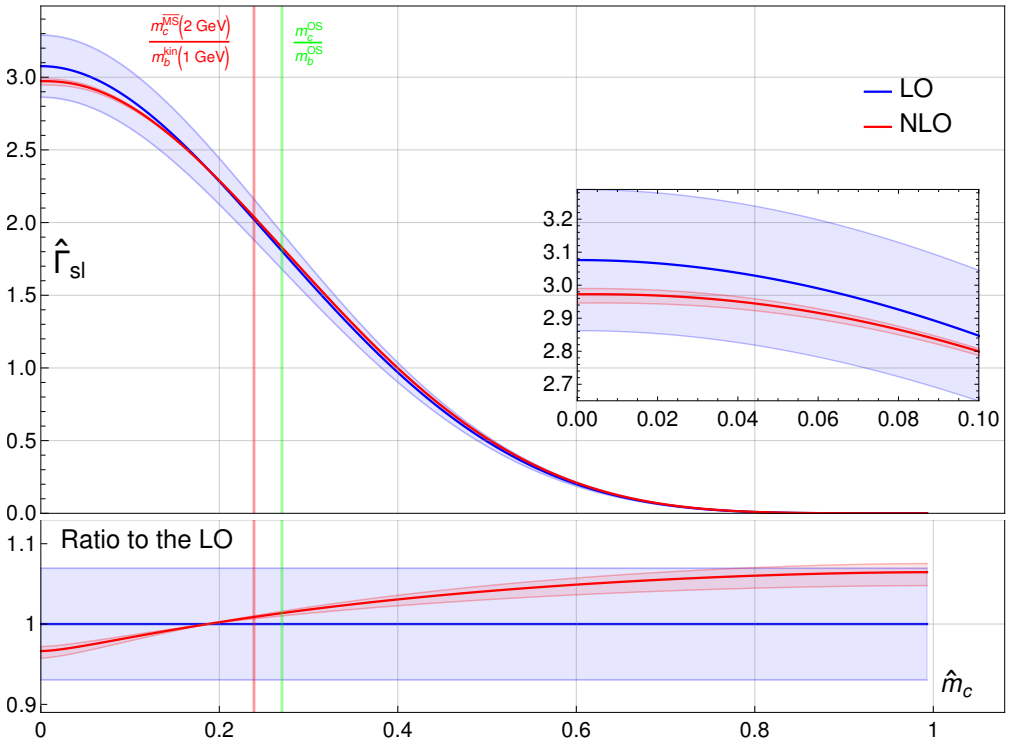

Figure 15: The normalized width of the semileptonic decay as a function of $\hat{m}_c$. The vertical red and green lines indicate the central values of $\hat{m}_c$ in the kinetic-$\overline{\text{MS}}$ and *OS*-*OS* renormalization schemes, respectively. The bottom panel depicts the ratio of the total width including the NLO correction to the LO approximation. The uncertainties were estimated in the same way as in figure 14.

With the divergent terms subtracted, one may investigate the individual contributions of each diagram. For this purpose it is useful to construct the $S^{(2b)}$, $S^{(2c)}$ and $S^{(2\otimes)}$ functions equivalent to the $S^{(2a)}$ function introduced in eq. (2.121) on page 97. These functions are shown in figure 12. Note that $S^{(2b)}$ vanishes as $q^2 \to (m_b - m_c)^2$ but $S^{(2c)}$ and $S^{(2\otimes)}$ are divergent in this limit, and only their sum tends to zero. The last point is illustrated in the bottom right panel of figure 12, which shows that the ratio $-S^{(2\otimes)}/S^{(2c)}$ tends to 1 for $q^2 \to (m_b - m_c)^2$. The cancellation of the phase-space endpoint singularities serves as an important crosscheck of the final result.

The functional dependence of the NLO correction on $\hat{q}^2$ is shown in figure 13. This curve has been obtained by adding the S functions of the four NLO two-loop diagrams and of the counterterm part. The spectrum normalized to the width of the semileptonic decay is shown in figure 14, both for the leading term and including the NLO correction. The perturbative uncertainty of the LO curve was estimated as $\pm\alpha_s\text{LO}/\pi$, while the uncertainty of the NLO was obtained by varying the renormalization scale μ between $m_b/2$ and $2m_b$. One can observe a very good behavior of the QCD perturbation series already at this order.

Finally, the spectrum can be integrated over q^2 to obtain the semileptonic decay width Γ_{sl} as a function of $\hat{m}_c$. This function is shown in figure 15 after normalizing it to the integral over $\hat{m}_c$, i.e.

$$\hat{\Gamma}_{sl} \equiv \frac{\int d\hat{q}^2 \frac{d\Gamma_{sl}}{d\hat{q}^2}}{\int d\hat{m}_c^2 \int d\hat{q}^2 d\frac{d\Gamma_{sl}}{d\hat{q}^2}}. \tag{3.188}$$

This figure illustrates the strong phase-space volume suppression of the semileptonic decay

channel at large $\hat{m}_c$. An analogous but much stronger suppression is observed for contributions with multiple charmed final-state particles. This observation will be investigated further in section 3.6.

3.5 Inclusive Spectrum at the NNLO

Our calculation of the $\mathcal{O}(\alpha_s^2)$ correction to the inclusive q^2 spectrum was based on the auxiliary width formula (3.68). The first step was to generate all the necessary three-loop Feynman diagrams that contribute to the inclusive auxiliary width $b \to X_c Q$ calculated using the formula (1.112). To this end, we utilized the `Fortran` program `qgraf` [227, 228]. The light quarks u, d, and s, were treated as a single massless quark, and the contributions from its loops were multiplied by 3. Using the QCD and the effective bcQ vertices as the input, we obtained 68 three-loop, 1PI $b \to b$ diagrams with exactly one Q-boson line. Four of these involved a 4-gluon vertex. At this order in QCD, diagrams with this vertex must necessarily contain a scaleless gluon loop attached to the gluon line of one of the four NLO diagrams. Another six diagrams did not contribute to the inclusive rate formula (3.68) because their contribution to $\mathrm{Im}\Sigma_{\mathrm{1PI}}$ vanished (see eq. (1.112)). This could be assessed prior to their calculation, as no kinematically allowed cut separating the two external lines exists. In these diagrams, the Q line is attached to a closed fermion loop instead of the main fermion line, meaning that a b-propagator would need to be cut, which is not kinematically allowed. The structure of the remaining 58 diagrams can also be obtained "by hand", by adding to one of the four NLO diagrams an element that increases the power of α_s by one. One may distinguish three types of such operations:

1. connecting the gluon line and a fermion line with a gluon, creating a 3-gluon vertex (8 1PI diagrams),

2. adding a closed loop (with b-, c-, or light quarks, ghosts, or gluons) on the gluon line (20 1PI diagrams),

3. including a second exchange of a gluon between two points on the main fermion line (30 1PI diagrams).

Out of these 58 diagrams, 19 come in pairs that are mirror images of each other. A diagram and its mirror image give the same contributions to the auxiliary width, due to the γ-matrix identity (3.174). This leaves 39 distinct diagrams that have to be computed. They are shown in figure 16, with the initial 5 corresponding to the first, the next 15 to the second, and the last 19 to the third type in the above list.

The next step was to generate the algebraic expressions corresponding to each of the 39 diagrams. To this end, a custom `Mathematica` program was developed. The most demanding task in terms of CPU time required was the symbolic simplification of large polynomials resulting from the Dirac traces. It was performed using a module written in the symbolic algebra manipulation program `FORM` [229–231]. The contribution of each diagram was written as a loop integral of a polynomial in integer powers of a basis of propagator denominators, with rational functions of $\hat{q}^2$, ${\hat{m}_c}^2$, D, and ξ_g as coefficients, similarly to the part of the NLO calculation described in section 1.7. Each term of these polynomials was recognized as an integrand of a scalar Feynman integral belonging to the integral family inherited from the considered diagram. There were 17664 three-loop scalar integrals found in total.

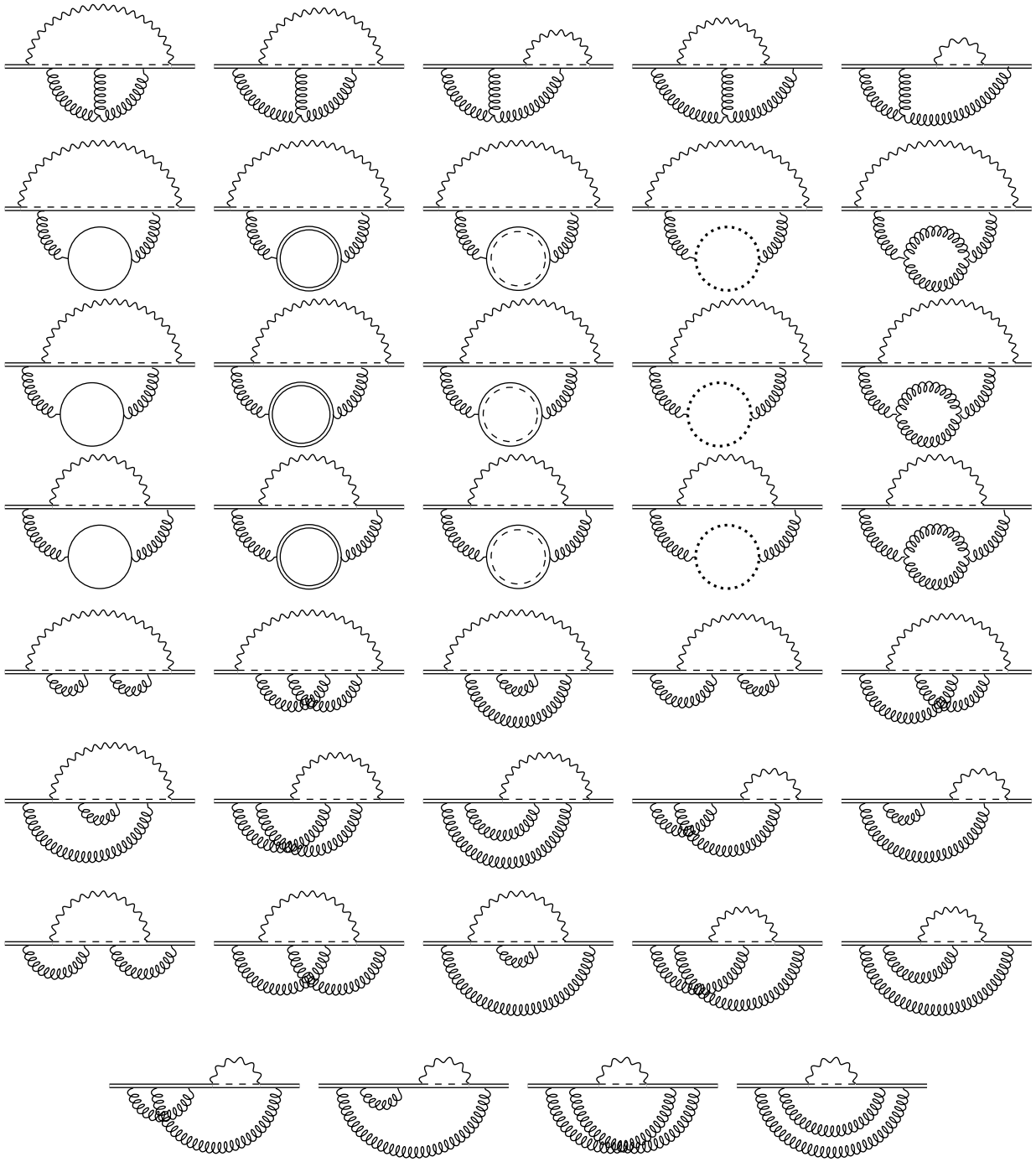

Figure 16: The 39 distinct three-loop diagrams contributing to the $b \to X_c Q$ decay width. The line drawing conventions follow the ones introduced in figure 6 on page 41 and eq. (1.242) on page 64. The massless quark propagators are depicted with a single continuous line.

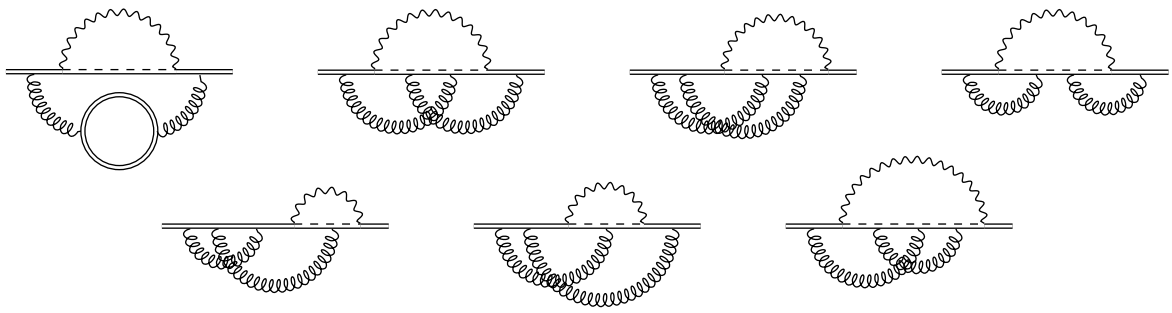

Figure 17: The seven diagrams that generate the integral families of all the three-loop MIs.

With the set of seed integrals established, the next step was to reduce their number using the IBP reduction. Using the program `Kira` 2.3 [157], the combined reduction for all 39 diagrams required 5.11 GB of memory, and was completed in 3972 seconds on the system specified below eq. (2.17) on page 74. After the reduction was completed, 7078 integrals were recognized as scaleless, and 2311 exactly equal to one of the other 8275 unique integrals. The latter number is the one that was quoted at the end of section 1.7. The IBP reduction allowed for expressing each of them, as well as the $b \to X_c Q$ width, as a linear combination of 151 MIs belonging to integral families inherited from seven diagrams shown in figure 17. The ξ_g-dependence of the coefficients of the MIs canceled out already at this stage, without the need for computing the individual MIs or preforming the renormalization. The Laurent expansions of the coefficients of some of the MIs started at $\mathcal{O}(\epsilon^{-3})$, meaning that the corresponding MIs had to be computed up to $\mathcal{O}(\epsilon^3)$.

Next, we assessed which of the three-loop MIs contribute a non-vanishing imaginary part to Σ_{1PI} in the inclusive width formula (1.112). With the `AMFlow` package available, the most straightforward approach was to compute all of them at a single point in the $(\hat{q}^2, \hat{m}_c^2)$ parameter space, at which $\hat{q}^2$ was sufficiently small for all exclusive partonic channels to be kinematically allowed. We found 97 MIs with non-zero imaginary parts for some values of $\hat{q}^2$. These integrals are shown in figures 18 and 19.

At this point, our approach diverged from the one taken by the competing group in ref. [67]. In that publication, the authors neglected all integrals where the only allowed cut crossed three charm lines, and in all the rest considered only the contributions from cuts crossing a single charm line (c.f. figure 2 in ref. [67] and the text below). The correction neglected in this way corresponds to the exclusive $b \to cc\bar{c}Q$ exclusive partonic decay or, equivalently, to the $b \to cc\bar{c}l\bar{\nu}_l$ contribution to the inclusive semileptonic q^2 spectrum. This channel is strongly suppressed by the small volume of the allowed phase-space, as will be described in the next section. With this simplification, the authors proceeded along the lines discussed in the Sample Calculation sections of this thesis, obtaining a result in terms of GPLs of weight 4 and lower. Their final results can be analyzed numerically with arbitrary precision using `GiNaC` [232] and `PolyLogTools` [181].

Instead of neglecting the triple-charm channel, we included its contribution to the q^2 spectrum at $\mathcal{O}(\alpha_s^2)$ by computing, with the help `AMFlow`, imaginary parts of all 97 required MIs at 682 points in the parameter space, with precision of 60 significant digits. The results of the scan over 200 values of $\hat{q}^2$ with $\hat{m}_c = 0.2384$ and $\mu = m_b$ for $\mathcal{O}(\epsilon^{-2})$, $\mathcal{O}(\epsilon^{-1})$, and $\mathcal{O}(\epsilon^0)$ terms of the bare part of the spectrum are shown in figure 20. The displayed normalized

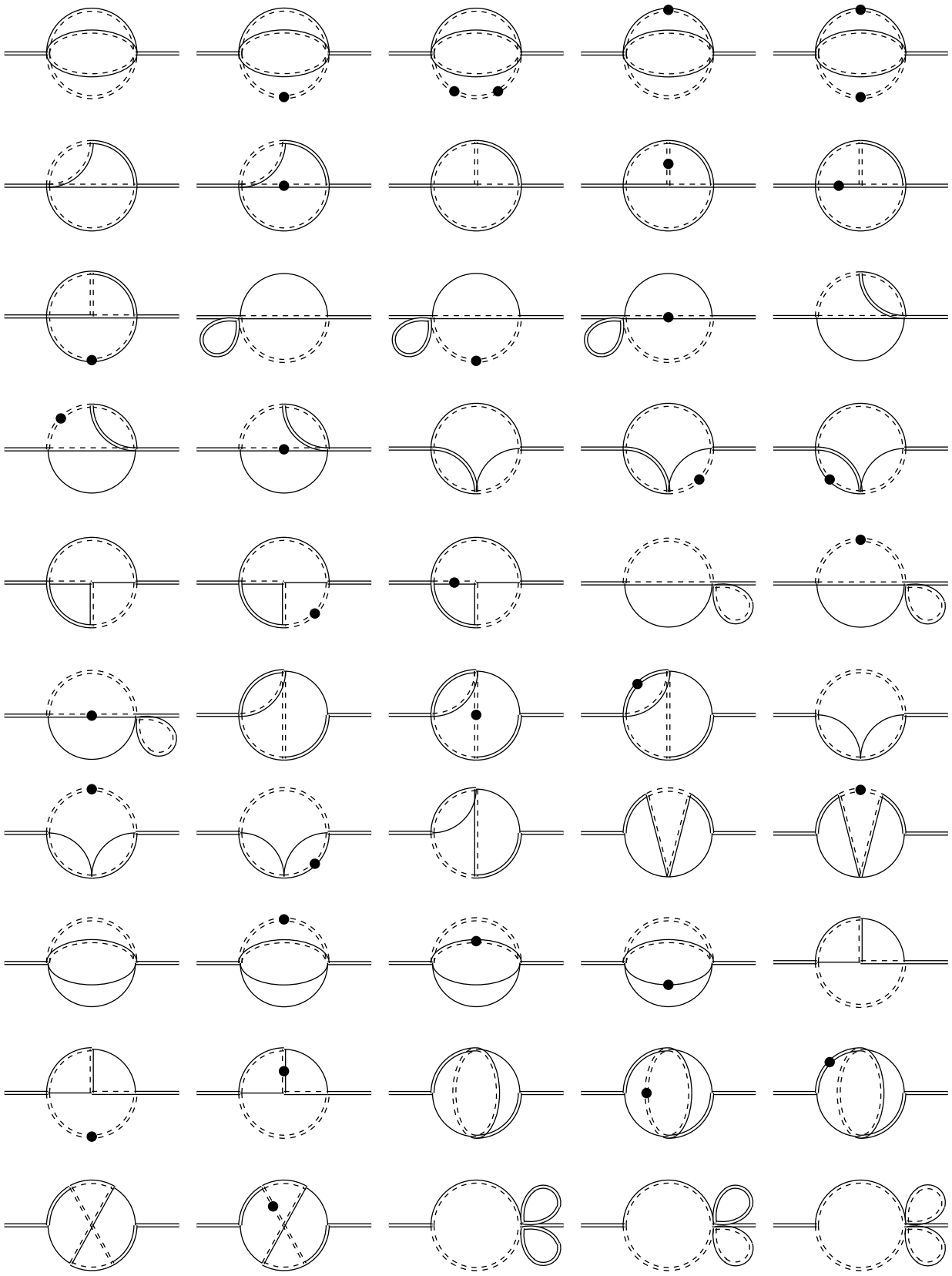

Figure 18: The first 50 (out of 97) three-loop MIs contributing to the inclusive auxiliary decay $b \to X_c Q$. The single lines denote massless propagators.

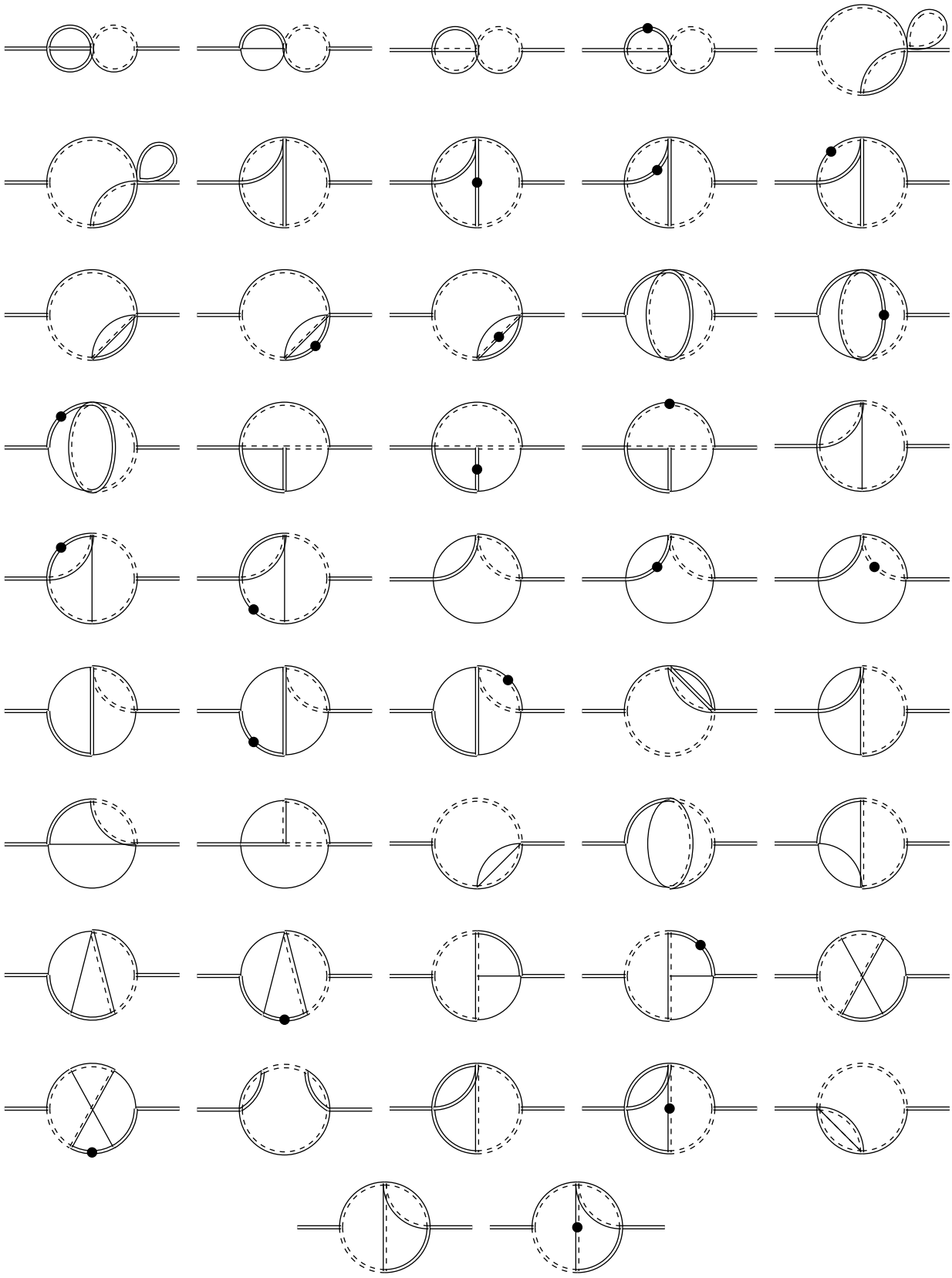

Figure 19: The last 47 (out of 97) three-loop MIs contributing to the inclusive auxiliary decay $b \to X_c Q$. The single lines denote massless propagators.

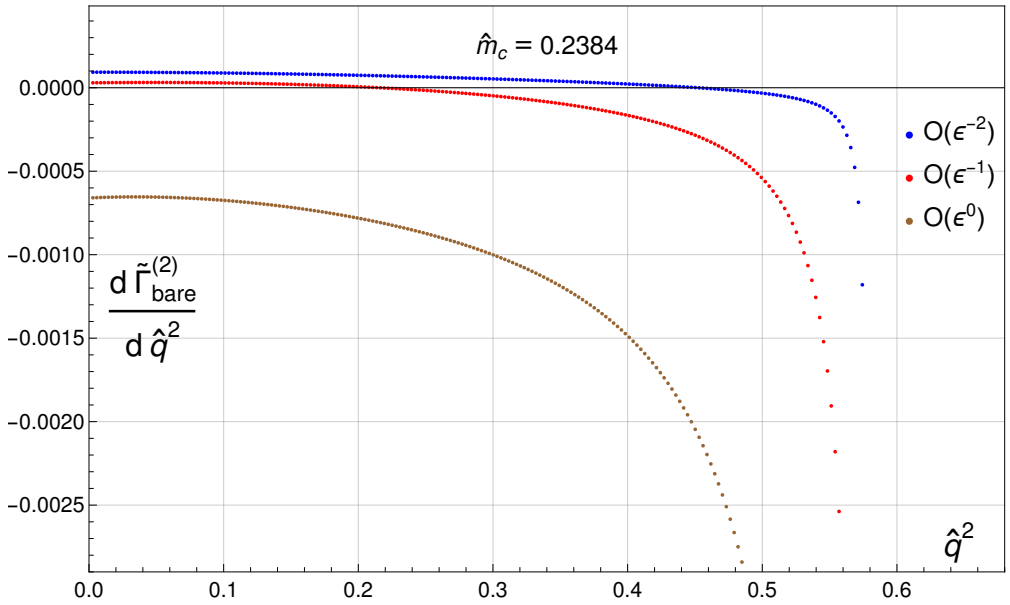

Figure 20: The bare term of the NNLO correction to the q^2 spectrum for $\hat{m}_c = 0.2384$ and $\mu = m_b$. The quantity $d\tilde{\Gamma}/d\hat{q}^2$ is defined in the text.

spectrum function $d\tilde{\Gamma}^{(2)}_{bare}$ is defined as

$$\frac{d\tilde{\Gamma}^{(2)}_{bare}}{d\hat{q}^2} \equiv \frac{1}{G_F^2|V_{cb}|^2 m_b^5} \frac{d\Gamma^{(2)}_{bare}}{d\hat{q}^2}. \tag{3.189}$$

Note that the finite part is divergent as $\hat{q}^2 \to (1-\hat{m}_c)^2$, just as observed for the diagram $(2c)$ in the calculation of the NLO correction. This divergence, together with the $\mathcal{O}(\epsilon^{-2})$ and $\mathcal{O}(\epsilon^{-1})$ terms, must be canceled by the contributions of lower-loop diagrams with counterterm insertions.

To renormalize the bare part, we need to derive a renormalization formula, similar to the one in eq. (3.184). In addition to the quark fields and masses that are renormalized in the on-shell scheme as before, at the NNLO one also needs to consider the renormalization of the coupling g_s. We renormalize it in the $\overline{\text{MS}}$ scheme with the central value of the renormalization scale μ chosen at m_b and then varied between $m_b/2$ and $2m_b$ to estimate the perturbative uncertainty. There are seven one-loop diagrams that contribute to the $\mathcal{O}(\alpha_s^2)$ correction:

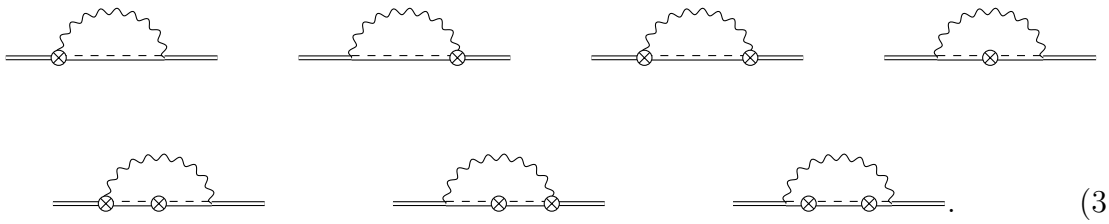

(3.190)

The first three of them are proportional to the LO diagram

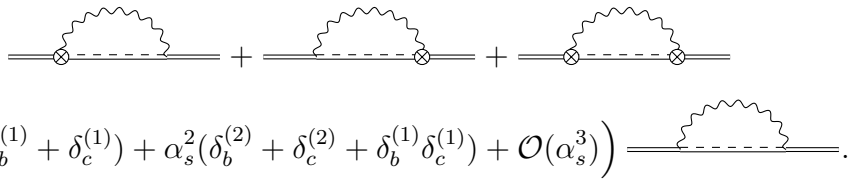

(3.191)

$$= \Big(\alpha_s(\delta_b^{(1)} + \delta_c^{(1)}) + \alpha_s^2(\delta_b^{(2)} + \delta_c^{(2)} + \delta_b^{(1)}\delta_c^{(1)}) + \mathcal{O}(\alpha_s^3)\Big)$$

The fourth diagram in eq. (3.190) can be written as in eq. (3.183), resulting in

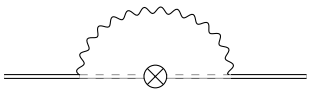

(3.192)

$$= \alpha_s^2 \left[-\delta_c^{(2)} + \left(\delta_{m_c}^{(2)} + \delta_c^{(1)}\delta_{m_c}^{(1)}\right) 2\hat{m}_c^2 \partial_{\hat{m}_c^2}\right]$$

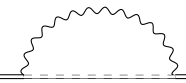

$$+ \mathcal{O}(\alpha_s^3).$$

Using eqs. (3.178) and (3.183), one can express the sum of the fifth and sixth diagram in eq. (3.190) as

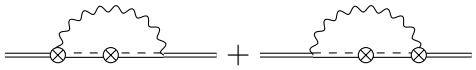

(3.193)

$$= \alpha_s^2 \left(\delta_b^{(1)} + \delta_c^{(1)}\right) \left(-\delta_c^{(1)} + \delta_{m_c}^{(1)} 2\hat{m}_c^2 \partial_{\hat{m}_c^2}\right)$$

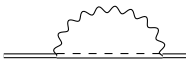

$$+ \mathcal{O}(\alpha_s^3)$$

Finally, the c-quark propagators together with the two counterterm insertions in the seventh diagram give

$$\begin{aligned}
&\mathcal{P}_c \left(-\delta_c \mathcal{P}_c^{-1} - i\left(\delta_{m_c} + \delta_c\delta_{m_c}\right) m_c\right) \mathcal{P}_c \left(-\delta_c \mathcal{P}_c^{-1} - i\left(\delta_{m_c} + \delta_c\delta_{m_c}\right) m_c\right) \mathcal{P}_c = \\
=&\delta_c^2 \mathcal{P}_c + 2i\delta_c\delta_{m_c} m_c \mathcal{P}_c^2 - m_c^2 \delta_{m_c}^2 \mathcal{P}_c^3 + \mathcal{O}(\alpha_s^3) = \\
=&\delta_c^2 \mathcal{P}_c - 4\delta_c\delta_{m_c} z\partial_z \mathcal{P}_c + \hat{m}_c^2 \delta_{m_c}^2 \partial_{\hat{m}_c^2} \mathcal{P}_c + 2\hat{m}_c^4 \delta_{m_c}^2 \partial_{\hat{m}_c^2}^2 \mathcal{P}_c + \mathcal{O}(\alpha_s^3).
\end{aligned} \tag{3.194}$$

In the last equality, the third power of the propagator has been written as

$$\mathcal{P}_c^3 = -\frac{1}{2}\partial_{m_c}^2 \mathcal{P}_c = -\partial_{m_c^2} \mathcal{P}_c - 2m_c^2 \partial_{m_c^2}^2 \mathcal{P}_c. \tag{3.195}$$

The last diagram in eq. (3.190) thus reads

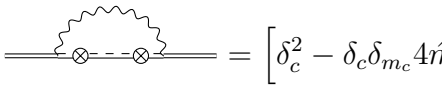

$$= \left[\delta_c^2 - \delta_c\delta_{m_c} 4\hat{m}_c^2 \partial_{\hat{m}_c^2} + \delta_{m_c}^2 \hat{m}_c^2 \partial_{\hat{m}_c^2} + \delta_{m_c}^2 2\hat{m}_c^4 \partial_{\hat{m}_c^2}^2\right]$$

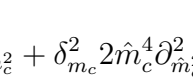

$$+ \mathcal{O}(\alpha_s^3). \tag{3.196}$$

Combining the results of eqs. (3.191), (3.192), (3.193), and (3.196) gives the one-loop counterterm contribution to the $\mathcal{O}(\alpha_s^2)$ correction in the simple form:

$$\frac{d\Gamma_{1loop}^{(2\otimes)}}{dq^2} = \left[\delta_b^{(2)} + \left(2\delta_{m_c}^{(2)} + 2\delta_b^{(1)}\delta_{m_c}^{(1)} + \left(\delta_{m_c}^{(1)}\right)^2\right) \hat{m}_c^2 \partial_{\hat{m}_c^2} + 2\left(\delta_{m_c}^{(1)}\right)^2 \hat{m}_c^4 \partial_{\hat{m}_c^2}^2\right] \frac{d\Gamma^{(0)}}{dq^2}. \tag{3.197}$$

Apart from the one-loop diagrams with one or two counterterms, one also needs to include two-loop diagrams with a single counterterm. These can be categorized by the NLO diagram into which the counterterm is inserted. For the diagram $(2a)$, there are eight possible insertions:

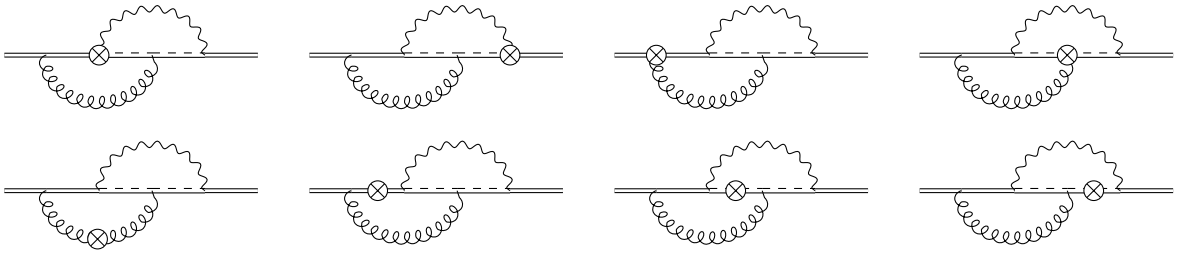

(3.198)

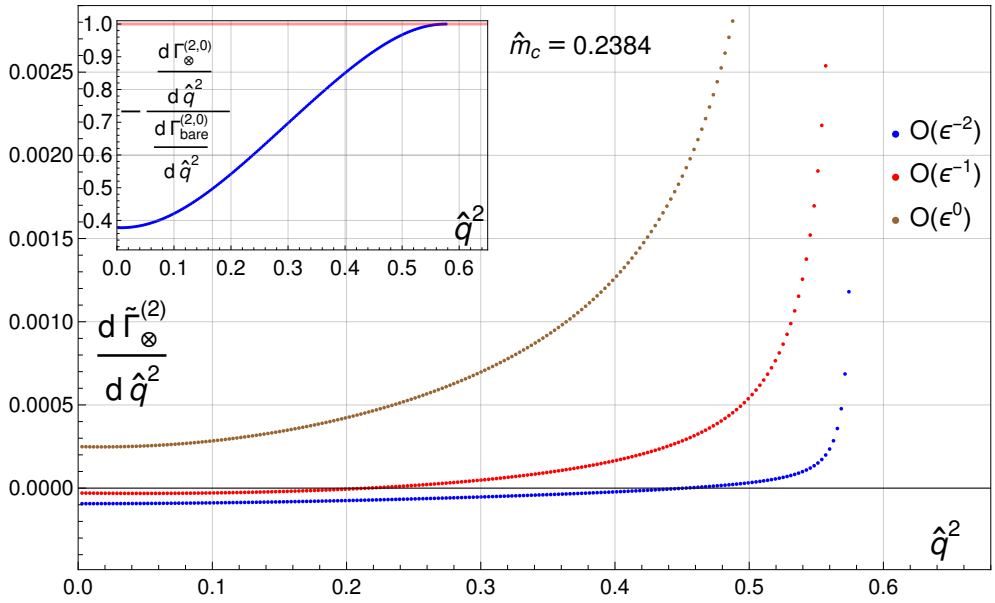

Figure 21: The counterterm part of the NNLO correction to the q^2 spectrum. The top-left panel illustrates the cancellation of the endpoint singularity of the $\mathcal{O}(\epsilon^0)$term between the bare and counterterm diagrams.

The first two are proportional to the diagram $(2a)$

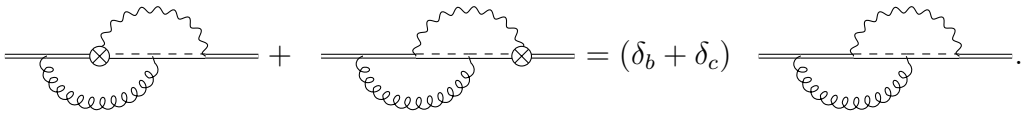

(3.199)

The next three can be combined using eq. (3.93)

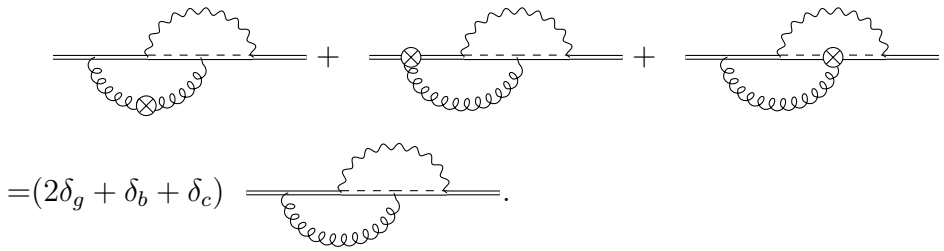

(3.200)

The last three diagrams in eq. (3.198) have a counterterm vertex inserted on a quark line. To compute the first of these, one can temporarily set the b-quark mass in the b propagator to $\widetilde{m}_b \neq m_b = \sqrt{p_b^2}$. Then, the $\partial_{\widetilde{m}_b}$ derivative can be used to express squares of the b propagators. Once the derivative is computed, $\widetilde{m}_b$ is set back to m_b. This procedure leads to a result analogous to eq. (3.183)

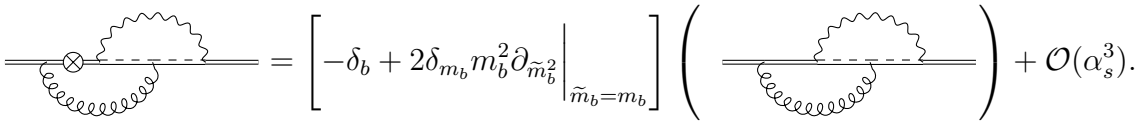

(3.201)

The two diagrams with counterterm insertions on the charm line can also be expressed through mass derivatives. If one denotes the left and right c-quark propagators as $\mathcal{P}_1$ and

$\mathcal{P}_2$ respectively, with all factors other than the c-quark propagators and c-line counterterms combined into a symbol $\mathcal{F}$, then

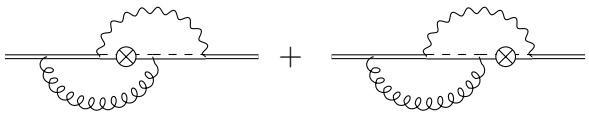

$$
\begin{aligned}
&= \mathcal{F}\left[\mathcal{P}_1\left(-\delta_c\mathcal{P}_1^{-1} - i\delta_{m_c}m_c\right)\mathcal{P}_1\mathcal{P}_2 + \mathcal{P}_1\mathcal{P}_2\left(-\delta_c\mathcal{P}_2^{-1} - i\delta_{m_c}m_c\right)\mathcal{P}_2\right] = \\
&= -2\delta_c\mathcal{F}\mathcal{P}_1\mathcal{P}_2 - i\delta_{m_c}m_c\mathcal{F}\left(\mathcal{P}_1^2\mathcal{P}_2 + \mathcal{P}_1\mathcal{P}_2^2\right) = -2\delta_c\mathcal{F}\mathcal{P}_1\mathcal{P}_2 + 2\delta_{m_c}\hat{m}_c^2\partial_{\hat{m}_c^2}\left(\mathcal{F}\mathcal{P}_1\mathcal{P}_2\right) = \\
&= \left[-2\delta_c + 2\delta_{m_c}\hat{m}_c^2\partial_{\hat{m}_c^2}\right]\left(\quad\right),
\end{aligned}
\tag{3.202}
$$

where the $\mathcal{O}(\alpha_s^3)$ term has been neglected. After putting together eqs. (3.201), (3.202), (3.199), and (3.200), the sum of all 8 counterterm insertions in the diagram $(2a)$ contributing to the $\mathcal{O}(\alpha_s^2)$ correction becomes

$$
\frac{d\Gamma^{(2\otimes)}_{(2a)}}{dq^2} = \left[2\delta_g^{(1)} + \delta_b^{(1)} + 2\delta_{m_c}^{(1)}\hat{m}_c^2\partial_{\hat{m}_c^2} + 2\delta_{m_b}^{(1)}m_b^2\partial_{\widetilde{m}_b^2}\Big|_{\widetilde{m}_b=m_b}\right]\frac{d\Gamma^{(1)}_{(2a)}}{dq^2}. \tag{3.203}
$$

Note that one could not simply use the result of eq. (2.117) to obtain the expression for $d\Gamma^{(2\otimes)}_{(2a)}/dq^2$, even if the $\mathcal{O}(\epsilon^1)$ term was analytically available, since the $\widetilde{m}_b$ derivative has to be taken prior to loop integration. Instead, the derivative should be applied already to the right hand side of eq. (1.253), resulting in different set of scalar integrals and different coefficients in table 2. The variable mass $\widetilde{m}_b$ can be set back to m_b prior to the IBP reduction. Fortunately, the resulting set of MIs is the same as in the calculation of the NLO correction.

The expressions obtained by inserting counterterms into the diagrams $(2a')$ and $(2b)$ can be rewritten along similar lines and yield analogous results:

$$
\begin{aligned}
\frac{d\Gamma^{(2\otimes)}_{(2a')}}{dq^2} &= \left[2\delta_g^{(1)} + \delta_b^{(1)} + 2\delta_{m_c}^{(1)}\hat{m}_c^2\partial_{\hat{m}_c^2} + 2\delta_{m_b}^{(1)}m_b^2\partial_{\widetilde{m}_b^2}\Big|_{\widetilde{m}_b=m_b}\right]\frac{d\Gamma^{(1)}_{(2a')}}{dq^2}, \\
\frac{d\Gamma^{(2\otimes)}_{(2b)}}{dq^2} &= \left[2\delta_g^{(1)} + \delta_b^{(1)} + 2\delta_{m_c}^{(1)}\hat{m}_c^2\partial_{\hat{m}_c^2} + 2\delta_{m_b}^{(1)}m_b^2\partial_{\widetilde{m}_b^2}\Big|_{\widetilde{m}_b=m_b}\right]\frac{d\Gamma^{(1)}_{(2b)}}{dq^2}.
\end{aligned}
\tag{3.204}
$$

As the diagram $(2c)$ does not have any b-quark lines, the $\partial_{\widetilde{m}_b}$ derivative term does not arise naturally. It can be added "by hand" to simplify the final result, since this derivative is 0. All other terms are the same as in the case of insertions into the other three NLO diagrams, giving

$$
\begin{aligned}
\frac{d\Gamma^{(2\otimes)}_{(2c)}}{dq^2} &= \left[2\delta_g^{(1)} + \delta_b^{(1)} + 2\delta_{m_c}^{(1)}z\partial_z + 0\right]\frac{d\Gamma^{(1)}_{(2c)}}{dq^2} \\
&= \left[2\delta_g^{(1)} + \delta_b^{(1)} + 2\delta_{m_c}^{(1)}\hat{m}_c^2\partial_{\hat{m}_c^2} + 2\delta_{m_b}^{(1)}m_b^2\partial_{\widetilde{m}_b^2}\Big|_{\widetilde{m}_b=m_b}\right]\frac{d\Gamma^{(1)}_{(2c)}}{dq^2}.
\end{aligned}
\tag{3.205}
$$

Combining the results for all 4 diagrams, the 2 loop renormalization formula at the $\mathcal{O}(\alpha_s^2)$ level reads

$$
\frac{d\Gamma^{(2\otimes)}_{2loop}}{dq^2} = \left[2\delta_g^{(1)} + \delta_b^{(1)} + 2\delta_{m_c}^{(1)}\hat{m}_c^2\partial_{\hat{m}_c^2} + 2\delta_{m_b}^{(1)}m_b^2\partial_{\widetilde{m}_b^2}\Big|_{\widetilde{m}_b=m_b}\right]\frac{d\Gamma^{(1)}_{bare}}{dq^2}. \tag{3.206}
$$

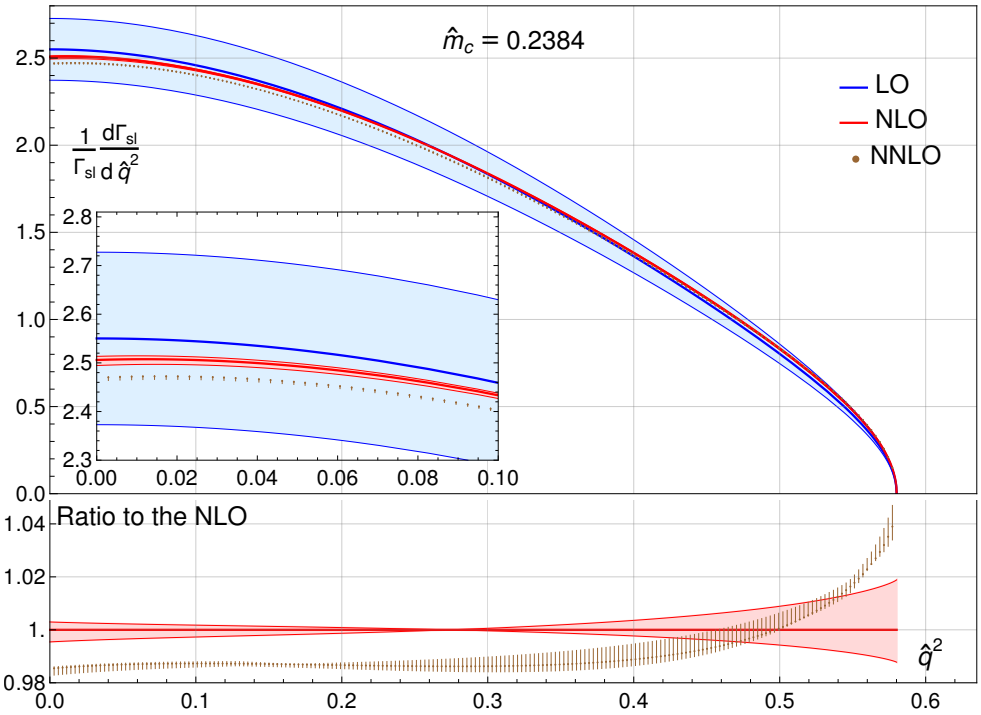

Figure 22: The numerical results for the renormalized NNLO correction to the q^2 spectrum. The NLO and NNLO uncertainties were assessed by varying the renormalization scale between $\mu = m_b/2$ and $\mu = 2m_b$. The brown strip in the bottom panel shows the ratio of the NNLO correction to the NLO term.

The sum of the right-hand-sides of eqs. (3.197) and (3.206) computed numerically using `AMFlow` at the same values of parameters as in figure 20 is shown in figure 21. The normalized spectrum $d\tilde{\Gamma}^{(2)}_{\otimes}/d\hat{q}^2$ is defined analogously to eq. (3.189). After combining these results with the bare part of the NNLO correction, both the $\mathcal{O}(\epsilon^{-2})$ and the $\mathcal{O}(\epsilon^{-1})$ term canceled out for all considered points in the parameter space to all 60 computed significant digits. The terms $\mathcal{O}(\epsilon^{-n})$ with $n \in \{3, 4, 5, 6\}$, canceled out among contributions from the bare diagrams before renormalization. The $\hat{q}^2 \to (1 - \hat{m}_c)^2$ singularity also canceled out in the physical result, as shown in the left panel of figure 21.

At this point, one can test the result by checking the cancellation of the μ dependence between the NNLO correction and the strong coupling multiplying the NLO term. The RGE (3.82) for $\alpha_s(\mu)$ can be solved up to the first non-leading correction, yielding

$$\alpha_s(\mu) = \alpha_s(\mu') \left(1 - \alpha_s(\mu')\beta_0 \log \frac{\mu}{\mu'} + \mathcal{O}(\alpha_s^2(\mu'))\right), \tag{3.207}$$

where $\mu' \sim m_b$ is some arbitrary reference scale, and the $\overline{\text{MS}}$-scheme value of β_0 was given in eq. (3.84). The number of active quark flavors in our approach was set to $n_f = 5$. The renormalized result for the q^2 spectrum at the leading order in the HQE and up to the NNLO term can then be written as

$$\frac{d\Gamma_{sl}}{dq^2} = \frac{d\Gamma^{(0)}}{dq^2} + \alpha_s(\mu') \left(1 - \alpha_s(\mu')\beta_0 \log \frac{\mu}{\mu'}\right) \frac{d\Gamma^{(1)}}{dq^2} + \alpha_s^2(\mu') \frac{d\Gamma^{(2)}}{dq^2}(\mu) + \mathcal{O}\left(\alpha_s^3(\mu')\right). \tag{3.208}$$

The nontrivial μ dependence of $d\Gamma^{(2)}/dq^2$ comes from the renormalization constants δ_X and the different powers p in the factor $\mu^{p\epsilon}$ multiplying the one-, two-, and three-loop parts of this

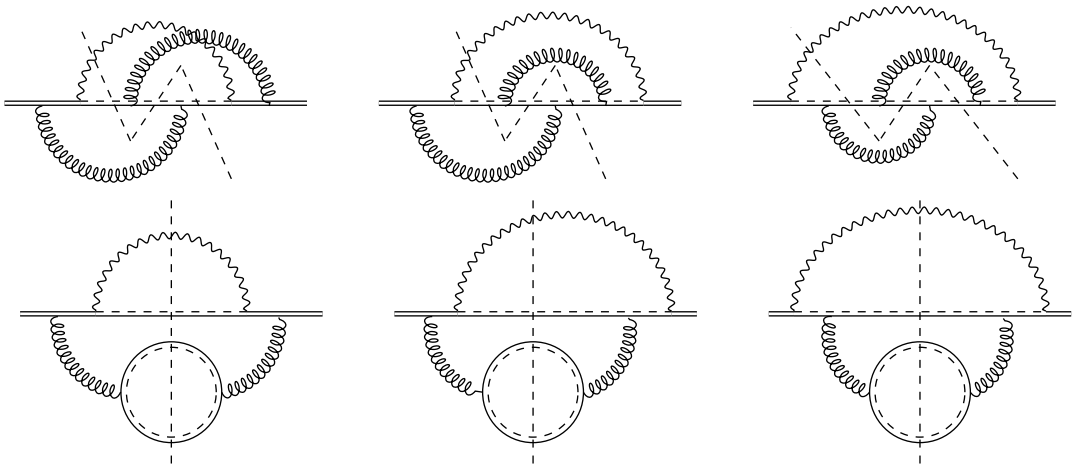

Figure 23: The six distinct diagrams with a triple-charm cut.

correction. Once the β_0 term is written explicitly as in the above equation, the dependence on μ must cancel out, and $d\Gamma_{sl}/dq^2$ becomes dependent on $\log(\mu'/m_b)$ only. This observation served as another crosscheck of the numerically calculated result. The scan of the spectrum for $\hat{m}_c = 0.2384$ is presented in figure 22, with the central value given for $\mu = m_b$, and the uncertainty obtained by varying μ between $m_b/2$ and $2m_b$.

3.6 Results

The Triple-Charm Channel

At this point, the calculation of the q^2 spectrum of the inclusive semileptonic decay in the leading order of the HQE and up to the NNLO in QCD is complete. When presenting our results in ref. [1], we decided to separate the inclusive NNLO correction into contributions coming from the final states with either one or three charm quarks, as in eq. (I.20). The former part was used for a direct comparison with the findings of ref. [67], where only the single-charm part, $d\Gamma^{(2)}_{1c}/dq^2$, was considered. This separation was performed by computing the triple-charm term separately, and subtracting it from the inclusive correction.

Contrary to the fully inclusive spectrum $d\Gamma^{(2)}/dq^2$, the contribution $d\Gamma^{(2)}_{3c}/dq^2$ corresponds to an exclusive partonic channel. However, the computation proceeds almost along the same lines as for the fully inclusive NNLO correction. Out of all 58 non-zero three-loop diagrams contributing to the spectrum at the NNLO, $d\Gamma^{(2)}_{3c}/dq^2$ is given by the ones that can be separated with a single cut into two parts, with each being a connected graph and involving one b-quark, one Q-boson, and three c-quark external lines. One finds eight diagrams in total, with 4 being in pairs with their mirror images. The six distinct cut diagrams are presented in figure 23. The contribution of each diagram is expressed as a linear combination of scalar integrals, which are then reduced to a basis of MIs. In this IBP reduction, it is beneficial to consider the integrals with indices larger than 1 as more complicated than the ones with negative indices. The MI basis obtained in this way has all indices smaller or equal to 1. According to the Cutkosky rules, the part of the inclusive spectrum that needs to be isolated comes from replacing

$$\frac{1}{k^2 - m^2 + i\varepsilon} \to -2\pi i \delta(k^2 - m^2) \tag{3.209}$$

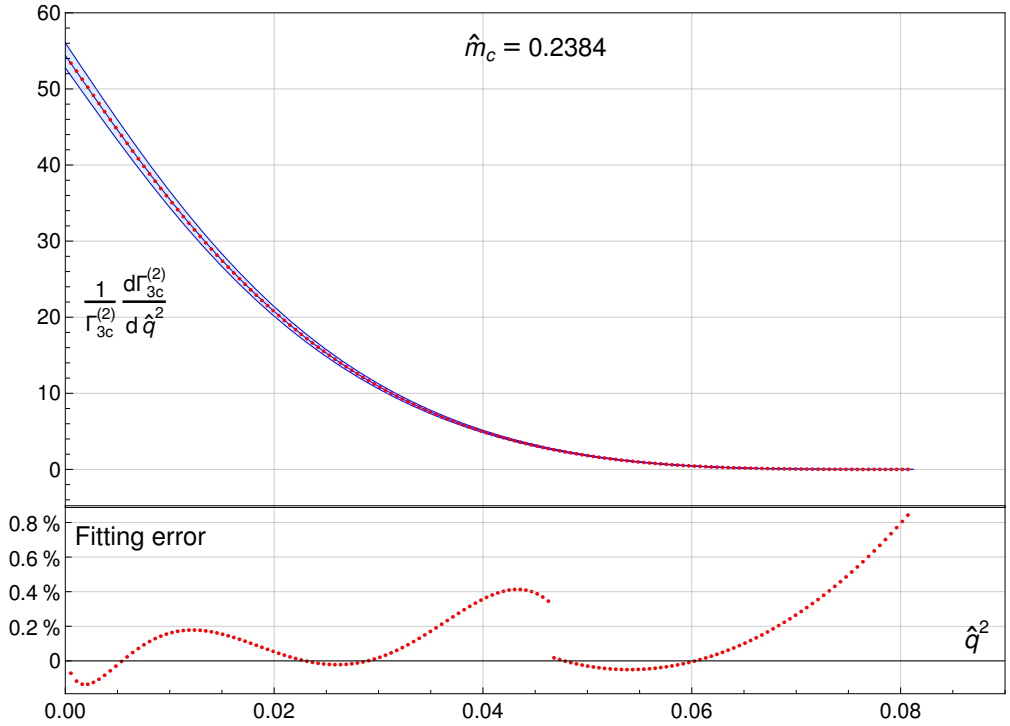

Figure 24: The contribution of the triple-charm channel to the NNLO correction for $\hat{m}_c = 0.2384$, normalized to its integral. The red points denote the numerical results obtained with `AMFlow`. The blue curve is the fit of eq. (3.211) with a global 3% uncertainty coming from combining the assumed 1.5% errors of the spectrum and the normalization integral. The bottom panel denotes the actual relative error of the fit when compared with the precise numerical result. The discontinuity of the fitting error occurs at $\hat{q}^2 = 0.0467$, where the second term of the ansatz (3.211) begins to contribute.

in the Q-boson and all c-quark lines. The MIs where at least one of the c lines or the Q line has a non-positive index should be set to 0 beforehand. The remaining 22 integrals belong to families inherited from the first and second diagram in figure 23. Using the Sochocki-Plemelj formula (3.101), the right hand side of the replacement (3.209) can be rewritten as a difference of two scalar propagators

$$-2\pi i\delta(k^2 - m^2) = \frac{1}{k^2 - m^2 + i\varepsilon} - \frac{1}{k^2 - m^2 - i\varepsilon}. \tag{3.210}$$

Each of the 22 cut MIs can therefore be calculated for different, numerical values of $\hat{m}_c^2$ and $\hat{q}^2$ using the auxiliary mass flow method, by considering the difference of the results obtained by evolving the auxiliary mass squared from $+i\infty$ and $-i\infty$. This approach of computing cut integrals is already implemented in `AMFlow` with a built-in interface. Certainly, the obtained result is UV-finite in the limit of $\epsilon \to 0$, as the considered correction comes from a tree-level process. We started with computing $d\Gamma_{3c}^{(2)}/dq^2$ at 150 values of $\hat{q}^2$ and $\hat{m}_c = 0.2384$. The result is shown in figure 24. To perform a fit, we assumed the following ansatz for $d\Gamma_{3c}^{(2)}/dq^2$ as a function of both $\hat{m}_c$ and $\hat{q}^2$:

$$\frac{d\Gamma_{3c}^{(2)}}{dq^2} = m_b^3 G_F^2 |V_{cb}|^2 L_{3c}^{\frac{7}{2}} \left[\sum_{kl} C_{kl} \hat{q}^{2k} \hat{m}_c^l + \Theta(10L_{3c} - 1) \sum_{mn} \tilde{C}_{mn} \hat{q}^{2m} \hat{m}_c^n \right], \tag{3.211}$$

C_{kl}	$k=0$	$k=1$	$k=2$
$l=0$	-0.000862940	-0.001237605	-0.002930817
$l=1$	0.022083312	0.058729219	0.115555544
$l=2$	-0.233051560	-0.929611726	-1.948951905
$l=3$	1.300169847	7.064296877	17.168143423
$l=4$	-4.046951098	-28.327414394	-82.170972154
$l=5$	6.666415074	57.939616602	202.387552617
$l=6$	-4.541480275	-47.726627340	-200.982999303

Table 3: Coefficients C_{kl} of the triple-charm fit (3.211).

$\tilde{C}_{mn}$	$m=0$	$m=1$	$m=2$	$m=3$	$m=4$
$n=0$	0.000877518	0.001621422	0.003642739	0.004746374	0.640253858
$n=1$	-0.022328502	-0.068057724	-0.138426420	-0.028111942	-20.337500422
$n=2$	0.234808565	1.020865993	2.251801608	-1.305831462	258.079023134
$n=3$	-1.306653472	-7.508277813	-19.200975797	19.197488356	-1635.101572743
$n=4$	4.059050049	29.397188800	88.978406754	-95.971405644	5172.363417944
$n=5$	-6.675376047	-58.957345285	-211.538554968	167.311712182	-6539.450493870
$n=6$	4.541480275	47.726627340	200.982999303	0	0

Table 4: Coefficients $\tilde{C}_{mn}$ of the triple-charm fit (3.211).

with $L_{3c} \equiv (\hat{q}^2 - (1+3\hat{m}_c)^2)\,(\hat{q}^2 - (1-3\hat{m}_c)^2)$. The integer powers k, l, m, and n, cover the ranges (0,2), (0,6), (0,4), and (0,6) respectively. The term involving $\Theta(10L_{3c}-1)$ was included to improve the accuracy in the region close to the triple-charm phase-space endpoint $\hat{q}^2 = (1-3\hat{m}_c)^2$. To find the fit coefficients C_{kl} and $\tilde{C}_{mn}$, we computed the triple-charm correction at additional 341 points, with the values of $\hat{m}_c$ between 0.14 and 0.29. The results were first published in ref. [1], and are presented here in tables 3 and 4. Comparing the fit (3.211) to the precise numerical values, we find a maximal deviation of around 1.5% for the points nearest to the endpoint, that quickly drops to less than 0.5% as $\hat{q}^2$ is lowered. We therefore assign a conservative fitting error of 1.5% in the calculation of the spectral moments, and in the comparison with the single-charm channel that will be described below.

The Single-Charm Channel

With the fit (3.211) at hand, the dominant, single-charm term $d\Gamma^{(2)}_{1c}/dq^2$ can be extracted by subtracting the triple-charm contribution from the inclusive NNLO correction presented in section 3.5. We computed the latter at 682 points, with $0.14 \le \hat{m}_c \le 0.29$ and $0 \le \hat{q}^2 \le (1-\hat{m}_c)^2$ using the method described in the previous section. For 341 of them that satisfied $\hat{q}^2 < (1-3\hat{m}_c)^2$, we also computed the $d\Gamma^{(2)}_{3c}/dq^2$ term. The numerical results for a fixed value of $\hat{m}_c$ are presented in figure 25. After subtracting the triple-charm contribution from the inclusive correction, we performed a fit to the following ansatz for the single-charm term:

$$\frac{d\Gamma^{(2)}_{1c}}{dq^2} = m_b^3 G_F^2 |V_{cb}|^2 L_{1c} \sum_{jkl=0} D_{jkl}\hat{m}_c^j \hat{q}^{2k} \log^l L_{1c}, \tag{3.212}$$

with $L_{1c} \equiv (\hat{q}^2 - (1+\hat{m}_c)^2)\,(\hat{q}^2 - (1-\hat{m}_c)^2)$. The indices j, k, and l, are bounded by 1, 7, and 8 respectively. The values of the coefficients D_{jkl} that were published in ref. [1] can also be found in tables 5, 6, 7, and 8 below. Thus obtained single-charm NNLO correction to the spectrum was then compared with the results of ref. [67] for 13600 points in the parameter

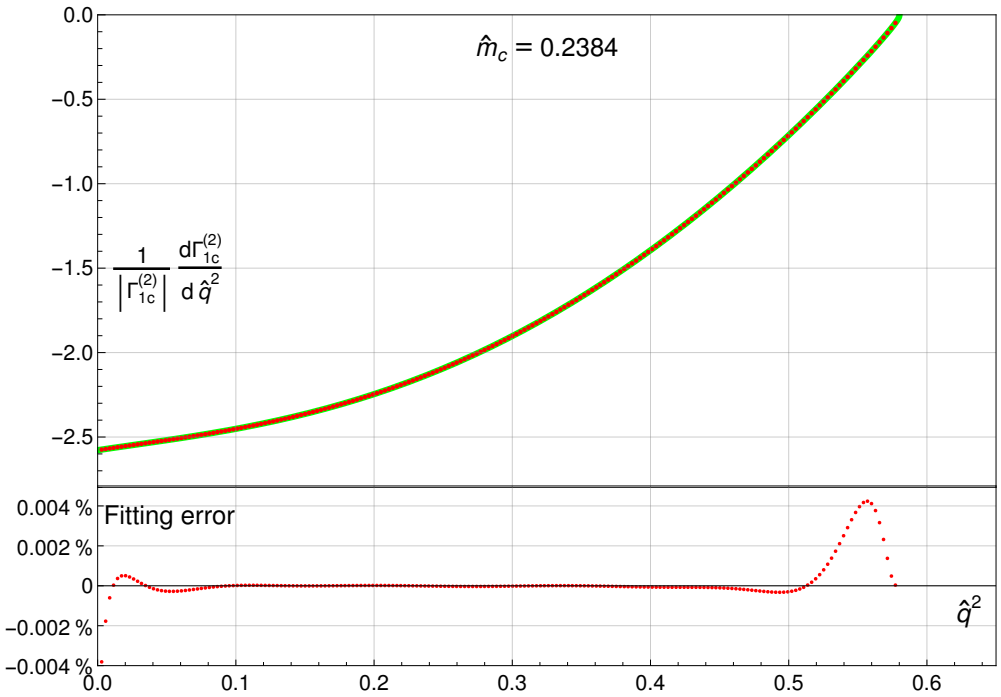

Figure 25: The contribution of the single-charm channel to the inclusive $\mathcal{O}(\alpha_s^2)$ correction, normalized to its integral over $\hat{q}^2$. The green band presents the result of the fit using the ansatz 3.212. The red points denote the numerical results obtained using `AMFlow`. The bottom panel shows the relative error of the fit.

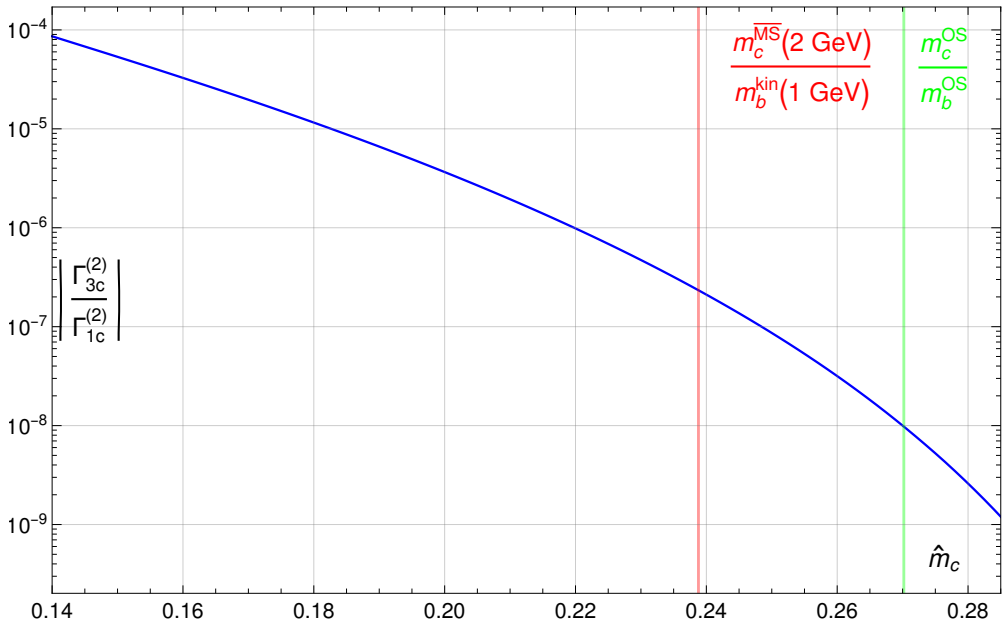

Figure 26: The ratio of $\Gamma_{3c}^{(2)} \equiv \int_0^{(1-3\hat{m}_c)^2} d\hat{q}^2 d\Gamma_{3c}^{(2)}/d\hat{q}^2$ and $\Gamma_{1c}^{(2)} \equiv \int_0^{(1-\hat{m}_c)^2} d\hat{q}^2 d\Gamma_{1c}^{(2)}/d\hat{q}^2$ as a function of $\hat{m}_c$.

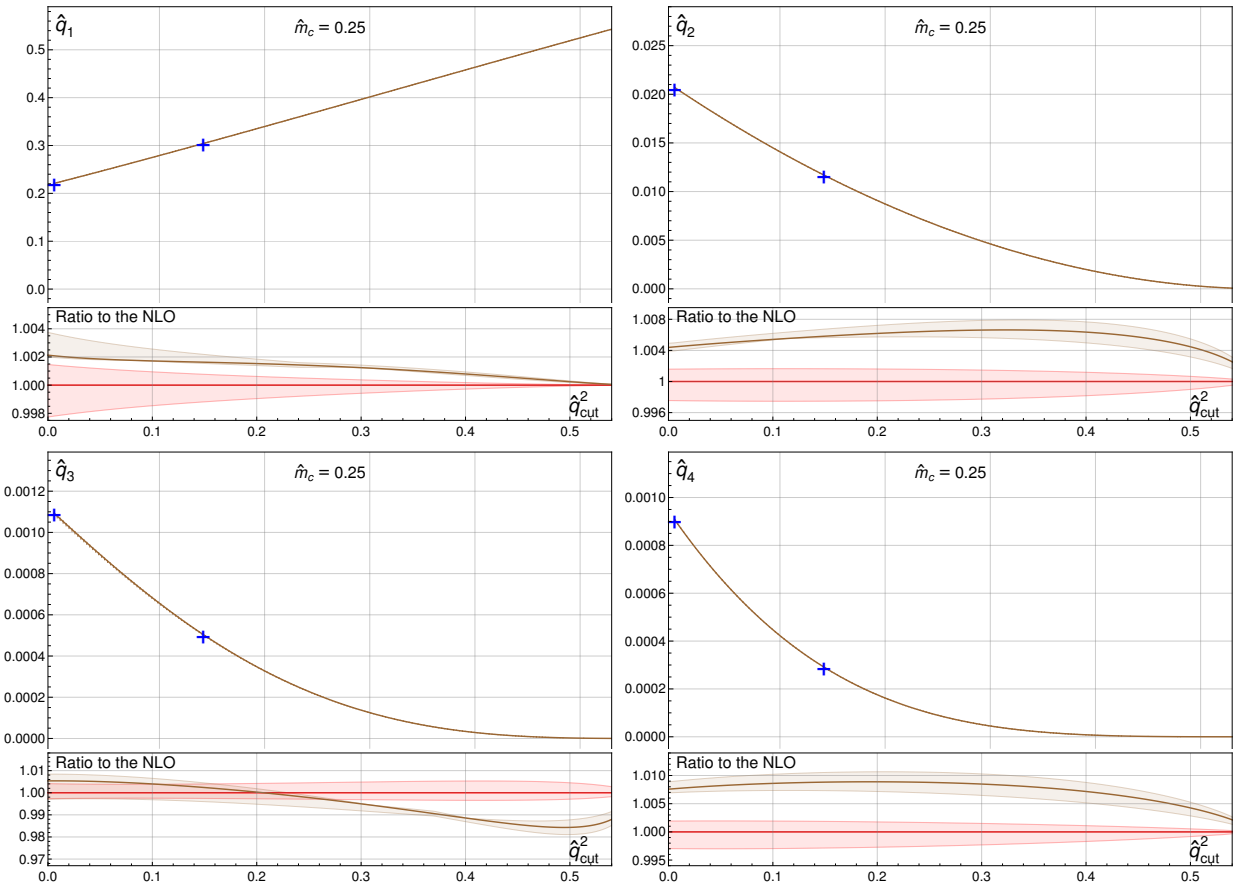

Figure 27: The centralized moments $\hat{q}_n$ for $n = 1 \ldots 4$ up to $\mathcal{O}(\alpha_s^2)$ as functions of the cut on small $\hat{q}^2$. The blue crosses denote the results given in eqs. (21) and (22) of ref. [67]. For a direct comparison with that publication, the value of $\hat{m}_c$ was set to 0.25. The NNLO to NLO ratios to the $\mathcal{O}(\alpha_s^1)$ results are shown by brown curves in the bottom panels.

space. We find that when the fit (3.212) is compared with the expression from ref. [67] given in terms of GPLs, the relative error never exceeds 5.2×10^{-4}. The numerical scan of the correction for $\hat{m}_c = 0.2384$ and the result of the fit are shown in figure 25.

The single-charm part of the NNLO correction to the spectrum is by far the dominant one. The triple-charm channel is kinematically allowed only for $\hat{q}^2 < (1-3\hat{m}_c)^2$, which for typical values of $\hat{m}_c$ constitutes less than 15% of the total allowed range of $\hat{q}^2$ in the semileptonic decay. Actually, at the hadronic level, there are only two kinematically allowed two-body final states with three valence charm quarks, namely $(D\eta_c)$ and (DJ/ψ), with the smallest possible invariant masses equal to $M_D + M_{\eta_c} \approx 4.85$ GeV$\approx 0.92 M_B$ and $M_D + M_{J/\psi} \approx 4.97$ GeV$\approx 0.94 M_B$, leaving only a tiny volume of the phase space for the outgoing particles. We found that for our reference value of $\hat{m}_c$, the $\hat{q}^2$ integral of $d\Gamma^{(2)}_{3c}/d\hat{q}^2$ is -2.428×10^{-7} times smaller than the corresponding integral of $d\Gamma^{(2)}_{1c}/d\hat{q}^2$ (see figure 26), while the ratio of the corrections to the spectrum for $\hat{q}^2 \to 0$ approaches 5.123×10^{-6}, and decreases rapidly with $\hat{q}^2$.

D_{0kl}	$k=0$	$k=1$	$k=2$	$k=3$
$l=0$	-0.00065492620361	-0.00390985766592	-0.00220565766436	0.15518605570268
$l=1$	-0.00142837487165	0.00696508473371	0.09405910531312	-0.06253133578189
$l=2$	0.00315708546717	-0.02325332865210	0.00374231943691	-2.02104356689117
$l=3$	-0.01566245331197	0.00539313247413	-0.16514145943056	0.50368450565789
$l=4$	-0.00314430463123	0.03298251534973	-0.24771235141673	0.79272863991011
$l=5$	-0.00116367410900	-0.00066823342187	-0.01632951298570	0.12789891805598
$l=6$	-0.00016427141654	-0.00086937186633	0.00406718033696	0.00295240291003
$l=7$	-0.00002838003168	-0.00013193918044	0.00091118101557	-0.00127493558773
$l=8$	-0.00000311384087	-0.00000605460509	0.00008807454959	-0.00020743224743

Table 5: Coefficients D_{0kl} of the single-charm fit (3.212) for k between 0 and 3.

D_{0kl}	$k=4$	$k=5$	$k=6$	$k=7$
$l=0$	-0.08570516624642	-2.60307981382978	5.46598388371161	-3.07155763105516
$l=1$	-4.45202557105393	12.27898482822888	-12.17665279523761	4.05283421170514
$l=2$	6.82900780658794	-8.98001675918627	4.79587351688384	-0.71420622887211
$l=3$	-0.22696886297429	-0.79009467604488	0.80044056001754	-0.12969467182270
$l=4$	-1.19412096570063	0.75616420973758	-0.12462741476560	-0.01366414279716
$l=5$	-0.29957244184153	0.30137080814560	-0.13593627512955	0.02437018661001
$l=6$	-0.03090584845561	0.04725296326283	-0.02906154255314	0.00673101795849
$l=7$	-0.00087783536997	0.00342046404978	-0.00276819278253	0.00074981715535
$l=8$	0.00013718255663	0.00010589907564	-0.00017873779555	0.00006418583561

Table 6: Coefficients D_{0kl} of the single-charm fit (3.212) for k between 4 and 8.

D_{1kl}	$k=0$	$k=1$	$k=2$	$k=3$
$l=0$	0.00037898651589	0.00517918021788	0.04112085070528	-0.21496054486301
$l=1$	0.00294905480007	-0.00603971843699	-0.21895793674020	-1.03193199304427
$l=2$	-0.01351315180078	-0.01995812054357	-0.22812429086629	3.41257368948131
$l=3$	0.01475940605979	0.00798442052509	0.20625870040905	-0.22965190841787
$l=4$	0.00361472380470	-0.04512665323742	0.27522405293211	-0.58912224362215
$l=5$	0.00135041781442	0.00257101526830	0.03190378201141	-0.15565929828791
$l=6$	0.00018496716551	0.00151028010054	-0.00216460072286	-0.01607688792361
$l=7$	0.00003136294993	0.00026420915586	-0.00084445521789	-0.00038980944792
$l=8$	0.00000345408063	0.00001942254381	-0.00010722136685	0.00009668851788

Table 7: Coefficients D_{1kl} of the single-charm fit (3.212) for k between 0 and 3.

D_{1kl}	$k=4$	$k=5$	$k=6$	$k=7$
$l=0$	-1.01037416347829	3.85777242049678	-4.82260835024637	2.43237146133600
$l=1$	7.28407942435662	-11.41492712861138	3.15489853106631	4.33118652047488
$l=2$	-6.95529309256300	2.97749311540542	2.87779195568835	-0.44612980575120
$l=3$	-0.81288724990409	1.05952773710921	0.58597841341702	-0.21167555956766
$l=4$	0.25138154880765	0.49282349653529	-0.24333580413142	0.01386846240050
$l=5$	0.20204027536542	-0.02532694776417	-0.04866750001498	0.01886365093423
$l=6$	0.04112674519580	-0.02440884452889	-0.00083229803405	0.00359648817752
$l=7$	0.00367275991399	-0.00340746780997	0.00055454715801	0.00030764562717
$l=8$	0.00017167412681	-0.00029973464715	0.00010242601552	0.00001903450238

Table 8: Coefficients D_{1kl} of the single-charm fit (3.212) for k between 4 and 7.

Moments of the spectrum

In the extraction of the SM value of $|V_{cb}|$, together with the b- and c-quark masses, as well as HQE matrix elements, one compares the SM predictions for moments of the semileptonic spectra with the corresponding measurements. For the phenomenological reasons mentioned in the Introduction, in the integrals defining the moments, it is necessary to exclude the region of small lepton energies, or, equivalently, small q^2. Once a prediction for the q^2 spectrum is obtained, it is straightforward to take this cut into account also on the theory side of the fit. The integrals defining the $\hat{q}^2$ moments considered in this thesis are

$$\hat{M}_n(\hat{q}^2_{cut}) \equiv \int\limits_{\hat{q}^2_{cut}}^{(1-\hat{m}_c)^2} d\hat{q}^2 \hat{q}^{2n} \frac{d\Gamma_{sl}}{d\hat{q}^2}. \tag{3.213}$$

Conventionally, one also defines the normalized moments:

$$\bar{M}_n(\hat{q}^2_{cut}) \equiv \frac{\hat{M}_n(\hat{q}^2_{cut})}{\hat{M}_0(\hat{q}^2_{cut})}, \tag{3.214}$$

and the centralized moments:

$$\begin{aligned} \hat{q}_1(\hat{q}^2_{cut}) \equiv& \bar{M}_1(\hat{q}^2_{cut}), \\ \hat{q}_n(\hat{q}^2_{cut}) \equiv& \sum_{j=0}^{n} \binom{n}{j} \bar{M}_j(\hat{q}^2_{cut}) \left(-\bar{M}_{n-j}(\hat{q}^2_{cut})\right)^{n-j}. \end{aligned} \tag{3.215}$$

Using the latter definition instead of the regular moments reduces correlations in the fit [33].

The first four centralized moments calculated using the partonic q^2 spectrum up to the NNLO in QCD are shown in figure 27. If only the single-charm NNLO correction was included, our result would be in prefect agreement with the values given in eqs. (21) and (22) of ref. [67]. To study the impact of the triple-charm term, one may define

$$\Delta\hat{q}^{3c}_n \equiv \hat{q}_n - \hat{q}^{1c}_n, \tag{3.216}$$

where the moment $\hat{q}^{1c}_n$ is computed by neglecting the triple-charm contribution at the NNLO. For the actual values of heavy quark masses, the ratio $\Delta\hat{q}^{3c}_n/\hat{q}_n$ can be at most $\mathcal{O}(10^{-7})$, far below the accuracy of present experiments.

Finally, the impact of the single-charm correction on the centralized moments for four sample values of $\hat{q}^2_{cut}$ is shown in figure 29. The single-charm NNLO correction to the moments $\Delta\hat{q}^{1c}_n$ is given by

$$\Delta\hat{q}^{1c}_n \equiv \hat{q}^{1c}_n - \hat{q}^{NLO}_n, \tag{3.217}$$

with $\hat{q}^{NLO}_n$ denoting the NLO approximation of the n-th centralized moment. The NNLO QCD term shifts the first moment by around 0.1%, the second and third by $\sim 0.5\%$, and the fourth by $\sim 0.8\%$, with the exact values depending on the chosen cut. The results presented above were obtained for quark fields and masses renormalized on shell. The behavior of the QCD perturbative series can be improved by instead adopting the kinetic renormalization scheme for the b quark mass [23–26]. While this conversion is known to enhance the precision of the semileptonic fits, it is beyond the scope of the present thesis.

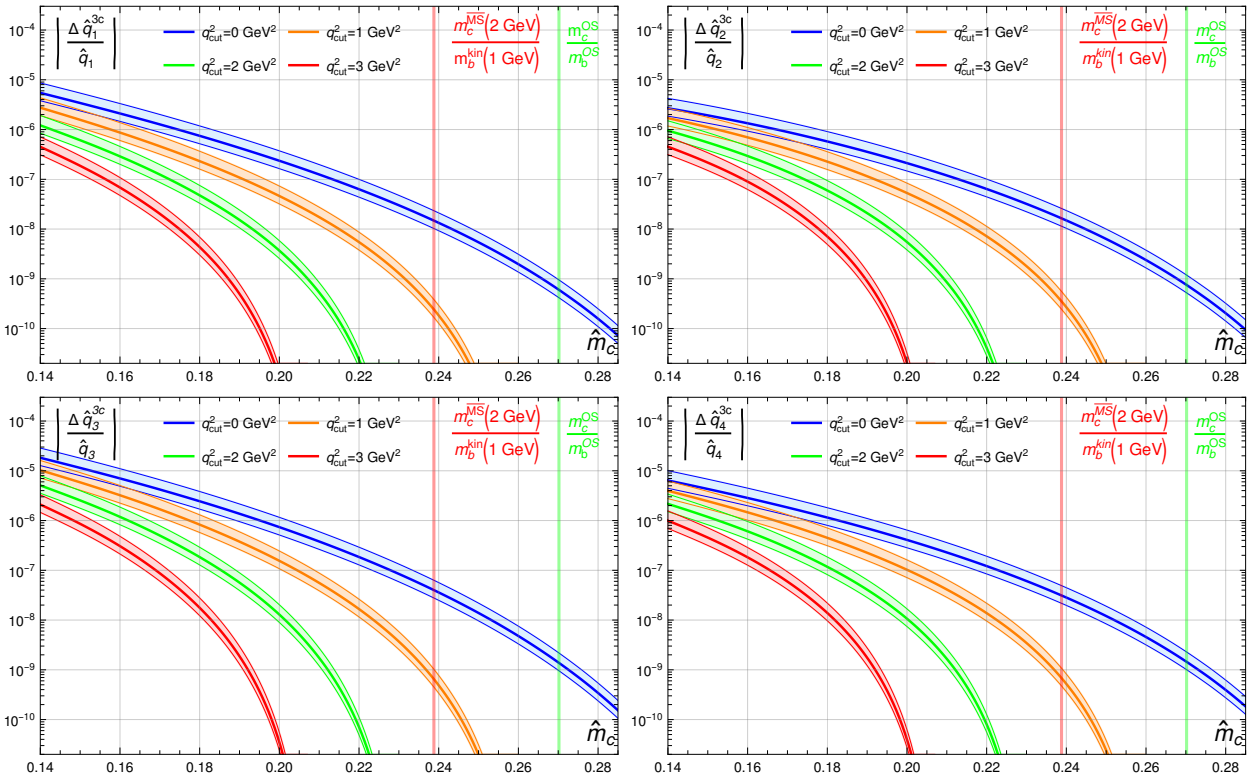

Figure 28: The dependence of the ratio $\Delta\hat{q}_n^{3c}/\hat{q}_n$ on $\hat{m}_c$ and the value of the cut on low q^2. The uncertainties come from varying the renormalization scale μ between $m_b/2$ and $2m_b$. The plots are identical as in figure 9 of our article [1].

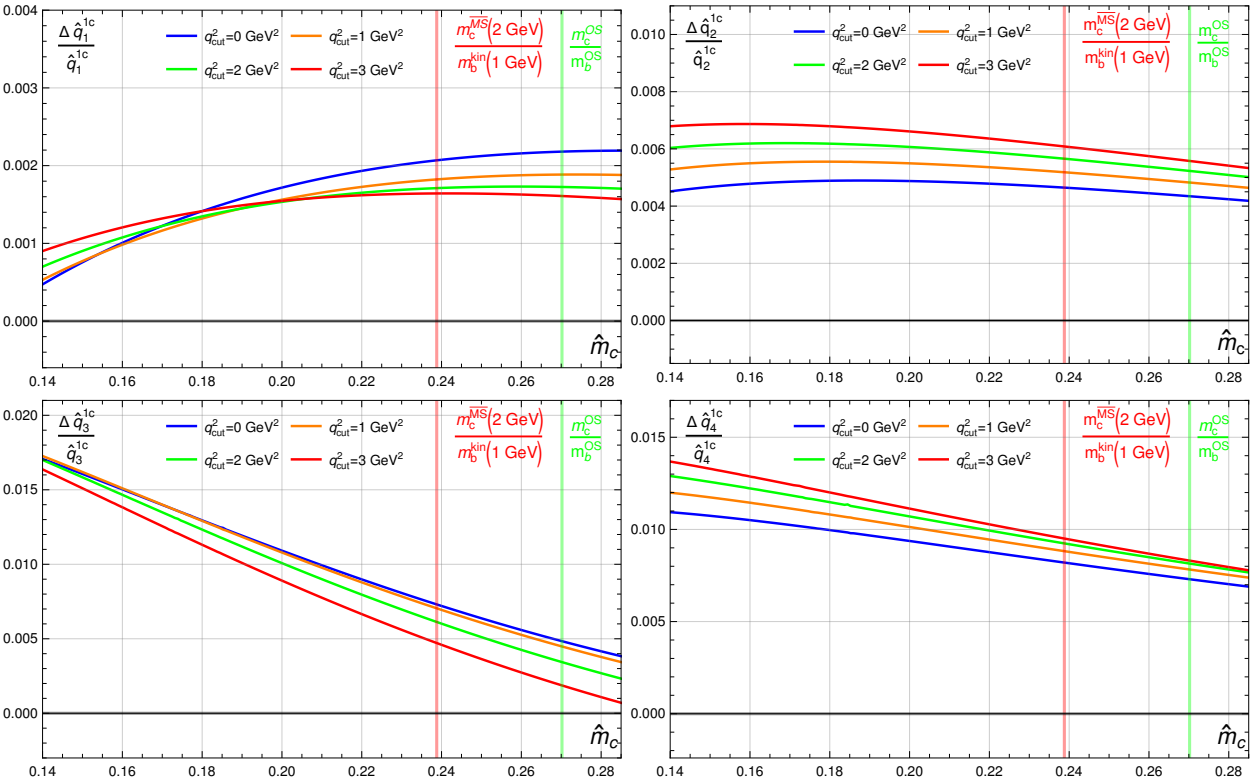

Figure 29: The relative impact of the single-charm NNLO correction on centralized moments of the q^2 spectrum. The renormalization scale choice uncertainty is omitted for clarity of the plots. The plots are identical as in figure 10 of our article [1].

Conclusions

The findings of the detailed investigation of the inclusive semileptonic decay of the B meson and the resulting extraction of physical parameters have now been serving physicists for over two decades. The analysis is still ongoing, with many observables and corrections yet to be tackled systematically. The work described in this thesis contributes to this field by concluding the calculation of the NNLO QCD correction to the spectrum in invariant mass of the lepton pair in the leading order in the Heavy Quark Expansion (referred to as the q^2 spectrum). Completing this project was motivated by the novel extraction method of the $|V_{cb}|$ CKM matrix element, based on the global fit of the q^2 moments of the semileptonic decay to the experimental data [33]. In this method, the fit depends on a smaller number of unknown, non-perturbative matrix elements when compared with the standard extraction procedures, thanks to the partial resummation of the HQE for reparametrization-invariant quantities [34].

The effects of the NNLO correction to the q^2 spectral moments in the BLM approximation have already been implemented in the most recent fit to the semileptonic experimental data in ref. [35]. By the time of publication of that article, the full NNLO and NNNLO corrections to the moments were known only for $q^2_{cut} = 0$ [66], and thus could not be utilized in the fit. Extending the analysis of the moments to non-zero values of q^2_{cut} was the motivation for computing the $\mathcal{O}(\alpha_s^2)$ correction to the q^2 spectrum. This dependence was easily derived once the q^2 spectrum was at hand. The results published in refs. [1, 67] and discussed in this thesis thus allow for including the full NNLO terms in the semileptonic fit.

The results presented here serve two main purposes. First, they provide an analysis of the dominant, single-charm contribution to the NNLO term, which verifies and confirms the findings of the parallel, independent calculation of ref. [67]. The result of the single-charm contribution to the spectrum was compared with the analytic expression provided by the authors of ref. [67] and confirmed for all 13600 considered points in the $(\hat{m}_c, \hat{q}^2)$ parameter space up to the 5.2×10^{-4} relative error. Moreover, the centralized q^2 moments for two sample points and with the quark fields and masses renormalized in the on-shell scheme were also found to be exactly equal to the values quoted in that publication. The single-charm correction turns out to affect the q^2 spectrum by at most 4% near the phase-space endpoint, and around 2% for most other values.

Second, the single-charm contribution has been supplemented with the correction corresponding to the triple-charm semileptonic decay channel. While the latter effect turned out to be very small for the observed values of the b and c quark masses, it was nevertheless important to compute it to complete the calculation of the inclusive NNLO correction. Before the quantitative treatment of the triple-charm channel was completed, this correction was being neglected purely on the basis of the small volume of the available phase-space. On the other hand, the width of the triple-charm channel is known to be divergent in the limit $\hat{m}_c \to 0$. The shape of the obtained ratio of the single- and triple-charm corrections as a function of $\hat{m}_c$ (see figure 26) confirms that a small variation in the computed 3-loop effect or the value of $\hat{m}_c$ could have had a large impact, and a thorough calculation was of interest.

The $\mathcal{O}(\alpha_s^2)$ correction to the spectrum was computed in a series of steps. First, a chain of effective theories was considered, in which the heavy electroweak degrees of freedom were

integrated out of the SM Green's function describing the semileptonic decay. Moreover, the calculation was simplified by replacing the lepton pair with an auxiliary vector boson Q. At the end of this procedure, one is left with a description based on perturbative QCD supplemented with a single fermion-gauge boson interaction vertex. Next, the amplitude was expressed as a linear combination of 3-loop integrals, and reduced to a basis of MIs using IBP identities between scalar integrals. The MIs were computed numerically using the auxiliary mass flow method for a large number of points in the $(\hat{m}_c, \hat{q}^2)$ space. The renormalization formula was derived, and the necessary 1- and 2-loop counterterm diagrams were computed using the same method. Finally, the results were fitted to a power-log ansatz.

Apart from the description of the calculation of the NNLO correction, the thesis aimed to provide a summary of the contemporary techniques employed in the computations of multi-loop, multi-scale Feynman diagrams in QFT. This is a dynamic and exciting area of research, with frequent breakthrough results opening new possibilities for precise phenomenological studies. All methods described in Chapter 2 are fundamentally based on the IBP identities, which may be viewed as identities stemming from the integral invariance under a redefinition of the integration variable. Both the ϵ-form approach and the auxiliary mass flow follow from the fact that the derivatives of all loop integrands can be expressed as different loop integrands, being therefore IBP reducible. The described computational methods were used extensively during the preparation of this thesis, and illustrated in numerous 1- and 2-loop examples.

Many natural extensions of the presented analysis of perturbative corrections to the semileptonic decay may be considered. A potentially significant effect may come from the leading electrodynamic correction. Going beyond the leading approximation in electroweak interactions presents a number of nontrivial complications. First, the auxiliary width approach described in section 3.1 breaks down because of the photon exchanges between the quark and lepton lines. Moreover, the masses of the outgoing leptons cannot be neglected because of collinear divergences in QED with massless fermions. To compute this correction in terms of GPLs, one would need to incorporate certain splitting function techniques[†] that allow for separating the logarithms $\log(m_l/m_b)$ and the part that is finite in the limit $m_l \to 0$. The computation of this correction by the present thesis' author is ongoing.

Since $\alpha_s^3(m_b) \sim \alpha_{em}$, the NNNLO QCD correction to the leading HQE contribution can be expected to be of similar size as the leading QED one. However, its calculation is likely to be much more arduous. A computation of the necessary 675 four-loop diagrams constitutes a computational challenge. Even generating the sets of seed integrals and their coefficients in the amplitude took around two weeks on the system described below eq. (2.17) in section 2.2. It is still unclear if the IBP reduction at this order is feasible with the contemporary algorithms. The direct computation of the single charm channel MIs using the ϵ-form method would be extremely difficult. The numerical approach employed in this thesis may also be too costly in terms of memory and CPU time. Evaluating the counterterm diagrams alone would be a larger project than the one presented in this thesis.

Going beyond the leading order in the HQE, a calculation of the NNLO QCD correction to the Wilson coefficients of the $\mathcal{O}(\hat{\Lambda}^2)$ and $\mathcal{O}(\hat{\Lambda}^3)$ operators in the HQE may be possible. The NLO QCD effects in the $\mathcal{O}(\hat{\Lambda}^4)$ and higher are also yet unknown. Here, as in all other calculations at the precision frontier of particle physics, one must weigh the potential phenomenological significance with the expected difficulty and the available computer resources.

[†]see for example refs. [233, 234] and the appendix B of ref. [235]

References

[1] Mateusz Czaja, Mikołaj Misiak, and Abdur Rehman. "Complete $\mathcal{O}(\alpha_s^2)$ corrections to the leptonic invariant mass spectrum in $b \to X_c l \overline{\nu}_l$ decay". *JHEP* 02 (2025), p. 021. arXiv: 2411.12866 [hep-ph].

[2] M. Czaja et al. "The $Q_{1,2}$–Q_7 interference contributions to $b \to s\gamma$ at $\mathcal{O}(\alpha_s^2)$ for the physical value of m_c". *Eur. Phys. J. C* 83.12 (2023), p. 1108. arXiv: 2309.14707 [hep-ph].

[3] A. A. Belavin, Alexander M. Polyakov, A. S. Schwartz, and Yu. S. Tyupkin. "Pseudoparticle Solutions of the Yang-Mills Equations". *Phys. Lett. B* 59 (1975). Ed. by J. C. Taylor, pp. 85–87.

[4] Gerard 't Hooft. "Computation of the Quantum Effects Due to a Four-Dimensional Pseudoparticle". *Phys. Rev. D* 14 (1976). Ed. by Mikhail A. Shifman. [Erratum: Phys.Rev.D 18, 2199 (1978)], pp. 3432–3450.

[5] R. Jackiw and C. Rebbi. "Vacuum Periodicity in a Yang-Mills Quantum Theory". *Phys. Rev. Lett.* 37 (1976). Ed. by J. C. Taylor, pp. 172–175.

[6] Curtis G. Callan Jr., R. F. Dashen, and David J. Gross. "The Structure of the Gauge Theory Vacuum". *Phys. Lett. B* 63 (1976). Ed. by J. C. Taylor, pp. 334–340.

[7] Varouzhan Baluni. "CP Violating Effects in QCD". *Phys. Rev. D* 19 (1979), pp. 2227–2230.

[8] R. J. Crewther, P. Di Vecchia, G. Veneziano, and Edward Witten. "Chiral Estimate of the Electric Dipole Moment of the Neutron in Quantum Chromodynamics". *Phys. Lett. B* 88 (1979). [Erratum: Phys.Lett.B 91, 487 (1980)], p. 123.

[9] Wen-Yuan Ai, Bjorn Garbrecht, and Carlos Tamarit. "CP Conservation in the Strong Interactions". *Universe* 10.5 (2024), p. 189. arXiv: 2404.16026 [hep-ph].

[10] V. Papadimitriou. "Luminosity determination at the Tevatron". *LHC Lumi Days*. Mar. 2011. arXiv: 1106.5182 [physics.ins-det].

[11] *Belle Collaboration website:* https://belle.kek.jp/. Accessed: 01-29-2025.

[12] Davide Zuliani. "Electroweak physics at LHCb". *Physica Scripta* 97 (Sept. 2022).

[13] *Belle II Collaboration website:* https://www.belle2.org/research/luminosity/index_html. Accessed: 01-29-2025.

[14] C. A. Baker et al. "An Improved Experimental Limit on the Electric Dipole Moment of the Neutron". *Phys. Rev. Lett.* 97 (2006), p. 131801. arXiv: hep-ex/0602020.

[15] T. Aushev et al. "Physics at Super B Factory" (Feb. 2010). arXiv: 1002.5012 [hep-ex].

[16] M. Beneke. "A Quark mass definition adequate for threshold problems". *Phys. Lett. B* 434 (1998), pp. 115–125. arXiv: hep-ph/9804241.

[17] Andre H. Hoang, Zoltan Ligeti, and Aneesh V. Manohar. "B decays in the upsilon expansion". *Phys. Rev. D* 59 (1999), p. 074017. arXiv: hep-ph/9811239.

[18] Andre H. Hoang, Zoltan Ligeti, and Aneesh V. Manohar. "B decay and the Υ mass". *Phys. Rev. Lett.* 82 (1999), pp. 277–280. arXiv: hep-ph/9809423.

[19] A. H. Hoang and T. Teubner. "Top Quark Pair Production Close to Threshold: Top Mass, Width and Momentum Distribution". *Phys. Rev. D* 60 (1999), p. 114027. arXiv: hep-ph/9904468.

[20] Antonio Pineda. "Determination of the bottom quark mass from the $\Upsilon(1S)$ system". *JHEP* 06 (2001), p. 022. arXiv: hep-ph/0105008.

[21] Andre H. Hoang, Ambar Jain, Ignazio Scimemi, and Iain W. Stewart. "Infrared Renormalization Group Flow for Heavy Quark Masses". *Phys. Rev. Lett.* 101 (2008), p. 151602. arXiv: 0803.4214 [hep-ph].

[22] Andre H. Hoang, Ambar Jain, Christopher Lepenik, Vicent Mateu, Moritz Preisser, Ignazio Scimemi, and Iain W. Stewart. "The MSR Mass and the $\mathcal{O}(\Lambda_{\rm QCD})$ Renormalon Sum Rule". *JHEP* 04 (2018), p. 003. arXiv: 1704.01580 [hep-ph].

[23] Ikaros I. Y. Bigi, Mikhail A. Shifman, N. Uraltsev, and Arkady I. Vainshtein. "High power n of m_b in beauty widths and $n = 5 \to \infty$ Limit". *Phys. Rev. D* 56 (1997). Ed. by Ikaros I Bigi, Paolo Gambino, and Thomas Mannel, pp. 4017–4030. arXiv: hep-ph/9704245.

[24] A. Czarnecki, K. Melnikov, and N. Uraltsev. "Non-Abelian Dipole Radiation and the Heavy Quark Expansion". *Phys. Rev. Lett.* 80 (1998), pp. 3189–3192. arXiv: hep-ph/9708372.

[25] Matteo Fael, Kay Schönwald, and Matthias Steinhauser. "Kinetic Heavy Quark Mass to Three Loops". *Phys. Rev. Lett.* 125.5 (2020), p. 052003. arXiv: 2005.06487 [hep-ph].

[26] Matteo Fael, Kay Schönwald, and Matthias Steinhauser. "On the relation between the $\overline{\rm MS}$ and the kinetic mass of heavy quarks". *Phys. Rev. D* 103.1 (2021), p. 014005. arXiv: 2011.11655 [hep-ph].

[27] Makoto Kobayashi and Toshihide Maskawa. "CP Violation in the Renormalizable Theory of Weak Interaction". *Prog. Theor. Phys.* 49 (1973), pp. 652–657.

[28] S. W. Herb et al. "Observation of a Dimuon Resonance at 9.5 GeV in 400 GeV Proton-Nucleus Collisions". *Phys. Rev. Lett.* 39 (1977), pp. 252–255.

[29] F. Abe et al. "Observation of Top Quark Production in $\bar{p}p$ Collisions". *Phys. Rev. Lett.* 74 (1995), pp. 2626–2631. arXiv: hep-ex/9503002.

[30] S. Abachi et al. "Observation of the Top Quark". *Phys. Rev. Lett.* 74 (1995), pp. 2632–2637. arXiv: hep-ex/9503003.

[31] S. Navas et al. "Review of particle physics". *Phys. Rev. D* 110.3 (2024), p. 030001.

[32] Chien-Yeah Seng, Mikhail Gorchtein, Hiren H. Patel, and Michael J. Ramsey-Musolf. "Reduced hadronic uncertainty in the determination of V_{ud}". *Phys. Rev. Lett.* 121.24 (2018), p. 241804. arXiv: 1807.10197 [hep-ph].

[33] Matteo Fael, Thomas Mannel, and K. Keri Vos. "V_{cb} Determination from Inclusive $b \to c$ Decays: An Alternative Method". *JHEP* 02 (2019), p. 177. arXiv: 1812.07472 [hep-ph].

[34] Thomas Mannel and K. Keri Vos. "Reparametrization Invariance and Partial Re-Summations of the Heavy Quark Expansion". *JHEP* 06 (2018), p. 115. arXiv: 1802.09409 [hep-ph].

[35] Gael Finauri and Paolo Gambino. "The q^2 moments in inclusive semileptonic B decays". *JHEP* 02 (2024), p. 206. arXiv: 2310.20324 [hep-ph].

[36] F. Abudinén et al. "Measurement of Lepton Mass Squared Moments in $B \to X_c l \bar{\nu}_l$ decays with the Belle II Experiment". *Phys. Rev. D* 107.7 (2023), p. 072002. arXiv: 2205.06372 [hep-ex].

[37] Ikaros I. Y. Bigi, Mikhail A. Shifman, N. G. Uraltsev, and A. I. Vainshtein. "On the Motion of Heavy Quarks inside Hadrons: Universal Distributions and Inclusive Decays". *Int. J. Mod. Phys. A* 9 (1994), pp. 2467–2504. arXiv: hep-ph/9312359.

[38] Mary K Gaillard, Benjamin W Lee, and Jonathan L Rosner. "Search for charm". *Reviews of Modern Physics* 47.2 (1975), p. 277.

[39] N. Cabibbo and L. Maiani. "The Lifetime of Charmed Particles". *Phys. Lett. B* 79 (1978), pp. 109–111.

[40] Ahmed Ali and E. Pietarinen. "Semileptonic Decays of Heavy Quarks in Quantum Chromodynamics". *Nucl. Phys. B* 154 (1979), pp. 519–534.

[41] Guido Altarelli, N. Cabibbo, G. Corbo, L. Maiani, and G. Martinelli. "Leptonic Decay of Heavy Flavors: A Theoretical Update". *Nucl. Phys. B* 208 (1982), pp. 365–380.

[42] Guido Corbo. "Semileptonic b Quark Decay in Quantum Chromodynamics". *Nucl. Phys. B* 212 (1983), pp. 99–108.

[43] Michael Trott. "Improving extractions of $|V_{cb}|$ and m_b from the Hadronic Invariant Mass Moments of Semileptonic Inclusive B Decay". *Phys. Rev. D* 70 (2004), p. 073003. arXiv: hep-ph/0402120.

[44] V. Aquila, P. Gambino, G. Ridolfi, and N. Uraltsev. "Perturbative corrections to semileptonic b decay distributions". *Nucl. Phys. B* 719 (2005), pp. 77–102. arXiv: hep-ph/0503083.

[45] Aneesh V. Manohar and Mark B. Wise. "Inclusive Semileptonic B and Polarized Λ_b Decays from QCD". *Phys. Rev. D* 49 (1994), pp. 1310–1329. arXiv: hep-ph/9308246.

[46] Ikaros I. Y. Bigi, Mikhail A. Shifman, N. G. Uraltsev, and Arkady I. Vainshtein. "QCD Predictions for Lepton Spectra in Inclusive Heavy Flavor Decays". *Phys. Rev. Lett.* 71 (1993). Ed. by Ikaros I Bigi, Paolo Gambino, and Thomas Mannel, pp. 496–499. arXiv: hep-ph/9304225.

[47] Martin Gremm and Anton Kapustin. "Order $1/m_b^3$ corrections to $B \to X_c l \bar{\nu}_l$ decay and their implication for the measurement of $\bar{Lambda}$ and λ_1". *Phys. Rev. D* 55 (1997), pp. 6924–6932. arXiv: hep-ph/9603448.

[48] Thomas Becher, Heike Boos, and Enrico Lunghi. "Kinetic corrections to $B \to X_c \ell \bar{\nu}$ at one loop". *JHEP* 12 (2007), p. 062. arXiv: 0708.0855 [hep-ph].

[49] Andrea Alberti, Paolo Gambino, and Soumitra Nandi. "Perturbative corrections to power suppressed effects in semileptonic B decays". *JHEP* 01 (2014), p. 147. arXiv: 1311.7381 [hep-ph].

[50] Thomas Mannel, Alexei A. Pivovarov, and Denis Rosenthal. "Inclusive semileptonic B decays from QCD with NLO accuracy for power suppressed terms". *Phys. Lett. B* 741 (2015), pp. 290–294. arXiv: 1405.5072 [hep-ph].

[51] Thomas Mannel and Alexei A. Pivovarov. "QCD corrections to inclusive heavy hadron weak decays at $\Lambda^3_{\rm QCD}/m^3_Q$". *Phys. Rev. D* 100.9 (2019), p. 093001. arXiv: 1907.09187 [hep-ph].

[52] Benjamin M. Dassinger, Thomas Mannel, and Sascha Turczyk. "Inclusive Semileptonic B decays to order $1/m_b^4$". *JHEP* 03 (2007), p. 087. arXiv: hep-ph/0611168.

[53] Thomas Mannel, Sascha Turczyk, and Nikolai Uraltsev. "Higher Order Power Corrections in Inclusive B Decays". *JHEP* 11 (2010), p. 109. arXiv: 1009.4622 [hep-ph].

[54] Stanley J. Brodsky, G. Peter Lepage, and Paul B. Mackenzie. "On the Elimination of Scale Ambiguities in Perturbative Quantum Chromodynamics". *Phys. Rev. D* 28 (1983), p. 228.

[55] Michael E. Luke, Martin J. Savage, and Mark B. Wise. "Charm Mass Dependence of the $\mathcal{O}(alpha_s^2 n_f)$ Correction to Inclusive $B \to X_c e \bar{\nu}_e$ Decay". *Phys. Lett. B* 345 (1995), pp. 301–306. arXiv: hep-ph/9410387.

[56] Kirill Melnikov. "$\mathcal{O}(alpha_s^2)$ corrections to semileptonic decay $b \to c l \bar{\nu}_l$". *Phys. Lett. B* 666 (2008), pp. 336–339. arXiv: 0803.0951 [hep-ph].

[57] Alexey Pak and Andrzej Czarnecki. "Mass effects in muon and semileptonic $b \to c$ decays". *Phys. Rev. Lett.* 100 (2008), p. 241807. arXiv: 0803.0960 [hep-ph].

[58] Alexey Pak and Andrzej Czarnecki. "Heavy-to-heavy quark decays at NNLO". *Phys. Rev. D* 78 (2008), p. 114015. arXiv: 0808.3509 [hep-ph].

[59] Matthew Dowling, Jan H. Piclum, and Andrzej Czarnecki. "Semileptonic decays in the limit of a heavy daughter quark". *Phys. Rev. D* 78 (2008), p. 074024. arXiv: 0810.0543 [hep-ph].

[60] Alexey Pak and Andrzej Czarnecki. "Mass effects in muon and semileptonic $b \to c$ decays". *Phys. Rev. Lett.* 100 (2008), p. 241807. arXiv: 0803.0960 [hep-ph].

[61] Kirill Melnikov. "$\mathcal{O}(alpha_s^2)$ corrections to semileptonic decay $b \to c l \bar{\nu}_l$". *Phys. Lett. B* 666 (2008), pp. 336–339. arXiv: 0803.0951 [hep-ph].

[62] Sandip Biswas and Kirill Melnikov. "Second order QCD corrections to inclusive semileptonic $b \to X_c l \bar{\nu}_l$ decays with massless and massive lepton". *JHEP* 02 (2010), p. 089. arXiv: 0911.4142 [hep-ph].

[63] Matteo Fael, Kay Schönwald, and Matthias Steinhauser. "Third order corrections to the semileptonic $b \to c$ and the muon decays". *Phys. Rev. D* 104.1 (2021), p. 016003. arXiv: 2011.13654 [hep-ph].

[64] Michael E. Luke and Aneesh V. Manohar. "Reparametrization invariance constraints on heavy particle effective field theories". *Phys. Lett. B* 286 (1992), pp. 348–354. arXiv: hep-ph/9205228.

[65] Thomas Mannel, Sascha Turczyk, and Nikolai Uraltsev. "Higher Order Power Corrections in Inclusive B Decays". *JHEP* 11 (2010), p. 109. arXiv: 1009.4622 [hep-ph].

[66] Matteo Fael, Kay Schönwald, and Matthias Steinhauser. "A first glance to the kinematic moments of $B \to X_c l \nu$ at third order". *JHEP* 08 (2022), p. 039. arXiv: 2205.03410 [hep-ph].

[67] Matteo Fael and Florian Herren. "NNLO QCD corrections to the q^2 spectrum of inclusive semileptonic B-meson decays". *JHEP* 05 (2024), p. 287. arXiv: 2403.03976 [hep-ph].

[68] Simon Badger, Matteo Becchetti, Colomba Brancaccio, Heribertus Bayu Hartanto, and Simone Zoia. "Numerical evaluation of two-loop QCD helicity amplitudes for $gg \to t\bar{t}g$ at leading colour" (Dec. 2024). arXiv: 2412.13876 [hep-ph].

[69] Long Chen, Xiang Chen, Xin Guan, and Yan-Qing Ma. "High Precision Results for Top-Quark Decay at N3LO in QCD". *PoS* ICHEP2024 (2025), p. 381.

[70] Niklas Schwanemann and Stefan Weinzierl. "Electroweak double-box integrals for Moller scattering" (Dec. 2024). arXiv: 2412.07522 [hep-ph].

[71] Dhimiter Canko and Mattia Pozzoli. "A first computation of three-loop master integrals for the production of two off-shell vector bosons with different masses" (Dec. 2024). arXiv: 2412.06972 [hep-ph].

[72] Felix Forner, Christoph Nega, and Lorenzo Tancredi. "On the photon self-energy to three loops in QED" (Nov. 2024). arXiv: 2411.19042 [hep-th].

[73] Thomas Dave and William J. Torres Bobadilla. "Helicity amplitudes in massless QED to higher orders in the dimensional regulator" (Nov. 2024). arXiv: 2411.07063 [hep-ph].

[74] Jian Wang, Xing Wang, and Yefan Wang. "Analytic decay width of the Higgs boson to massive bottom quarks at order α_s^3" (Nov. 2024). arXiv: 2411.07493 [hep-ph].

[75] Yao Ji, Bo-Xuan Shi, Jian Wang, Ye-Fan Wang, Yu-Ming Wang, and Hui-Xin Yu. "Next-to-Next-to-Leading-Order QCD Prediction for the Pion Form Factor" (Nov. 2024). arXiv: 2411.03658 [hep-ph].

[76] Dmitry Chicherin, Johannes Henn, Jaroslav Trnka, and Shun-Qing Zhang. "Positivity properties of five-point two-loop Wilson loops with Lagrangian insertion" (Oct. 2024). arXiv: 2410.11456 [hep-th].

[77] Christoph Nega. "The Electron Self-Energy at 2 and 3 Loops". *PoS* LL2024 (2024), p. 009.

[78] Michael E. Peskin and Daniel V. Schroeder. "An Introduction to Quantum Field Theory" (1995).

[79] Steven Weinberg. "The Quantum theory of fields. Vol. 1: Foundations" (June 2005).

[80] S. Pokorski. "Gauge Field Theories" (Jan. 2005).

[81] M. Srednicki. "Quantum field theory" (Jan. 2007).

[82] C. Itzykson and J. B. Zuber. "Quantum Field Theory". International Series In Pure and Applied Physics (1980).

[83] James D. Bjorken and Sidney D. Drell. "Relativistic Quantum Mechanics". International Series In Pure and Applied Physics (1965).

[84] Matthew D. Schwartz. "Quantum Field Theory and the Standard Model" (Mar. 2014).

[85] Franz Mandl and Graham Shaw. "Quantum Field Theory" (1985).

[86] Brian C. Hall. "Lie Groups, Lie Algebras, and Representations". Graduate Texts in Mathematics (2015).

[87] J.P. Serre. "Lie Algebras and Lie Groups: 1964 Lectures given at Harvard University". Lecture Notes in Mathematics (2009).

[88] Alexander Kirillov Jr. “An Introduction to Lie Groups and Lie Algebras”. Cambridge Studies in Advanced Mathematics (2008).

[89] G. C. Wick. “The Evaluation of the Collision Matrix”. *Phys. Rev.* 80 (1950), pp. 268–272.

[90] Joshua Ellis. “TikZ-Feynman: Feynman diagrams with TikZ”. *Comput. Phys. Commun.* 210 (2017), pp. 103–123. arXiv: 1601.05437 [hep-ph].

[91] P. V. Dong, L. T. Hue, H. T. Hung, H. N. Long, and N. H. Thao. “Symmetry Factors of Feynman Diagrams for Scalar Fields”. *Theor. Math. Phys.* 165 (2010), pp. 1500–1511. arXiv: 0907.0859 [hep-ph].

[92] L. D. Faddeev and V. N. Popov. “Feynman Diagrams for the Yang-Mills Field”. *Phys. Lett. B* 25 (1967). Ed. by Jong-Ping Hsu and D. Fine, pp. 29–30.

[93] H. Lehmann, K. Symanzik, and W. Zimmermann. “On the formulation of quantized field theories”. *Nuovo Cim.* 1 (1955), pp. 205–225.

[94] R. E. Cutkosky. “Singularities and discontinuities of Feynman amplitudes”. *J. Math. Phys.* 1 (1960), pp. 429–433.

[95] Gerard ’t Hooft. “Renormalizable Lagrangians for Massive Yang-Mills Fields”. *Nucl. Phys. B* 35 (1971). Ed. by J. C. Taylor, pp. 167–188.

[96] Gerard ’t Hooft and M. J. G. Veltman. “Regularization and Renormalization of Gauge Fields”. *Nucl. Phys. B* 44 (1972), pp. 189–213.

[97] W. Pauli and F. Villars. “On the Invariant Regularization in Relativistic Quantum Theory”. *Rev. Mod. Phys.* 21 (1949), pp. 434–444.

[98] C. G. Bollini and J. J. Giambiagi. “Lowest order divergent graphs in ν-dimensional space”. *Phys. Lett. B* 40 (1972), pp. 566–568.

[99] Gerard ’t Hooft and M. J. G. Veltman. “Regularization and Renormalization of Gauge Fields”. *Nucl. Phys. B* 44 (1972), pp. 189–213.

[100] T. Huber and Daniel Maitre. “HypExp: A Mathematica package for expanding hypergeometric functions around integer-valued parameters”. *Comput. Phys. Commun.* 175 (2006), pp. 122–144. arXiv: hep-ph/0507094.

[101] Tobias Huber and Daniel Maitre. “HypExp 2, Expanding Hypergeometric Functions about Half-Integer Parameters”. *Comput. Phys. Commun.* 178 (2008), pp. 755–776. arXiv: 0708.2443 [hep-ph].

[102] Michael S. Chanowitz, M. Furman, and I. Hinchliffe. “The Axial Current in Dimensional Regularization”. *Nucl. Phys. B* 159 (1979), pp. 225–243.

[103] F. Jegerlehner. “Facts of life with γ_5”. *Eur. Phys. J. C* 18 (2001), pp. 673–679. arXiv: hep-th/0005255.

[104] William A. Bardeen, R. Gastmans, and B. E. Lautrup. “Static quantities in Weinberg’s model of weak and electromagnetic interactions”. *Nucl. Phys. B* 46 (1972), pp. 319–331.

[105] D. A. Akyeampong and Robert Delbourgo. “Dimensional regularization, abnormal amplitudes and anomalies”. *Nuovo Cim. A* 17 (1973), pp. 578–586.

[106] P. Breitenlohner and D. Maison. “Dimensionally Renormalized Green’s Functions for Theories with Massless Particles. 2.” *Commun. Math. Phys.* 52 (1977), p. 55.

[107] P. Breitenlohner and D. Maison. "Dimensional Renormalization and the Action Principle". *Commun. Math. Phys.* 52 (1977), pp. 11–38.

[108] W. Siegel. "Inconsistency of Supersymmetric Dimensional Regularization". *Phys. Lett. B* 94 (1980), pp. 37–40.

[109] Otto Nachtmann and Werner Wetzel. "Spontaneous Breaking of Chiral Symmetry in Quantum Chromodynamics". *Phys. Lett. B* 81 (1979), pp. 211–214.

[110] S. Aoyama and M. Tonin. "The Dimensional Regularization of Chiral Gauge Theories and Generalized Slavnov-Taylor Identities". *Nucl. Phys. B* 179 (1981), pp. 293–323.

[111] Andrzej J. Buras and Peter H. Weisz. "QCD Nonleading Corrections to Weak Decays in Dimensional Regularization and 't Hooft-Veltman Schemes". *Nucl. Phys. B* 333 (1990), pp. 66–99.

[112] Steven A. Gottlieb and J. T. Donohue. "The Axial Vector Current and Dimensional Regularization". *Phys. Rev. D* 20 (1979), p. 3378.

[113] D. Espriu and R. Tarrach. "Renormalization of the Axial Anomaly Operators". *Z. Phys. C* 16 (1982), p. 77.

[114] A. M. Bruque, A. L. Cherchiglia, and M. Pérez-Victoria. "Dimensional regularization vs methods in fixed dimension with and without γ_5". *JHEP* 08 (2018), p. 109. arXiv: 1803.09764 [hep-ph].

[115] A. C. D. Viglioni, A. L. Cherchiglia, A. R. Vieira, Brigitte Hiller, and Marcos Sampaio. "γ_5 algebra ambiguities in Feynman amplitudes: Momentum routing invariance and anomalies in $D = 4$ and $D = 2$". *Phys. Rev. D* 94.6 (2016), p. 065023. arXiv: 1606.01772 [hep-th].

[116] Ruggero Ferrari. "γ_5 in Dimensional Regularization: a Novel Approach" (May 2016). arXiv: 1605.06929 [hep-th].

[117] Ruggero Ferrari. "Managing γ_5 in Dimensional Regularization and ABJ Anomaly" (Mar. 2014). arXiv: 1403.4212 [hep-th].

[118] E. Cartan. "Sur la structure des groupes de transformations finis et continus". Thèses présentées a la Faculté des Sciences de Paris pour obtenir le grade de docteur ès sciences mathématiques (1894).

[119] Jean Dieudonné. "On Semi-Simple Lie Algebras". *Proceedings of the American Mathematical Society* 4.6 (1953), pp. 931–932.

[120] *Mathematics StackExchange thread:* https://math.stackexchange.com/questions/298287/prove-that-every-bilinear-associative-form-in-a-simple-lie-algebra-is-a-multiple. Accessed: 02-27-2025.

[121] Issai Schur. "Neue Begründung der Theorie der Gruppencharaktere". *Sitzungsberichte der Königlich Preussischen Akademie der Wissenschaften zu Berlin* (1905), pp. 406–432.

[122] Samuel Abreu, Ruth Britto, and Claude Duhr. "The SAGEX review on scattering amplitudes Chapter 3: Mathematical structures in Feynman integrals". *Journal of Physics A: Mathematical and Theoretical* 55.44 (Nov. 2022), p. 443004.

[123] F. V. Tkachov. "A theorem on analytical calculability of 4-loop renormalization group functions". *Phys. Lett. B* 100 (1981), pp. 65–68.

[124] K. G. Chetyrkin and F. V. Tkachov. "Integration by parts: The algorithm to calculate β-functions in 4 loops". *Nucl. Phys. B* 192 (1981), pp. 159–204.

[125] T. Gehrmann and E. Remiddi. "Differential equations for two-loop four-point functions". *Nucl. Phys. B* 580 (2000), pp. 485–518. arXiv: hep-ph/9912329.

[126] R. N. Lee. "Group structure of the integration-by-part identities and its application to the reduction of multiloop integrals". *JHEP* 07 (2008), p. 031. arXiv: 0804.3008 [hep-ph].

[127] O. V. Tarasov. "Reduction of Feynman graph amplitudes to a minimal set of basic integrals". *Acta Phys. Polon. B* 29 (1998). Ed. by T. Riemann and J. Blumlein, p. 2655. arXiv: hep-ph/9812250.

[128] A. V. Smirnov and V. A. Smirnov. "S-bases as a tool to solve reduction problems for Feynman integrals". *Nucl. Phys. B Proc. Suppl.* 160 (2006). Ed. by J. Blumlein, S. Moch, and T. Riemann, pp. 80–84. arXiv: hep-ph/0606247.

[129] Janusz Gluza, Krzysztof Kajda, and David A. Kosower. "Towards a Basis for Planar Two-Loop Integrals". *Phys. Rev. D* 83 (2011), p. 045012. arXiv: 1009.0472 [hep-th].

[130] Alessandro Georgoudis, Kasper J. Larsen, and Yang Zhang. "Azurite: An algebraic geometry based package for finding bases of loop integrals". *Comput. Phys. Commun.* 221 (2017), pp. 203–215. arXiv: 1612.04252 [hep-th].

[131] Zvi Bern, Michael Enciso, Harald Ita, and Mao Zeng. "Dual Conformal Symmetry, Integration-by-Parts Reduction, Differential Equations and the Nonplanar Sector". *Phys. Rev. D* 96.9 (2017), p. 096017. arXiv: 1709.06055 [hep-th].

[132] David A. Kosower. "Direct Solution of Integration-by-Parts Systems". *Phys. Rev. D* 98.2 (2018), p. 025008. arXiv: 1804.00131 [hep-ph].

[133] S. Laporta. "High-precision calculation of multiloop Feynman integrals by difference equations". *Int. J. Mod. Phys. A* 15 (2000), pp. 5087–5159. arXiv: hep-ph/0102033.

[134] A. V. Smirnov and A. V. Petukhov. "The Number of Master Integrals is Finite". *Lett. Math. Phys.* 97 (2011), pp. 37–44. arXiv: 1004.4199 [hep-th].

[135] Philipp Kant. "Finding linear dependencies in integration-by-parts equations: A Monte Carlo approach". *Comput. Phys. Commun.* 185 (2014), pp. 1473–1476. arXiv: 1309.7287 [hep-ph].

[136] Jonas Klappert, Sven Yannick Klein, and Fabian Lange. "Interpolation of dense and sparse rational functions and other improvements in FireFly". *Comput. Phys. Commun.* 264 (2021), p. 107968. arXiv: 2004.01463 [cs.MS].

[137] Richard Zippel. "Probabilistic algorithms for sparse polynomials". *Symbolic and Algebraic Computation*. Ed. by Edward W. Ng. Berlin, Heidelberg: Springer Berlin Heidelberg, 1979, pp. 216–226.

[138] Jennifer de Kleine, Michael Monagan, and Allan Wittkopf. "Algorithms for the nonmonic case of the sparse modular GCD algorithm". ISSAC '05. Beijing, China: Association for Computing Machinery, 2005, pp. 124–131.

[139] Michael Ben-Or and Prasoon Tiwari. "A deterministic algorithm for sparse multivariate polynomial interpolation". *Proceedings of the Twentieth Annual ACM Symposium on Theory of Computing*. STOC '88. Chicago, Illinois, USA: Association for Computing Machinery, 1988, pp. 301–309.

[140] Annie Cuyt and Wen-shin Lee. "Sparse interpolation of multivariate rational functions". *Theoretical Computer Science* 412.16 (2011). Symbolic and Numerical Algorithms, pp. 1445–1456.

[141] Paul S. Wang. "A p-adic algorithm for univariate partial fractions". *Proceedings of the Fourth ACM Symposium on Symbolic and Algebraic Computation*. SYMSAC '81. Snowbird, Utah, USA: Association for Computing Machinery, 1981, pp. 212–217.

[142] Charalampos Anastasiou and Achilleas Lazopoulos. "Automatic integral reduction for higher order perturbative calculations". *Journal of High Energy Physics* 2004.07 (Sept. 2004), p. 046.

[143] C. Studerus. "Reduze – Feynman integral reduction in C++". *Comput. Phys. Commun.* 181 (2010), pp. 1293–1300. arXiv: 0912.2546 [physics.comp-ph].

[144] A. von Manteuffel and C. Studerus. "Reduze 2 - Distributed Feynman Integral Reduction" (Jan. 2012). arXiv: 1201.4330 [hep-ph].

[145] R. N. Lee. "Presenting LiteRed: a tool for the Loop InTEgrals REDuction" (Dec. 2012). arXiv: 1212.2685 [hep-ph].

[146] Roman N. Lee. "LiteRed 1.4: a powerful tool for reduction of multiloop integrals". *J. Phys. Conf. Ser.* 523 (2014). Ed. by Jianxiong Wang, p. 012059. arXiv: 1310.1145 [hep-ph].

[147] A. V. Smirnov. "Algorithm FIRE – Feynman Integral REduction". *JHEP* 10 (2008), p. 107. arXiv: 0807.3243 [hep-ph].

[148] A. V. Smirnov and V. A. Smirnov. "FIRE4, LiteRed and accompanying tools to solve integration by parts relations". *Comput. Phys. Commun.* 184 (2013), pp. 2820–2827. arXiv: 1302.5885 [hep-ph].

[149] Alexander V. Smirnov. "FIRE5: A C++ implementation of Feynman Integral REduction". *Comput. Phys. Commun.* 189 (2015), pp. 182–191. arXiv: 1408.2372 [hep-ph].

[150] A. V. Smirnov and F. S. Chukharev. "FIRE6: Feynman Integral REduction with modular arithmetic". *Comput. Phys. Commun.* 247 (2020), p. 106877. arXiv: 1901.07808 [hep-ph].

[151] Philipp Maierhöfer, Johann Usovitsch, and Peter Uwer. "Kira—A Feynman integral reduction program". *Comput. Phys. Commun.* 230 (2018), pp. 99–112. arXiv: 1705.05610 [hep-ph].

[152] Philipp Maierhöfer and Johann Usovitsch. "Kira 1.2 Release Notes" (Dec. 2018). arXiv: 1812.01491 [hep-ph].

[153] P. Maierhöfer and J. Usovitsch. "Recent developments in Kira". *CERN Yellow Reports: Monographs* 3 (2020). Ed. by A. Blondel, J. Gluza, S. Jadach, P. Janot, and T. Riemann, pp. 201–204.

[154] Jonas Klappert, Fabian Lange, Philipp Maierhöfer, and Johann Usovitsch. "Integral reduction with Kira 2.0 and finite field methods". *Comput. Phys. Commun.* 266 (2021), p. 108024. arXiv: 2008.06494 [hep-ph].

[155] Fabian Lange, Philipp Maierhöfer, and Johann Usovitsch. "Developments since Kira 2.0". *SciPost Phys. Proc.* 7 (2022), p. 017. arXiv: 2111.01045 [hep-ph].

[156] Johann Usovitsch. "Kira and the block-triangular form". *PoS* LL2022 (2022), p. 071.

[157] Fabian Lange, Johann Usovitsch, and Zihao Wu. "Towards the next Kira release". *PoS* LL2024 (2024), p. 070. arXiv: 2407.01395 [hep-ph].

[158] Zihao Wu, Janko Boehm, Rourou Ma, Hefeng Xu, and Yang Zhang. "NeatIBP 1.0, a package generating small-size integration-by-parts relations for Feynman integrals". *Comput. Phys. Commun.* 295 (2024), p. 108999. arXiv: 2305.08783 [hep-ph].

[159] Zihao Wu, Janko Böhm, Rourou Ma, Johann Usovitsch, Yingxuan Xu, and Yang Zhang. "Performing integration-by-parts reductions using NeatIBP 1.1 + Kira" (Feb. 2025). arXiv: 2502.20778 [hep-ph].

[160] Xin Guan, Xiao Liu, Yan-Qing Ma, and Wen-Hao Wu. "Blade: A package for block-triangular form improved Feynman integrals decomposition". *Comput. Phys. Commun.* 310 (2025), p. 109538. arXiv: 2405.14621 [hep-ph].

[161] A. V. Kotikov. "Differential Equation Method: The Calculation of N Point Feynman Diagrams". *Phys. Lett. B* 267 (1991). [Erratum: Phys.Lett.B 295, 409–409 (1992)], pp. 123–127.

[162] Johannes M. Henn. "Multiloop integrals in dimensional regularization made simple". *Phys. Rev. Lett.* 110 (2013), p. 251601. arXiv: 1304.1806 [hep-th].

[163] A. B. Goncharov. "Multiple polylogarithms, cyclotomy and modular complexes". *Math Res. Letters* 5 (1998), pp. 497–516. arXiv: 1105.2076 [math.AG].

[164] Roman N. Lee. "Reducing differential equations for multiloop master integrals". *JHEP* 04 (2015), p. 108. arXiv: 1411.0911 [hep-ph].

[165] Roman N. Lee and Andrei A. Pomeransky. "Normalized Fuchsian form on Riemann sphere and differential equations for multiloop integrals" (July 2017). arXiv: 1707.07856 [hep-th].

[166] A. Blondel et al. "Standard model theory for the FCC-ee Tera-Z stage, section E.8". *Mini Workshop on Precision EW and QCD Calculations for the FCC Studies : Methods and Techniques*. Vol. 3/2019. CERN Yellow Reports: Monographs. Geneva: CERN, Sept. 2018. arXiv: 1809.01830 [hep-ph].

[167] Mario Prausa. "epsilon: A tool to find a canonical basis of master integrals". *Comput. Phys. Commun.* 219 (2017), pp. 361–376. arXiv: 1701.00725 [hep-ph].

[168] Oleksandr Gituliar and Vitaly Magerya. "Fuchsia: a tool for reducing differential equations for Feynman master integrals to epsilon form". *Comput. Phys. Commun.* 219 (2017), pp. 329–338. arXiv: 1701.04269 [hep-ph].

[169] Christoph Meyer. "Algorithmic transformation of multi-loop master integrals to a canonical basis with CANONICA". *Comput. Phys. Commun.* 222 (2018), pp. 295–312. arXiv: 1705.06252 [hep-ph].

[170] Roman N. Lee. "Libra: A package for transformation of differential systems for multiloop integrals". *Comput. Phys. Commun.* 267 (2021), p. 108058. arXiv: 2012.00279 [hep-ph].

[171] Long-Bin Chen, Hai Tao Li, Zhao Li, Jian Wang, Yefan Wang, and Quan-feng Wu. "Analytic three-loop QCD corrections to top-quark and semileptonic $b \to u$ decays". *Phys. Rev. D* 109.7 (2024), p. L071503. arXiv: 2309.00762 [hep-ph].

[172] Tongzhi Yang. "Renormalization of twist-two operators and four-loop splitting functions in QCD". *PoS* RADCOR2023 (2024), p. 056.

[173] Saurav Goyal, Roman N. Lee, Sven-Olaf Moch, Vaibhav Pathak, Narayan Rana, and V. Ravindran. "Next-to-Next-to-Leading Order QCD Corrections to Polarized Semi-Inclusive Deep-Inelastic Scattering". *Phys. Rev. Lett.* 133 (2024), p. 211905. arXiv: 2404.09959 [hep-ph].

[174] Manuel Egner, Matteo Fael, Kay Schönwald, and Matthias Steinhauser. "Nonleptonic B-meson decays to next-to-next-to-leading order". *JHEP* 10 (2024), p. 144. arXiv: 2406.19456 [hep-ph].

[175] Yao Ji, Bo-Xuan Shi, Jian Wang, Ye-Fan Wang, Yu-Ming Wang, and Hui-Xin Yu. "Next-to-Next-to-Leading-Order QCD Prediction for the Pion Form Factor" (Nov. 2024). arXiv: 2411.03658 [hep-ph].

[176] Jia-Le Ding, Hai Tao Li, and Jian Wang. "Next-to-next-to-leading order threshold soft function for tW production" (Feb. 2025). arXiv: 2502.18648 [hep-ph].

[177] Taushif Ahmed et al. "NNLO phase-space integrals for semi-inclusive deep-inelastic scattering" (Dec. 2024). arXiv: 2412.16509 [hep-ph].

[178] Long-Bin Chen, Jian Wang, and Yefan Wang. "Analytic NNLO QCD corrections to top quark pair production in electron-positron collisions". *JHEP* 09 (2024), p. 014. arXiv: 2405.18912 [hep-ph].

[179] A. V. Belitsky, L. V. Bork, J. M. Grumski-Flores, and V. A. Smirnov. "Three-leg form factor on Coulomb branch". *JHEP* 11 (2024), p. 169. arXiv: 2402.18475 [hep-th].

[180] Jens Vollinga. "GiNaC: Symbolic computation with C++". *Nucl. Instrum. Meth. A* 559 (2006). Ed. by J. Blumlein, W. Friebel, T. Naumann, T. Riemann, P. Wegner, and D. Perret-Gallix, pp. 282–284. arXiv: hep-ph/0510057.

[181] Claude Duhr and Falko Dulat. "PolyLogTools — polylogs for the masses". *JHEP* 08 (2019), p. 135. arXiv: 1904.07279 [hep-th].

[182] Claude Duhr. "Mathematical aspects of scattering amplitudes". *Theoretical Advanced Study Institute in Elementary Particle Physics: Journeys Through the Precision Frontier: Amplitudes for Colliders*. 2015, pp. 419–476. arXiv: 1411.7538 [hep-ph].

[183] Jonathan Borwein, David Bradley, David Broadhurst, and Petr Lisoněk. "Special values of multiple polylogarithms". *Transactions of the American Mathematical Society* 353.3 (2001), pp. 907–941.

[184] Vladimir A. Smirnov. "Asymptotic expansions in momenta and masses and calculation of Feynman diagrams". *Mod. Phys. Lett. A* 10 (1995), pp. 1485–1500. arXiv: hep-th/9412063.

[185] M. Beneke and Vladimir A. Smirnov. "Asymptotic expansion of Feynman integrals near threshold". *Nucl. Phys. B* 522 (1998), pp. 321–344. arXiv: hep-ph/9711391.

[186] Vladimir A. Smirnov. "Problems of the strategy of regions". *Phys. Lett. B* 465 (1999), pp. 226–234. arXiv: hep-ph/9907471.

[187] V.A. Smirnov. "Renormalization and Asymptotic Expansions". Progress in Physics: Birkhäuser (1991).

[188] Vladimir A. Smirnov. "Applied asymptotic expansions in momenta and masses". *Springer Tracts Mod. Phys.* 177 (2002), pp. 1–262.

[189] Xiao Liu, Yan-Qing Ma, and Chen-Yu Wang. "A Systematic and Efficient Method to Compute Multi-loop Master Integrals". *Phys. Lett. B* 779 (2018), pp. 353–357. arXiv: 1711.09572 [hep-ph].

[190] S. Laporta. "High-precision ϵ expansions of three loop master integrals contributing to the electron $g-2$ in QED". *Phys. Lett. B* 523 (2001), pp. 95–101. arXiv: hep-ph/0111123.

[191] B. A. Kniehl, A. F. Pikelner, and O. L. Veretin. "Three-loop massive tadpoles and polylogarithms through weight six". *JHEP* 08 (2017), p. 024. arXiv: 1705.05136 [hep-ph].

[192] David J. Broadhurst. "Massive three - loop Feynman diagrams reducible to SC* primitives of algebras of the sixth root of unity". *Eur. Phys. J. C* 8 (1999), pp. 311–333. arXiv: hep-th/9803091.

[193] Matthias Steinhauser. "MATAD: A Program package for the computation of MAssive TADpoles". *Comput. Phys. Commun.* 134 (2001), pp. 335–364. arXiv: hep-ph/0009029.

[194] Y. Schroder and A. Vuorinen. "High-precision epsilon expansions of single-mass-scale four-loop vacuum bubbles". *JHEP* 06 (2005), p. 051. arXiv: hep-ph/0503209.

[195] Thomas Luthe, Andreas Maier, Peter Marquard, and York Schroder. "Complete renormalization of QCD at five loops". *JHEP* 03 (2017), p. 020. arXiv: 1701.07068 [hep-ph].

[196] Thomas Luthe. "Fully massive vacuum integrals at 5 loops". PhD thesis. Bielefeld U., 2015.

[197] Xiao Liu and Yan-Qing Ma. "Multiloop corrections for collider processes using auxiliary mass flow". *Phys. Rev. D* 105.5 (2022), p. L051503. arXiv: 2107.01864 [hep-ph].

[198] Xiao Liu and Yan-Qing Ma. "AMFlow: A Mathematica package for Feynman integrals computation via auxiliary mass flow". *Comput. Phys. Commun.* 283 (2023), p. 108565. arXiv: 2201.11669 [hep-ph].

[199] Helaman Ferguson and David Bailey. "A Polynomial Time, Numerically Stable Integer Relation Algorithm" (Jan. 1992).

[200] Helaman Ferguson, David Bailey, and Steve Arno. "Analysis Of PSLQ, An Integer Relation Finding Algorithm". *Mathematics of Computation* 68 (Dec. 1998).

[201] K. G. Chetyrkin, Johann H. Kuhn, and M. Steinhauser. "RunDec: a Mathematica package for running and decoupling of the strong coupling and quark masses". *Comput. Phys. Commun.* 133 (2000), pp. 43–65. arXiv: hep-ph/0004189.

[202] Barbara Schmidt and Matthias Steinhauser. "CRunDec: a C++ package for running and decoupling of the strong coupling and quark masses". *Comput. Phys. Commun.* 183 (2012), pp. 1845–1848. arXiv: 1201.6149 [hep-ph].

[203] Florian Herren and Matthias Steinhauser. "Version 3 of RunDec and CRunDec". *Comput. Phys. Commun.* 224 (2018), pp. 333–345. arXiv: 1703.03751 [hep-ph].

[204] Aneesh V. Manohar and Mark B. Wise. "Heavy quark physics". 10 (2000).

[205] Sheldon L. Glashow. "The renormalizability of vector meson interactions". *Nucl. Phys.* 10 (1959), pp. 107–117.

[206] Abdus Salam and John Clive Ward. "Electromagnetic and weak interactions". *Phys. Lett.* 13 (1964), pp. 168–171.

[207] Steven Weinberg. "A Model of Leptons". *Phys. Rev. Lett.* 19 (1967), pp. 1264–1266.

[208] Abdus Salam. "Weak and Electromagnetic Interactions". *Conf. Proc. C* 680519 (1968), pp. 367–377.

[209] Jorge C. Romao and Joao P. Silva. "A resource for signs and Feynman diagrams of the Standard Model". *Int. J. Mod. Phys. A* 27 (2012), p. 1230025. arXiv: 1209.6213 [hep-ph].

[210] F. Englert and R. Brout. "Broken Symmetry and the Mass of Gauge Vector Mesons". *Phys. Rev. Lett.* 13 (9 Aug. 1964), pp. 321–323.

[211] Peter W. Higgs. "Broken Symmetries and the Masses of Gauge Bosons". *Phys. Rev. Lett.* 13 (16 Oct. 1964), pp. 508–509.

[212] David J. Gross and Frank Wilczek. "Ultraviolet Behavior of Nonabelian Gauge Theories". *Phys. Rev. Lett.* 30 (1973). Ed. by J. C. Taylor, pp. 1343–1346.

[213] H. David Politzer. "Reliable Perturbative Results for Strong Interactions?" *Phys. Rev. Lett.* 30 (1973). Ed. by J. C. Taylor, pp. 1346–1349.

[214] William E. Caswell. "Asymptotic Behavior of Nonabelian Gauge Theories to Two Loop Order". *Phys. Rev. Lett.* 33 (1974), p. 244.

[215] D. R. T. Jones. "Two Loop Diagrams in Yang-Mills Theory". *Nucl. Phys. B* 75 (1974), p. 531.

[216] O. V. Tarasov, A. A. Vladimirov, and A. Yu. Zharkov. "The Gell-Mann-Low Function of QCD in the Three Loop Approximation". *Phys. Lett. B* 93 (1980), pp. 429–432.

[217] S. A. Larin and J. A. M. Vermaseren. "The three-loop QCD β function and anomalous dimensions". *Phys. Lett. B* 303 (1993), pp. 334–336. arXiv: hep-ph/9302208.

[218] T. van Ritbergen, J. A. M. Vermaseren, and S. A. Larin. "The four-loop β function in Quantum Chromodynamics". *Phys. Lett. B* 400 (1997), pp. 379–384. arXiv: hep-ph/9701390.

[219] M. Czakon. "The Four-Loop QCD β-Function and Anomalous Dimensions". *Nucl. Phys. B* 710 (2005), pp. 485–498. arXiv: hep-ph/0411261.

[220] P. A. Baikov, K. G. Chetyrkin, and J. H. Kühn. "Five-Loop Running of the QCD coupling constant". *Phys. Rev. Lett.* 118.8 (2017), p. 082002. arXiv: 1606.08659 [hep-ph].

[221] John C. Collins. "Renormalization : An Introduction to Renormalization, the Renormalization Group and the Operator-Product Expansion". Cambridge Monographs on Mathematical Physics 26 (1984).

[222] Kenneth G. Wilson. "Non-Lagrangian Models of Current Algebra". *Phys. Rev.* 179 (5 Mar. 1969), pp. 1499–1512.

[223] Kenneth G. Wilson. "Operator-Product Expansions and Anomalous Dimensions in the Thirring Model". *Phys. Rev. D* 2 (8 Oct. 1970), pp. 1473–1477.

[224] Stefan Hollands and Robert M. Wald. "The Operator Product Expansion in Quantum Field Theory" (Dec. 2023). arXiv: 2312.01096 [hep-th].

[225] P. Marquard, L. Mihaila, J. H. Piclum, and M. Steinhauser. "Relation between the pole and the minimally subtracted mass in dimensional regularization and dimensional reduction to three-loop order". *Nucl. Phys. B* 773 (2007), pp. 1–18. arXiv: hep-ph/0702185.

[226] S. Bekavac, A. Grozin, D. Seidel, and M. Steinhauser. "Light quark mass effects in the on-shell renormalization constants". *JHEP* 10 (2007), p. 006. arXiv: 0708.1729 [hep-ph].

[227] Paulo Nogueira. "Automatic Feynman Graph Generation". *J. Comput. Phys.* 105 (1993), pp. 279–289.

[228] P. Nogueira. "Feynman graph generation and propagator mixing, I". *Comput. Phys. Commun.* 269 (2021), p. 108103.

[229] J.A.M. Vermaseren. "Symbolic Manipulation with FORM". *CAN (Computer Algebra Nederland)* (1991).

[230] D. Fliegner, A. Retey, and J. A. M. Vermaseren. "Parallelizing the symbolic manipulation program FORM". *6th International Workshop on New Computing Techniques in Physics Research: Software Engineering, Artificial Intelligence Neural Nets, Genetic Algorithms, Symbolic Algebra, Automatic Calculation*. June 1999. arXiv: hep-ph/9906426.

[231] J. A. M. Vermaseren. "New features of FORM" (Oct. 2000). arXiv: math-ph/0010025.

[232] Jens Vollinga. "GiNaC: Symbolic computation with C++". *Nucl. Instrum. Meth. A* 559 (2006). Ed. by J. Blumlein, W. Friebel, T. Naumann, T. Riemann, P. Wegner, and D. Perret-Gallix, pp. 282–284. arXiv: hep-ph/0510057.

[233] Matteo Cacciari and Stefano Catani. "Soft gluon resummation for the fragmentation of light and heavy quarks at large x". *Nucl. Phys. B* 617 (2001), pp. 253–290. arXiv: hep-ph/0107138.

[234] Matteo Cacciari and Einan Gardi. "Heavy quark fragmentation". *Nucl. Phys. B* 664 (2003), pp. 299–340. arXiv: hep-ph/0301047.

[235] Maciej Kaminski, Mikolaj Misiak, and Michal Poradzinski. "Tree-level contributions to $B \to X_s\gamma$". *Phys. Rev. D* 86 (2012), p. 094004. arXiv: 1209.0965 [hep-ph].